

TARGETING INFLAMMATORY MEDIATOR SIGNALLING IN PERICYTES TO
RESOLVE TISSUE FIBROSIS

REBECCA ELLEN BIGNOLD

Doctor of Philosophy

ASTON UNIVERSITY

June 2022

©Rebecca Ellen Bignold, 2022

Rebecca Ellen Bignold asserts their moral right to be identified as the
author of this thesis

This copy of the thesis has been supplied on condition that anyone who consults
it is understood to recognise that its copyright belongs to its author and that
no quotation from the thesis and no information derived from it may be
published without appropriate permission or acknowledgement.

Aston University

Targeting Inflammatory Mediator Signalling in Pericytes to Resolve Tissue Fibrosis

Rebecca Ellen Bignold

Doctor of Philosophy

2022

Abstract: The migration of pericytes from the vasculature towards the inflamed airway is a key contributor to airway remodelling, a hallmark of allergic asthma. However, the mechanisms contributing to this event are not yet known. Various growth factors, cytokines and matrikines have been linked to airway remodelling or allergic asthma, although how they interact with pericytes and effect their migration is yet to be determined. These factors may be useful, druggable targets for future asthma treatments. Pericyte migration was observed via Transwell and scratch assays and the expression of indicators of fibrosis including periostin and N-cadherin were assessed via immunostaining and ELISA and the IL-13 inhibitor cinnamaldehyde was explored as a drug to target this migration. In order to better observe pericyte uncoupling from endothelial cells and their subsequent migration, 3D co-cultures of pericytes and endothelial cells were constructed via magnetic levitation and analysed using immunostaining. As an in vivo corollary, the house dust mite mouse model of allergic asthma was utilised and lung tissue, tracheobronchial whole mounts, bronchoalveolar lavage fluid and whole lung digests were harvested and used to assess the effect of the CXCL12 neutraligand LIT-927 on airway remodelling. The results demonstrate increased pericyte migration following treatment with TGF- β , EGF or periostin and under inflammatory conditions in vivo. The impact of periostin was further explored, with the expression of periostin by pericytes increased by TGF- β and periostin secretion driven by IL-13, which was successfully inhibited with cinnamaldehyde treatment. Spheroids of pericytes and endothelial cells were successfully constructed, although further optimisation of the staining method is needed. CXCL12 neutralization with LIT-927 was found to reduce symptoms of respiratory distress and impede the uncoupling of pericytes while not affecting the immune response or the expression of CXCR4 on pericytes. Overall, cinnamaldehyde and LIT-927 are promising future drugs for treating allergic asthma.

Keywords: Pericyte · Airway Remodelling · Allergic Asthma · Migration · TGF- β · Periostin · Cinnamaldehyde · Spheroid · CXCL12 · LIT-927

Personal Acknowledgements

I'd like to thank everyone who has helped me and offered me support and guidance throughout my journey as a researcher.

I'd firstly like to offer the biggest thanks to my supervisor, Dr Jill Johnson who has helped me grow into the researcher I am today. Her expertise in the field has been invaluable and her personal support has really helped me to achieve my potential. Thank you for continually pushing me in the right places and encouraging me to pursue greater things.

I'd also like to thank Professor Andrew Devitt, Dr Stephane Gross, Dr Ewan Ross and Wayne Fleary who have offered me technical support throughout my time at Aston University.

I have had the opportunity to work with many talented and enthusiastic colleagues including Humaa Asif, Annelise Garrison, Emma Pugh, Usama Kasu, Inderpreet Ragbotra, and Maxwell Dobney. Thanks for keeping me sane!

Also, thank you to the Emmas at Clarendon Academy, Emma Cooper, Emma John and Emma Prior, for encouraging me to pursue a career in science. You helped to lay a very good foundation for me to build on and I am incredibly grateful.

Finally, I would like to thank my family, Mum, Dad and Lizzie for your encouragement and reassurance throughout my education. And to Craig, for putting up with me throughout the most stressful part of my life so far.

Collaborator Acknowledgements

I acknowledge that data shown within Chapter 4 of this thesis has been previously published in *Frontiers in Allergy*.

BIGNOLD, R. & JOHNSON, J. 2021. Matricellular protein periostin promotes pericyte migration in fibrotic airways. *Frontiers in Allergy*, 2

I acknowledge that data shown within Chapter 6 of this thesis has been previously published as a pre-print in Research Square and is under review for publication in *Respiratory Research*.

BIGNOLD, R., SHAMMOUT, B., ROWLEY, J., REPICI, M., SIMMS, J. & JOHNSON, J. 2022. CXCL12 drives pericyte accumulation and airway remodeling in allergic airway disease. Research Square.

[signature redacted]

Rebecca Bignold

Table of Contents

Chapter 1 – Introduction

1.1 Asthma	1
1.2 Pericytes	5
1.3 Pericytes and Chronic Inflammatory Disease	9

Chapter 2 – Materials and Methods

2.1 Cell Culture	13
2.2 Growth Factor Treatment.....	13
2.3 Transwell Assays	14
2.4 Scratch Assays	14
2.5 ELISA.....	15
2.6 3D Cultures.....	15
2.7 In Vivo House Dust Mite Model	15
2.8 Sample Collection	16
2.9 Preparation of Single Cell Suspension from Mouse Lung	16
2.10 Staining of Lung Cells for Flow Cytometry	17
2.11 Flow Cytometry	17
2.12 Fluorescence Imaging	18
2.13 Image Analysis	19
2.14 Bioinformatics	20
2.15 Statistical Analysis	20

Chapter 3 - The Migration of Pericytes In Vitro Can Be Modulated By Growth Factors, Cytokines & Matrikines in the Microenvironment Including TGF- β , VEGF & Periostin

3.1 Introduction	22
------------------------	----

3.2 Results	24
3.3 Discussion	46
Chapter 4 – Matricellular Protein Periostin Promotes Pericyte Migration in Fibrotic Airways and Can Be Abrogated By Cinnamaldehyde	
4.1 Introduction	49
4.2 Results	51
4.3 Discussion	90
Chapter 5 – A New Dimension: Spheroids Containing a Co-Culture of Endothelial Cells and Pericytes Can Be Constructed Via Magnetic Levitation	
5.1 Introduction	98
5.2 Results	101
5.3 Discussion	119
Chapter 6 – CXCL12 Drives Pericyte Accumulation and Airway Remodelling in Allergic Airway Disease	
6.1 Introduction	125
6.2 Results	127
6.3 Discussion	141
Chapter 7 – General Discussion	
7.1 Chapter 3	145
7.2 Chapter 4	148
7.3 Chapter 5	153
7.4 Chapter 6	155
7.5 Disruptions	159
Chapter 8 - References.....	161
Chapter 9 – Supplementary Information	196

Abbreviations

AI	Artificial intelligence
Akt	Protein kinase B
AMPK	AMP-activated protein kinase
ANOVA	Analysis of variance
ARCHA	Aston Research Centre for Healthy Ageing
ARRIVE	Animal Research: Reporting of In Vivo Experiments
AU	Arbitrary units
AW	Airway
BAL	Bronchoalveolar lavage
BTM	Bottom
BV	Blood vessel
CIN	Cinnamaldehyde
COPD	Chronic obstructive pulmonary disease
COVID	SARS-CoV-2
CTK	Cytokine
CV	Coefficient of variation
CXCL12	C-X-C motif chemokine ligand 12
CXCR4	C-X-C motif chemokine receptor 4
DAPI	Diamindino-2-phenylindole
DMEM	Dulbecco's modified eagle medium
ECM	Extracellular matrix
EDTA	Ethylenediaminetetraacetic acid
EGF	Epidermal growth factor
EGFR	Epidermal growth factor receptor
ELISA	Enzyme-linked immunosorbent assay
EMBL-EBI	European Molecular Biology Laboratory – European Bioinformatics Institute
EMT	Epithelial to mesenchymal transition
ERK	Extracellular signal-regulated kinase

FCS	Foetal calf serum
FDA	Food and Drug Administration
FGF	Fibroblast growth factor
GEO	Gene Expression Omnibus
GF	Growth factor
GM-CSF	Granulocyte-macrophage colony-stimulating factor
HDM	House dust mite
HIV	Human immunodeficiency virus
HPLPC	Human placental pericytes
HUVEC	Human umbilical vein endothelial cells
ICAM-1	Intercellular adhesion molecule 1
IFN-γ	Interferon gamma
IL	Interleukin
ILD	Interstitial lung disease
ILK	Integrin-linked kinase
IPF	Idiopathic pulmonary fibrosis
LFA-1	Lymphocyte function-associated antigen 1
LIT	LIT-927
Macs	Macrophages
MAPK	Mitogen-activated protein kinases
MSC	Mesenchymal stem cell
N-cad	N-cadherin
NCBI	National Centre for Biotechnology Information
NG2	Neural/glial antigen 2
NGS	Normal goat serum
NHS	National Health Service
NK	Natural killer
Ns	Not significant
Ox	Oxidative
PBS	Phosphate buffered saline
PCR	Polymerase chain reaction

PDGF	Platelet-derived growth factor
PDGFR	Platelet-derived growth factor
PI3K	Phosphoinositide 3-kinase
PLCγ	Phospholipase C gamma
PM	Pericyte medium
POSTN	Periostin
PSTN	Periostin
RNA	Ribonucleic acid
RPMI	Roswell Park Memorial Institute
Smad	“Small mothers against decapentaplegic”
TGF-β	Transforming growth factor beta
TNF-α	Tumour necrosis factor alpha
UV	Ultraviolet
VEGF	Vascular endothelial growth factor
VEH	Vehicle
α-SMA	Alpha-smooth muscle actin

List of Figures

Figure 1.1	Diagram depicting the four aspects of airway remodelling seen in asthma	4
Figure 1.2	The involvement of pericytes in the airway remodelling observed in asthmatic lungs	10
Table 2.1	Growth factors and cytokines used and their general working concentrations	14
Table 2.2	Antibodies used in flow cytometry experiments	17
Table 2.3	Primary antibodies used in immunofluorescent staining	18
Figure 3.1	There is no significant difference in pericyte migration towards serum free media measured with Transwell assay following growth factor treatment	24
Figure 3.2	Pericytes treated with TGF- β migrate less towards media containing FCS than untreated pericytes	26
Figure 3.3	There is no significant difference in pericyte migration towards media containing PDGF-BB measured with Transwell assays following growth factor treatment	27
Figure 3.4	Pericytes significantly migrated more towards media containing FCS than serum free media or media containing PDGF-BB	28
Figure 3.5	Pericyte nuclei are clearly visible on Transwell membranes using a DAPI stain	29
Figure 3.6	Pericytes grown in pericyte media migrate more than those grown in DMEM	30
Figure 3.7	Pericytes grown in pericyte media and treated with TGF- β migrate more than those grown in DMEM and treated with TGF β	31
Figure 3.8	Untreated pericytes do not preferentially migrate towards either living or dead macrophages	32
Figure 3.9	Treatment with VEGF or TGF- β encouraged pericyte migration towards living macrophages	33
Figure 3.10	There was no difference in the migration of pericytes towards dead macrophages following growth factor treatments	34

Figure 3.11	There is no difference in migration towards serum free DMEM, FCS or CXCL12 by untreated pericytes	36
Figure 3.12	Pericytes treated with TGF- β migrate more towards medium containing CXCL12 and medium containing FCS than serum-free medium	37
Figure 3.13	Pericytes treated with periostin migrate less towards medium containing FCS than untreated pericytes	38
Figure 3.14	Pericytes treated with TGF- β and periostin migrate less towards medium containing CXCL12 than untreated pericytes	39
Figure 3.15	Pericytes treated with TGF- β or periostin appear in clumps on Transwell membranes	40
Figure 3.16	Pericytes treated with TGF- β or EGF migrate significantly more than untreated pericytes in scratch assays	41
Figure 3.17	Pericytes treated with periostin migrate significantly more than untreated pericytes in scratch assays	43
Figure 3.18	Graphical depiction of method used to construct wells for the dual surface assay	44
Figure 3.19	The method for the dual surface assay does not yield interpretable results	45
Figure 4.1	The gene for periostin is increased in humans with allergic asthma	51
Figure 4.2	The gene for periostin is increased in wild type mice given HDM but not in IL-13 knockouts	52
Figure 4.3	The increase and decrease of gene expression in IPF lungs compared to healthy lungs	53
Figure 4.4	The gene expression of periostin in lungs with interstitial lung disease compared to healthy lungs	54
Figure 4.5	The expression of POSTN in asthmatic lung cell types	55
Figure 4.6	Protein interactions of periostin	56
Figure 4.7	Pericytes migrate into the cell free space more when treated with TGF- β or periostin	57
Figure 4.8	Pericytes migrate more when treated with either TGF- β or periostin	58
Figure 4.9	Treating pericytes with periostin did not increase their migration towards either serum free medium or medium containing FCS in Transwell assays	59

Figure 4.10	TGF- β or periostin treatment increases the expression of periostin by pericytes	60
Figure 4.11	Treating pericytes with periostin increases their expression of periostin	61
Figure 4.12	Periostin and CD146 positive cells form a robust ring around airways that were exposed to HDM	63
Figure 4.13	Periostin and PDGFR β positive cells form a robust ring around airways that were exposed to HDM	64
Figure 4.14	HDM-exposed lung tissue expressed significantly more periostin than PBS tissue	65
Figure 4.15	BAL from HDM-exposed mice contained slightly more secreted periostin than PBS mice	66
Figure 4.16	IL-13 treatment caused pericytes to secrete significantly more periostin than other cytokines	67
Figure 4.17	Periostin expression by pericytes peaked at around 3 days of TGF- β treatment	68
Figure 4.18	Periostin expression by pericytes remained constant throughout 9 days of IL-13 treatment	69
Figure 4.19	Periostin expression by pericytes increased with time following combined TGF- β and IL-13 treatments	70
Figure 4.20	α -SMA expression by pericytes slightly increased with time following TGF- β treatment	71
Figure 4.21	α -SMA expression by pericytes remained relatively constant throughout the 9 days of IL-13 treatment	72
Figure 4.22	α -SMA expression by pericytes increased with time following a combined TGF- β and IL-13 treatment	73
Figure 4.23	There was no significant difference in the expression of N-cadherin by pericytes following TGF- β and/or periostin treatment	74
Figure 4.24	Treatment with EGF and periostin increased the expression of N-cadherin by pericytes	75
Figure 4.25	There was no significant difference in the expression of N-cadherin by pericytes following TGF- β and/or periostin treatment	76
Figure 4.26	There was no significant difference in the expression of periostin by pericytes following TGF- β and/or periostin treatment	77

Figure 4.27	There was no significant difference in the expression of periostin by pericytes following EGF and/or periostin treatment	78
Figure 4.28	There was no significant difference in the expression of periostin by pericytes following TGF- β , EGF and/or periostin treatment	79
Figure 4.29	Cinnamaldehyde treatment successfully inhibited IL-13-mediated periostin secretion by pericytes at concentrations higher than 1nM	80
Figure 4.30	Treatment with cinnamaldehyde did not affect the migration of TGF- β -treated pericytes	81
Figure 4.31	Treatment with cinnamaldehyde reduced the effect of IL-13 treatment on the migration of pericytes	82
Figure 4.32	Treatment with cinnamaldehyde reduced the effect of periostin treatment on the migration of pericytes	83
Figure 4.33	Treatment with cinnamaldehyde did not affect the expression of periostin by TGF- β treated pericytes.	84
Figure 4.34	Treatment with cinnamaldehyde did not affect the expression of periostin by IL-13 treated pericytes	85
Figure 4.35	Treatment with cinnamaldehyde did not affect the expression of periostin by periostin treated pericytes	86
Figure 4.36	Treatment with cinnamaldehyde significantly increased the expression of N-cadherin in pericytes treated with TGF- β	87
Figure 4.37	Treatment with cinnamaldehyde did not affect the expression of N-cadherin by IL-13 treated pericytes	88
Figure 4.38	Treatment with cinnamaldehyde decreased the expression of N-cadherin in pericytes treated with periostin	78
Figure 4.39	Hypothesised mechanism of periostin, how it contributes to migration and is inhibited by cinnamaldehyde	91
Figure 5.1	Methods for spheroid and organoid formation	99
Figure 5.2	Various characteristics of spheroids can be observed using DAPI staining	101
Figure 5.3	There was no difference in the length of the spheroids following VEGF or H ₂ O ₂ treatment	102
Figure 5.4	Spheroids treated with H ₂ O ₂ had a more consistent area than VEGF or untreated spheroids	103

Figure 5.5	The density of VEGF treated spheroids had a more variable density than the other treatments.	105
Figure 5.6	Spheroids can have varying levels of structural integrity and may break apart even in the absence of treatment	106
Figure 5.7	VEGF treated spheroids showed a greater expression of N-cadherin	107
Figure 5.8	VEGF treated spheroids showed a greater expression of SM22	109
Figure 5.9	VEGF treated spheroids showed a greater expression of CD31	110
Figure 5.10	Following all treatments SM22 was the stain with the highest expression, with VEGF treatment resulting in the highest expression overall	111
Figure 5.11	Untreated and TGF- β treated spheroids contained areas with reduced cell densities	112
Figure 5.12	Many treatments resulted in a reduced cell mass in the core of the spheroids as well as irregularities around the outside of the spheroids	113/114
Figure 5.13	There is great variation in staining intensities within treatment groups	115
Figure 5.14	3D spheroids can be represented in various ways such as maximum projections, 3D representation videos or as a GIF scanning through individual images in the Z-stack	117
Figure 5.15	Images of spheroids and growth plates before and after mounting showing rings of cells that are left in the wells after spheroid removal	118
Figure 6.1	The dosing schedule used in the HDM model	127
Figure 6.2	HDM treated mice had more immune cells present in their bronchoalveolar lavage fluid than PBS treated mice	128
Figure 6.3	HDM treated mice had a lower percentage of macrophages present in their bronchoalveolar lavage fluid than PBS treated mice	129
Figure 6.4	HDM treated mice had a higher percentage of eosinophils present in their bronchoalveolar lavage fluid than PBS treated mice	130
Figure 6.5	HDM treated mice had a higher percentage of neutrophils present in their bronchoalveolar lavage fluid than PBS treated mice	131
Figure 6.6	Mice treated with HDM had higher symptom scores than PBS mice, with those given LIT-927 having significantly lower scores than those given just the vehicle	132

Figure 6.7	Mice treated with HDM had higher symptom scores than PBS mice, with those given LIT-927 having significantly lower scores following intervention at week 3.	133
Figure 6.8	Pericytes were observed uncoupling from the vasculature more in the mice just exposed to HDM than those exposed to HDM and treated with LIT-927	134
Figure 6.9	More pericytes had uncoupled in HDM only tracheas than the control tracheas and those given HDM and LIT-927	135
Figure 6.10	Both conditions exposed to HDM had more CXCR4+ pericytes within their lungs than either control condition	136
Figure 6.11	HDM-exposed lungs had a thick and continuous layer of smooth muscle around the airways, which was interrupted following treatment with LIT-927	137
Figure 6.12	HDM-exposed lungs had a thick and continuous layer of smooth muscle around the airways, which was thinner following treatment with LIT-927	138
Figure 6.13	The amount of α -SMA stain was greater in lungs exposed to only HDM compared to controls and the lungs given HDM and LIT-927	139
Figure 6.14	Hypothesis on the effect of HDM and LIT-927 treatment in the different conditions tested	140
Figure 7.1	Outcomes of this thesis	159
Supplementary Figure 8.1	QR code linking to 3D representation of untreated spheroid	196
Supplementary Figure 8.2	QR code linking to 3D representation of TGF- β treated spheroid	197
Supplementary Figure 8.3	QR code linking to 3D representation of periostin treated spheroid	198
Supplementary Figure 8.4	QR code linking to video of individual stacks of an untreated spheroid	199
Supplementary Figure 8.5	QR code linking to video of individual stacks of a TGF- β treated spheroid	100
Supplementary Figure 8.6	QR code linking to video of individual stacks of a periostin treated spheroid	201
Supplementary Figure 8.7	Manufacturers protocol for the human periostin ELISA DueSet by R&D Systems	202

Chapter 1 - Introduction

Pericytes are a relatively recently characterised cell type that are considered to be a type of tissue-resident mesenchymal stem cell (MSC) (Wong et al., 2015). In many ways, pericytes are similar to the more well-known bone marrow-resident MSC, but there are some differences in the range of function of these cell types. It has been shown that alterations to pericyte function may be a contributing factor to allergic asthma through the induction of structural changes (fibrosis) that have a negative impact on lung function. The symptoms of various fibrotic lung diseases, such as chronic obstructive pulmonary disorder (COPD), idiopathic pulmonary fibrosis (IPF) and asthma, have been attributed to the recruitment of pericytes areas of immune cell infiltration. While fibrosis in these conditions can be triggered by multiple different factors, there are many consistencies in the downstream mechanisms that lead to fibrosis (Liu et. al., 2021). Crucially, pericyte recruitment to sites of inflammation has been observed in a wide range of fibrotic diseases of the liver, kidneys, and heart (Mederacke et al., 2013, Shaw et al., 2018, Ytrehus et al., 2018). Based on our partial understanding of the mechanisms driving pericyte recruitment into fibrotic foci, it is hypothesised that pericyte migration into sites of inflammation is a key event in the development of tissue fibrosis (Hung et al., 2013).

1.1 Asthma

One of the most common conditions in modern society and the most common lung disease, asthma is defined as chronic inflammation of the lungs and airways, particularly after exposure to certain allergens (Janson, 1998). Over 5.4 million people in the UK alone are suffering from asthma according to AsthmaUK.org, with around 1,500 people dying from asthma attacks a year. This number is steadily escalating, having increased by 33% between 2008 and 2018 in the UK (Iacobucci, 2019). This costs the NHS (National Health Service) around £1 billion a year on asthma care alone (AsthmaUK, 2019). Asthma is thought to be induced by aeroallergen exposure and exacerbated through excessive inflammatory responses driven by the immune system (Johnson et al., 2004, Barnes, 2008b). It has been studied extensively using both in vitro and in vivo methods, leading to the development of various forms of treatment. Despite the range of treatment options available including bronchodilators and corticosteroids, asthma is still yet to be cured and remains a chronic disease. However, an exploration of the key role of pericytes in asthma may yield promising results in the search for a cure.

1.1.2 The Immune Response in Asthma

It is well documented that in allergic asthma, the immune response is triggered by the release of IgE molecules resulting from a hypersensitivity response to the allergen (Eseribese et al., 2015). Immune cells such as eosinophils and mast cells contribute to the increased inflammation that is characteristic of the disease (Jatakanon et al., 1999). Eosinophils are recruited by IL(interleukin)-5 releasing Th2 cells as well as epithelial cells which release IL-25, IL-33 and GM-CSF (granulocyte macrophage colony-stimulating factor). Epithelial cells can recruit dendritic cells, which further coordinate both the innate and adaptive immune responses through the release of cytokines such as IL-4, IL-12 and IFN- γ (interferon gamma). NK (natural killer) cells are also recruited, which increase proinflammatory signals including IFN- γ , IL-4, IL-5 and IL-13 as well as TNF- α (tumour necrosis factor) (Eseribese et al., 2015). It is thought that Th2 cytokines such are released in milder cases of asthma whilst Th1 and Th17 cytokines are mostly seen in severe asthma (Al-Muhsen et al., 2011). This has also been corroborated using long-term mouse studies showing that mice skew towards a neutrophil dominant Th17 response to asthma after around 10 days of HDM (house dust mite) treatment (Johnson et al., 2011). The Th2 response is traditionally associated with the reaction to allergens. The differentiation of Th0 cells to Th2 cells is driven by IL-4, which increases the production of IgE and initiates the immune response. Hypersecretion of mucus along with airway hyperresponsiveness, which are widely associated with asthma, are likely triggered by IL-13 during the Th2 response (Caminati et al., 2018). These all work to exacerbate inflammation and can overall lead to structural changes (Barnes, 2008a). These structural changes, including airway smooth muscle thickening and fibrotic stiffening of the airway wall, contribute to the well-known symptoms of asthma, i.e. wheezing and dyspnoea (Barnes, 2008b).

Despite it being a highly prevalent condition, and one which is largely understood at a molecular basis, the structural changes characteristic of allergic asthma remain intractable to currently available therapeutics, highlighting a significant research gap. One of the most useful methods in the study of asthma is the use of animal models. However, as asthma is a complex disease, it has proven difficult to develop a completely effective animal model for research. Each model therefore focuses on different aspects of asthma. The bleomycin-induced murine model is also often used to model other fibrotic lung conditions such as idiopathic pulmonary fibrosis. However, this model does not truly mimic the conditions observed in allergic asthma as it does not trigger a Th2-polarised, allergen-specific immune response (Chaudhary et al., 2006). Previously, the most commonly used allergen in the study of asthma was ovalbumin. This is likely due to its cheap price as it can be easily mass produced from chicken eggs. Although it is able to induce inflammation in species such as mice and rats, providing a suitable adjuvant such as aluminium hydroxide is used, ovalbumin exposure does not trigger asthma in humans. Moreover, mice eventually develop inhalation tolerance to

ovalbumin (Swirski et al., 2004), rendering this model useless for the study of chronic pathology. Therefore, it is thought to be a less effective model as it cannot be directly related back to humans (Aun et al., 2017). A different, relatively newer animal model uses house dust mite (HDM) extract to induce an inflammatory response; over 80% of asthmatics are sensitive to HDM. It has been shown that exposure to HDM extract, in the absence of any additional stimulation, significantly induces a Th2-polarised immune response in mice. This was apparent through the increase of various inflammatory markers such as Th2-related cytokines, eosinophil infiltration in the lung, airway smooth muscle thickening, and collagen deposition (Johnson et al., 2004); crucially, inhalation tolerance does not occur in this model. This clinically relevant response is useful to study the long-term physiological changes that occur in asthma, such as airway hyperresponsiveness and specific aspects of tissue remodelling.

1.1.2 Airway Remodelling

Airway remodelling is a term used to describe four key changes in lung physiology, particularly of the airway walls, that are associated with allergic asthma (Figure 1). One of the most well-known aspects is the overproduction of mucus or mucus gland hyperplasia (Boulet, 2017). Within the airway epithelium, secretory cells known as goblet cells secrete mucus into the lumen of the airway in order to protect the epithelium and trap pathogens. This is normally removed quickly by the ciliated cells of the airway epithelium. However, in asthma, the increased amount of mucus is not removed effectively and can even lead to death, with mucosal-derived asphyxia being the most common cause of asthma-related death (Bonser and Erle, 2017). Asphyxia can also occur when the airway smooth muscle surrounding the airways thickens and contracts.

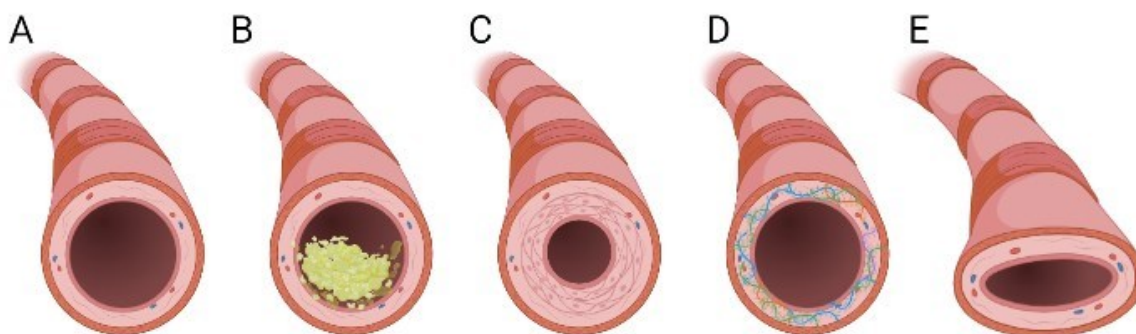


Figure 1.1 – Diagram depicting the four aspects of airway remodelling seen in asthma. Any combination of these physiological changes may be seen in each case, often with many of them interacting and contributing to the pathogenesis of the disease. It shows the cross section of an airway with the airway wall in pink and the lumen in the centre of each airway. A healthy airway has a large unobstructed lumen and relatively thin wall (A) whilst in diseased airways, the lumen space can be reduced by the failure to remove mucus (B) as well as the recruitment of vascular smooth muscle cells to the airway wall (C). Fibrosis and myofibroblasts also play a large role, causing the increased deposition of ECM (extracellular matrix) proteins (D) and the constriction of airway smooth muscle (E), thus reducing airflow. Adapted from (James and Wenzel, 2007).

The thickening of airway smooth muscle occurs due to the increased proliferation of smooth muscle cells as well as the overall size and contractility of the cells (Jones et al., 2016). An essential part of the thickening of the airway is the increased rate of angiogenesis through exuberant VEGF (vascular endothelial growth factor) production (Tatari et al., 2019). This prevents the death of cells within the inflamed tissue and allows the continued thickening of the airway wall. Studies have suggested that a combination of growth factors and other cytokines work in tandem to produce these new blood vessels. Vascular endothelial growth factor (VEGF) and various angiopoietins produced from endothelial cells initiate the vascular formation by recruiting fibroblasts and vascular smooth muscle cells, whilst transforming growth factor-beta (TGF- β) is released during vessel maturation and encourages the deposition of extracellular matrix (ECM) proteins as well as preventing endothelial cell proliferation (Alagappan et al., 2013). Other studies, however, have identified other factors that may be involved, such as FGF (fibroblast growth factor), TNF- α , and IL-8 (Walters et al., 2008). The fibroblasts and vascular smooth muscle cells recruited during both angiogenesis and airway thickening may also pose an additional problem. Both cell types are able to deposit large amounts of ECM proteins such as collagen, particularly in response to TGF- β . This can cause the formation of scar tissue (fibrosis) around the airways and constriction of the airway, as well as reducing the size of the airway lumen, thus reducing airflow (O'Dwyer and Moore, 2017).

Myofibroblasts are one of the key cell types that are involved in wound healing where they produce and arrange extracellular matrix (Hinze, 2016). Therefore, dysregulated myofibroblasts greatly

contribute to many forms of fibrosis including asthma as they are responsible for much of the increased deposition of ECM proteins and airway thickening. However, the source of these myofibroblasts is hotly debated. It has been established that myofibroblasts are not resident in tissue and instead differentiate from other cell types in response to injury causing a change in the cell environment such as increased levels of TGF- β and increased extracellular strain often caused by the extracellular matrix. Previous studies using cell lineage tracing strategies have investigated the hypothesis that the progenitors of myofibroblasts are varied, including fibroblasts, epithelial or endothelial cells as well as fibrocytes from the bone marrow (Hinz et al., 2007, Johnson et al., 2011, Mederacke et al., 2013). This is often referred to as EMT, or epithelial to mesenchymal transition. EMT has been shown to occur in several biological contexts, each with their own distinct functions which have been categorised into 3 types. Type 1 refers to developmental EMT which occurs during organ formation and is most useful for transplantation as they do not result in fibrosis (Thiery et al., 2009). Type 2, on the other hand, is activated by fibrosis and inflammation and is useful in wound healing responses. However, this response can be prolonged and eventually lead to the death of the organ (Marconi et al., 2021). Type 3 EMT occurs in cells that have undergone mutations, such as cancerous cells, thus increasing their ability to metastasize and spread the cancer to other organs (Smith & Bhowmich, 2016, Kalluri & Weinberg, 2009). However, taken together, these cell types appear to make relatively minor contributions to the development of airway remodelling. Recently, Johnson et al. demonstrated that pericytes are a major source of myofibroblasts and contribute to airway remodelling in allergic airway disease (shown in Figure 1.2) (Johnson et al., 2015).

1.2 Pericytes

Pericytes were first characterised by Charles Rouget in 1873, and are therefore referred to as Rouget cells (van Dijk et al., 2015). They were then renamed pericytes by Dore in 1923 (Dore-Duffy and Cleary, 2011). However, pericytes are still rarely researched. This is likely due to the intrinsic difficulty in culturing cells with stem cell properties, in that they can freely differentiate in vitro. They are also incredibly heterogeneous both in vivo and in vitro. This causes difficulties in identifying the cell type in mixed cultures and when staining. The expression of markers by pericytes can also vary with species, the location of the vessel, or other local physiological conditions (Diaz-Flores et al., 2009). Therefore, it is suggested that multiple markers are used in tandem in order to ensure correct identification (van Dijk et al., 2015). The most common pericyte markers used are α -smooth muscle actin (α -SMA) and NG2 (neural/glial antigen 2), specifically for arteriolar and capillary pericytes, respectively (Diaz-Flores et al., 2009).

Pericytes are always found surrounding the endothelial cells that form blood vessels. They are embedded within the same basement membrane as endothelial cells, allowing them to be referred to as mural cells, much like vascular smooth muscle cells (Armulik et al., 2005). These cells can be found throughout the body; however, most studies have focused on pericytes in the kidney, lungs, and blood brain barrier. It has been suggested that the mesenchymal stem cell capacity of pericytes indicates that they may be precursor cells of myofibroblasts (Wong et al., 2015, Hung et al., 2013). This is due to their similar characteristics such as marker expression and ability to differentiate into osteoblasts, chondrocytes, and adipocytes under healthy conditions. MSC are a type of pluripotent stem cell which reside in the bone marrow throughout the body in adults. As with pericytes, MSC can differentiate into osteoblasts, chondroblasts, and adipocytes, with specific differentiation driven by a combination of different growth factors and other environmental cues (Izadpanah et al., 2006). This newly discovered and abundant tissue-resident stem cell niche may allow future therapies to be developed. However, considerable evidence demonstrates that pericytes can contribute to disease, as they can differentiate into scar-forming myofibroblasts during chronic inflammation, particularly in the lungs (Hung et al., 2013, Rowley and Johnson, 2014, Wong et al., 2015). Due to fate-mapping methods in a case of renal fibrosis, this transition contributes to fibrosis more than previously thought (Humphreys et al., 2010).

1.2.1 Pericyte Roles

As previously mentioned, due to their apparent heterogeneity, pericytes are able to fulfil a variety of roles depending on species and location within the body. They do this via the secretion of a mixture of growth factors and cytokines. The coverage of blood vessels by pericytes aids in their stabilisation by allowing the diameter of the vessel to be regulated. This improves resistance to high blood pressure and also contributes to the migration and proliferation of nearby cells during angiogenesis through the secretion of VEGF and Ang1 (Diaz-Flores et al., 2009). For this reason, there is often a higher concentration of pericytes found at blood vessel junctions (van Dijk et al., 2015). Pericytes also contribute to overall tissue homeostasis through the regulation of the permeability of the endothelium. This is mediated by nitric oxide, a potent vasodilator, and VEGF and is particularly important in the blood brain barrier. VEGF can induce the dissociation of pericytes from the endothelium, thus decreasing the area of endothelial cell that is covered and therefore increasing vessel permeability. It has also been observed that pericytes can display macrophage-like properties as well as interacting with macrophages themselves (Diaz-Flores et al., 2009).

Cultured pericytes are morphologically distinct from many other types of cell, although they do share several characteristics with fibroblasts. The culturing conditions for pericytes, however, are very specific and differ from that of fibroblasts, such as their requirement for a lower concentration

of foetal calf serum and glucose. Therefore, manufactured selective medium can be used in order to distinguish them from fibroblasts and endothelial cells in culture (Tigges et al., 2012). Pericytes exhibit fibroblast-like protrusions with a circular central cell body. Within the cell, the nucleus appears large whilst the mitochondria are small and electron dense (Diaz-Flores et al., 2009). Pericytes are also able to form adhesion plaques in order to embed into the subendothelium around blood vessels. These plaques contain high levels of fibronectin, highlighting their similarity to other fibroblastic cell types (Armulik et al., 2005). Pericytes are most commonly found surrounding small capillaries throughout the body, while vascular smooth muscle cells instead cover larger vessels (van Dijk et al., 2015). Pericytes often wrap around the entirety of the vessel, although they can exhibit a variety of wrapping patterns, resulting in 10-50% coverage of the endothelium (Armulik et al., 2005). These variations relate to the function of that particular pericyte; for example, during angiogenesis, pericytes tend to span the vessel longitudinally (Dore-Duffy and Cleary, 2011). It is thought that the coverage pattern of vessels by pericytes contributes to their differing roles as this can modulate cell function and physiological factors such as blood flow.

Pericytes are no longer thought to be just structural cells and are now known to interact in depth with their surrounding environment. For this reason, pericytes have shown to express a variety of different receptors for cytokines and growth factors. The receptor for TGF- β , TGF β R2 is expressed on both pericytes and endothelial cells, thus allowing crosstalk between these often-associated cell types (Armulik et al., 2011, Butsabong et al., 2021). As pericytes are known to aid in angiogenesis, it is not surprising that studies have shown that pericytes express a receptor for VEGF, VEGFR1 (Eilken et al., 2017). Less commonly, studies have also shown that pericytes likely express the EGFR receptor for EGF (epidermal growth factor), especially in tumour environments and that heparin-binding EGF-like growth factor may increase this expression (Nolan-Stevaux et al., 2010, Sun et al., 2021). One of the relatively newly discovered signalling pathways involving pericytes is the CXCL12/CXCR4 (C-X-C motif chemokine ligand 12/C-X-C chemokine receptor 4) pathway. Studies have shown that pericytes in the lung as well as in other locations such as around bones, express the α V β 3 receptor CXCR4 (Stephenson et al., 2020, Xu et al., 2020). This thesis will also explore this further in Chapter 6 and the accompanying research article (Bignold et al., 2022). Periostin, a matrikine explored further within this thesis, is thought to interact with several different receptors including α V β 5, and α 6 β 4 (Dorafshan, et al., 2022, Gonzalez-Gonzalez & Alonso, 2018). α V β 5 has been shown to be expressed by pericytes and has been implicated in increased vascular leakage in renal injury (McCurley et al., 2017). The other two integrins mentioned seem to be expressed on endothelial cells but their expression on pericytes has not been explored (Kemp et al., 2022).

1.2.2 Difficulties in Pericyte Research

There are many hurdles to overcome when carrying out research on pericytes. One of which is the characterisation and isolation of pericytes due to the inherent heterogeneity within the populations (Prazeres et al., 2017). The most common markers used for pericyte identification are PDGFR β (platelet-derived growth factor receptor beta) and NG2 as well as CD31 and CD45 which are negative in pericytes (Yuan et al., 2015, Wilson et al., 2018). However, PDGFR β is also present on bone marrow leukocytes, megakaryocytes, macrophages and T cells, and NG2 is expressed by glial cells (Demoulin & Montano-Almendras, 2012, Zhu et al., 2016). There are also several cell types that are very difficult to distinguish from pericytes, both due to their similar expression of markers and their co-localisation. One of these is fibroblasts which, along with pericytes, also express CD44, CD73, CD90, CD105 and PDGFR α as well as having similar morphological appearances (Barron et al., 2016, Hung et al., 2019). Another cell type which are often confused with pericytes are mesenchymal stem cells which are known to share the markers CD29, CD49a, CD47 and CD105 with pericytes (Garrison et al., 2023).

There are also differences in marker expression depending on the location of the pericytes. Much of the research performed involving pericytes is focused on pericytes found within the brain, however studies have hinted to the organotypicity of pericytes and therefore data based on pericytes in the brain may not be applicable to lung pericytes (Vanlandewijck et al., 2018). Pericytes also express different markers depending on the type of blood vessel they reside on and are affected by changes in disease states as well as differing culture conditions (Armulik et al., 2011). For examples, studies have shown that whilst pericytes residing around lung capillaries are negative for α -SMA, pericytes found on venules near alveolar septa are positive for α -SMA (Johnson et al., 2015, Kapanci et al., 1992). This highlights the difficulties of studying pericytes even within specific organs. These varying markers and expressions in pericytes results in an expansive and diverse pool of study designs which can lead to incorrect assumptions and inferences. Standardisation of markers would allow research to be more readily comparable and more robust conclusions drawn, thus forwarding the field of pericyte research.

Due to these variable markers, the isolation of pericytes is also a very challenging task. Studies have been able to isolate primary human and mouse pericytes from cardiac tissue using fluorescence activating cell sorting (FACS) and a panel of 6 markers (CD140b+NG2+CD146+CD31-CD34-CD45-), kidney tissue using flow cytometry and 4 markers (PDGFR β +NG2+CD45-PECAM-), bone marrow via microbead cell sorting and 3 markers (CD146+CD34-CD45-) and umbilical cord by explant outgrowth and magnetic sorting using 2 markers (NG2+CD31-) (Lee et al., 2019, Lemos et al., 2016, Mangialardi et al., 2019, Cathery et al., 2020). Lung pericytes have proven difficult to isolate due to the fibrous nature of the lung tissue leading to low yields of pericytes (Dore-Duffy & Esen, 2018). However,

studies have successfully isolated pericytes with markers such as PDGFR β , 3G5, NG2 and CD146 using methods involving magnetic bead sorting with and without the addition of FACS as well as cell-selective culture conditions (Wilson et al., 2018, Yuan et al., 2015, Yuan et al., 2020, Bagley et al., 2006, Meng et al., 2021, Yamaguchi et al., 2020). The range of methods and markers used once again highlights the need for an industry standard to be developed.

1.3 Pericytes and Chronic Inflammatory Disease

One of the most promising areas of research in asthma is into the role of pericytes in allergic airway inflammation. Pericytes have already been associated with other forms of inflammatory disease, in particular kidney fibrosis and liver fibrosis (Lin et al., 2008, Mederacke et al., 2013). It is thought that pericytes may encourage the recruitment of inflammatory cells, with the gaps between adjacent pericytes having a decreased expression of laminin, thus encouraging immune cell diapedesis (Kratzer et al., 2013). This can increase the population of leukocytes and therefore increase the inflammatory response. It has also been suggested that the secretion of VEGF and Ang2 by pericytes can be an indicator of the severity of the asthma as they contribute to angiogenesis and the overall stability of vessels (Kratzer et al., 2013).

Studies have observed increased migration of pericytes away from blood vessels in inflammation, resulting in a larger surface area of exposed endothelial cells in conditions such as asthma. This movement is thought to be induced by cytokines such as ICAM-1 (intercellular adhesion molecule 1) and LFA-1 (lymphocyte function-associated antigen 1), which are increased in inflamed tissue (Rowley and Johnson, 2014, Proebstl et al., 2012). These enlarged gaps between pericytes allow neutrophils to enter the tissue, thus increasing the immune response to the allergen and therefore exacerbating asthma (shown in Figure 1.2) (Proebstl et al., 2012).

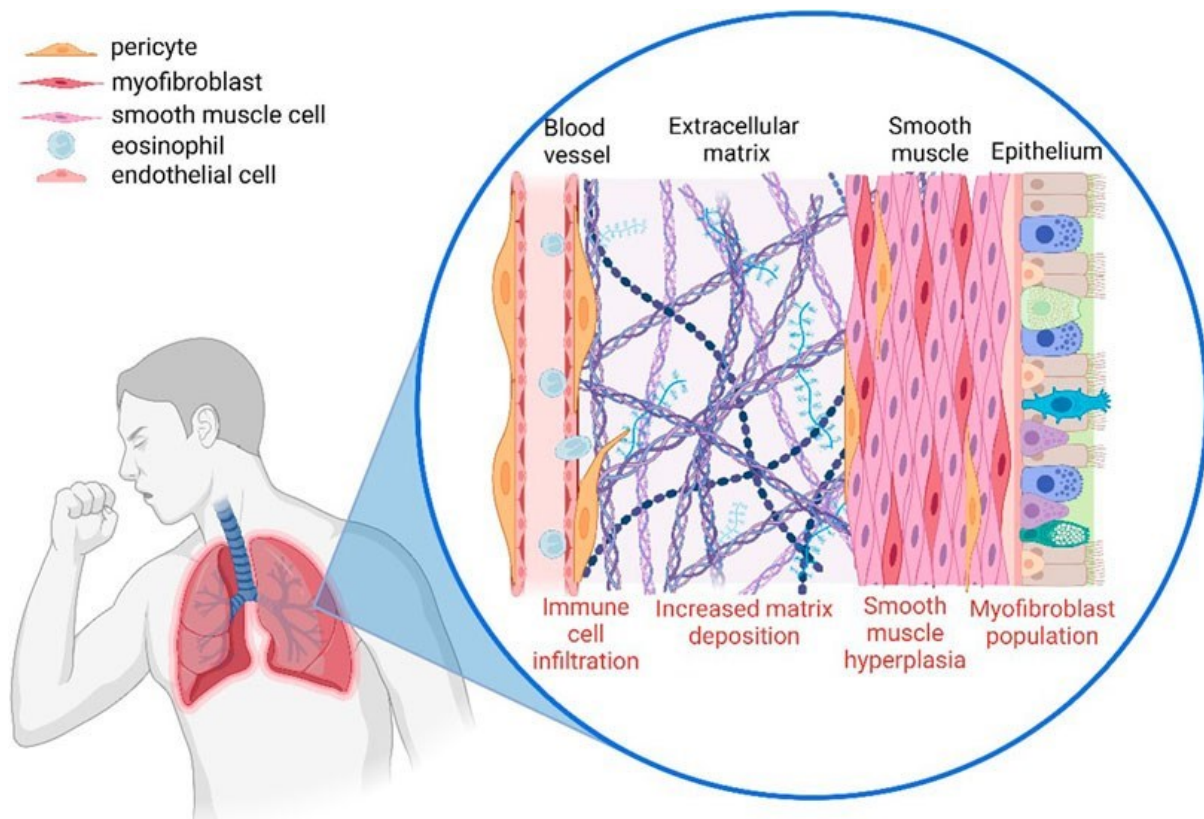


Figure 2.2 – The involvement of pericytes in the airway remodelling observed in asthmatic lungs. Pericytes modulate immune infiltration, detach from the blood vessel and migrate towards the site of inflammation where they increase deposition of extracellular matrix components, and also contribute to vascular leakage (Created with BioRender.com). Originally published in Garrison et al., 2023.

1.3.1 PDGF-BB (platelet derived growth factor)

Another important factor in the effect of pericytes on asthma is platelet-derived growth factor (PDGF)-BB/PDGFR- β signalling. The family of platelet-derived growth factors is involved in the regulation of mesenchymal cell types, including vascular smooth muscle cells and pericytes. It is known that this signalling pathway is involved in the attachment and subsequent disassociation of pericytes from endothelial cells. In conditions where PDGF-BB/ PDGFR β signalling is reduced, such as a defect in the maturation of the PDGF-BB precursor in the HDM model (Johnson et al., 2015), the interactions between pericytes and endothelial cells are decreased and pericytes dissociate from the vessels (Johnson et al., 2015). This study also tested multiple aspects of allergic asthma, such as airway hyperreactivity and airway resistance, both of which were increased in house dust mite (HDM) treated mice when PDGFR β was blocked and pericyte uncoupling was enhanced. Johnson et al. also showed, using lineage tracing, the accumulation of pericytes within the airway walls of HDM-exposed mice. This indicates that pericytes make a significant contribution to airway wall remodelling. Reduced PDGFR β activity was also observed in HDM mice, suggesting that the artificial modification of PDGF-BB/PDGFR β signalling may be a useful tool in the treatment of asthma,

although more research must be performed to fully understand the pathways involved (Johnson et al., 2015).

1.3.2 Periostin

A relatively new area of research has emerged that ties in the interaction of the immune response and growth factor release on pericytes in asthma. Periostin, which was originally referred to as osteoblast-specific factor 2, is a matricellular protein which is a component of the extracellular matrix that is not involved with maintaining the cellular structure (O'Dwyer and Moore, 2017). Its exact function is still contested but is likely to involve the modulation of some cellular processes. It is widely accepted that an increase in periostin can be linked to asthma, with several studies observing that asthmatic patients had high serum periostin levels as well as an increase (3.7-fold) in periostin expression in bronchial cells (Caminati et al., 2018, Lopez-Guisa et al., 2012). Studies have also shown that periostin affects the inflammation observed in asthma and therefore contributes to airway remodelling (Bentley et al., 2014, Li et al., 2015). The exact origin of periostin is currently unknown; however, many studies suggest that it is produced in response to IL-4 and IL-13, two cytokines that are typical in the Th2 immune response and that are upregulated in asthma. Yokota et al. state that periostin can bind to $\alpha v\beta 1$, $\alpha v\beta 3$, and $\alpha v\beta 5$ receptors on macrophages (Yokota et al., 2017). This interaction may facilitate macrophage recruitment (Zhou et al., 2015). Periostin also closely modulates the effect of TGF- β . Both of these molecules are able to affect the other, in a positive feedback loop, allowing the production of TGF- β and the resulting inflammation to become dysregulated. Ashley et al. demonstrated that treatment of TGF- β and periostin increases the production of the other (Ashley et al., 2017), while Naik et al. found that treating lung mesenchymal cells with TGF- β tripled periostin production (Naik et al., 2012). Periostin also increases TGF- β production and further dysregulation of TGF- β release by inhibiting Smad7, a protein which acts as a regulator for TGF- β production, thus inducing the uncontrolled production and release of TGF- β (Kanaoka et al., 2018). One of the ways in which TGF- β contributes to airway remodelling and inflammation is by promoting epithelial-to-mesenchymal transition (EMT), which Hu et al. concluded is mediated by periostin (Hu et al., 2015). How periostin interacts with pericytes is widely debated. Although some studies suggest that pericytes produce periostin, other studies suggest that it comes from fibrocytes and bronchial smooth muscle cells (Chen et al., 2018b, Nakama et al., 2017, Ashley et al., 2017, Makita et al., 2018). However, as with many of the studies focusing on the origin of periostin, they fail to rule out the possibility that pericytes may be involved by using inefficient markers and cell isolation techniques. Many studies also suggest that periostin is involved in the migration and proliferation of pericytes, although the exact mechanisms behind this interaction are yet to be explained (Jackson-Boeters et al., 2009, Chen et al., 2018b, Yokota et al., 2017). This

protein seems to link pericytes and TGF- β with the Th2 response and airway remodelling observed in asthma, yet the mechanistic details of these interactions have not been elucidated. This area of research is promising and highlights possible drug targets that may have a holistic effect on airway remodelling.

1.4 Study Aims

The hypothesis of this thesis is that the factors affecting pericyte migration within allergic asthma can be targeted and negated resulting in a reduction of pericyte migration in vitro and airway remodelling in vivo. This study aims to explore the effect of various growth factors, cytokines and matrikines on the migration of pericytes with the view to inhibit this migration in vitro and abrogate airway remodelling in an in vivo model of allergic asthma.

To do this, the factors that may contribute to pericyte migration (such as growth factors, cytokine and matrikines) were investigated using two forms of migration assay: Transwell and scratch assays. Two of these factors, periostin and CXCL12, were selected to investigate in further chapters. The relationship between periostin and pericytes was analysed via further scratch assays so demonstrate migration, immunostaining to check for expression of periostin both in cultured pericytes and in lung tissue, and ELISA (enzyme linked immunosorbent assay) to investigate the secretion of periostin. An IL-13 inhibitor, cinnamaldehyde, was also investigated as a possible route to reduce the effect of periostin. This was shown via ELISA and scratch assay. An alternative to traditional, 2D culture methods was also explored as a better way to model blood vessels. This was attempted via magnetic levitation of pericytes and endothelial cells using iron nanoparticles. The effectiveness of this was assessed through several rounds of immunostaining. Finally, the CXCL12/CXCR4 gradient was targeted in vivo via the use of a novel neutraligand administered to mice undergoing the HDM model of asthma. Symptoms were monitored during the administration of the HDM and lung tissue and bronchoalveolar lavage fluid was collected for investigation via immunostaining, flow cytometry and differential cell counts.

Chapter 2 - Materials and Methods

2.1 Cell Culture

HPLPCs (human placental pericytes cells) from Promocell (Germany) were cultured for use in experimentation. This cell line was used as they are currently the only non-brain or retinal derived pericyte cell line commercially available. Initial investigations have shown that human placental and pulmonary pericytes express similar cell surface markers and consistent morphological characteristics (although this has not been published). Due to the pandemic, primary lung tissue was scarcely available, and I did not have the ethical approval nor the facilities to work with primary human tissue. The cells were received from Promocell at passage 2 and cultured until passage 10 in a 1:3 seeding density as beyond this they began to display an altered phenotype. All experiments were performed on cells between passage 6 and 10. All pericytes were cultured in specific pericyte growth medium (Promocell, Germany) and split using trypsin-EDTA (Ethylenediaminetetraacetic acid) (Sigma-Aldrich Ltd., Missouri, USA). HUVECs (human umbilical vein endothelial cells) from Promocell (Germany) were cultured in EGM medium (Lonza, Switzerland) and split similarly to HPLPCs. A549 human epithelial cells (Sigma/Merck, Germany) were cultured in DMEM (Dulbecco's Modified Eagle Medium) containing high glucose without pyruvate (Lonza, Basel, Switzerland) and split similarly to the other cell lines. Cells were cultured in well plates coated in a gelatine mixture of autoclaved distilled water with 5% gelatine (Sigma-Aldrich Ltd., Missouri, USA). This was done to ensure rapid attachment of the cell monolayer. THP-1 monocytes were kindly provided by Prof A. Devitt (Aston University). They were maintained in uncoated T25 flasks in RPMI medium (Roswell Park Memorial Institute) (Lonza, Basel, Switzerland) with 10% FCS (foetal calf serum). They were transformed into unpolarised macrophages through a treatment of vitamin D₃, also obtained from Prof Devitt. In order to kill the macrophages to perform certain assays, cells were exposed to UV (ultraviolet) light for 10 minutes to initiate apoptosis.

2.2 Growth Factor Treatment

Various recombinant growth factors and cytokines were used to treat HPLPCs throughout these experiments. Table 1 contains an overview of the concentration used for each growth factor. These were added to the growth medium every 48 hours until the stated treatment course was complete.

Table 2.1 - Growth factors and cytokines used and their general working concentrations

Growth Factor/Cytokine	Concentration	Manufacturer
TGF- β	10 ng/ml	R&D Systems, Minneapolis, USA
EGF	10 ng/ml	Biolegend, California, USA
VEGF	10 ng/ml	Biolegend, California, USA
Periostin	100 ng/ml	Biolegend, California, USA
PDGF- β	300 ng/ml	Biolegend, California, USA
CXCL12	500ng/ml	Biolegend, California, USA
IL-13	100 ng/ml	Biolegend, California, USA
Cinnamaldehyde	1mM / 132mg/ml	Sigma-Aldrich, Missouri, USA
H ₂ O ₂	50 ng/ml	Biolegend, California, USA
TNF- α	10 ng/ml	Biolegend, California, USA

2.3 Transwell Assays

Cells were treated with various growth factors at varying concentrations and timescales as stated in the individual figure legends. Post treatment, medium was added to three columns in a 24 well plate, one containing DMEM (Dulbecco modified eagle medium) without serum (Lonza, Basel, Switzerland), one with DMEM with added 10% heat treated FCS (foetal calf serum) (Gibco/Thermo Fischer Scientific, Massachusetts, USA), and DMEM without serum with added 300 ng/ml of PDGF-B (BioLegend, California, USA). 500ng/ml CXCL12 (Biolegend, California, USA) and cultured macrophages (1 million cell/ml) were also used as attractants. One Transwell insert with 8 μ m pores (Merck, Germany) was placed in each well before 100 μ l of a pericyte cell suspension at 2×10^5 cells/ml in DMEM without serum was added into each insert. The plate was then incubated for 24 hours at 37°C in 5% O₂ atmosphere. The medium was then removed from the insert and the inner membrane swabbed carefully to remove cells that had not migrated. The cells were then fixed in cold 100% EtOH (CEAC, Aston University) for 10 minutes. After fixing, the membranes were cut from the insert, dipped in ddH₂O, and mounted onto a slide for imaging. Fluoroshield mounting medium with DAPI (Diamindino-2-phenylindole) (Sigma-Aldrich Ltd., St. Louis, USA) was used to stain cell nuclei by adding several drops to each membrane. The slides were visualised under UV light at 100x magnification using a fluorescence microscope and then cell counts were analysed using ImageJ software.

2.4 Scratch Assays

HPLPCs were cultured until between passage 6–10 in pericyte-specific medium (Promocell) with 1% antibiotic/antimycotic (ThermoFisher, Massachusetts, USA). Once a monolayer of pericytes was formed they were treated with the growth factor stated in the individual figure legends. Following treatment, a p200 pipette tip was used to scratch the monolayer and form a wound once in each well. The cells were then washed with PBS (phosphate buffered saline) and transferred to serum-free low-glucose Dulbecco's Modified Eagle's Medium (DMEM; Sigma-Aldrich) with 1% antibiotic/antimycotic (Sigma-Aldrich) in order to arrest cell proliferation. Images of each scratch were taken at 100x before and after 24 h of incubation at 37°C and 5% CO₂. The area of each scratch was calculated with ImageJ and the difference between the areas before and after the incubation were used to calculate the distance that was migrated in pixels².

2.5 ELISA

Anti-periostin ELISAs (R&D Systems, Minnesota, US) were performed on supernatant harvested from cultured HPLPCs treated the various cytokines mentioned previously or supernatant from polarised macrophages (obtained from colleagues) and on bronchoalveolar lavage fluid harvested from HDM treated (and control) mice prepared as described in sections 2.7 and 2.8. All ELISAs were performed as per the manufacturer's instructions (Supplementary Figure 9.7).

2.6 3D cultures

Pericyte and endothelial cell cultures were prepared in a 1:5 ratio at 2.5×10^6 cells in 1ml of pericyte medium and endothelial cell medium (1:1 ratio). Then, 1 μ l of Nanoshuttle (Greiner Bio-One Ltd., Austria) solution was added per 10,000 cells used before centrifuging and resuspending three times at 100 *g* for 5 minutes each time, which allowed the Nanoshuttle particles to incorporate into the cells. After the last centrifugation, the pellet was resuspended in a mix of 5 ml of pericyte medium and 5 ml of endothelial cell medium; 100 μ l of this suspension was added to each well of a 96-well plate before topping up each well with an extra 150 μ l of medium (1:1 pericyte/endothelial cell media). A magnet array plate holder was used to levitate the cells allowing the spheroids to form. Cells were maintained for 5 days before they were treated with the relevant growth factors. Following the required length of treatment, spheroids were washed three times with PBS and fixed with 4% paraformaldehyde. They were incubated at room temperature for 15 minutes and then immunostained using the techniques which will be described.

2.7 In vivo house dust mite model

All animal procedures were carried out in strict accordance with the approved protocol and recommendations for proper use and care of laboratory animals (Animals (Scientific Procedures) Act

1986). All experiments on animals were conducted according to United Kingdom Home Office regulations (project license P75A73BEB held by the Principle Investigator) and animal handling was performed by qualified personnel. All studies were performed and reported according to the revised ARRIVE guidelines (du Sert et al., 2020).

Thirty female C57Bl/6 mice (6-8 weeks old) were purchased from Charles River and housed at the Aston University central animal facility under specific pathogen-free conditions. The mice were provided with food and water and exposed to a 12-hour light-dark cycle. All mice were handled in compliance with UK Home Office regulations on animal care and welfare (Animals (Scientific Procedures) Act 1986). Allergic airway disease was induced using a previously described protocol (Johnson et al., 2004). In brief, on five days per week over the course of five consecutive weeks, mice were anesthetized with isoflurane (Sigma-Aldrich, Missouri, USA) before being challenged with house dust mite allergen (HDM). HDM extract (Citeq, The Netherlands) was suspended in sterile phosphate buffered saline (PBS) at a final concentration of 2.5 mg/ml. Ten microlitres of the solution was administered intranasally; control mice received 10 μ l of sterile PBS using the same protocol. LIT-927 was obtained from Axon Medchem (Groningen, The Netherlands) and was diluted to 197 ng/ml in methyl- β -cyclodextrin (Sigma, Missouri, USA) 10% w/v and delivered intranasally (10 μ l) immediately before allergen exposure.

2.8 Sample collection

All mice were euthanised humanely using a pentobarbital overdose administered intraperitoneally. Different samples were then collected from individual mice for separate analyses. Bronchoalveolar lavage fluid was harvested for immune cell counts. Procedures requiring materials from mice included lung section immunostaining, flow cytometry and cell culture. The lungs were surgically removed and processed for immunostaining as described below. Whole lungs were taken and digested for analysis via flow cytometry.

2.9 Preparation of single cell suspension from mouse lung

Bilateral thoracotomy was performed to expose the pleural cavity. A small incision was made in the left ventricle, and 10 ml ice cold PBS was flushed through the circulatory system via the right ventricle using a 21G needle and 10 ml syringe. The lungs were removed and placed in an Eppendorf tube with 0.5 ml DMEM pen/strep (1%). Lungs were finely minced with scissors, and 0.5 ml DMEM pen/strep with 0.195WU/ml Liberase™ thermolysin (Roche Diagnostics, Switzerland) and DNase I (Sigma-Aldrich, Missouri, USA) added before incubating at 37°C for 45 min.

Reaction was terminated using 1ml FBS with EDTA (5 mM), and samples were kept on ice hereafter. Digested tissue was mechanically dissociated by pulping through a 100 µm cell strainer (Miltenyi, Germany) using a syringe plunger, washed twice in RPMI buffer (RPMI, pen/strep, HEPES (25mM), EDTA (5mM) and FBS (10%), 1200 rpm, 4°C, 6 min) before filtering through a 70 µm filter (Miltenyi, Germany) to create a single cell suspension.

2.10 Staining of lung cells for flow cytometry

Cells were diluted to 10-50 x 10⁶ cells/ml in staining buffer (PBS, 10% FBS, EDTA (5mM), and Fc receptor blocked with anti-CD26/32 (1:100, Biolegend, California, USA) for 10 min on ice. Cells were aliquoted into 100 µl/well V-bottomed 96-well plates (Corning, New York, USA), centrifuged (1200rpm, 5 min, 4°C), and resuspended in staining buffer containing antibodies pre-conjugated to fluorophores (see Table 2.2) for 30 mins ice in the dark. Cells were washed twice to remove unbound antibody before fixing in 100 µl/well IC fixation buffer (eBioscience, California, USA) for 20 min ice in the dark, washing, and re-suspending in 200 µl PBS. Stained samples were stored at 4°C, in the dark.

Table 2.2 – Antibodies used in flow cytometry experiments

Antibody	Target	Fluorophore	Host	Concentration	Manufacturer
CD31	Endothelial cells	PerCp-Cy5.5	Rat	1:80	Biolegend, California, USA
CD45	Pan-leukocytes	PerCP-Cy5.5	Rat	1:80	Biolegend, California, USA
Ter119	Erythrocytes	PerCP-Cy5.5	Rat	1:80	Biolegend, California, USA
CD146	Pericytes	PE-Cy7	Rat	1:80	Biolegend, California, USA
PDGFRβ	Pericytes	APC	Rat	1:20	Biolegend California, USA
CXCR4	Marker of interest	PE	Mouse	1:40	Biolegend, California, USA

2.11 Flow cytometry

Single colour compensation controls using VersaComp antibody capture beads (Beckman Coulter, California, USA) and Fluorescence Minus One (FMO) controls were prepared at time of staining following the same protocol. Stained controls were stored at 4°C in the dark. All flow cytometry analyses were performed on a Cytoflex flow cytometer equipped with 405 nm, 488 nm (530/30 – FITC/AF488, 695/40 – PerCp-Cy5.5), 561nm (585/15 – PE, 780/60 – PE-Cy7) and 640 nm (670/14 – APC) lasers and filters. Data were analysed using FlowJo (Treestar, Oregon, USA) software. Cells were first selected using forward scatter and side scatter and doublets were removed. Cells that were positive for Ter119, CD45 and CD31 were then excluded and the cells that were positive for both CD146 and PDGFRβ were selected. The expression of CXCR4 in those cells was then assessed.

2.12 Fluorescence imaging

Immunostaining was performed on cultured human pericytes (HPLPC) and the large airways (tracheobronchial wholemounts) and lung tissue from mice.

HPLPC were cultured as previously described on coverslips coated in 2% gelatine. Upon completion of the desired experiment, medium was removed, and cells were fixed with cold 100% ethanol for 10 minutes. Cells were then washed with PBS and blocked with 5% NGS (normal goat serum; Sigma-Aldrich, Missouri, USA) in 0.3% Triton-X-100/PBS for 60 minutes. The primary antibodies (shown in Table 2) selected for that experiment were then added and incubated at room temperature for 60 minutes before being removed and washed again with PBS. The secondary antibodies (all from Invitrogen) corresponding to the primaries used were then added at 1:500 and incubated for 60 minutes. All antibodies were diluted in 0.3% Triton-X-100/PBS. Following this, the antibodies were removed, and the coverslips were washed with PBS before being mounted with Fluoroshield (Sigma-Aldrich, Missouri, USA) mounting medium containing DAPI.

Table 3 - Primary antibodies used in immunofluorescent staining

Antibody	Host	Concentration	Manufacturer
PDGFR β	Rat/Mouse	1:200	Abcam, UK
Periostin	Rabbit	1:200	Abcam, UK
CD146	Mouse	1:200	Biolegend, California, USA
N-cadherin	Rat	1:200	Abcam, UK
SM22	Rabbit	1:200	Abcam, UK
CD31	Hamster	1:500	Abcam, UK
Isolectin	From <i>Griffonia simplicifolia</i> (directly conjugated with AlexaFluor™ 488)	1:200	ThermoFisher, Massachusetts, USA
α -SMA	Mouse (directly conjugated with Cy3)	1:1000	Sigma-Aldrich, Missouri, USA
NG2	Rabbit	1:250	Millipore, Germany

Whole lungs and tracheas were taken from the mice and stored in sucrose solution to cryopreserve the sample. Sucrose was rinsed off using PBS. The large airways (trachea and bronchi prepared and stained as a whole mount) were cleaned of extraneous tissue and pinned down onto Sylgard-coated plates (Sigma-Aldrich, Missouri, USA). Whole lungs were embedded in TissueTek OCT (Sakura

Finetech, UK) and frozen at -80°C . Sections ($10\ \mu\text{m}$) were then cut using a cryostat (Leica, Germany) and mounted on Superfrost Plus slides (Fisher Scientific, UK). The slides were stored at -80°C . Prior to staining, slides were warmed to room temperature. A hydrophobic marker was used to outline the tissue sections before they were blocked with 5% NGS in 0.3% Triton-X-100/PBS for 2 h. After this, the blocking solution was washed off with PBS and the slides were incubated overnight at room temperature with primary antibodies against periostin raised in rabbit (Abcam), α -SMA raised in mouse (Abcam, UK), or CD31 raised in Armenian hamster (Biolegend, California, USA). Following incubation, the primary antibody was washed off with PBS containing 0.3% Triton-X, and the secondary antibody (AlexaFluor488 goat anti-rabbit (Invitrogen, UK), AlexaFluor555 goat anti-mouse (Invitrogen, UK), or AlexaFluor649 goat anti-hamster (Invitrogen, UK) was added and incubated again for 2 h. Slides were then washed again with PBS and mounted using Fluoroshield with DAPI (Sigma-Aldrich, Missouri, USA). Lung sections and tracheobronchial wholemounts were imaged at the ARCHA (Aston Research Centre for Healthy Aging) Advanced Imaging Facility at Aston University, employing a SP5 TCS II MP confocal microscope (Leica, Germany), an EVOS XL microscope, or a widefield fluorescent microscope (Leica, Germany).

2.13 Image Analysis

Image analysis was performed on images using the open-source software ImageJ version 1.52 (Schneider et al., 2012). Images were loaded individually onto the program before being converted to 8-bit black and white or split (for images with multiple colours) which results in black and white channels. The threshold for the image was then set to highlight only the areas of interest. This was kept constant in each channel throughout each experiment to allow comparison. For images from Transwell assays where cells were to be counted, the image was then set to binary before a watershed was applied. This was to attempt to distinguish cells within multi-cell clumps although this was not always accurate. Particles were then measured with the size greater than 15 pixels in order to reduce counting debris. Results from Transwell assays were normalised to untreated cells in the presence of serum free media. Manual cell counting was performed on immunostained images as cell numbers were less due to a higher magnification used. To quantify stain, following thresholding, the integrated density of the stain is measured and then manually divided by the number of observed cells in the image. This was to account for variation in the number of cells within the image as the intensity per cell can now be estimated. This workflow is slightly altered in the images of the 3D spheroids where instead of manually counting cells, a region of interest encapsulating the spheroid was drawn and integrated density was calculated within that region of interest. This was similar to the technique used on images of lung slices where a region of interest was drawn around the airway in each image at a consistent width either side of the epithelium. The

intensity of stain within this region of interest was then calculated in order to control for images with several airways or blood vessels. ImageJ was also used to measure the size of the scratches in images from scratch assays. Again, the drawing tool was used to highlight a region of interest where the scratch occurred in the image and the area of that region of interest was measured.

2.14 Bioinformatics

Data gained from online sources was included in this thesis due to being unable to access a wet lab during the COVID-19 pandemic. The NCBI GEO (National Institutes of Health Gene Expression Omnibus) database was searched for POSTN (the gene for periostin) and allergic asthma (Barrett et. al., 2013). Once suitable data sets were identified, the data was searched for POSTN using the Curated Dataset Browser which resulted in the readout displayed in this thesis. In addition, the IPF Lung Atlas was used to further explore the expression of POSTN in fibrotic lungs (Neumark et. al., 2020). The gene explorer tool was used on the individual data sets in order to search for POSTN and this data could also be limited to cell type using the cell explorer. Further investigation into POSTN in asthma was completed using the Wellcome Sanger Institute Lung Cell Atlas (accessed at asthma.cellgeni.sanger.ac.uk) (Vieira Braga et. al., 2019). The dataset of “Asthma airway atlas others” was selected and POSTN was selected as the gene of interest. The readout of this is included within this thesis. The interactions of POSTN was also investigated using the IntAct database by EMBL-EBI (European Molecular Biology Laboratory – European Bioinformatics Institute) (Orchard et. al., 2013). POSTN was searched and the human protein was selected. The readout was included in this thesis.

2.15 Statistical Analysis

All results are shown as mean \pm standard error of the mean. GraphPad Prism 8 was used for data processing and statistical analyses. Differences were evaluated by one-way analysis of variance (ANOVA) for multiple groups with the Tukey post hoc test, or by two-way ANOVA with Šídák's multiple comparisons test. Differences were deemed to be statistically significant when a p-value less than 0.05 was obtained (* $p < 0.05$, ** $p < 0.01$, *** $p < 0.001$, **** $p < 0.0001$).

Chapter 3 – The Migration of Pericytes In Vitro Can Be Modulated By Growth Factors, Cytokines & Matrikines in the Microenvironment Including TGF- β , VEGF & Periostin

3.1 Introduction

In normal tissue pericytes reside around the endothelial cell layer of blood vessels. This connection is mediated by peg and socket connections and modulation of cytokines within the microenvironment (Sweeney et al., 2018)). There, pericytes are able to modulate various pathways such as angiogenesis and vessel permeability (Bergers & Song, 2005). However, in fibrotic tissues it has been observed that pericytes dissociate from the blood vessels and migrate towards the inflamed airway (Johnson et al., 2015). This migration is a key event contributing to airway remodelling observed in asthma. By migrating away from the blood vessels, the permeability of the vessel is increased which dysregulates the cytokines in the microenvironment (Aguilera & Brekken, 2014). The movement of cells towards the airways both thickens the smooth muscle layer surrounding the airways and contributes to the resident myofibroblast population, thus furthering the excess deposition of ECM proteins into the airway subepithelium (Chang et al., 2012). The mechanisms behind this migration, however, are largely unknown.

In order to prevent the migration of pericytes using a drug, the initial triggers of this process must be understood. For this reason, extensive study of the cellular environment which initiates the largest increase in migration was carried out, using various growth factors and cytokines. TGF-beta has been long linked to fibrotic microenvironments with some even concluding that it is one of the key mediators of fibrosis (Biernacka, Dobaczewski & Frangogiannis, 2011). TGF-beta can stimulate many different signalling pathways such as MAPK (Mitogen-activated protein kinases), PI3K (phosphoinositide 3-kinase)/Akt and Rho, allowing it to have varying effects including the regulation of ECM deposition, tumour cell migration and differentiation of fibroblasts into myofibroblasts (Vasiukov et al., 2020, Muraoka et al., 2002, Thannickal et al., 2003). As increased ECM deposition, cell migration and differentiation into myofibroblasts have all been linked to pericytes in the context of fibrosis, TGF-beta was an obvious growth factor of interest.

EGF was explored mainly due to its role in angiogenesis and pericyte recruitment to blood vessels (Stratman et al., 2010). As EGF is also thought to be increased in uncontrolled asthma and can be measured in sputum samples, the increased concentration of EGF within the airways may contribute instead to the recruitment of pericytes towards the airways where they can then contribute to airway

remodelling (Takamasu et al., 2011). As this contribution of EGF to pericyte migration is not fully known, it was thought that EGF would be an interesting growth factor to explore.

Along similar lines to EGF, VEGF was also explored for its links to angiogenesis and pericyte interaction with endothelial cells (Eilken et al., 2017). As pericytes both produce VEGF and carry the receptor for VEGF it could be assumed that pericytes are highly sensitive to VEGF within the microenvironment. Several studies have also implicated VEGF as a mediator for Th2 inflammation and a factor effecting aspects of remodelling such as mucus metaplasia and subepithelial fibrosis via the modulation of cytokines such as IL-13 (Lee et al., 2011). The direct implications of VEGF on pericyte migration are still debated and so the inclusion of VEGF into this study was decided.

The expression of CXCL12 (also known as SDF-1) has been linked to the development and progression of asthma, Studies have suggested that the increased expression of CXCL12 in asthmatic lungs can lead to the inflammation of the epithelium and subsequent migration and proliferation of smooth muscle cells (Wei, Chen & He, 2021). The receptor for CXCL12, CXCR4 can be found on pericytes, therefore allowing pericytes to react to the increasing concentration of CXCL12, thus indicating a potential role for CXCL12 in pericyte migration towards asthmatic airways (Hamdan, Zhou & Kleinerman, 2014).

Macrophages are often implicated with exacerbating inflammation, especially in allergic asthma. Both tissue-resident and bone marrow-derived macrophages contribute to the conditions of the microenvironment by skewing towards an M2 phenotype (Draijer & Peters-Golden, 2017, Girodet et al., 2016). This encourages the activation of Th2 cells as well as the production of inflammatory molecules such as TGF- β (Abdelaziz et al., 2020). For this reason, a pilot study was performed including healthy macrophages and damaged macrophages (in order to stimulate vesicle formation) to see if they modulated cytokine release by pericytes and subsequently a change in migration.

Periostin is slightly different to the other factors explored in this chapter in that it is a matrikine. This means that it is a bioactive peptide derived from the extracellular matrix (Burgess et al., 2021). Matrikines have similar properties and structures to traditional cytokines and are often involved in processes such as angiogenesis (Winkler et al., 2020). However, some studies have also highlighted their induction of matrix metalloproteinases such as MMP-2 which has been shown to influence cell migration (Winkler et al., 2020, Aguilera & Brekken, 2014). Periostin itself has been linked to allergic asthma, with high serum concentrations of periostin being indicative of asthma severity and eosinophilia (Takahashi et al., 2019). This link to asthma and to cell migration highlights the potential effects of periostin on pericytes and therefore periostin was investigated within this study.

Various forms of migration assays were utilised in order to obtain a broader view of pericyte migratory capacity and the impact of inflammatory/profibrotic mediators on this ability. Transwell assays were used as explained in Chapter 2, “Materials and Methods”. As a control, pericytes that had previously been treated with growth factors were transferred to serum free DMEM and were allowed to migrate towards a well containing serum free DMEM. The absence of an attractant should show the innate capacity of the cells to migrate spontaneously without an initiating signal.

3.2 Results

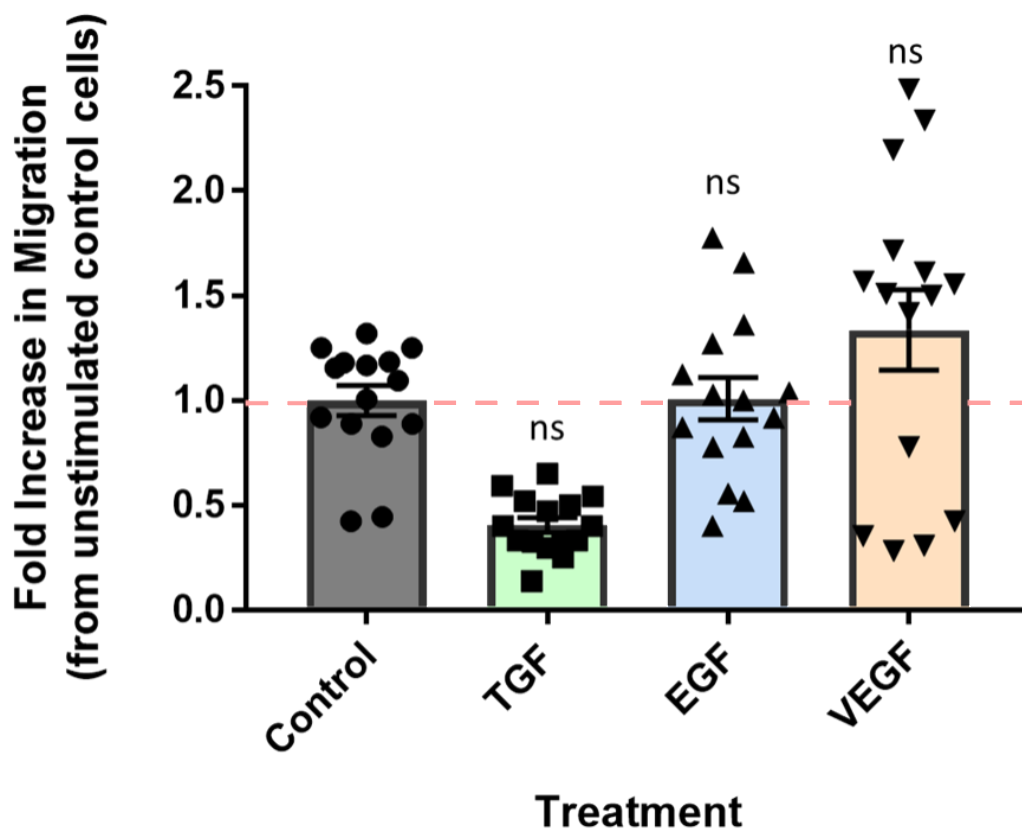


Figure 3.1 – There is no significant difference in pericyte migration towards serum free media measured with Transwell assay following growth factor treatment. Transwell assay performed as stated in “Methods”. Pericytes were treated with 10 ng/ml of the corresponding growth factor for 7 days. Cells were then starved in DMEM without serum and put in the top of the assay. The lower medium also contained DMEM without serum. After 24 h, membranes were collected and processed as in “Methods”, with the cell counts being normalised to the unstimulated control cells. The resulting average of each condition is shown. 15 counts were taken from 3 membranes per condition. “ns” indicates results were not significant to $p < 0.05$ compared to untreated control by one-way analysis of variance (ANOVA) for multiple groups with the Tukey post hoc test. Pink line represents the normalising control by one-way analysis of variance (ANOVA) for multiple groups with the Tukey post hoc test.

Although results were not significant to $p < 0.05$, a trend was apparent between growth factor treatments. There was a slight increase in migration of pericytes treated with VEGF and a slight decrease in cells treated with TGF- β . It was expected that any difference seen was not significant as serum-free medium does not encourage migration towards itself. The slight increase in migration displayed by pericytes treated with VEGF, however, may indicate an increase in migratory capacity. This was understandable as VEGF is increased during angiogenesis, where pericytes are recruited to newly formed blood vessels and would therefore migrate.

Following this initial experiment, a universal attractant of foetal calf serum (FCS) was used which can attract all cell types as it is required for growth. However, FCS is known to also contain many different growth factors including EGF, PDGF and FGF, and although all FCS used was heat treated, some growth factors may still remain and cause confounding effects (Naseer et al., 2009). Medium containing 10% FCS was placed in the bottom well of the Transwell assay in order to encourage pericytes to migrate through the membrane.

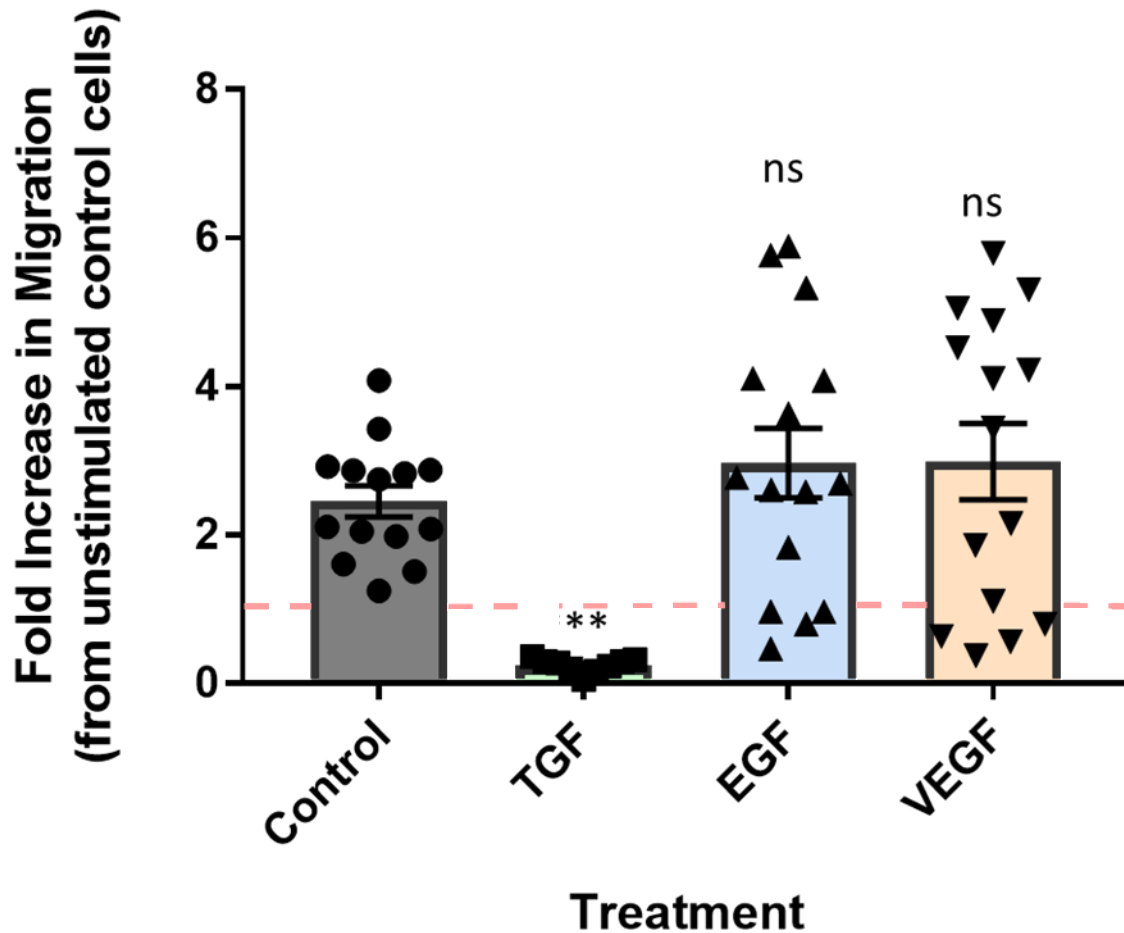


Figure 3.3- Pericytes treated with TGF- β migrate less towards media containing FCS than untreated pericytes. Transwell assay performed as stated in "Methods". Pericytes were treated with 10 ng/ml of the corresponding growth factor for 7 days. Cells were then starved in DMEM without serum and put in the top of the assay. The lower medium also contained DMEM with 10% FCS. After 24 h, membranes were collected and processed as in "Methods", with the cell counts being normalised to the control cells in DMEM without serum in each experiment. The resulting average of each condition is shown. 15 counts were taken from 3 membranes per condition. "***" indicates significance to $p < 0.01$ compared to untreated control by one-way analysis of variance (ANOVA) for multiple groups with the Tukey post hoc test. The pink line represents the normalising control.

Overall, pericytes migrated more towards serum containing FCS than serum without FCS (see Figure 3.1 and 3.2). This can be seen as the untreated cells showed a 3.5-fold increase in migration when migrating towards FCS compared to their migration towards serum free medium. Unexpectedly, the cells treated with TGF- β prior to the migration assay migrated significantly less than the untreated cells ($p = 0.0058$). This was unexpected as previous research has suggested that TGF- β treatment increases the migration of mesenchymal cells (Liu et al., 2019b, Zhao et al., 2016, Melzer et al., 2017).

As well as a universal attractant, a specific pericyte attractant was tested. PDGF-BB is a protein secreted by endothelial cells and it mediates the connection between pericytes and endothelial cells. Therefore, pericytes should migrate towards medium containing 300 µg/ml PDGF-BB.

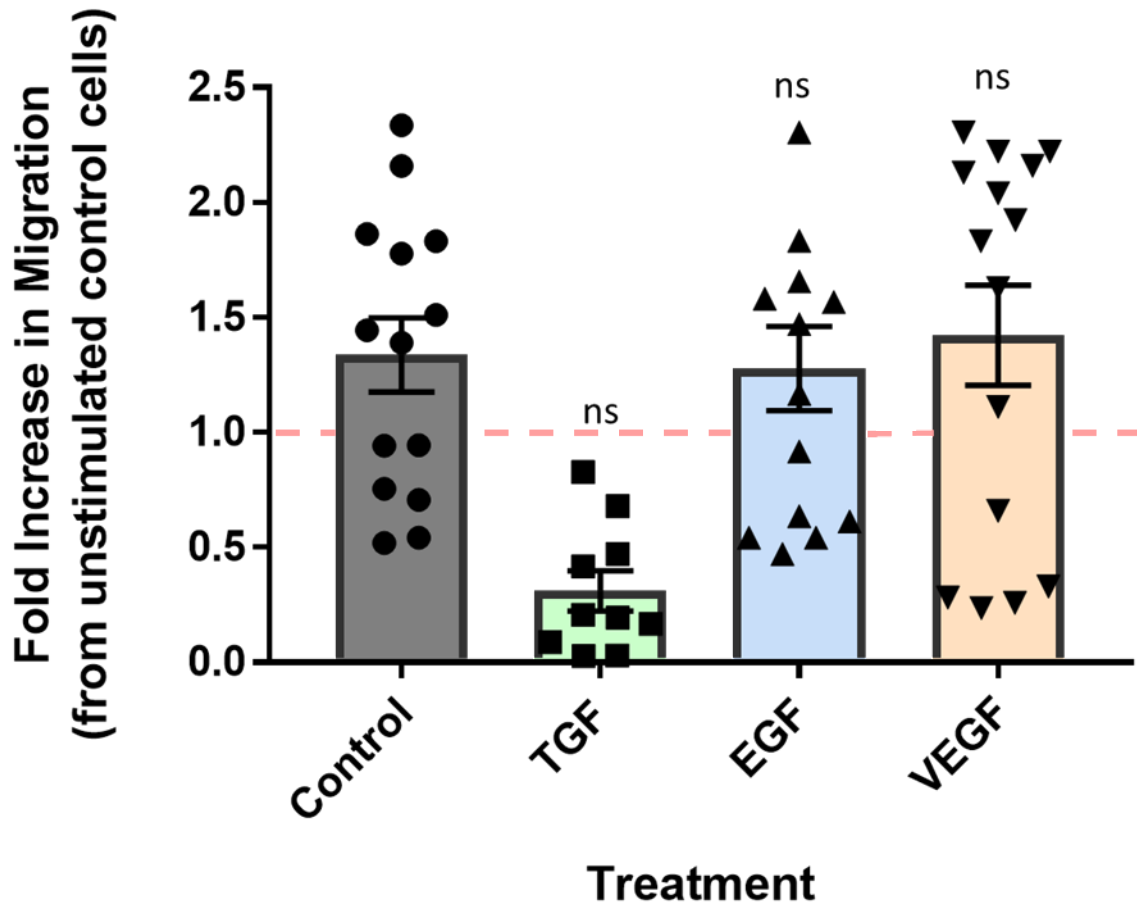


Figure 3.3 – There is no significant difference in pericyte migration towards media containing PDGF-BB measured with Transwell assays following growth factor treatment. Transwell assay performed as stated in “Methods”. Pericytes were treated with 10 ng/ml of the corresponding growth factor for 7 days. Cells were then starved in DMEM without serum and put in the top of the assay. The lower medium also contained DMEM with 300 µg/ml PDGF-BB. After 24 h, membranes were collected and processed as in “Methods”, with the cell counts being normalised to the control cells in DMEM without serum in each experiment. The resulting average of each condition is shown. 15 counts were taken from 3 membranes per condition. “ns” indicates results were not significant to $p < 0.05$ compared to untreated control by one-way analysis of variance (ANOVA) for multiple groups with the Tukey post hoc test. Pink line represents the normalising control.

The migration towards PDGF-BB shows a similar trend to the previous two migration studies (Figure 3.1 and 3.2). As with the migration without an attractant, the results are not significant to $p < 0.05$ and yet show a slight difference between treatment groups. Overall, the pericytes migrated more than those without an attractant but less than those migrating towards medium containing FCS.

Again, as with all previous results, cells treated with TGF- β seemed to show a reduction in migration compared to unstimulated cells.

To show the relative migration towards the three different attractants used, this data was presented again in a separate graph.

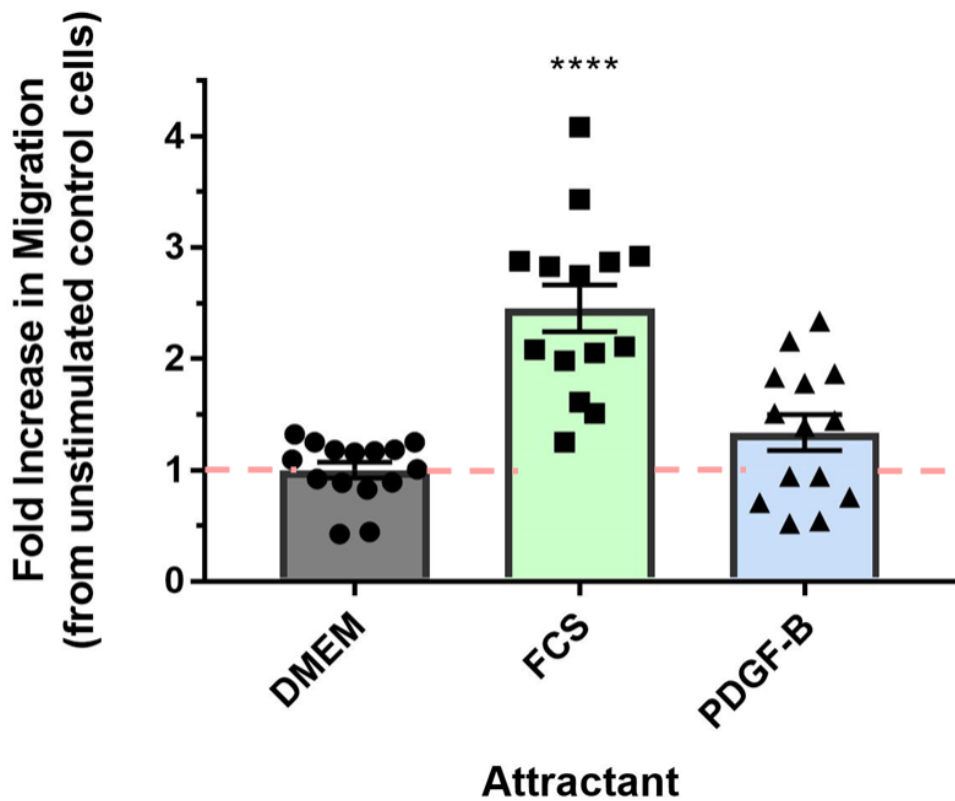


Figure 3.4 – Pericytes significantly migrated more towards media containing FCS than serum free media or media containing PDGF-BB measured with Transwell. Transwell assay performed as stated in “Methods”. Untreated pericytes were starved in DMEM without serum and put in the top of the assay. The lower medium also contained DMEM without serum, DMEM with 10% FCS or DMEM with 300 $\mu\text{g/ml}$ PDGF-BB. After 24 h, membranes were collected and processed as in “Methods”, with the cell counts being normalised to the control cells in DMEM without serum in each experiment. The resulting average of each condition is shown. 15 counts were taken from 3 membranes per condition. “****” = $p < 0.0001$ compared to cells migrating towards serum free media by one-way analysis of variance (ANOVA) for multiple groups with the Tukey post hoc test. Pink line represents the normalising control.

Figure 3.4 indicates that pericytes significantly migrated more towards FCS than PDGF-BB. This is to be expected as FCS is a universal cell attractant, although it is unusual that pericytes did not migrate significantly towards PDGF-B.

These results were obtained by performing a Transwell assay. This assay is described in “Methods” and results in the production of a membrane stained with DAPI which is imaged at 100x magnification.

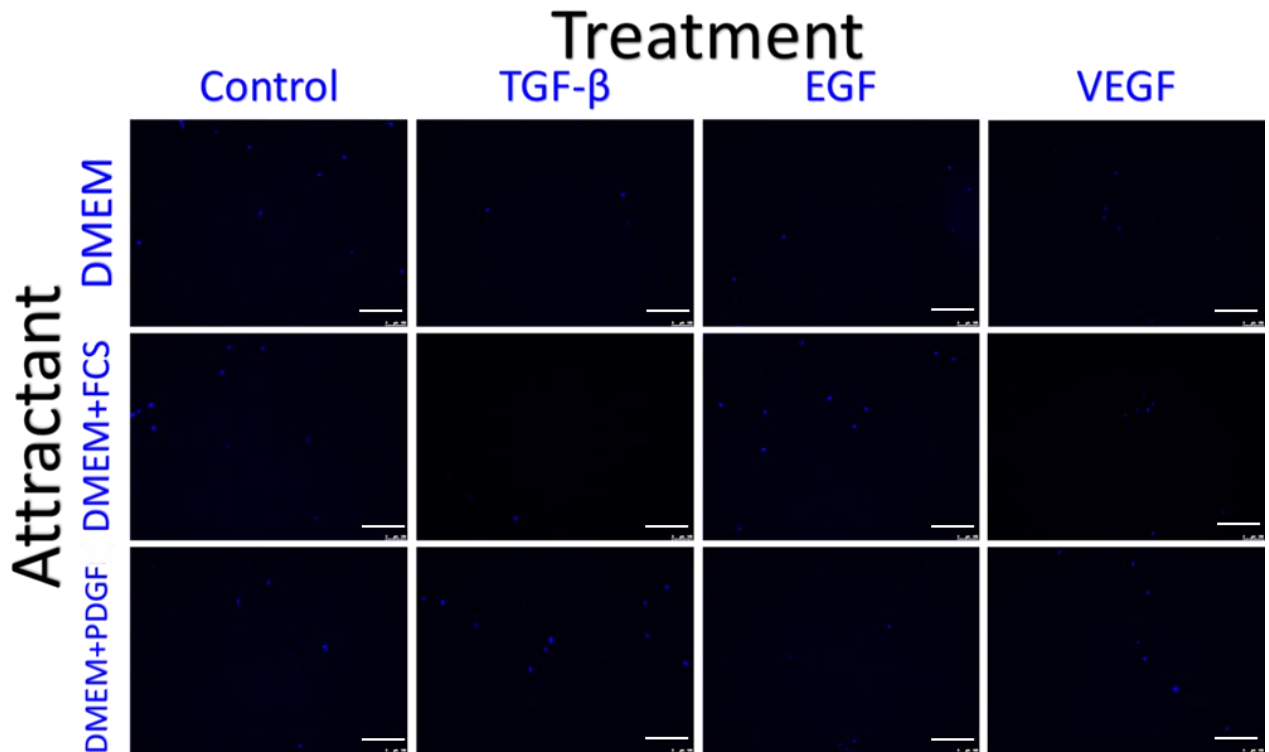


Figure 3.5 – Pericyte nuclei are clearly visible on Transwell membranes using a DAPI stain, Representative images of Transwell membranes taken using widefield microscopy at 100x magnification. Transwell assays were performed as in “Methods” with cells stimulated by 10ng/ml of either TGF-β, EGF, VEGF or without stimulation and migrated towards either serum free DMEM, DMEM containing 10% FCS or DMEM containing 300μl/ml PDGF-B. Membranes were stained with DAPI and subsequent counts were taken using ImageJ. Scale bars = 200μm.

Five images such as the ones shown in Figure 3.5 were taken and analysed per membrane. ImageJ was utilised to identify single cells and enumerate the total cells on a membrane. This was achieved by selecting an appropriate threshold to distinguish each cell. These “particles” were then measured and the totals averaged in order to achieve the enumeration of the assays (Figures 3.1-3.3). As each image from each condition varied in the number of cells, standard deviations were relatively high. There was also a difference in the intensity of the DAPI signal between the different membranes. This could be due to errors whilst handling the samples or natural variation between the cells.

The overall lack of significance along with the odd reduction in migration observed with cells treated with TGF-β was postulated to be due to the culture medium. All growth factor treatments were performed in pericyte medium, which is designed to preserve the stem cell properties of the cells and prevent spontaneous differentiation. It is possible that this would prevent the growth factors from inducing a change in morphology or expression patterns of the pericytes and therefore prevent

a change in migration. Therefore a study was carried out to the effects of culturing in pericyte medium as well as DMEM. Cells were grown in the stated medium prior to performing the assay.

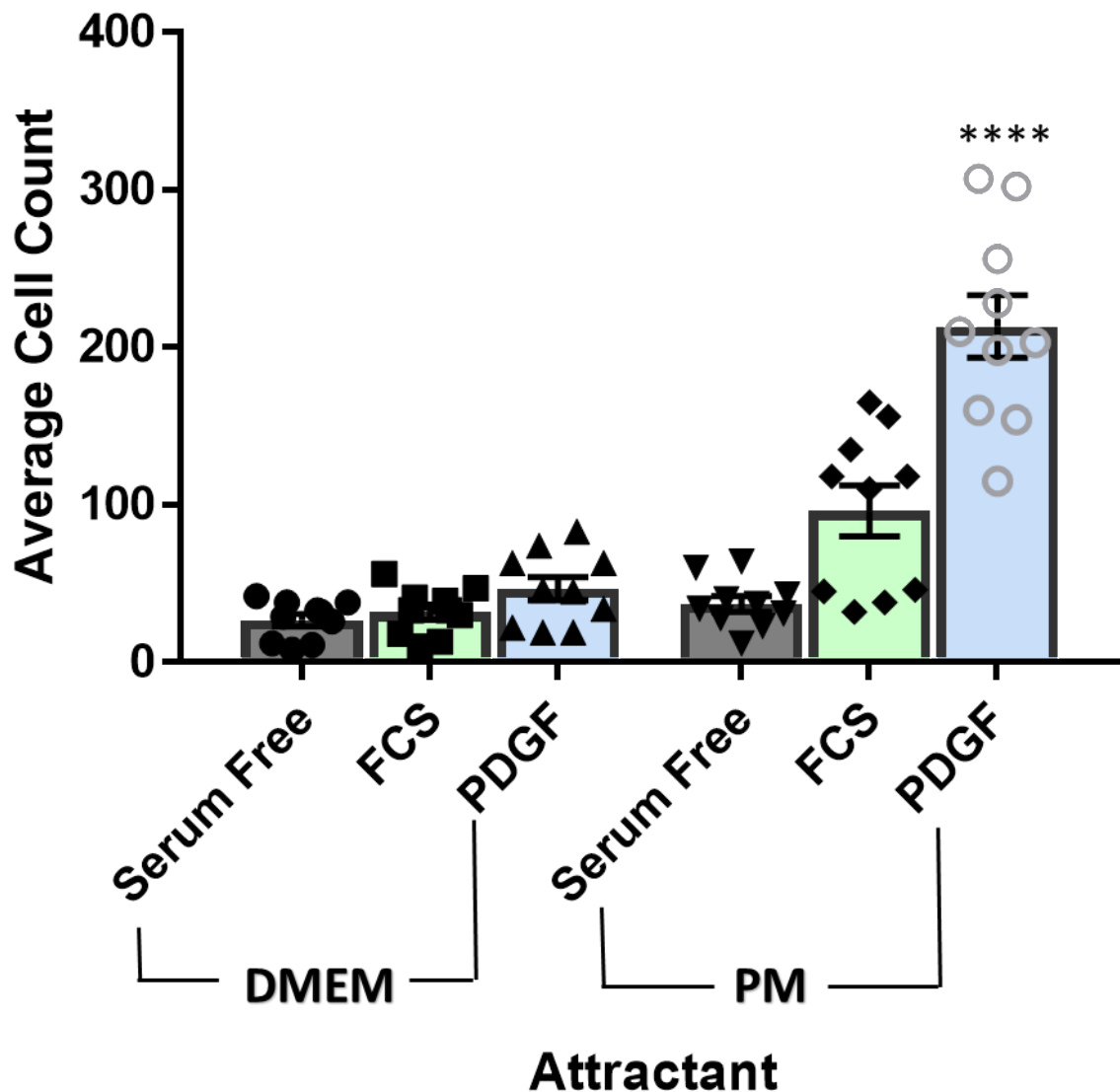


Figure 3.6 – Pericytes grown in pericyte media migrate more than those grown in DMEM. Transwell assay performed as in "Methods". Cells were grown in either DMEM or pericyte medium (PM). All cells migrated towards either DMEM without serum, with 10% FCS or 300µg/ml PDGF-B. The mean of 10 counts from 2 membranes per condition have been plotted. "****" = $p < 0.0001$ compared to serum free pericyte medium control by one-way analysis of variance (ANOVA) for multiple groups with the Tukey post hoc test.

Overall, cells that were grown in pericyte medium migrated more than those grown in DMEM, with the condition that were grown in pericyte medium and migrated towards PDGF-BB showing significantly more migration ($p < 0.0001$). In general, again, cell migrated towards medium containing FCS or PDGF-BB more than medium without serum. All cells represented in Figure 3.6 were

unstimulated cells, although the same experiment was also repeated with cells stimulated with 10ng/ml TGF- β . Cells were treated in the relevant medium for 24 hours.

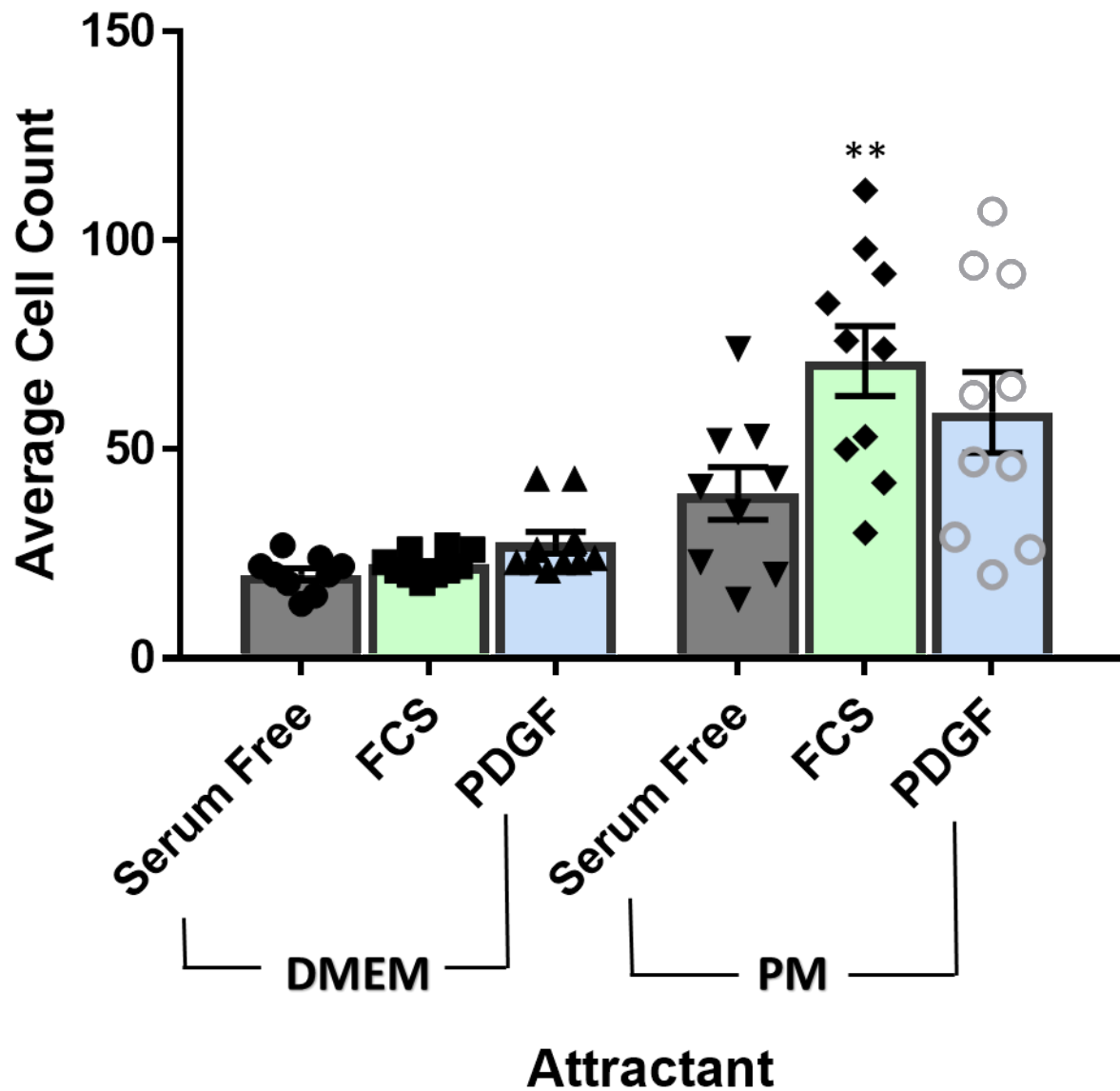


Figure 3.7 – Pericytes grown in pericyte media and treated with TGF- β migrate more than those grown in DMEM and treated with TGF β . Transwell assay performed as in "Methods". Cells were grown in either DMEM or pericyte medium (PM) and treated with 10ng/ml TGF- β for 24 hours prior to the assay. All cells migrated towards either DMEM without serum, with 10% FCS or 300 μ g/ml PDGF-B. The mean of 10 counts from 2 membranes per condition have been plotted. "****" = $p < 0.01$ compared to serum free DMEM control by one-way analysis of variance (ANOVA) for multiple groups with the Tukey post hoc test.

As with unstimulated cells, those grown in pericyte medium migrated more than those grown in DMEM. When compared to untreated cells in Figure 3.7, it is apparent that the migration towards

PDGF-B by cells grown in pericyte medium is significantly reduced ($p < 0.0001$). This may indicate that TGF- β treatment prevents the cells from interacting with PDGF-B.

One of the events that occurs during fibrosis is the influx of macrophages to the inflamed tissue. For this reason it was hypothesised that pericytes may respond to signals given out by these macrophages and therefore may migrate towards them.

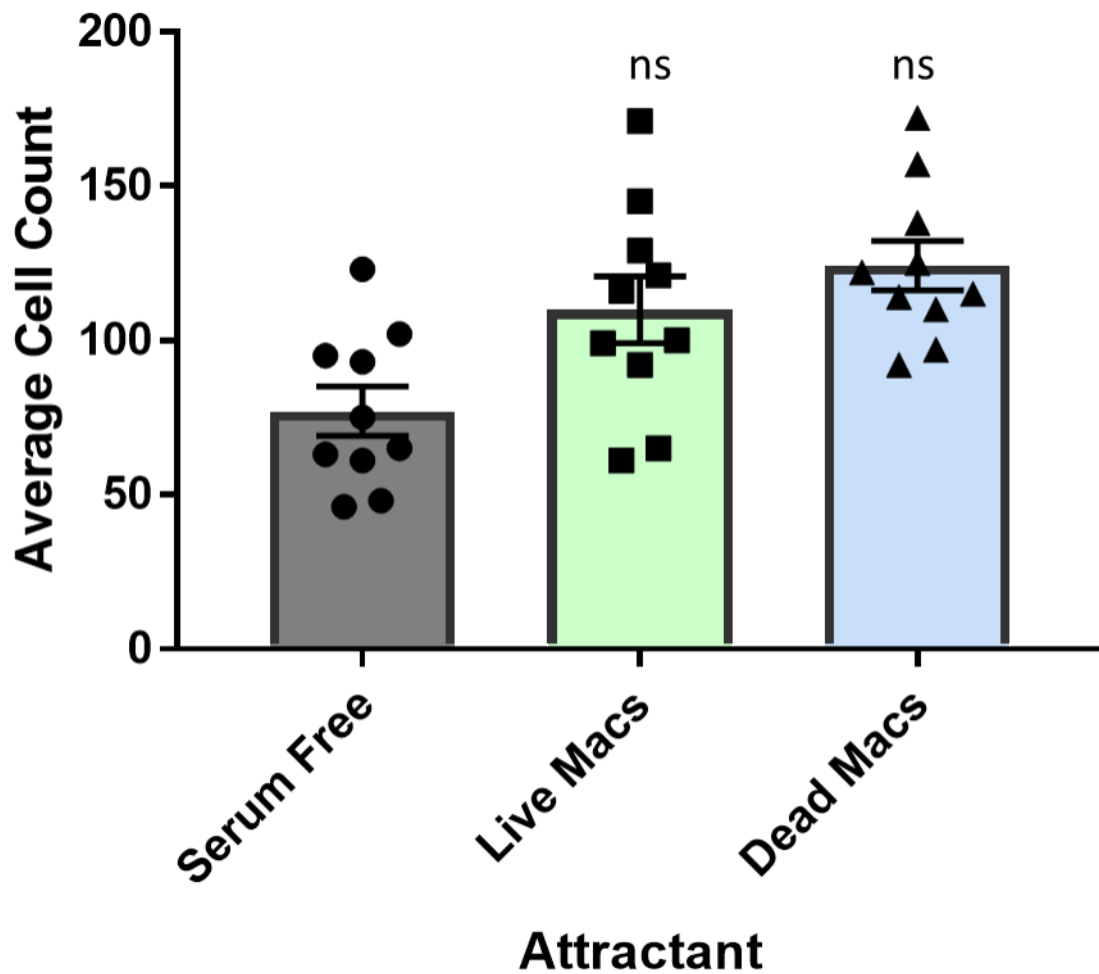


Figure 3.8 – Untreated pericytes do not preferentially migrate towards either living or dead macrophages. Transwell assay performed as in "Methods". Cells were grown in pericyte medium and migrated towards either DMEM without serum, DMEM with living macrophages, or DMEM with UV-killed macrophages, both at 1 million cells per ml. The mean of 5 counts from 2 membranes have been plotted. Results are a combination of 2 experiments. "ns" indicates results were not significant to $p < 0.05$ compared to the serum free control by one-way analysis of variance (ANOVA) for multiple groups with the Tukey post hoc test.

It was apparent that untreated cells failed to migrate significantly towards both forms of macrophages. Unfortunately, both experiments displayed considerable variability and therefore no results were significant. There was a slight increase in migration towards the macrophages suggesting that untreated pericytes may interact with macrophages but not to a significant level. Both live macrophages and dead macrophages were used in order to elucidate whether pericytes would react in response to signals from healthy macrophages or pro-inflammatory cytokines or reactive oxygen species released upon its death although these signals were not specifically explored in this study (Chiarelli-Neto et al., 2023). The lack of significance may be due to the pericytes not interacting with the macrophages or may just be due to a low concentration of macrophages and a subsequent reduction in cytokines for the pericytes to react to. As control cells did not respond to the macrophages significantly, further Transwells were performed to see if pre-treatment of cells with growth factors would modulate the pericyte's ability to respond to macrophage signals.

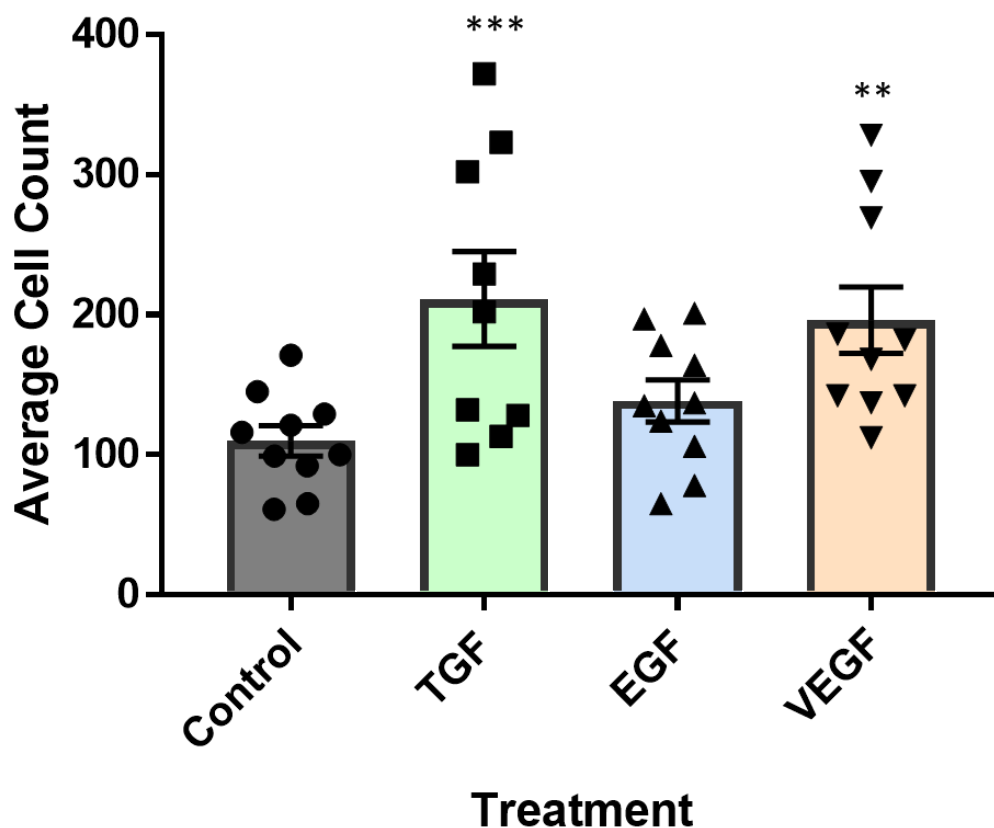


Figure 3.9 – Treatment with VEGF or TGF- β encouraged pericyte migration towards living macrophages. Transwell assay performed as in "Methods". Cells were grown in pericyte medium and were treated with 10ng/ml of the corresponding growth factor for 24 hrs and migrated towards DMEM containing living macrophages at 1 million cells per ml. The mean of 5 counts from 2 membranes have been plotted. Results are a combination of 2 experiments. "***" = $p < 0.01$, "****" = $p < 0.001$ compared to the control by one-way analysis of variance (ANOVA) for multiple groups with the Tukey post hoc test.

Interestingly, there was a significant variation in the migration towards living macrophages with different growth factor treatments. Pericytes that were treated with TGF-beta or VEGF migrated more towards living macrophages. This may suggest that TGF-beta and VEGF treatment make pericytes more susceptible to signals on macrophages or vesicles released by living macrophages. The pericytes treated with EGF exhibited similar migration as those without treatment. Therefore EGF is unlikely to affect the expression of macrophage interacting proteins in pericytes.

This assay was repeated using UV killed macrophages instead of living macrophages in order to see if treatments induce a different response to macrophages which have been damaged.

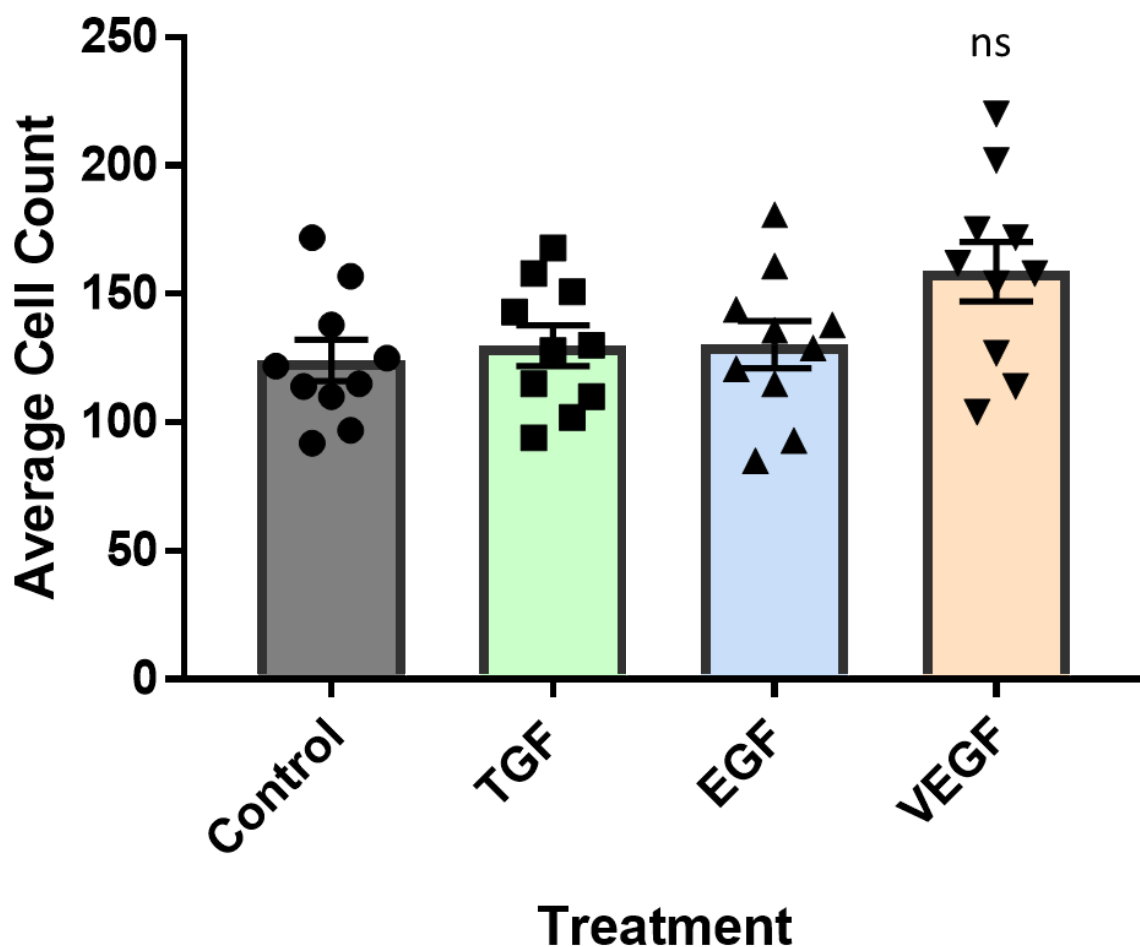


Figure 3.10 – There was no difference in the migration of pericytes towards dead macrophages following growth factor treatments. Transwell assay performed as in "Methods". Cells were grown in pericyte medium and were treated with 10ng/ml of the corresponding growth factor for 24 hrs and migrated towards DMEM containing UV killed macrophages at 1 million cells per ml. The mean of 5 counts from 2 membranes have been plotted. Results are a combination of 2 experiments. "ns" indicates results were not significant to $p < 0.05$ compared to the control by one-way analysis of variance (ANOVA) for multiple groups with the Tukey post hoc test.

The response of treated pericytes to dead macrophages was very different compared to living macrophages. There was no significant difference in pericyte migration to dead macrophages between each treatment. As there is a significant difference towards living macrophages, this suggests that there is a difference in the signals produced by living and dead macrophages. This could affect pericyte response in fibrotic tissue as the extent of fibrosis is associated with the state of the macrophages. Also, the fact that pericytes respond to macrophage signals indicates that the increased presence of macrophages in inflammation must be considered when combatting pericyte migration.

In addition to receiving pro-fibrotic signals aid the pericytes capacity to migrate, they also must respond to a signal which directs them to migrate towards the fibrotic tissue, in this case, the inflamed airway. Möhle et al. first suggested that the CXCR4/CXCL12 gradient may be responsible for attracting these pericytes by describing the migration of CD34+ progenitor cells we now know may be pericytes (Möhle et al., 1998). CXCR4 is a receptor found on the surface of pericytes and it is thought that the fibrotic microenvironment contains a greater concentration of CXCL12, thus increasing migration. This was tested using recombinant CXCL12 as an attractant in Transwell assays.

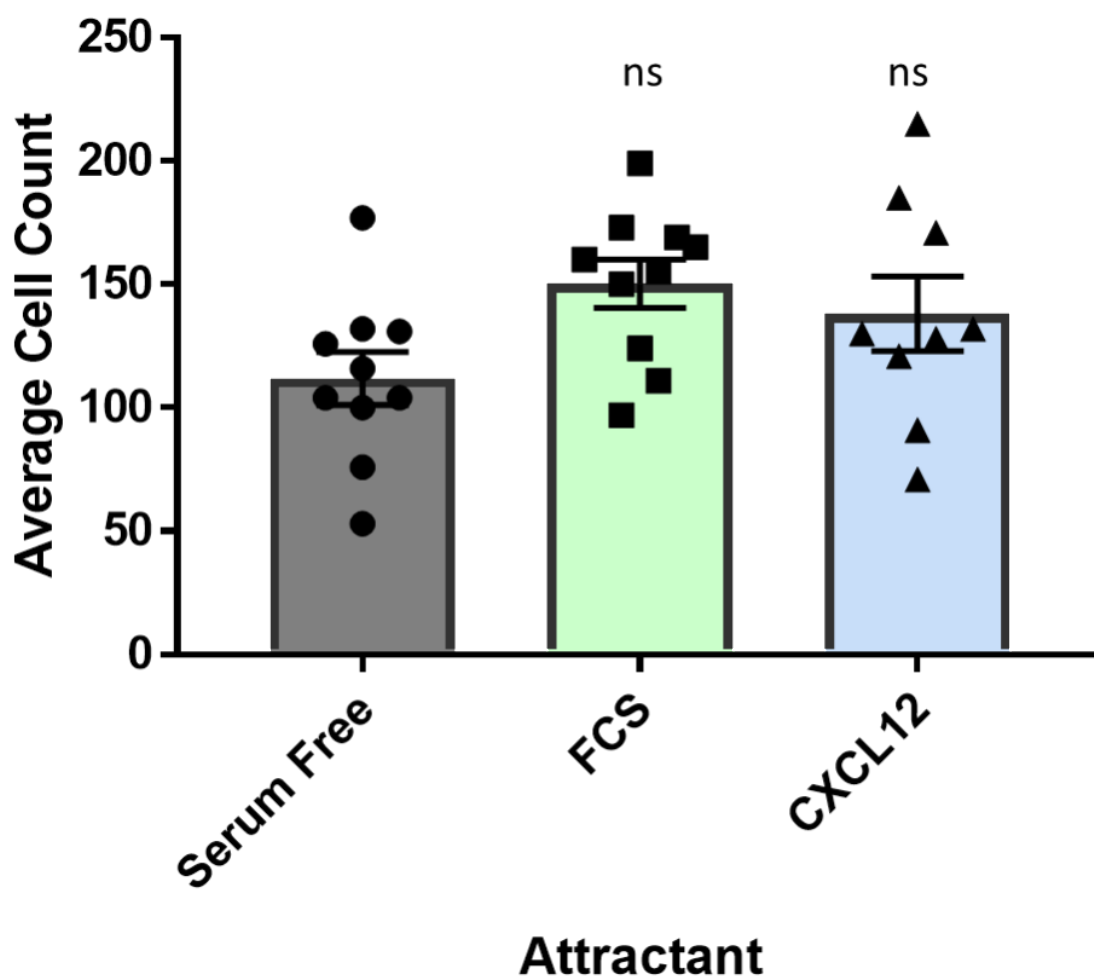


Figure 3.11 – There is no difference in migration towards serum free DMEM, FCS or CXCL12 by untreated pericytes. Transwell assay performed as in "Methods". Cells were grown in pericyte medium migrated towards either DMEM without serum, DMEM with 10% FCS or 500ng/ml of CXCL12. The mean of 5 counts from 2 membranes have been plotted. "ns" indicates results were not significant to $p < 0.05$ compared to the serum free control by one-way analysis of variance (ANOVA) for multiple groups with the Tukey post hoc test.

Using both the universal cellular attractant and the ligand CXCL12 which is thought to be unregulated in fibrotic tissue as well as in asthma, these Transwell assays suggest that healthy, unstimulated pericytes do not freely migrate towards either attractant. Even though there is a slight increase in migration towards FCS and to a lesser extent CXCL12, this was not significant. This may either be due to the small sample size of the assay or due to the minimal migratory capacity of the pericytes under normal conditions. In order for pericytes to migrate, these results suggest that they may need to be primed in order to migrate toward an attractant.

To test this idea, these assays were repeated following stimulation with the inflammatory/profibrotic mediator TGF- β in order to prime pericytes for migration.

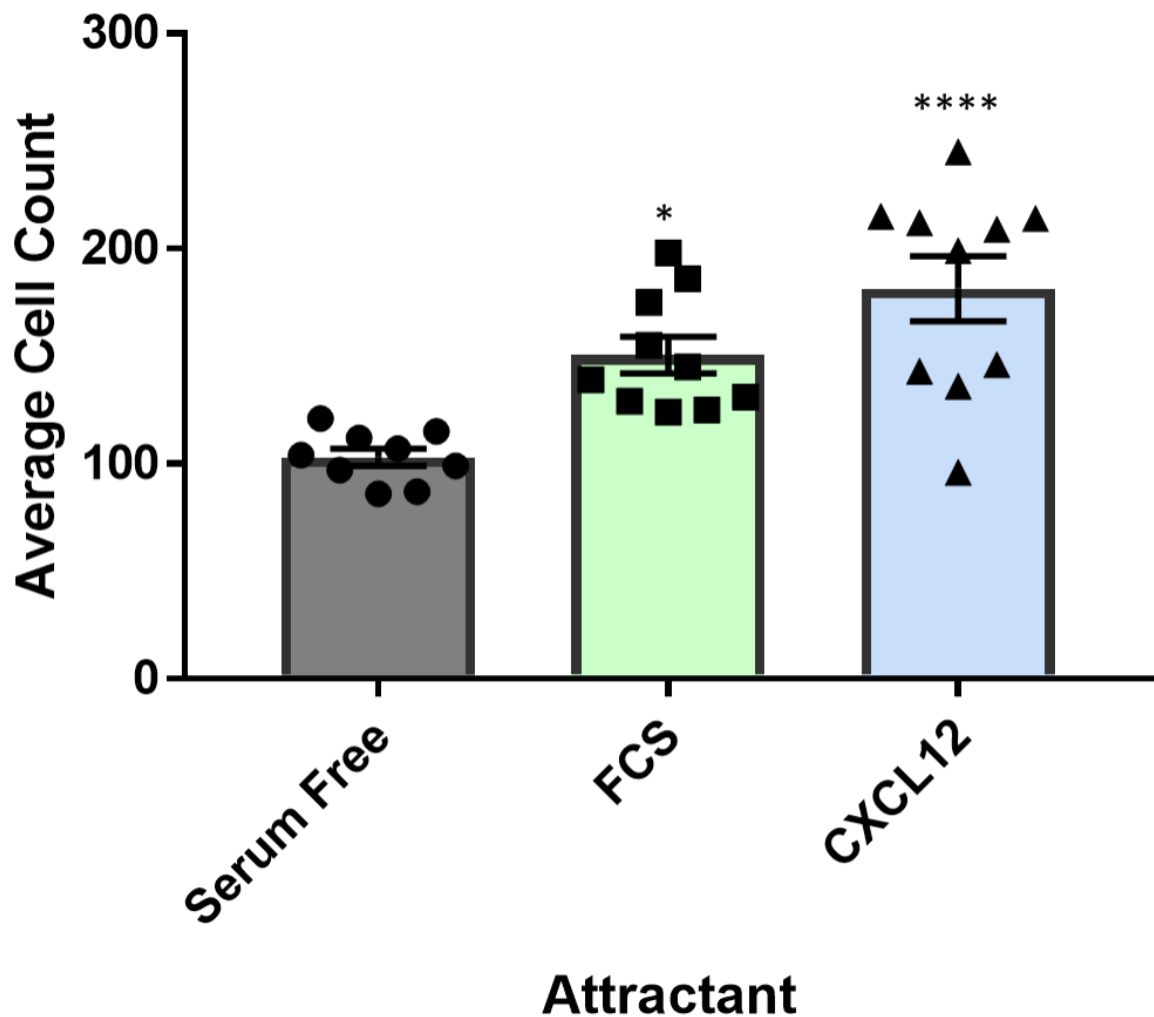


Figure 3.12 – Pericytes treated with TGF- β migrate more towards medium containing CXCL12 and medium containing FCS than serum-free medium. Transwell assay performed as in "Methods". Cells were grown in pericyte medium and treated with 10ng/ml TGF- β for 24hrs before they migrated towards either DMEM without serum, DMEM with 10% FCS or 500ng/ml of CXCL12. The mean of 5 counts from 2 membranes have been plotted. "*" = $p < 0.05$, "****" = $p < 0.0001$ compared to the serum free control by one-way analysis of variance (ANOVA) for multiple groups with the Tukey post hoc test.

Pericytes treated with TGF- β significantly migrated towards both medium containing FCS ($p = 0.0108$) and medium containing CXCL12 ($p < 0.0001$). The treatment with TGF- β caused an increased migration to stimuli overall than untreated pericytes as more pericytes had migrated in Figure 3.12 than seen in Figure 3.11 which shows untreated cells. The stimulated pericytes showed a greater amount of migration towards the CXCL12 attractant than both the control and the medium containing FCS.

Periostin is a molecule which is thought to interact TGF- β (Ashley et. al., 2017). It has been linked to asthma in humans but its interaction with pericytes is yet unknown (Takahashi et al., 2019). Its capacity to modulate the migration of pericytes was tested using Transwell assays and FCS as an attractant to provide both signals theoretically needed to induce migration, both a priming signal and a chemoattractant.

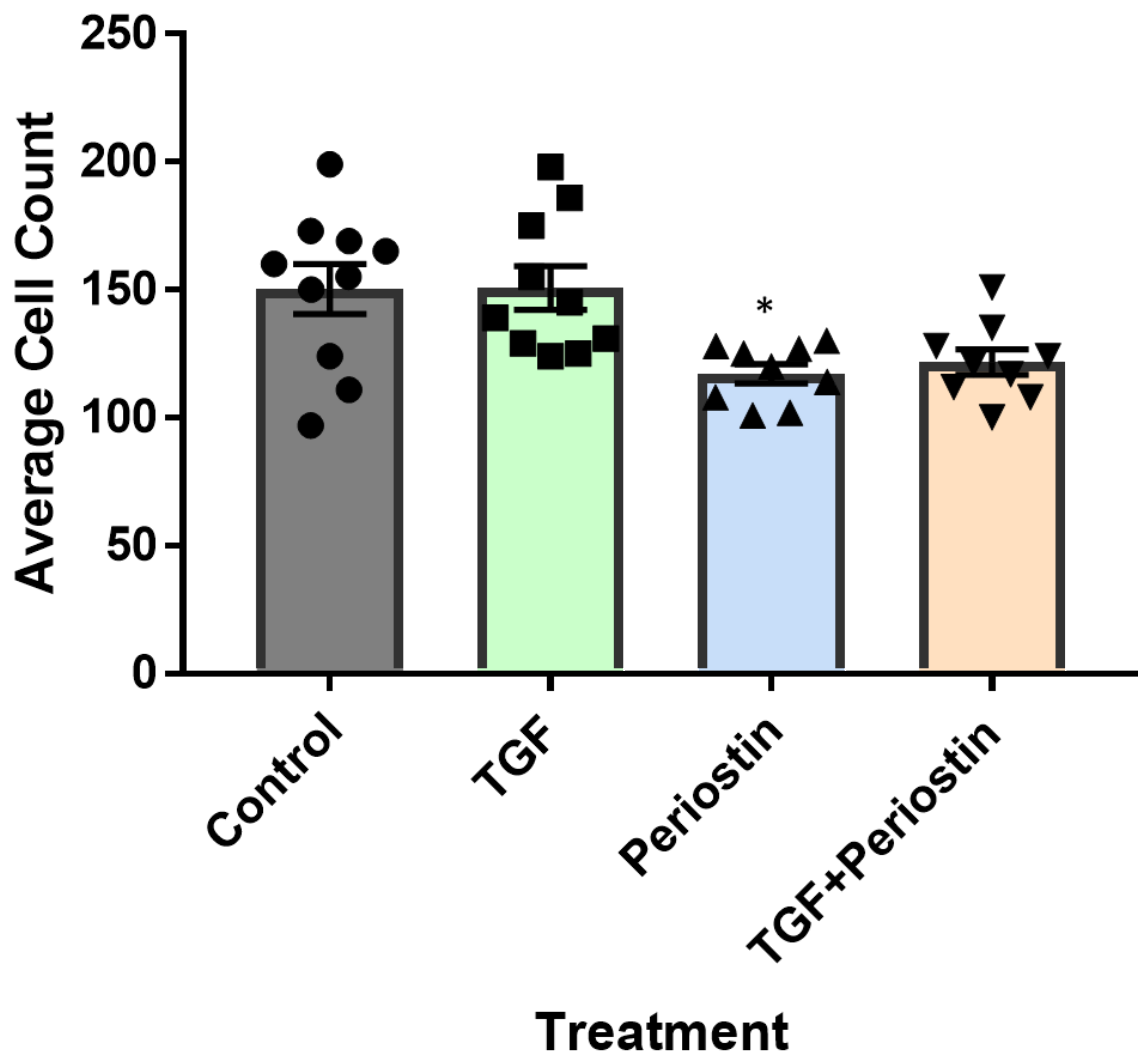


Figure 3.13 – Pericytes treated with periostin migrate less towards medium containing FCS than untreated pericytes. Transwell assay performed as in “Methods”. Cells were grown in pericyte medium and treated with 10 ng/ml of TGF- β and/or 100 ng/ml of periostin for 48 hours. All cells migrated towards DMEM with 10% FCS. The mean of 5 counts from 2 membranes have been plotted. “*” indicates significance of $p < 0.05$ compared to cells treated with TGF- β by one-way analysis of variance (ANOVA) for multiple groups with the Tukey post hoc test.

Unexpectedly, treatment with periostin and treatment with combined TGF- β and periostin resulted in a reduced pericyte migration towards FCS, with periostin treatment showing a significant decrease

($p=0.0181$). This was unusual as TGF- β treatment increased migration and periostin was thought to crosstalk with TGF- β as well as activate similar pathways and therefore, theoretically, should have also increased pericyte migration (Nanri et al., 2020, Ouanouki, Lamy & Annabi, 2018, Hu et al., 2015).

In order to further investigate this phenomena a different pericyte specific attractant was tested to see if the same phenomena would be observed.

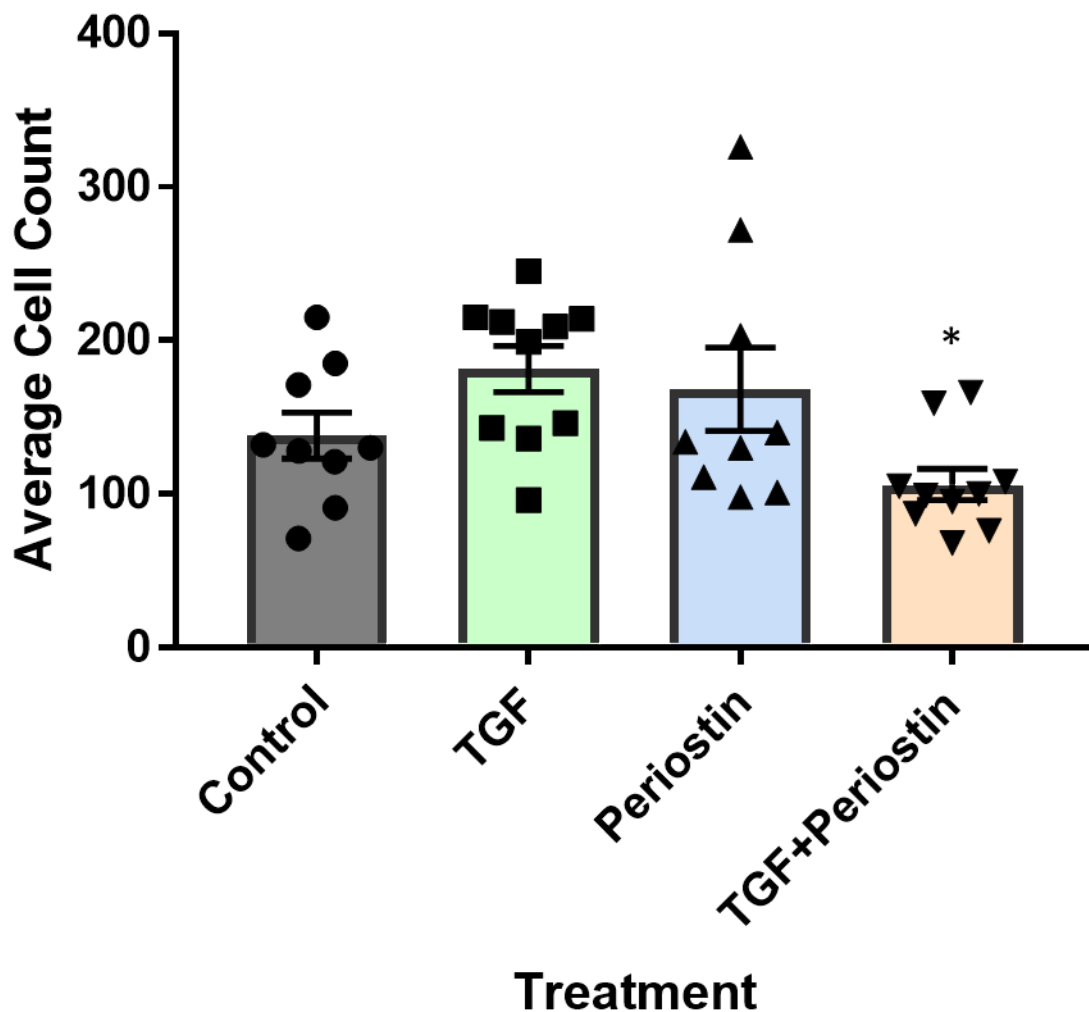


Figure 3.14 – Pericytes treated with TGF- β and periostin migrate less towards medium containing CXCL12 than untreated pericytes. Transwell assay performed as in “Methods”. Cells were grown in pericyte medium and treated with 10 ng/ml of TGF- β and/or 100 ng/ml of periostin for 48 hours. All cells migrated towards DMEM with 500ng/ml CXCL12. The mean of 5 counts from 2 membranes have been plotted. “*” indicates significance of $p<0.05$ compared to cells treated with TGF- β by one-way analysis of variance (ANOVA) for multiple groups with the Tukey post hoc test.

Similar to Figure 3.12 and Figure 3.13, Figure 3.14 shows that migration was reduced with periostin treatment when compared to TGF- β . However, overall migration increased towards CXCL12. A theory behind the unusual results outlined in Figure 3.12-3.14 is that periostin caused pericytes to associate more strongly with each other via its cell adhesion role in wound healing and scar formation and therefore produce large clumps which would be unable to squeeze through the 8 μ m pores in the Transwell membranes (Yokota et al., 2017, Michaylira et al., 2012). Also, if they were able to make their way through the membrane, ImageJ analysis would be unable to distinguish between individual cells and would instead count several cells as a singular cell resulting in a lower count. Therefore, this method requires optimisation or more advanced post processing.

To test this, images were taken of the Transwell membranes using DAPI to mark cell nuclei.

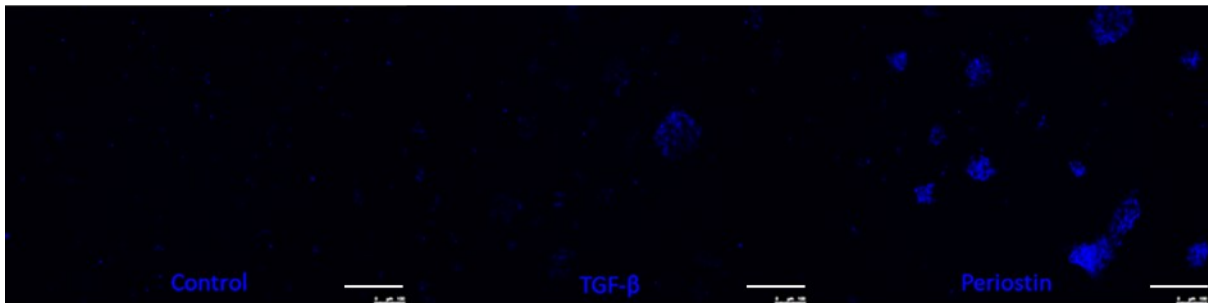


Figure 3.15 – Pericytes treated with TGF- β or periostin appear in clumps on Transwell membranes. Images show examples of counts of pericytes migrating towards media with 10% FCS to demonstrate cell clumping observed in the treated conditions. Cells were grown in pericyte medium and treated with 10 ng/ml of TGF- β or 100 ng/ml of periostin for 48 hours. Following transwell assay, cells were stained with DAPI and imaged at 100x magnification. Scale bars = 200 μ m.

Figure 3.15 shows representative images of Transwell membranes after migration has occurred. It is clear to see that there is an increased number of cells present when they were treated with TGF- β or periostin. However, the ImageJ analysis records a lower number due to the clumping of cells which registered on the software as singular cells. Therefore, Transwell assays with subsequent analysis by ImageJ may not be a suitable method for analysing pericyte migration at this concentration of cells.

As it was the movement of the pericytes through the membrane of the Transwell insert as well as the limited surface area available to the cells which likely contributed to the clumping of the cells, an additional method of migration analysis was used. Cells were prepared in a similar way as those used in the previous experiments. Pericytes were cultured in pericyte medium containing various treatments for 48 hours. This is to ensure the growth factors fully take effect on the cells. The cells were then transferred to serum free DMEM in order to arrest cell proliferation and to ensure any differences observed were due to migration rather than additional proliferation. A scratch was then made in the monolayer, approximately 400 μ m wide and the cells were left to migrate for 24 hours at

37°C. The images taken before and after this incubation were analysed to determine the distance the cells migrated in 24 hours.

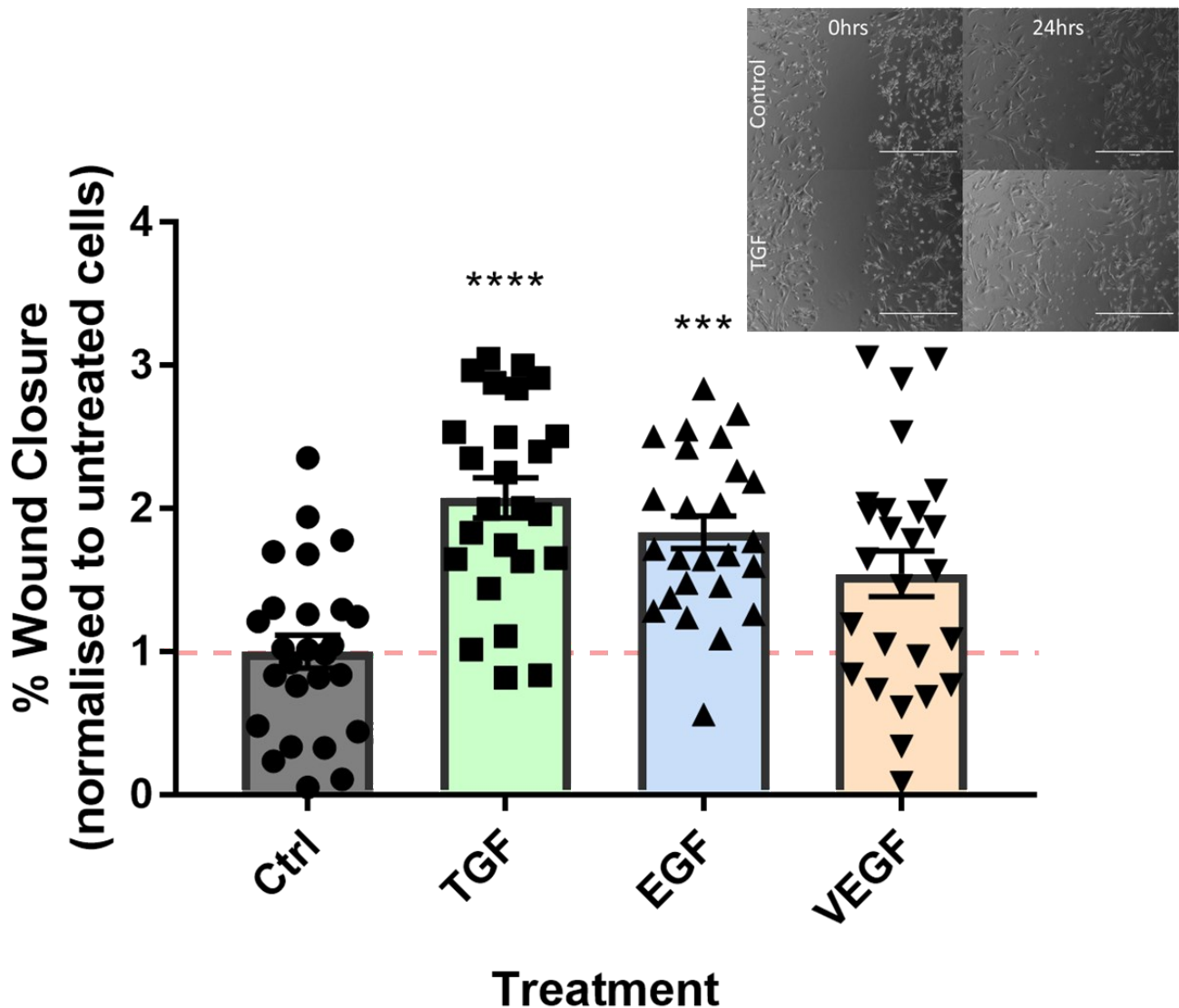


Figure 3.16 – Pericytes treated with TGF- β or EGF migrate significantly more than untreated pericytes in scratch assays. Scratch assay performed on pericytes that were grown in pericyte medium and treated with 10 ng/ml of TGF- β , EGF or VEGF for 48 hours. Cells were transferred into medium lacking serum and a scratch was made in each monolayer using a p200 pipette tip. Images were taken at 100x magnification immediately after scratching and at 24 hours later. The size of the scratches were determined using ImageJ and average % wound closure was calculated. Data from 3 independent experiments, containing 5 or 10 technical replicates per experiment, normalised to the untreated cells. N=25, “***” = $p < 0.001$, “****” = $p < 0.0001$ in respect to untreated cells. Pink line represents the normalising control. Inset contains representative images from the scratches taken for reference by one-way analysis of variance (ANOVA) for multiple groups with the Tukey post hoc test. Scale bars = 1000 μ m.

A significant increase in migrating cells was observed in all treated cells compared to untreated cells, with the greatest migration observed with both TGF- β treatment and EGF treatment (both $p < 0.0001$, VEGF = $p = 0.0145$). This reflects results shown by others, as both TGF- β and EGF are thought to encourage migration of mesenchymal stem cells. As this was observed using a scratch method but not with the Transwell method it can be suggested that the TGF- β treatment in particular had altered the cells so they were unable to pass through the membrane rather than reduce the migration ability of the cells. This data supports the idea of targeting TGF- β or EGF pathways to prevent pericyte migration during fibrosis. The large size of the error bars in all treatment groups in Figure 3.16 is likely due to natural variation between experiments as some natural slight variation of confluence was present, especially as some treatments encourage proliferation. However, due to the large number of repeats, these results were statistically significant.

This method was also repeated to investigate the effect of treatment with periostin and PDGF-B.

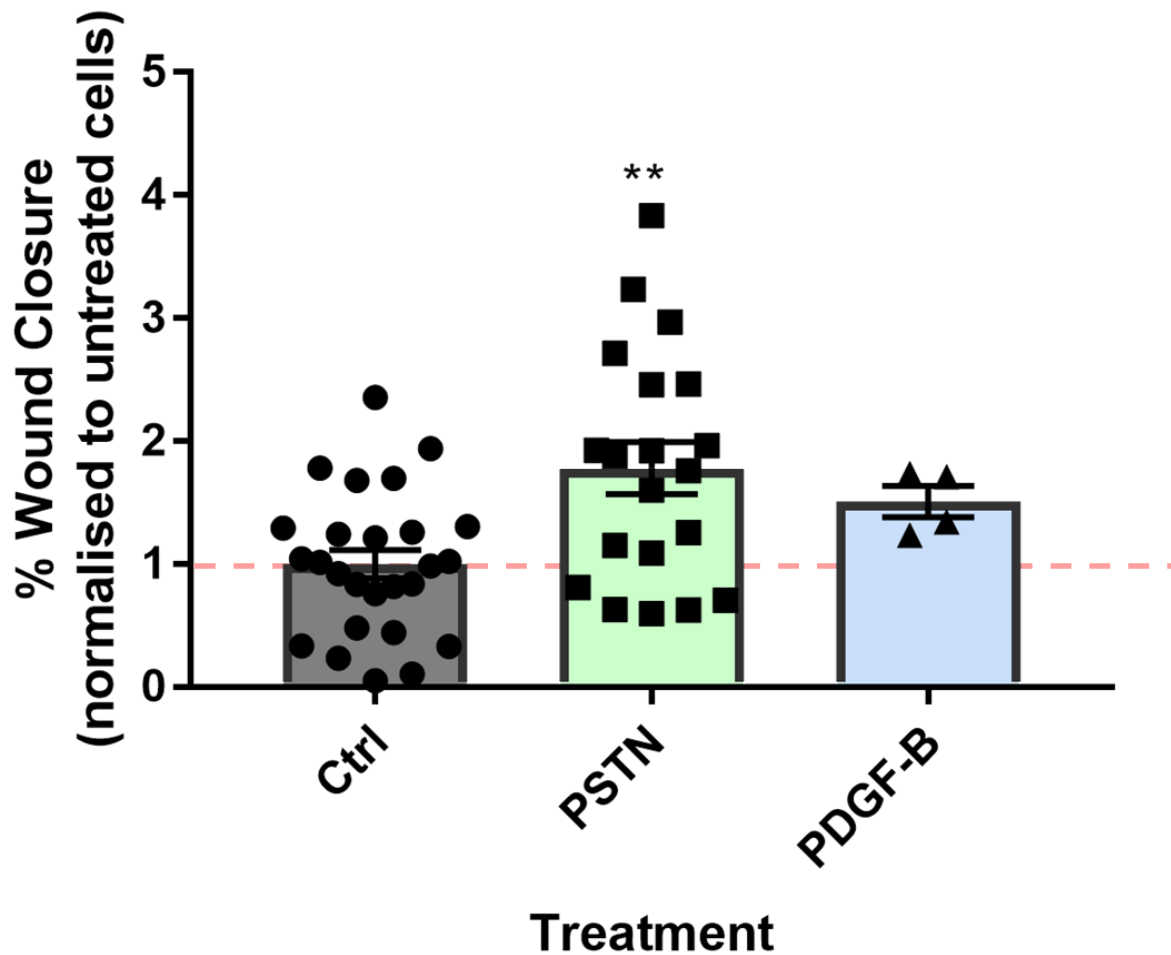


Figure 3.17 – Pericytes treated with periostin migrate significantly more than untreated pericytes in scratch assays. Scratch assay performed on pericytes that were grown in pericyte medium and treated with 100ng/ml periostin or 300µg/ml PDGF-B for 48 hours. Cells were transferred into medium lacking serum and a scratch was made in each monolayer using a p200 pipette tip. Images were taken at 100x magnification immediately after scratching and at 24 hours later. The size of the scratches were determined using ImageJ and average difference in sizes were calculated. Control data from 3 independent experiments (5 or 10 technical replicates per experiment), periostin data from 2 independent experiments (9 or 10 technical replicates per experiment), PDGF-B data from 1 experiment. All data normalised to the untreated cells from that experiment. $n_{\text{Control}}=25$, $n_{\text{Periostin}}=19$, $n_{\text{PDGF-B}}=4$ “***” = $p < 0.01$ in respect to untreated cells by one-way analysis of variance (ANOVA) for multiple groups with the Tukey post hoc test.

Much like previous treatments with TGF-β, EGF, and VEGF, treatments with periostin and PDGF-B also encourage migration. Both of these treatments, however, seem to increase migration less than was observed with TGF-β or EGF treatments. With periostin treatment yielding significant results ($p=0.0036$) and PDGF-B treatment being almost significant ($p=0.1334$) however, does suggest that the targeting of both of these pathways by inhibitory molecules may yield positive results in reducing pericyte migration during fibrosis.

In order to explore the migration of pericytes in a more complex environment, a method was tested which allowed the interaction between three cell types found in the airway: endothelial cells,

epithelial cells, and pericytes. 0.45µm Transwell inserts were inverted, and the outer membrane was coated with gelatine. At the same time standard round coverslips were placed in a 24 well plate and were also coated in gelatine. Endothelial cells or epithelial cells were then seeded on each surface and allowed to grow for 48 hours. During this time, pericytes were treated with TGF-β for 48 hours in separate flasks. After 48 hours the surfaces were combined into the wells as shown in Figure 3.17, and the pericytes were transferred into serum free medium and added to each well. This was supposed to indicate if there was a bias in the direction which the pericytes would migrate in fibrotic conditions compared to healthy conditions. Rather than with Transwell assays which tested the ability of pericytes to migrate toward specific chemoattractants, this method demonstrated if there was anything intrinsic to the cells themselves that influenced migration, such as cell surface proteins. Both orientations of the cells were included in order to negate the effect of gravity. It was hypothesised that pericytes treated with TGF-β would be observed on the surfaces containing epithelial cells compared to those containing endothelial cells and vice versa for the untreated pericytes. This was because in fibrotic airways pericytes migrate away from the endothelium towards the epithelium.

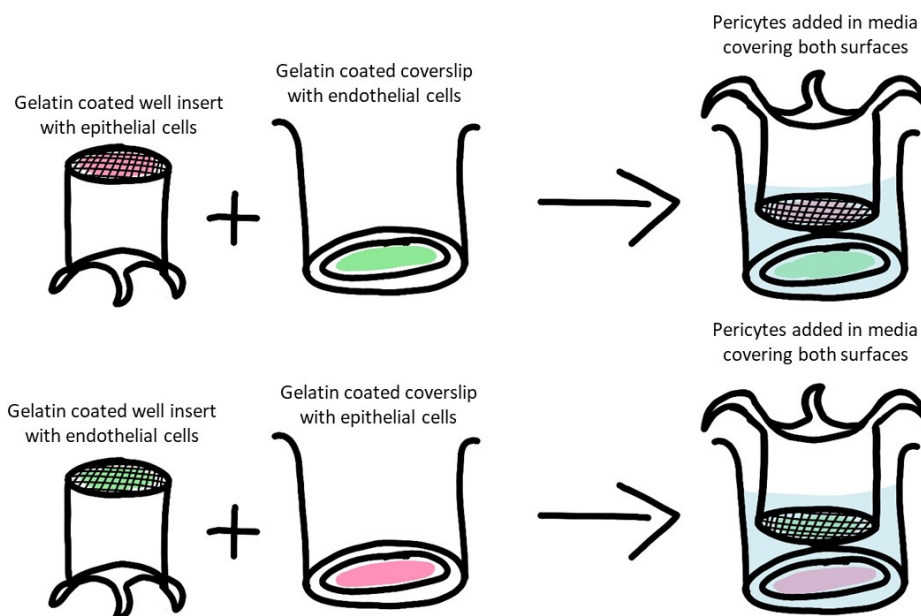


Figure 3.18 - Graphical depiction of method used to construct wells for the dual surface assay

However, this method did not obtain any meaningful results. Robust markers for pericytes (NG2) were unavailable at the time of this study due to supply issues and the PDGFR antibody used did not

work as desired. This resulted in being unable to tell where the pericytes migrated as highlighted in Figure 3.19.

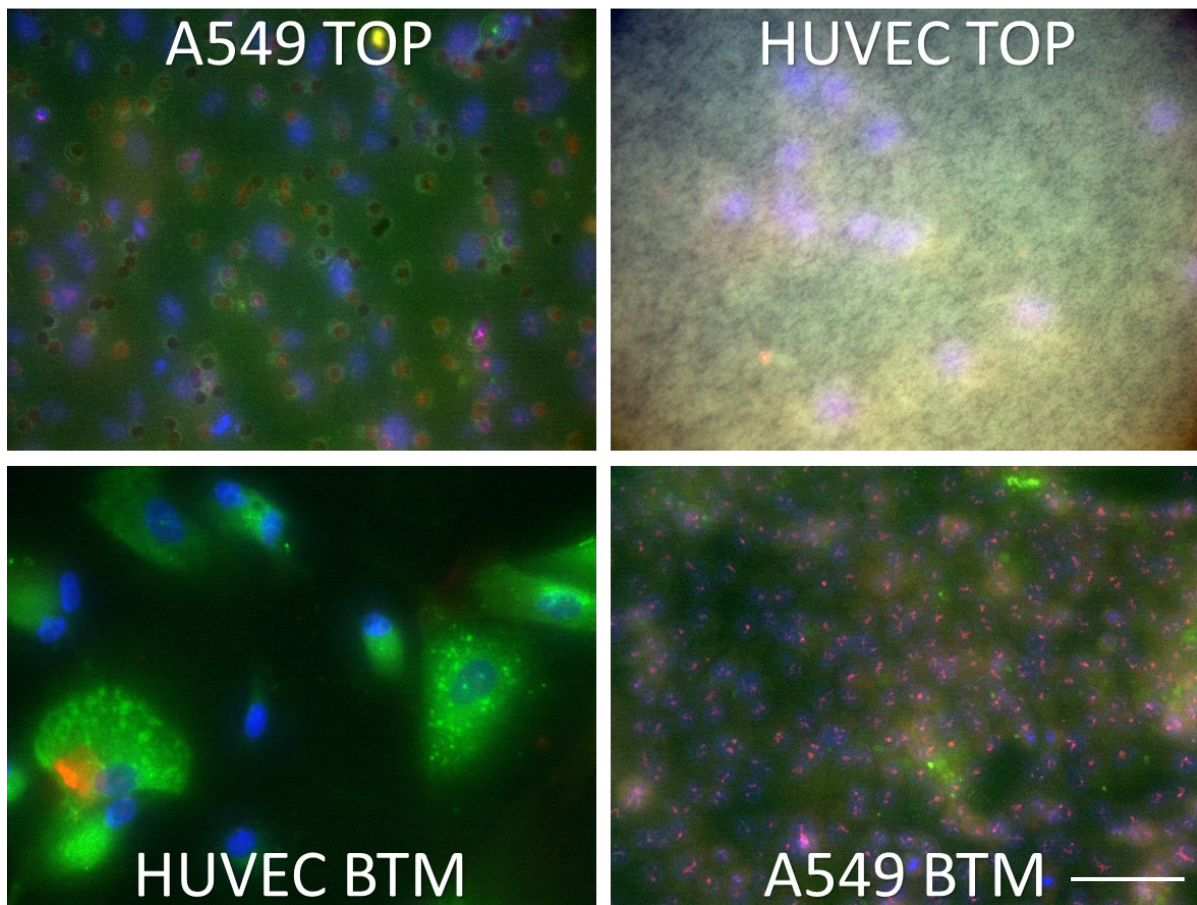


Figure 3.19 – The method for the dual surface assay does not yield interpretable results. Immunostaining performed on cells assayed as described in Figure 3.18. All cells were untreated. Cells were stained with an anti-CD31 antibody (green), an anti-PDGFR β antibody (red) and the nuclear stain DAPI (blue). Images were taken at 400x magnification. Scale bar = 100 μ m.

These images are an example of what was seen in all wells of the experimental plate. The PDGFR β pericyte stain did not behave as expected and therefore it was impossible to identify which cell layer the pericytes preferentially chose to migrate to. It is also possible that the pericytes did not bind to either surface as they were only given 24 hrs to adhere. If this method is to be used in the future it should undergo extensive optimisation in order for the visualisation of pericytes to be possible.

More optimisation needs to be done considering this method in order to establish ideal culture durations and cell concentrations. A variety of different stains should also be explored to find the best staining profile in order to highlight all three of the cell types. In addition, pre-staining the different cell populations may allow easier tracking through the membranes as differences in cell types would be more distinct. Other assays may also be modified to explore this directional effect,

such as using live cell imaging or employing matrix such as Matrigel in order to establish a more robust area for migration.

3.3 Discussion

Overall, the exploration into the migration of pericytes under fibrotic conditions is an important platform on which further research into the impact of inflammatory mediators in asthma can be based. Although, in this chapter, migration of pericytes away from blood vessels and towards the airway wall is framed as a detrimental effect, there are circumstances where this movement would be advantageous. Pericytes are known to play roles within wound healing as a stationary component of the vessel wall such as the management of the clotting cascade and infiltration of immune cells such as macrophages (Bodnar et al., 2016). In addition, as tissue remodelling is a key event in wound healing, it may be that pericytes migrate to areas of injury, for example in the airway wall, and contribute to maintaining structural stability through the production of ECM proteins (Deigelmann & Evans, 2004). However, as pericytes leaving the vasculature often increases vascular permeability and dysregulation, this may lead to an influx of immune cells and an exacerbation of the inflammation (Ferland-McCollough et al., 2017). Nevertheless, it is important to acknowledge that not all pericyte migration may be detrimental and therefore inhibitors that prevent all migration of pericytes should be avoided.

Of the growth factors that were explored, TGF- β was shown to produce a robust increase in pericyte migration in scratch assays. This result was not seen in Transwell assays due to experimental constraints. This highlights the importance of using a diverse range of methods to explore migration as certain treatments or natural characteristics of the cells may impact results. Both EGF and VEGF was also shown to increase migration of pericyte, although not as much as TGF- β . This indicates that a complex interplay between various growth factors, cytokines, and chemokines in the microenvironment of the fibrotic airway is likely to contribute to the increased pericyte migration observed previously in vivo (Johnson et al., 2015, Kemp et al., 2020). In addition, periostin, a profibrotic matrikine, was briefly explored. This was pinpointed as a possible contributor to migration as it has been suggested to work alongside TGF- β to contribute to tissue fibrosis (Ashley et al., 2017). The results of both the Transwell assays and the scratch assays suggest that treatment with periostin yields similar results to treatment with TGF- β , such as the increased migration of pericytes in scratch assays (Figures 3.15/3.16) as well as the cell clumping observed on Transwell membranes (Figure 3.15). Periostin, therefore, may become a key target in reducing pericyte migration in allergic asthma (Bignold & Johnson, 2021a, Wu et al., 2018). The increased pericyte migration observed towards both living and dead macrophages is also an area which may be fruitful to explore. This apparent attraction suggests that macrophages may release important cytokines

within extracellular vesicles which encourage migration upon their arrival at inflamed tissue (Wang et al., 2020). However, as this is an incredibly complex system, it falls beyond the scope of this thesis, although it would likely be a fruitful avenue to pursue.

Treatment times were altered throughout these experiments, building on optimisation done by other members of the lab. For example, the 7-day treatment with TGF- β shown in Figures 3.1-3.3 was changed to 24 hours in Figure 3.7. This was in order to investigate the unusual effect of a reduction of migration following TGF- β treatment which literature suggests is thought to increase migration (Liu et al., 2019b, Zhao et al., 2016, Melzer et al., 2017). This optimisation should be further explored by continuing to test various concentrations and time scales of growth factor treatments. Figure 3.3 suggests that treatment with TGF- β reduced the pericytes ability to respond to PDGF-BB. The cause of this is yet unknown although it may be due to the differentiation brought on by TGF- β and the subsequent increase in PDGFR α expression in fibrotic myofibroblasts (Bonner, 2004). However, this is also unusual, as TGF- β treatment has also shown to upregulate expression of PDGFR β and therefore would make the pericytes more reactive to PDGF-BB (Andrae, Gallini & Betsholtz, 2008). Therefore, it is likely that this unusual result is down to poor method. Figures 3.12, 3.13 and 3.14 involved pericytes migrating towards CXCL12. CXCL12 is normally produced within the bone marrow in order to maintain the hematopoietic stem cell population (Rankin, 2012). However, in fibrotic lung diseases, damage to epithelial cells have been shown to increase the expression of CXCL12 which then encourages the migration of mesenchymal stem cells to the site of injury (Xu et al., 2006). Studies have also shown a strong expression of CXCL12 in the lumen of fibrotic airways as well as within the smooth muscle layers (Jaffar et al., 2020). The receptor for CXCL12, CXCR4 is present on several different cell types including epithelial cells, myeloid cells and importantly, pericytes (Jaffar et al., 2020, Xiang et al., 2019). Xiang et al. demonstrated that untreated pericytes expressed CXCR4 but that this expression can be increased, in this case, via treatment with PDGF-BB (Xiang et al., 2019). This suggests that pericytes do not need to be primed in order to express CXCR4 and therefore respond to CXCL12, but that this expression can be modulated through growth factor treatments.

Figure 3.15 highlights a distinct flaw in the methodology used for some experiments within this chapter. Both ImageJ and traditional manual methods could not distinguish between different cells within the large clumps seen in Figure 3.15. This flaw was avoided by changing method of measuring migration but could also be aided by the use of artificial intelligence (AI). Several groups have started to harness AI in image analysis due to its high throughput nature and ability to consistently perform (Morelli et al., 2021). Unfortunately, to harness the power of AI, a high level of computing power and technical knowledge would be needed which was not available within this project.

Ideally more work should also be completed relating to the migration of pericytes, as much of the methodology used was not ideal, due to the variation between experiments and between methods. The conditions used in the scratch assay experiments should be observed using live cell imaging methods which were unavailable at the time these experiments were undertaken (Pijuan, et al., 2019). This would allow the observation of the migration and would show the optimum time these experiments should be incubated. It would also allow the speed of the migration to be calculated which would likely vary between treatments due to the differences in cell metabolism in response to the treatments. In order to decrease the variation between scratch assays, the formation of the scratch could be automated by utilising well inserts which have a built-in cell-free space, produced by Ibbidi (Huang et al., 2019). This would ensure the wound size started out at a consistent size and would prevent the cell damage and build up of dead cells resulting from making a physical scratch through the cell monolayer. Including these extra methods would solidify the results observed in this chapter and further highlight the avenues that can be explored further in order to reduce pericyte migration in allergic asthma and thereby have a positive impact on lung structure and function.

The implications of exploring mediators such as growth factors and cytokines as drivers of pericyte migration is to highlight possible targets for intervention in order to reduce the abhorrent pericyte migration seen in fibrotic airways (Johnson et al., 2015). One of the key findings in this chapter is the effect of CXCL12. Movement of pericytes towards CXCL12 had not previously been explored and therefore is further discussed in Chapter 6 and in the accompanying published research paper (Bignold et al., 2022). To further study how growth factor treatments affect the sensitivity of pericytes to CXCL12, the expression of CXCR4 on pericytes following treatments with various growth factors should be explored via immunostaining or flow cytometry, as this may indicate the mechanism behind the interactions with CXCL12. In addition to growth factors, pericytes experienced increased migration in the presence of macrophages. This also may be linked to the CXCL12 axis as macrophages are known to be a source of CXCL12 especially in fibrotic tissue such as within tumours (Sanchez-Martin et al., 2011). However, this conclusion cannot be specifically drawn as factors produced by the macrophages in these experiments were not explored. This would be an interesting avenue of further study as the cross-talk between pericytes and macrophages undoubtedly has wide-reaching effects within fibrotic tissue. Another interesting aspect of growth factor treatment is its effect on the extracellular matrix composition, in particular TGF- β and periostin as both are known to exacerbate extracellular matrix deposition in lung fibrosis (O'Dwyer & Moore, 2017). However this is beyond the scope of this thesis and is currently being investigated as part of another research project within our lab.

Chapter 4 – Matricellular Protein Periostin Promotes Pericyte Migration in Fibrotic Airways and Can Be Abrogated By Cinnamaldehyde

4.1 Introduction

Allergic asthma is a common, yet complex condition involving the constriction of airways, airway wall thickening and overall reduction in airflow and increased airway hyperresponsiveness. The pathophysiology of asthma can be categorised by three aspects of airway remodelling: mucus hyperplasia, airway smooth muscle alterations, and deposition of extracellular matrix (ECM) proteins. The causes of remodelling are a much contested topic, but the general consensus is that myofibroblasts are responsible for the accumulation of contractile elements and ECM proteins in the airway wall. Pericytes are mesenchymal progenitor cells associated with the tissue microvasculature, and have been shown in organ fibrosis of varying aetiology to be a primary source of myofibroblasts. (Johnson et al., 2015, Kuppe et al., 2021, Xavier et al., 2017 Picoli et al., 2019, Birbrair et al., 2014, Hannan et al., 2020). In healthy tissue, pericytes maintain the structure and function of blood vessels and help control the transport of cells and molecules in and out of the vasculature (Ribatti, Nico & Crivellato, 2011). However, during fibrosis driven by inflammatory cytokines such as TGF- β and as observed in allergic asthma, pericytes have been observed to uncouple from capillaries within the airway wall and accumulate within and around airway smooth muscle bundles, with elevated expression of the myofibroblast marker α -smooth muscle actin (α -SMA) and a demonstrable contribution to airway hyperactivity in an allergen-driven model of allergic asthma (Johnson et al., 2015). N-cadherin antibodies were also used to observe myofibroblast characteristics and migratory capacity of pericytes (Shenoy, et al., 2016). Additionally, pericytes are also thought to be the prime source of ECM proteins in the lung (both through their contribution to the myofibroblast population and the secretion of proteins themselves) and are major contributors to several different fibrotic lung conditions such as pulmonary fibrosis and interstitial lung disease (Yamaguchi et al., 2020, Su et al., 2021, Hung et al., 2013, Bagnato & Harari, 2015).

The complex interplay between inflammatory mediators that results in the uncoupling and migration of pericytes is an important area of investigation. By identifying the main driving force in this process, pericyte migration could be inhibited or even prevented, leading to improved lung function in allergic asthma. One inflammatory mediator that deserves attention in this regard is periostin, which is an extracellular matrix-derived bioactive peptide (matrikine) that has recently been

implicated in Type 2-mediated tissue fibrosis (Burgess et al., 2021). Periostin is a matricellular protein that was first identified as a cell adhesion protein in 1993 (Takeshita et al., 1993). However, it is widely now associated with fibrosis and other pro-fibrotic cytokines. It has strong links with allergic asthma, with high serum levels of periostin being used as a biomarker of asthma severity as well as other fibrotic lung conditions including IPF where blood periostin levels can predict the progression of the disease and is elevated in the lungs of various other ILDs (interstitial lung diseases) such as usual interstitial pneumonia (Takahashi et al., 2019, Naik et al., 2012, Okamoto et al., 2011). It has also been strongly linked to TGF- β , one of the most infamous pro-fibrotic cytokines, as a co-regulatory relationship has been suggested between these two mediators (Ashley et al., 2017). The effects of periostin were also abrogated via targeting the induction of periostin production, IL-13, by a potent inhibitor, cinnamaldehyde (Mitamura et al., 2018).

4.2 Results

Initially, several online databases were searched in order to establish the significance of periostin in several fibrotic lung diseases and to observe whether the gene for periostin expression, POSTN, is upregulated.

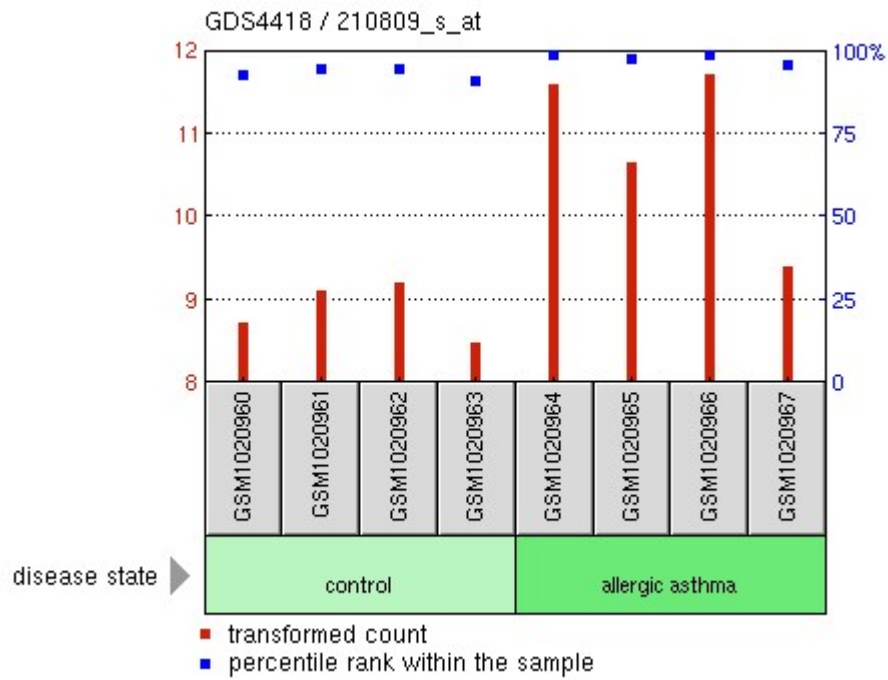


Figure 4.1 – The gene for periostin is increased in humans with allergic asthma. periostin gene expression data obtained from RNA from biopsies performed by Chamberland et. Al. Data accessible at NCBI GEO database (Edgar, Domrachev & Lash., 2002), accession GSE41649 (Chamberland et. al., 2009).

An expression profile was constructed from an array performed on the bronchial biopsies of patients with allergic asthma. The transformed counts of POSTN for 3 of the 4 patients with asthma was higher than the control.

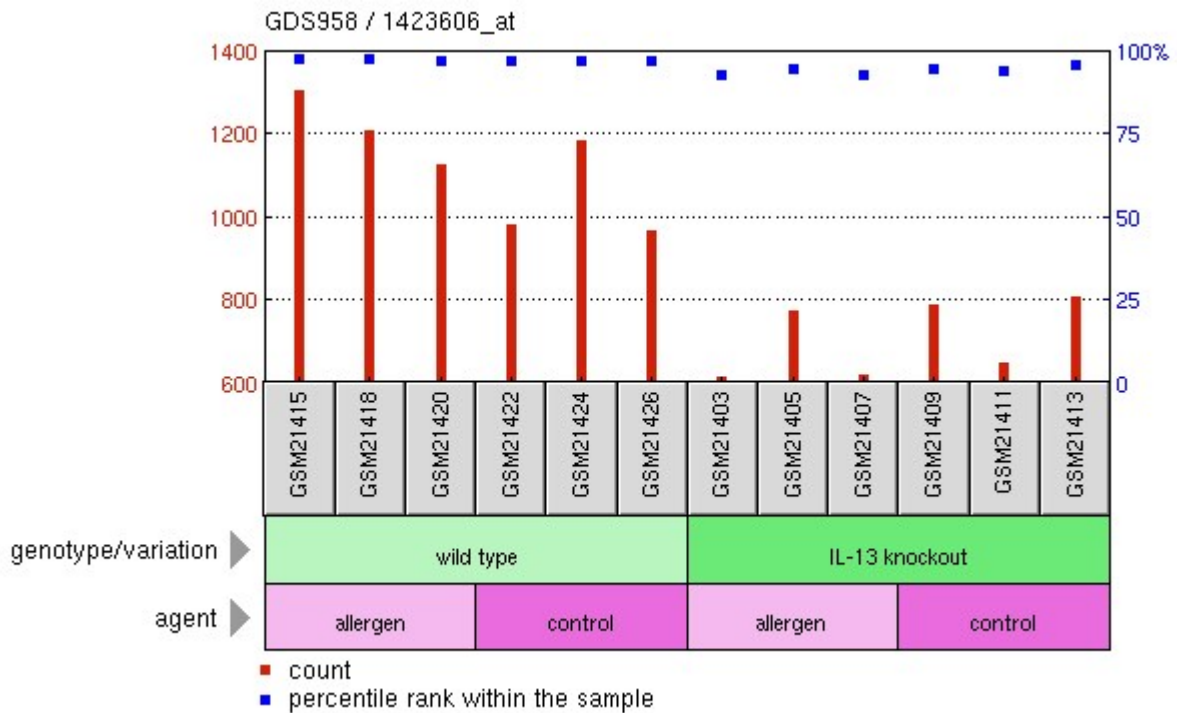


Figure 4.2 – The gene for periostin is increased in wild type mice given HDM but not in IL-13 knockouts. Gene expression data obtained from mouse lung tissue. The mice were either wild-type or IL-13 knockout which were treated with either house dust mite or a control. Data accessible at NCBI GEO database (Edgar, Domrachev & Lash, 2002), accession GSE1301.

This dataset indicates that POSTN RNA is dependent on IL-13 as all mice which were unable to produce IL-13 had a vast reduction in POSTN RNA. There was a little difference in POSTN RNA in wild type mice with those treated with HDM having a slightly higher expression than the control treated mice.

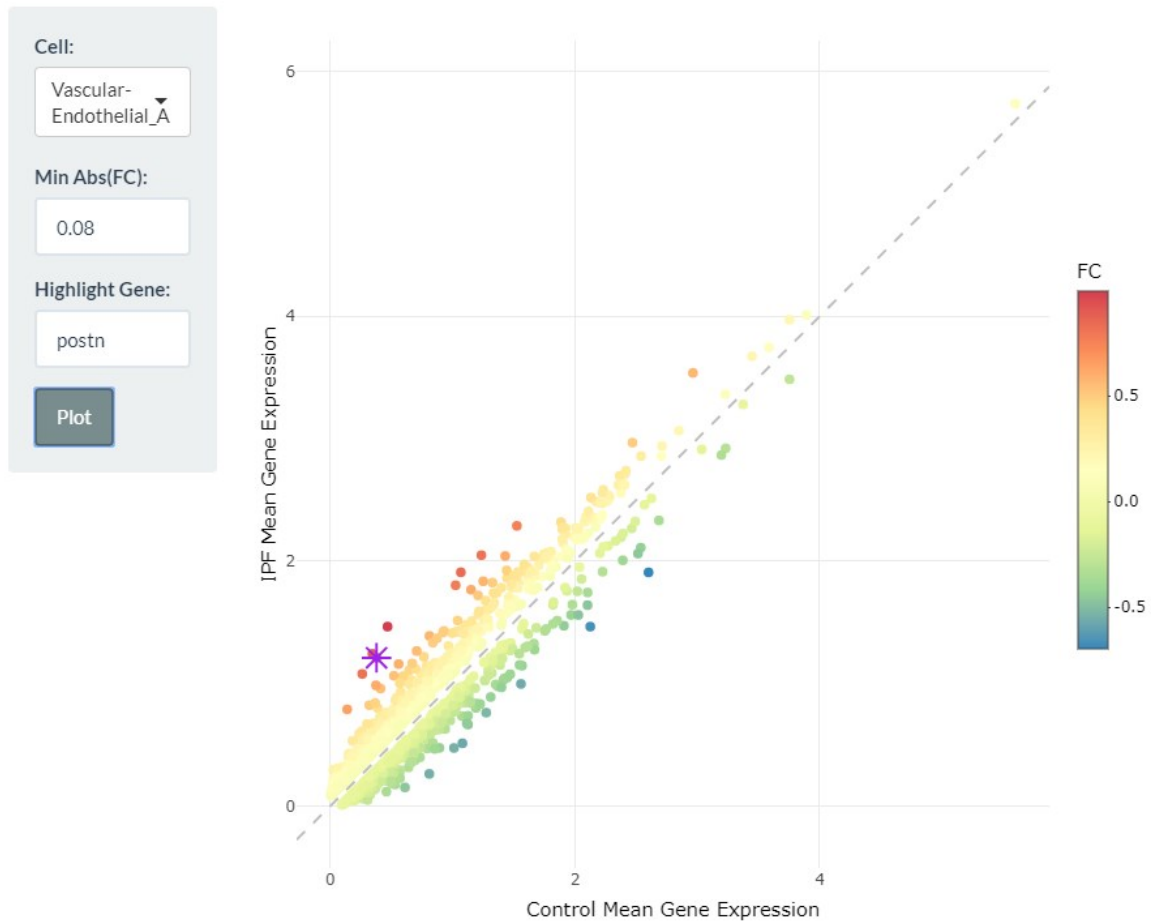


Figure 4.3 – The increase and decrease of gene expression in IPF lungs compared to healthy lungs using single cell RNA-seq. The purple asterisk indicates *POSTN*. Data obtained from IPF Cell Atlas and Adams et al. (Neumark et al., 2020, Adams et al. 2020).

Figure 4.3 indicates the genes which are upregulated and downregulated in lung vascular endothelial cells with idiopathic pulmonary fibrosis. The purple asterisk shows that *POSTN* is strongly upregulated in IPF endothelial cells than the control endothelial cells.

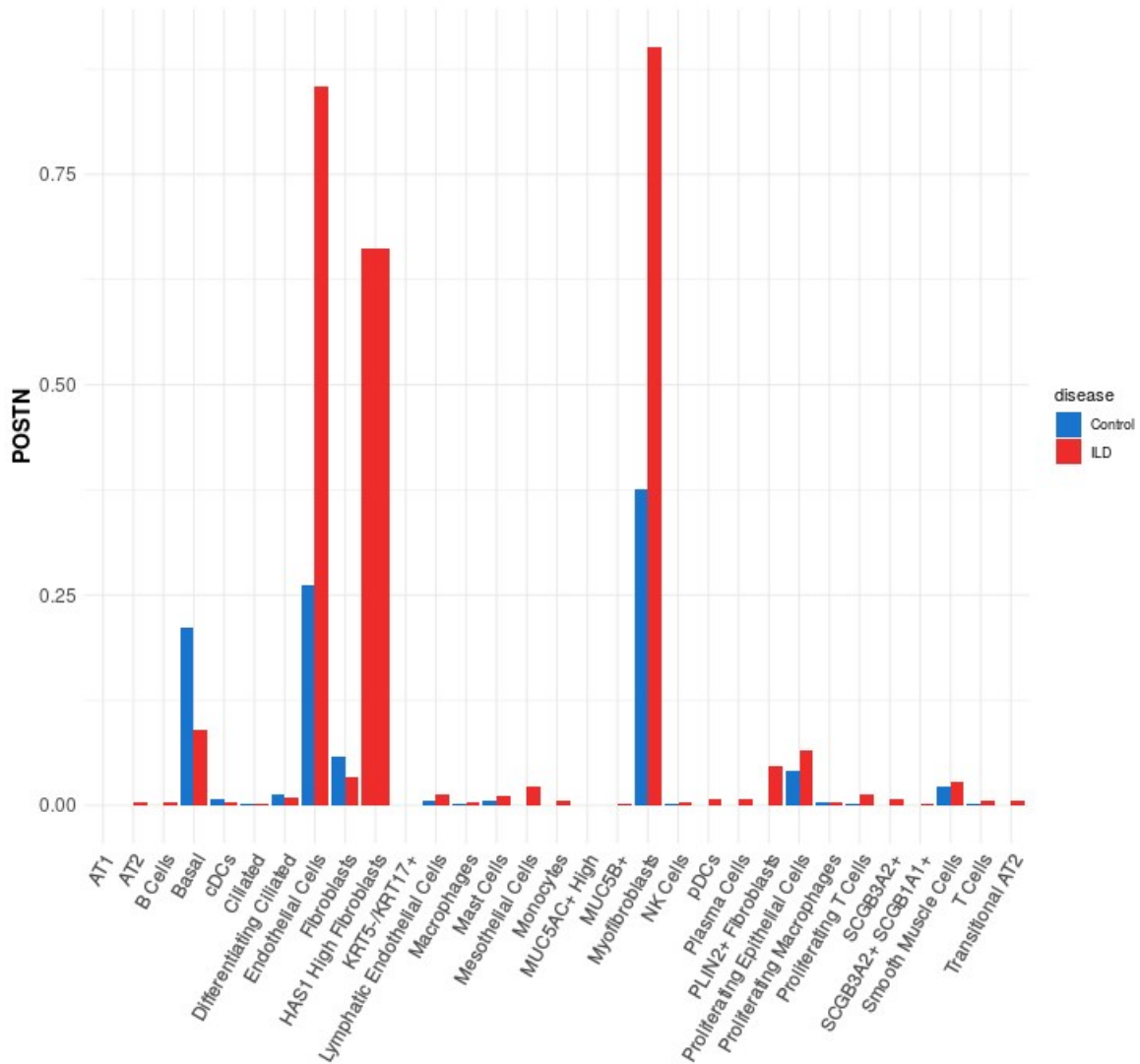


Figure 4.4 – The gene expression of periostin in lungs with interstitial lung disease compared to healthy lungs using single-cell RNA-sequencing. All data obtained from IPF Cell Atlas and Habermann et al. (Neumark et al., 2020, Habermann et al., 2020)

Figure 4.4 highlights the expression of POSTN in each cell type in ILD lungs vs healthy lungs. In myofibroblasts and endothelial cells POSTN expression is relatively high in healthy lungs compared to other cell types. This expression only increased further in the ILD lungs.

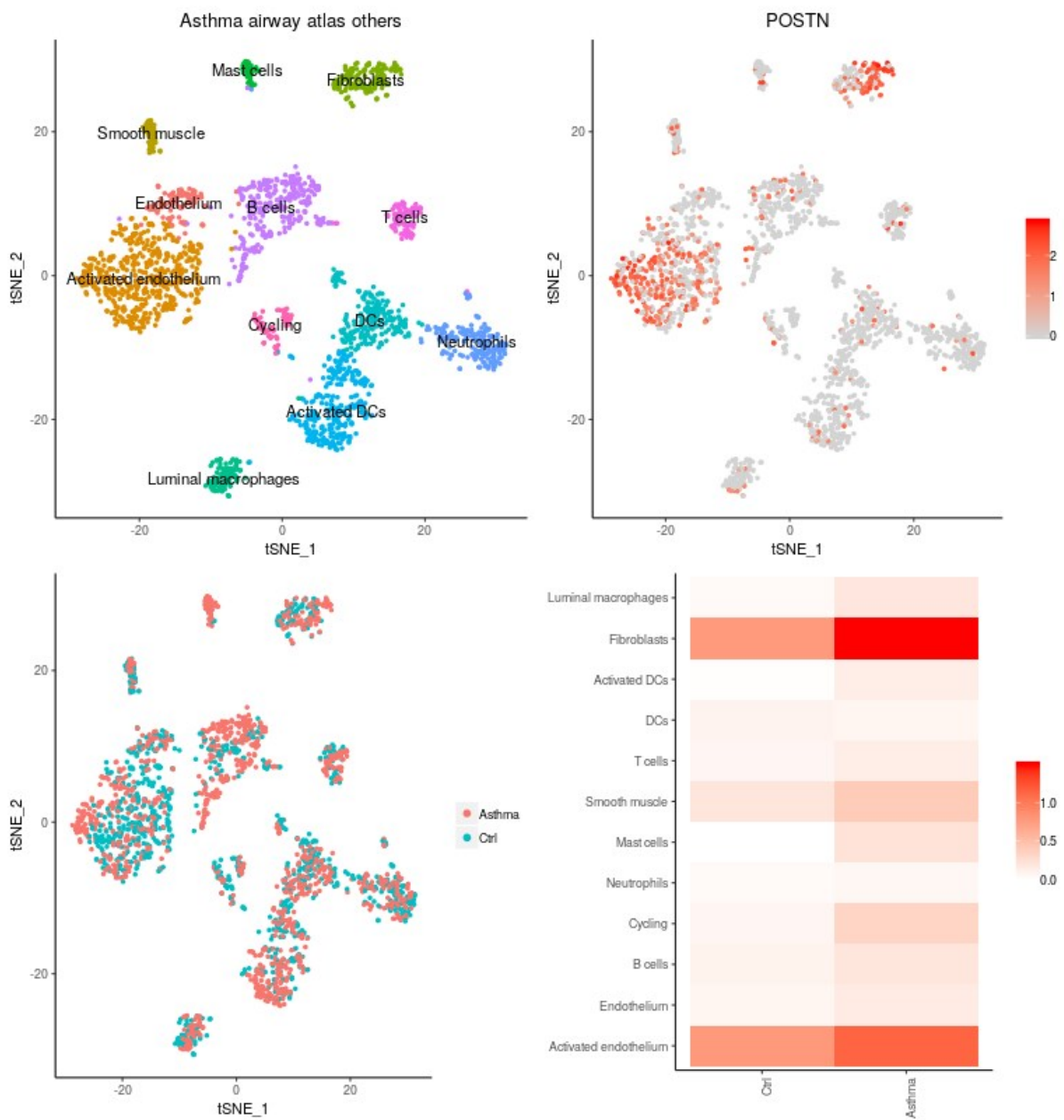


Figure 4.5 –The expression of POSTN in asthmatic lung cell types using single-cell transcriptomics. All data obtained from the Wellcome Sanger Institute Cell Atlas (<https://asthma.cellgeni.sanger.ac.uk/>, Regev et al., 2017)

Figure 4.5 shows that POSTN expression is clustered in the activated endothelium and in fibroblasts in particular. Expression in both of these areas is higher in asthmatic lungs than in the control lungs. There is very little POSTN expression in the other cell types tested although, in general, all expression of POSTN was higher in asthmatic lungs except in dendritic cells and neutrophils in which is it the same as in control lungs.

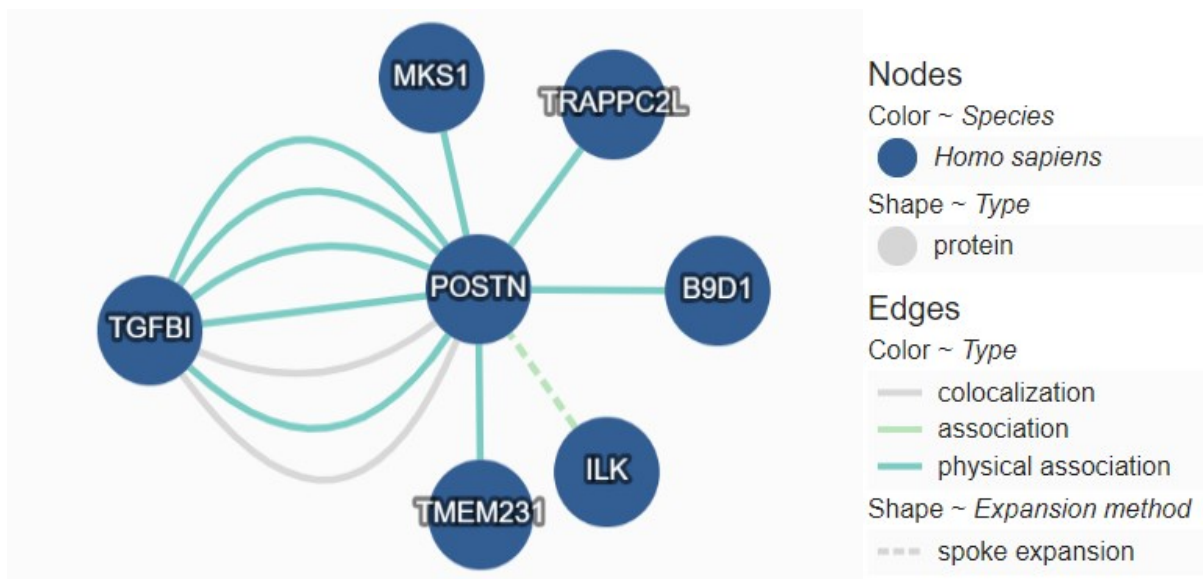


Figure 4.6 – Protein interactions of periostin. Data obtained from IntAct database by EMBL-EBI which includes many different data sets using a variety of methods such as pull-down affinity chromatography, confocal microscopy and anti bait coimmunoprecipitation (Orchard et al., 2013).

Figure 4.6 shows several protein interactions periostin is thought to have. It shows there are strong links between periostin and TGF- β 1 through co-localisation and physical interaction. Most of the other proteins mentioned are involved with the transport of proteins across membranes. The interactions with TGF- β were determined by anti-bait co-immunoprecipitation, pull down and confocal microscopy methods.

Taken together, this bioinformatics assessment highlighted the importance of the gene encoding periostin in various fibrotic lung conditions such as ILD and IPF. Thus, we elected to assess periostin expression in pericytes in response to fibrotic stimuli in order to simulate fibrotic conditions and observe the effect of the protein periostin on pericytes. We performed this by utilising scratch assays, immunostaining and ELISAs in order to observe periostin levels and its effect on the migration of pericytes.

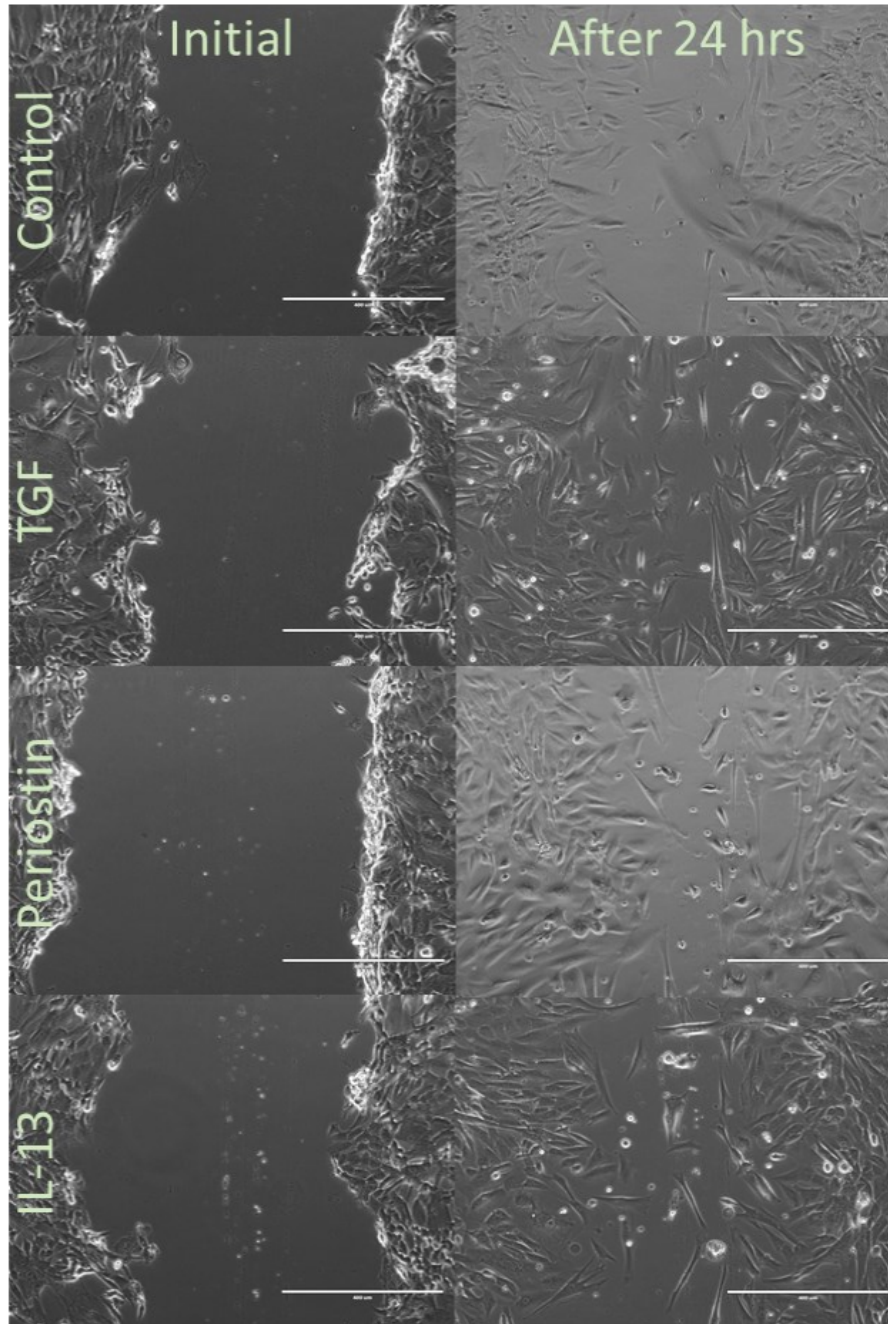


Figure 4.7 – Pericytes migrate into the cell free space more when treated with TGF- β or periostin. Representative images from scratch assay performed on pericytes that were grown in pericyte medium and treated with 10 ng/ml of TGF- β , 100ng/ml of IL-13 or 100 ng/ml of periostin for 48 hours. Cells were transferred into serum-free medium and a scratch was made in each monolayer using a p200 pipette tip. Images were taken at 100x magnification immediately after scratching at 24 hours later. N=6, representative of 2 independent experiments. Scale bar = 400 μ m.

The representative images selected from the scratch assay show that all pericytes exhibit migration

after 24 hours irrespective of their treatment. However, it was also apparent that treatment with TGF- β , periostin or IL-13 increased the ability of pericytes to migrate and therefore resulted in a smaller wound after 24 hours. The images also show that there may have been increased cell death in the TGF- β and IL-13 conditions due to the increased number unadhered cells present following the 24-hour incubation. This may have increased the size of the wound as cells were removed, although the wound still had a clear boundary which allowed it to still be measured accurately.

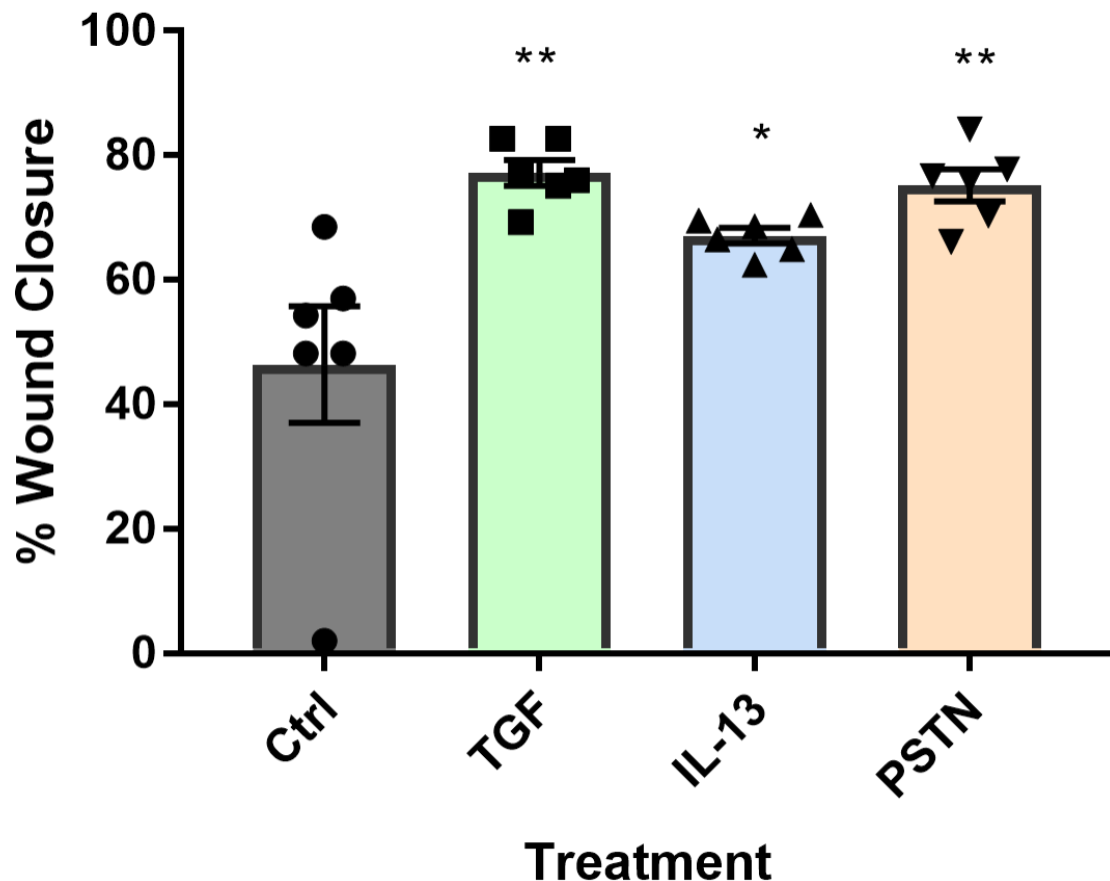


Figure 4.8 – Pericytes migrate more when treated with either TGF- β or periostin. Scratch assay performed on pericytes that were grown in pericyte medium and treated with 10 ng/ml of TGF- β , 100 ng/ml of IL-13 or 100 ng/ml of periostin for 48 hours. Cells were transferred into serum-free medium and a scratch was made in each monolayer using a p200 pipette tip. Images were taken at 100x magnification immediately after scratching at 24 hours later. The size of the scratches were determined using ImageJ and percentage wound closure was calculated. n=6 from 2 independent experiments (each consisting of 3 technical replicates), “***” = $p < 0.01$, “*” = $p < 0.05$ vs. untreated cells by one-way analysis of variance (ANOVA) for multiple groups with the Tukey post hoc test.

Figure 4.8 shows the numerical analysis of the images that were represented in Figure 4.7. It shows that treatment with TGF- β or periostin significantly increased the migration of pericytes compared to the untreated pericytes ($p=0.0154$, $p=0.0277$). However, the IL-13 treatment only slightly

increased migration and therefore the results were not significant. As the pericytes were incubated in serum free medium, cell proliferation is arrested and therefore any increase in cell mass in the wound is likely to be from pericytes which have moved into the area. Data from previous experiments (in Chapter 3) were chosen not to be included within this analysis, allowing this data to not require normalisation.

As well as scratch assays, Transwell assays were also utilised to explore the migration of pericytes in response to periostin. Serum free was used to simulate non-directional movement and FCS was then added in order to attract the pericytes. Pericytes treated with TGF- β and untreated cells significantly migrated more towards FCS rather than serum free medium ($p=0.0018$, $p=0.0151$). However, treatment with periostin did not induce an increase in migration, even towards medium containing FCS.

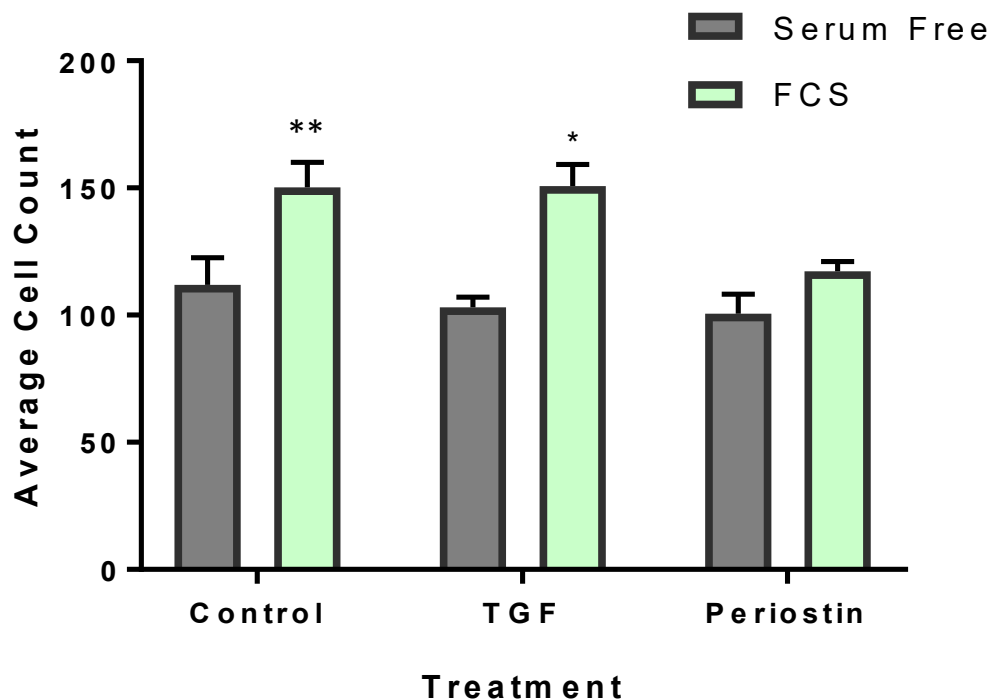


Figure 4.9 - Treating pericytes with periostin did not increase their migration towards either serum free medium or medium containing FCS in Transwell assays. Transwell assay performed on pericytes that were grown in pericyte medium and treated with 10 ng/ml of TGF- β or 100 ng/ml of periostin for 48 hours. All cells migrated towards either DMEM without serum or DMEM with 10% FCS. The mean of 5 counts from 2 membranes have been plotted. Images show examples of counts of cells migrating towards media with 10% FCS to demonstrate cell clumping observed in the treated conditions. "***" = $p < 0.01$, "**" = $p < 0.05$ to serum free cells by two-way ANOVA with Šidák's multiple comparisons test.

It is well documented that periostin can be produced by epithelial cells in vivo and therefore we also assessed the periostin expression by pericytes in vitro.

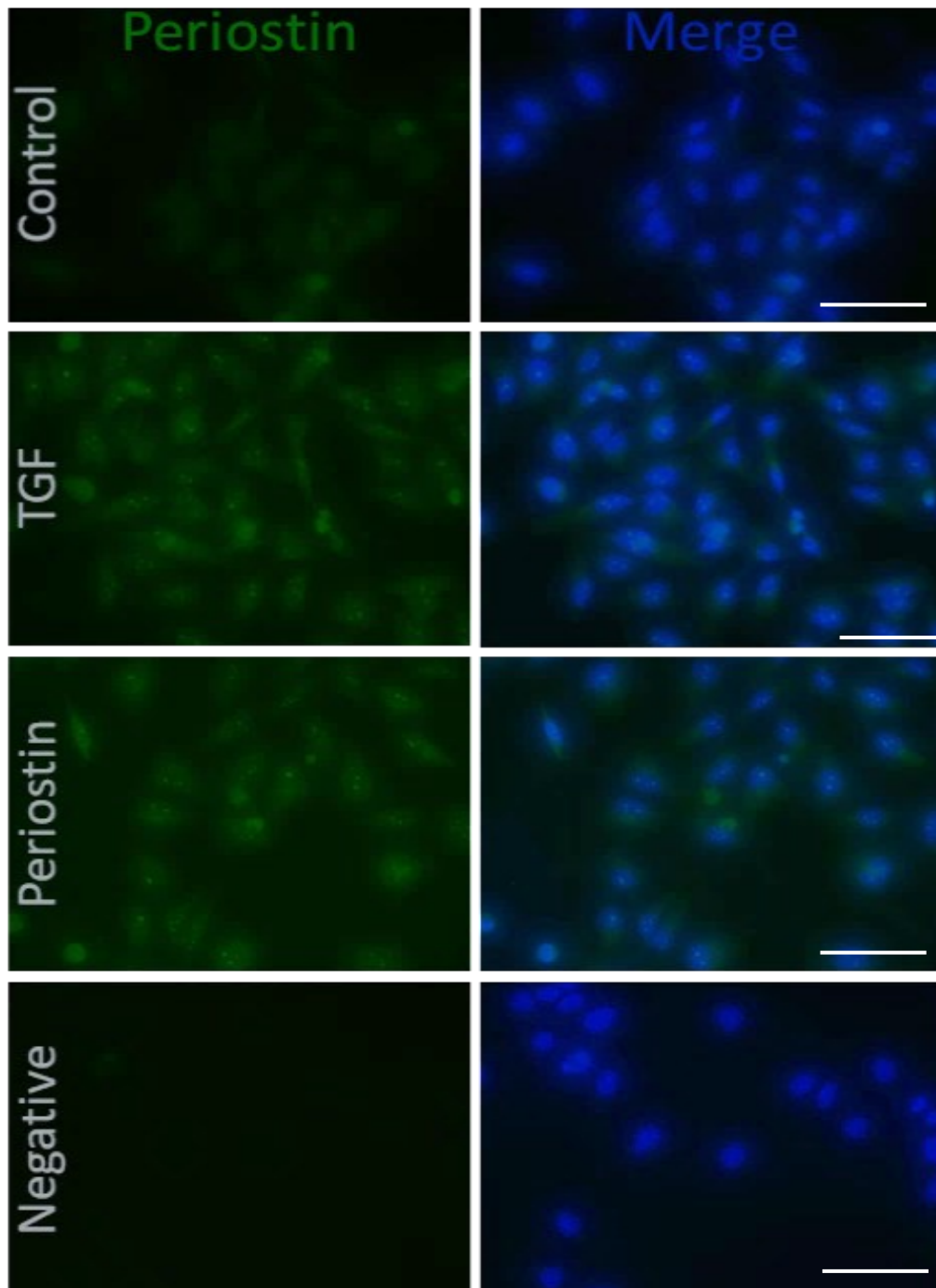


Figure 4.10 – TGF- β or periostin treatment increases the expression of periostin by pericytes. Immunostaining performed on pericytes grown in pericyte medium and treated with 10 ng/ml of TGF- β or 100 ng/ml of periostin for 24 hours. Cells were stained with an anti-periostin antibody (green) and the nuclear stain DAPI (blue). Images were taken at 400x magnification. Negative control contains just the secondary antibody and DAPI to control for non-specific binding. Scale bars = 100 μ m

Cultured pericytes were treated with pro-fibrotic cytokines TGF- β and periostin in order to simulate the conditions of fibrosis seen in allergic asthma. Untreated pericytes are shown to spontaneously produce low levels of periostin. These images show that this production is increased with the treatment of TGF- β and periostin. There is a similar number of cells in each image although this slight natural variation was reduced by calculating the expression of periostin per cell.

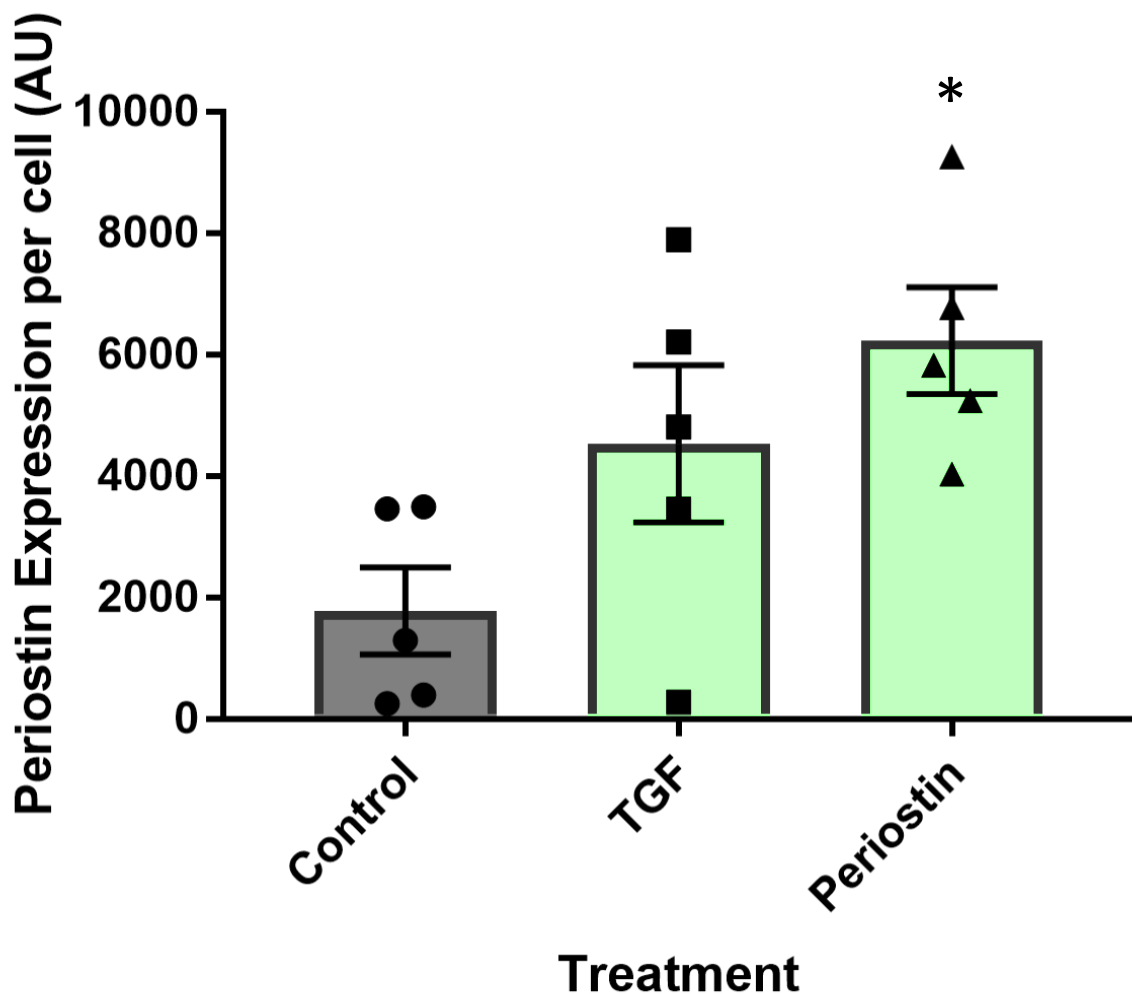


Figure 4.114 – Treating pericytes with periostin increases their expression of periostin. Immunostaining performed on pericytes grown in pericyte medium and treated with 10 ng/ml of TGF- β or 100 ng/ml of periostin for 24 hours. Cells were stained with an anti-periostin antibody (green) and the nuclear stain DAPI (blue). Images were taken at 400x magnification and intensity of periostin stain was calculated with ImageJ. Intensity of stain per field of view was divided by the number of cells in order to determine periostin expression per cell. * $p < 0.05$, $n = 5$, by one-way analysis of variance (ANOVA) for multiple groups with the Tukey post hoc test.

Following morphometric analysis by Image J of images including those seen in Figure 4.10, Figure 4.11 shows that periostin treatment significantly increased periostin production compared to the control ($p = 0.0205$), although TGF- β treatment increased periostin production almost as much. The

insignificance of the TGF- β treated group ($p=0.165$) is likely due to the larger spread of the data, which could be solved by performing more repeats.

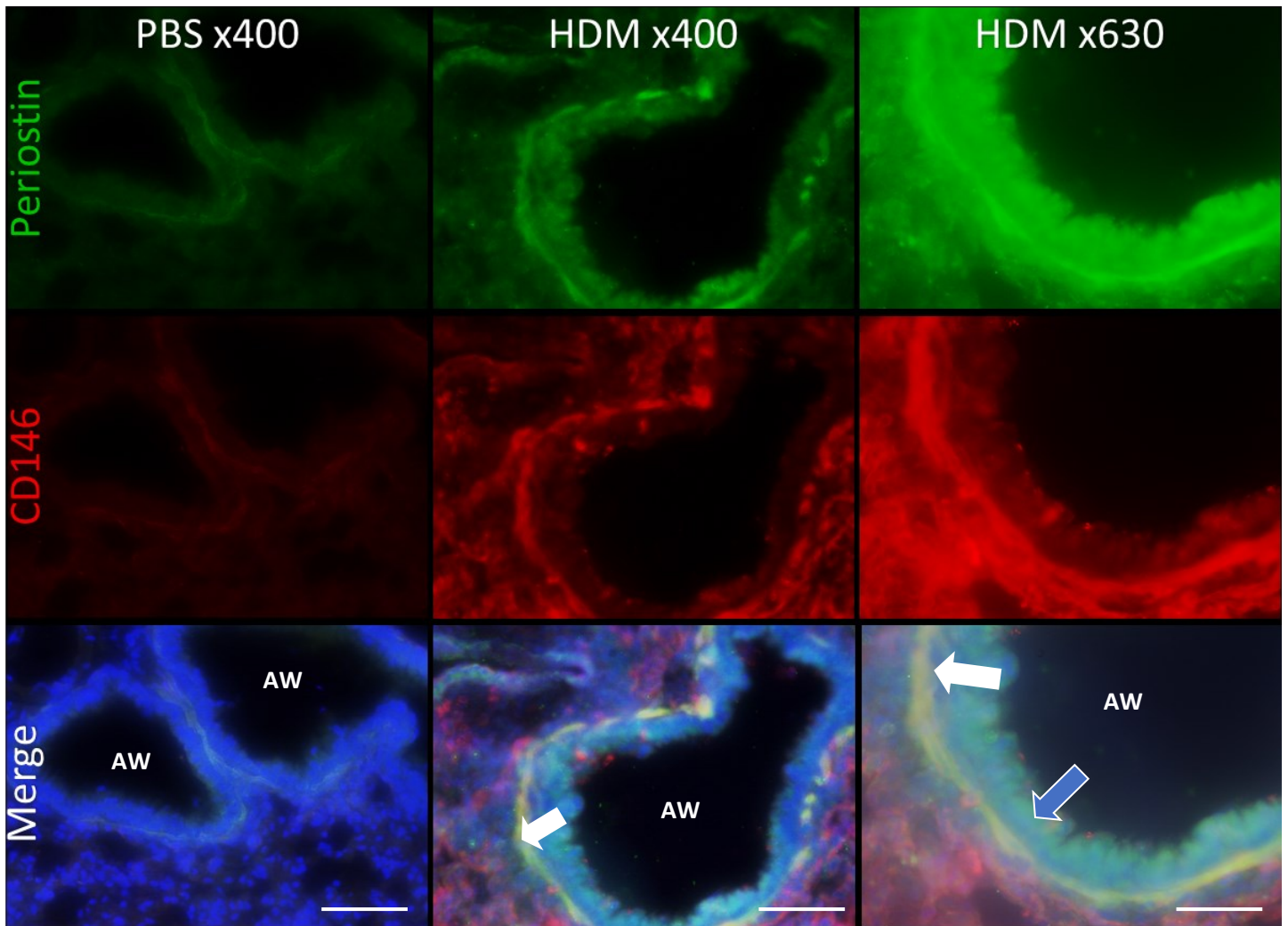


Figure 4.12 – Periostin and CD146 positive cells form a robust ring around airways that were exposed to HDM. Female C57/Bl6 mice (6-8 weeks old) were exposed to either sterile PBS (10 μ L) or house dust mite extract (HDM; 25 μ g in 10 μ L) five days a week for 5 consecutive weeks. At the end of the protocol, lung sections obtained from PBS control and HDM-exposed mice were stained with an anti-periostin antibody (green), an anti-CD146 antibody (red) and the nuclei stain DAPI (blue). Images were taken at 400x and 630x magnification as stated. White arrows indicate periostin and CD146 positive cells. Blue arrow indicates periostin present in the epithelium. “AW” = airway. Scale bars = 300 μ m.

Fibrotic lung tissue has been shown to exhibit increased levels of periostin expression, as compared to healthy control lungs. These fibrotic lungs also showed aspects of remodelling including thickened smooth muscle. This can be seen visually in Figure 4.12, which shows a robust ring of cells within the subepithelium which stained strongly for periostin as well as CD146, a pericyte marker. This ring of cells was not present in any of the lungs which had not been exposed to HDM. Conversely, PBS treated lungs showed a very low level of periostin expression overall. Periostin is also clearly visible within the epithelial cells surrounding the airways which has also been previously described by several studies including Burgess et al. (Burgess et al., 2019).

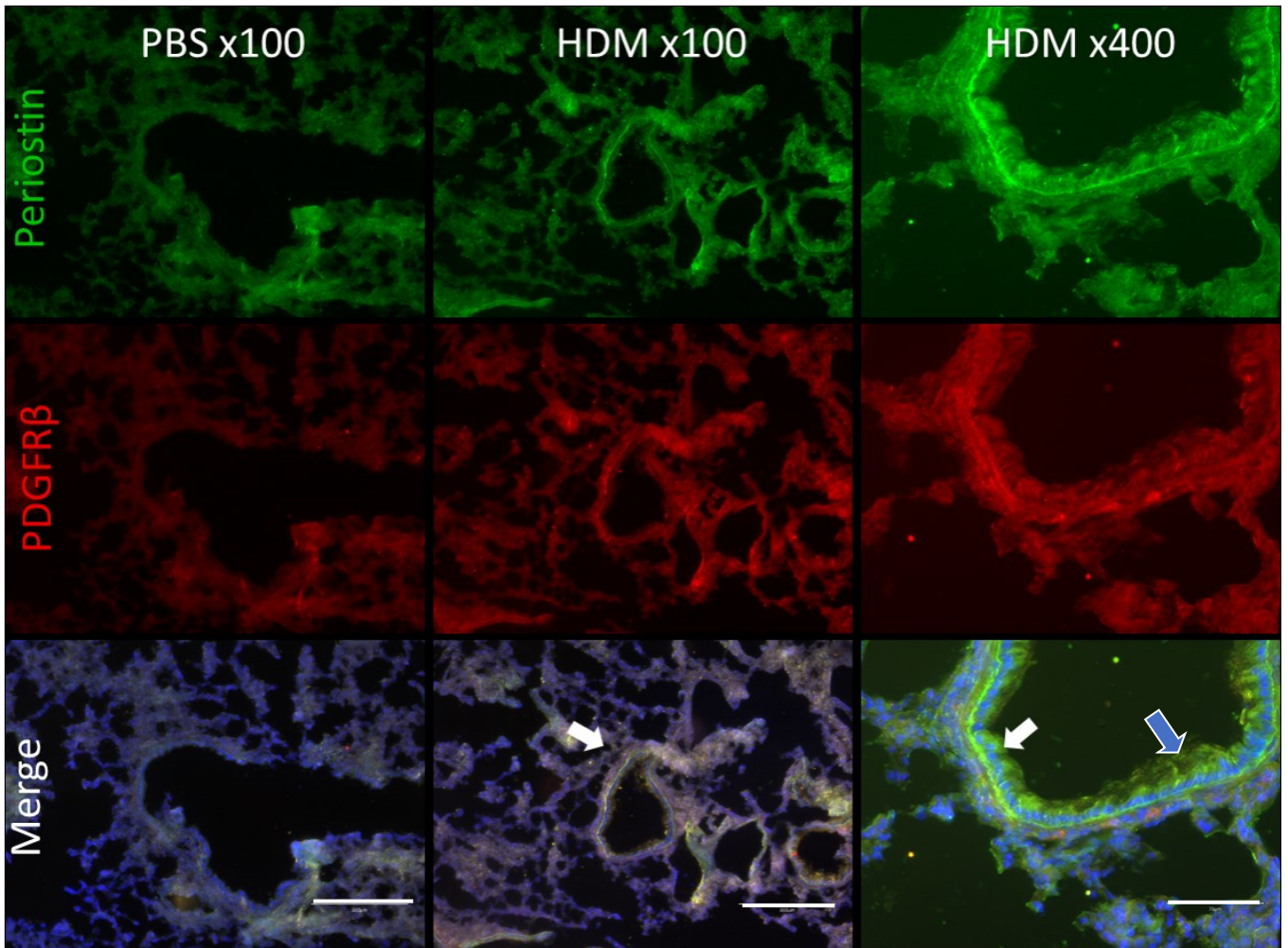


Figure 4.13 - Periostin and PDGFR β positive cells form a robust ring around airways that were exposed to HDM. Female C57/Bl6 mice (6-8 weeks old) were exposed to either sterile PBS (10 μ L) or house dust mite extract (HDM; 25 μ g in 10 μ L) five days a week for 5 consecutive weeks. At the end of the protocol, lung sections obtained from PBS control and HDM-exposed mice were stained with an anti-periostin antibody (green), an anti-PDGFR β antibody (red) and the nuclei stain DAPI (blue). Images were taken at 100x and 400x magnification as stated. White arrows indicate periostin and PDGFR β positive cells. Blue arrow indicates periostin present in the epithelium. Scale bars = 300 μ m

Figure 4.13 corroborates the results shown in Figure 4.12. Again, a robust layer of periostin positive cells is observed around the fibrotic airway wall and is also positive for a pericyte marker, in this case PDGFR β . This suggests these cells are pericytes. There is also periostin signal once again present in the epithelium in addition to the layer of cells within the airway wall. The magnification of the images in Figure 4.13 is not as large as that shown in Figure 4.12 and so it is harder to see the exact location of the stains. The quality of the tissue is also not as good and therefore there is minimal basement membrane surrounding the airway to observe the surrounding area. This also makes it difficult to observe other aspects of remodelling although these mice did show symptoms of

respiratory distress following exposure to HDM. The negative control, PBS treated lung tissue, also has airways without this strong double positive layer of cells.

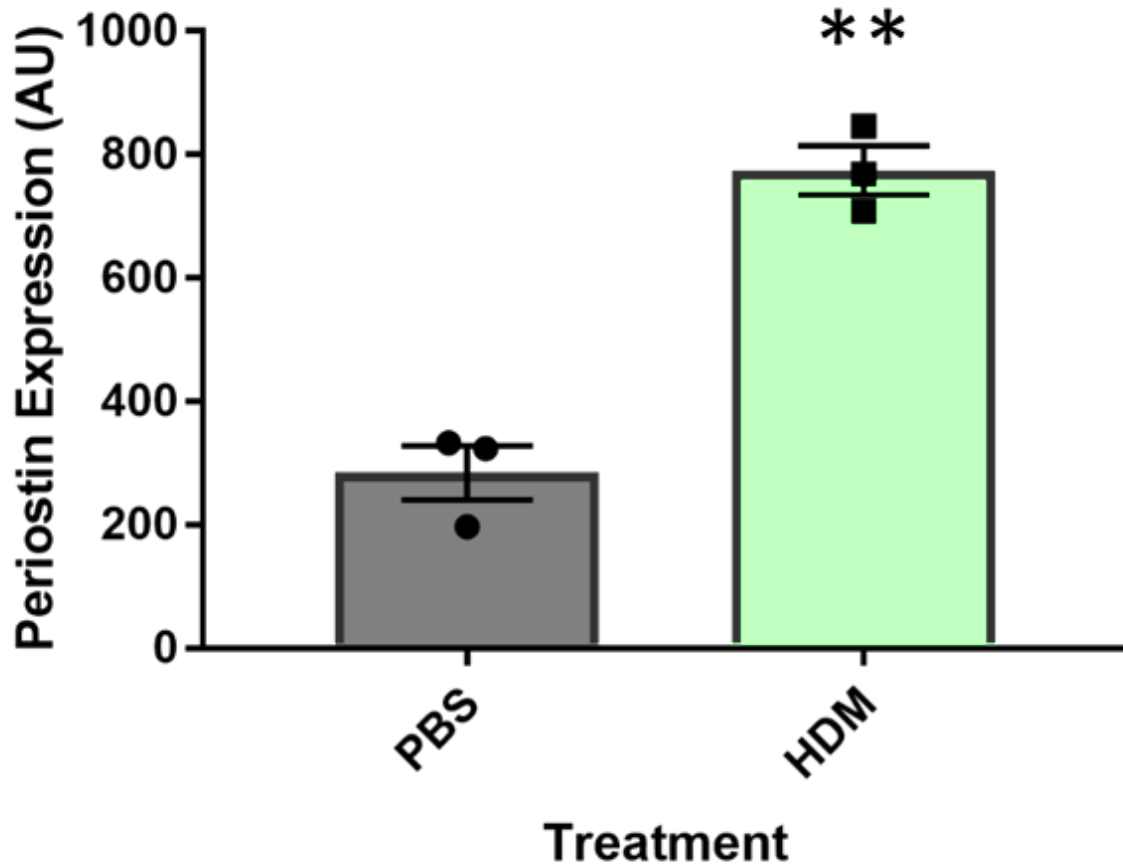


Figure 4.14 – HDM-exposed lung tissue expressed significantly more periostin than PBS tissue. Female C57/Bl6 mice (6-8 weeks old) were exposed to either sterile PBS (10 μ L) or house dust mite extract (HDM; 25 μ g in 10 μ L) five days a week for 5 consecutive weeks. At the end of the protocol, lung sections obtained from PBS control and HDM-exposed mice were stained with an anti-periostin antibody (green) and the nuclei stain DAPI (blue). Images were taken at 400x and 630x magnification as stated. Arrows indicate periostin positive cells. Expression of periostin was calculated in the area of interest around each airway using ImageJ. “***” = $p < 0.01$, $n = 3$, by one-way analysis of variance (ANOVA) for multiple groups with the Tukey post hoc test.

The images from the previous experiment were analysed with ImageJ. A region of interest was selected at a consistent distance around the airways. This confirmed that lungs that were exposed to HDM had significantly higher expression of periostin than control lungs given PBS ($p = 0.0012$). A triple stain could be performed with a pericyte marker in order to confirm the identity of the periostin positive cells.

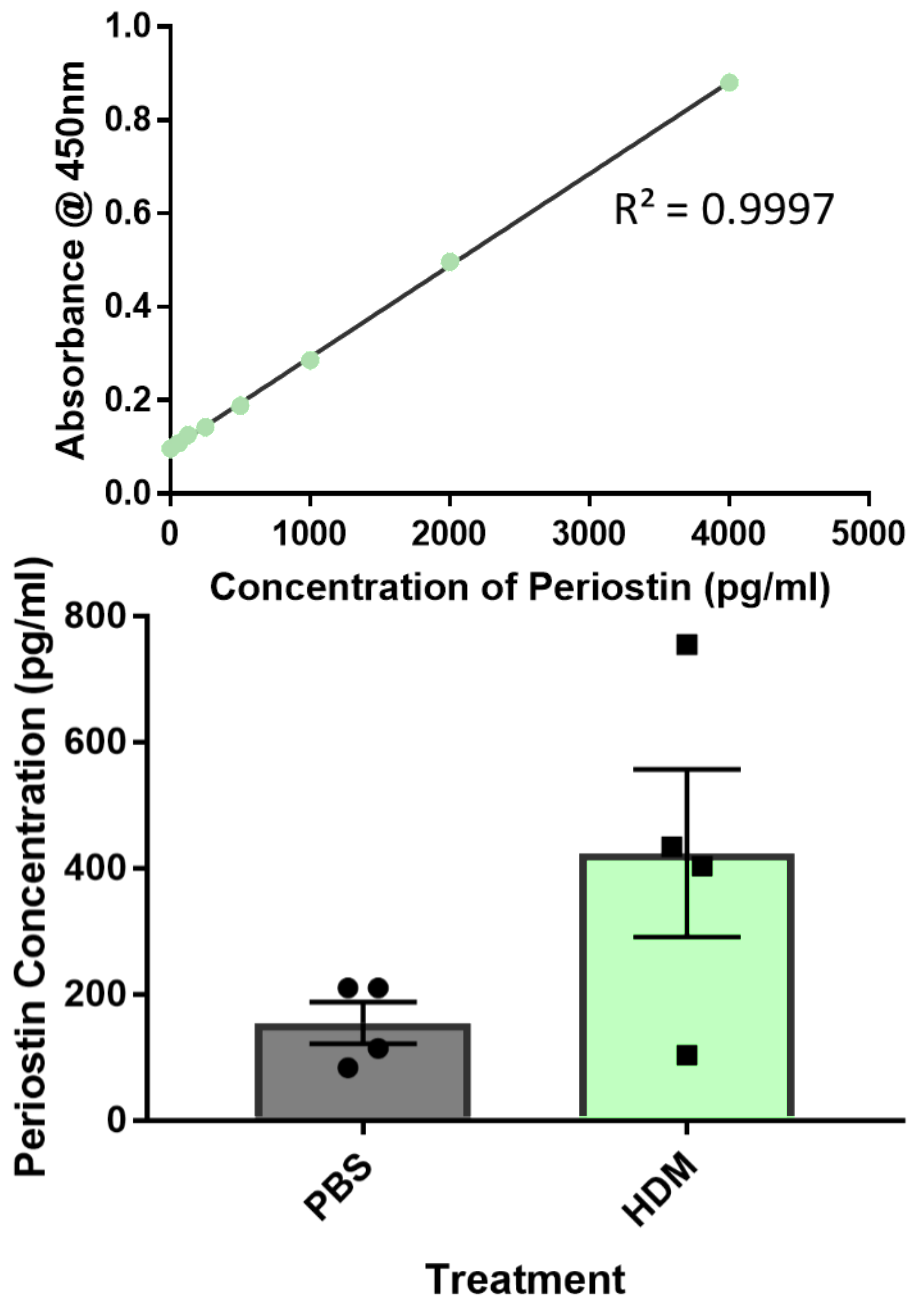


Figure 4.15 – BAL from HDM-exposed mice contained slightly more secreted periostin than PBS mice. Female C57/Bl6 mice (6-8 weeks old) were exposed to either sterile PBS (10 μ L) or house dust mite extract (HDM; 25 μ g in 10 μ L) five days a week for 5 consecutive weeks. At the end of the protocol, bronchoalveolar lavage samples were harvested. The periostin content of the lavage fluid was assessed via ELISA. Results were not significant ($p < 0.05$), by one-way analysis of variance (ANOVA) for multiple groups with the Tukey post hoc test

Fluid obtained from HDM treated mice via bronchoalveolar lavage was assessed with a periostin-specific ELISA to test for serum periostin concentration. HDM lavage contained slightly more secreted periostin than control PBS mice although this was not significant. This may be due to the natural variation in biological systems as there is a wide range of data in the HDM condition. The R^2 value is very close to 1 which suggests the assay was performed accurately.

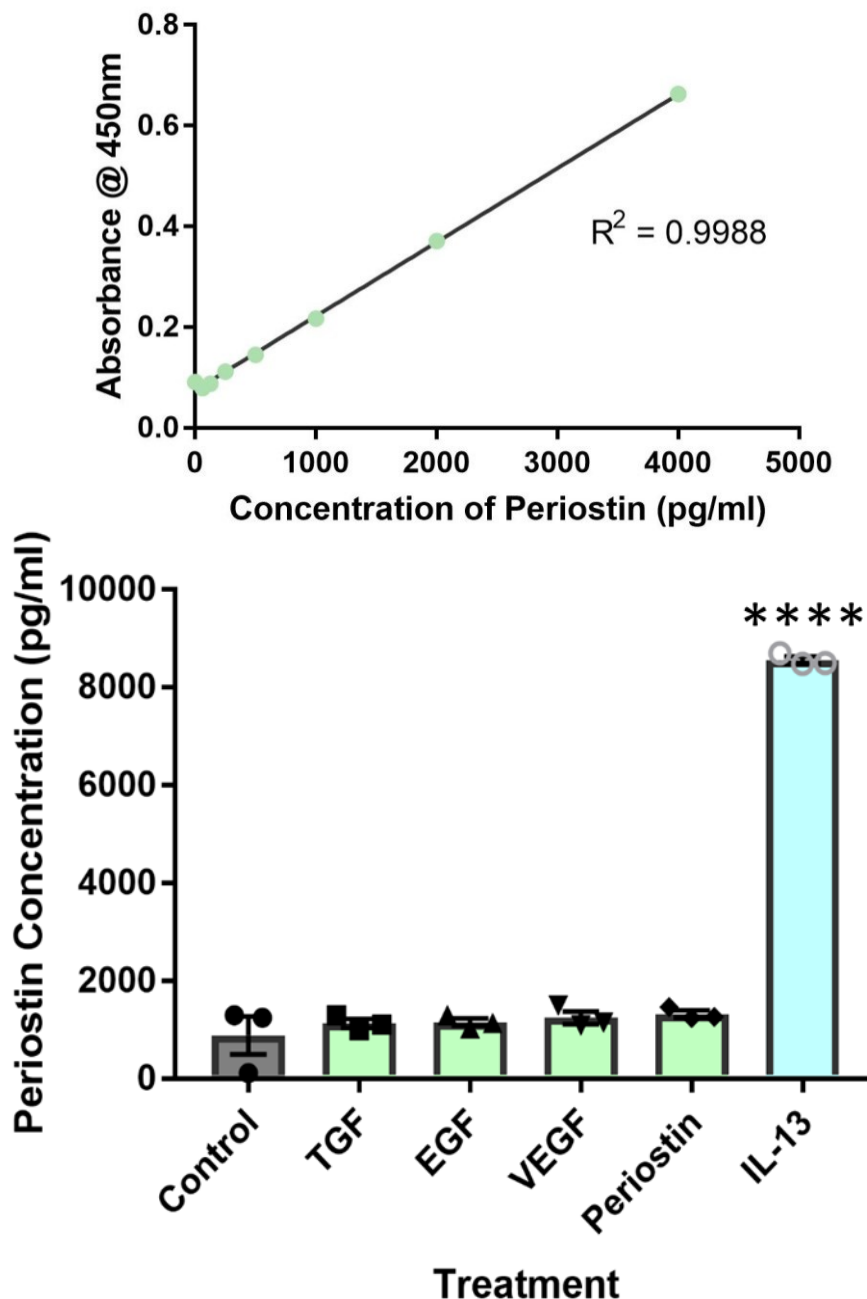


Figure 4.16 – IL-13 treatment caused pericytes to secrete significantly more periostin than other cytokines. Cultured pericytes were treated with 10ng/ml TGF- β , 10ng/ml EGF, 10ng/ml VEGF, 100ng/ml IL-13 or 100ng/ml Periostin in pericyte medium for 7 days before the supernatant was harvested. The periostin content was assessed using an anti-periostin ELISA kit. “****” = $p < 0.0001$, $n = 3$, by one-way analysis of variance (ANOVA) for multiple groups with the Tukey post hoc test.

ELISAs were utilised to measure the free periostin protein levels produced by treated cultured pericytes. Various growth factors were explored in order to examine the relationship between cytokines which are thought to be involved in inflammation and fibrosis and periostin. Most growth factor treatments did not induce the production of free periostin in cultured pericytes as supernatants from pericytes treated with TGF- β , EGF, VEGF and periostin contained the same concentration of periostin as the supernatant from untreated cells. Conversely, the supernatants from pericytes treated with IL-13 contained a greatly increased concentration of periostin, an almost sevenfold increase.

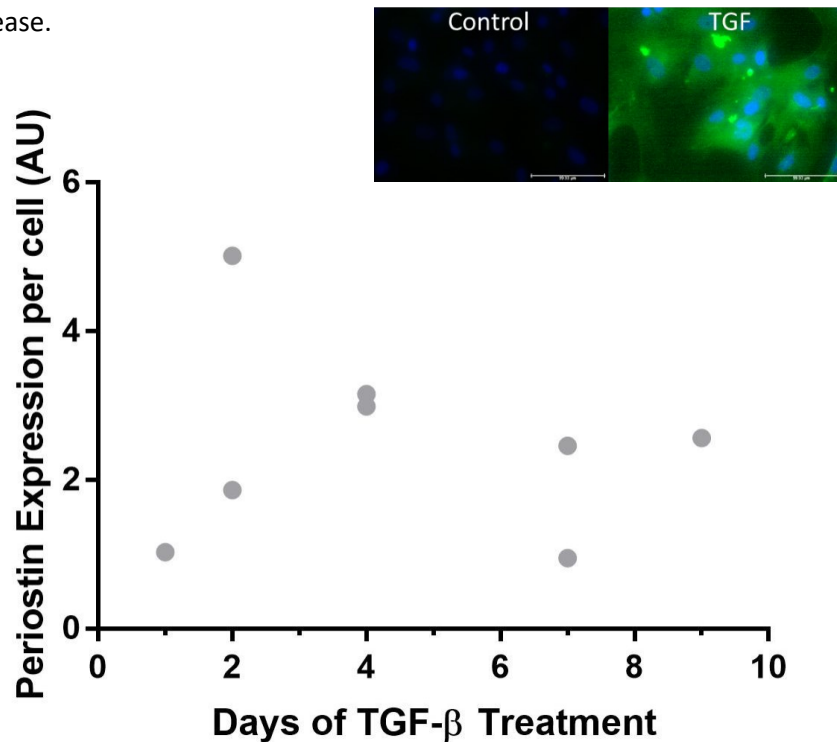


Figure 4.17 - Periostin expression by pericytes peaked at around 3 days of TGF- β treatment. Immunostaining performed on pericytes grown in pericyte medium and treated with 10 ng/ml of TGF- β for 24, 48, 96, 168 or 216 hours. Cells were supplemented with TGF- β every 2 days to maintain the treatment. Cells were stained with an anti-periostin antibody and intensity of periostin stain at 400x magnification was calculated with ImageJ. Intensity of stain per field of view was divided by the number of cells in order to determine periostin expression per cell. Results were normalised to 24 hours of TGF- β treatment. $n=1-2$, all results are not significant. Inset includes representative staining images. Scale bars = 100 μ m.

Various time points were explored in this pilot study in order to see if extended exposure to growth factors influenced a change in the expression of periostin. There is no significant difference in the expression of periostin after treating pericytes with TGF- β for up to 9 days. This is likely due to the low N numbers used in this study. Larger N numbers were attempted but long exposure to TGF- β reduced cell viability, preventing cells surviving to the end of the experiment in order to be stained. There was also a large variation between pericytes in the same group which could, again, be due to cell death in certain well.

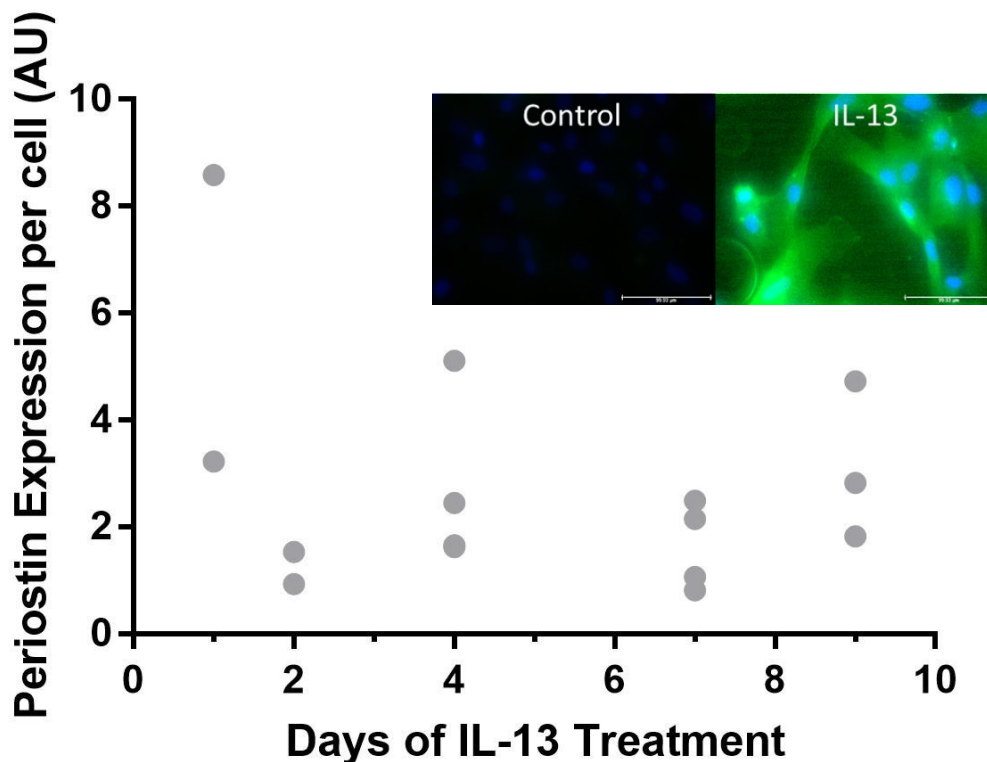


Figure 4.18 – Periostin expression by pericytes remained constant throughout 9 days of IL-13 treatment. Immunostaining performed on pericytes grown in pericyte medium and treated with 100 ng/ml of IL-13 for 24, 48, 96, 168 or 216 hours. Cells were supplemented with IL-13 every 2 days to maintain the treatment. Cells were stained with an anti-periostin antibody and intensity of periostin stain at 400x magnification was calculated with ImageJ. Intensity of stain per field of view was divided by the number of cells in order to determine periostin expression per cell. n=2-4, all results are not significant. Inset includes representative staining images. Scale bars = 100µm.

Again, several time points were explored in order to explore the effect of extended IL-13 treatment on the production of periostin by pericytes. Although there was no significant difference between each treatment group, a slight trend can be seen. The highest production of periostin came after 1 day of IL-13 treatment and longer treatments resulted in a lower expression of periostin. Similar to in Figure 4.18, there was no significant difference between treatments which is likely due to the low n numbers and therefore should be repeated several times to increase the n numbers and fully elucidate the trend.

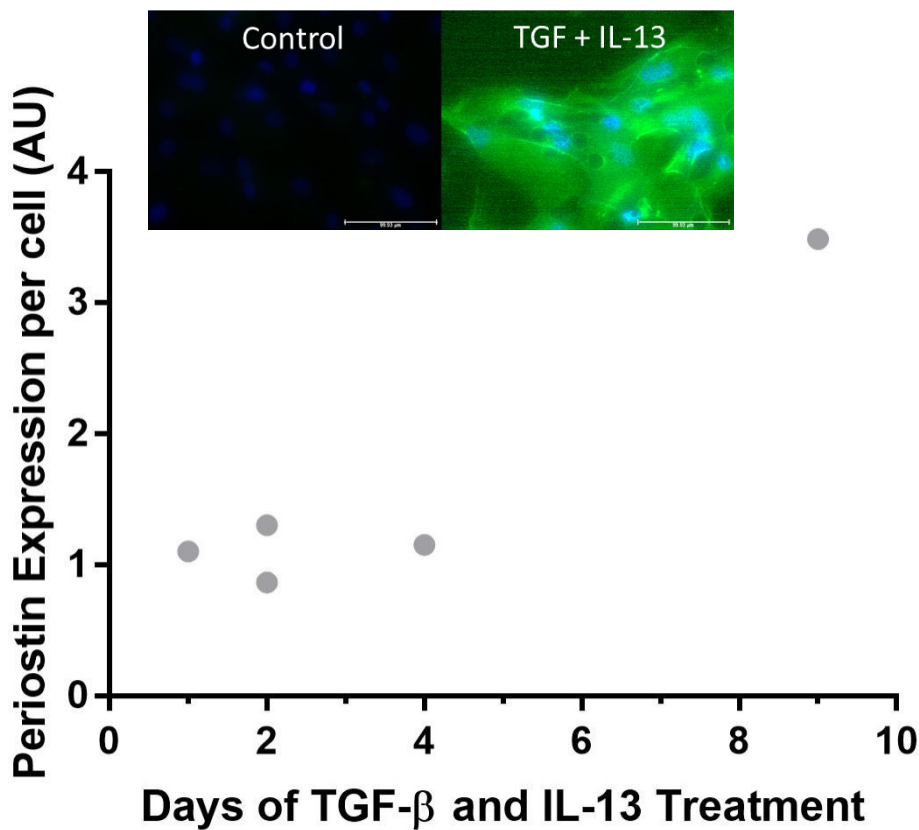


Figure 4.19 - Periostin expression by pericytes increased with time following combined TGF- β and IL-13 treatments. Immunostaining performed on pericytes grown in pericyte medium and treated with 10 ng/ml of TGF- β and 100 ng/ml of IL-13 for 24, 48, 96, 168 or 216 hours. Cells were supplemented with TGF- β and IL-13 every 2 days to maintain the treatment. Cells were stained with an anti-periostin antibody and intensity of periostin stain at 400x magnification was calculated with ImageJ. Intensity of stain per field of view was divided by the number of cells in order to determine periostin expression per cell. n=1-2, all results are not significant. Inset includes representative staining images. Scale bars = 100 μ m.

Treatment with both TGF- β and IL-13 together was explored to see if it would produce an additive, synergistic or suppressive effect. This was also explored across several days to see if longer treatments will have a different effect. Similar to both Figure 4.17 and 4.18, treatments resulted in increased cell death and caused the low n numbers which is likely to cause the non-significance of the results. Despite this, there is a slight trend, with the 9 day treatment causing an increase in periostin production. This experiment should be repeated in order to fully ascertain the effect of both of these treatments on periostin expression.

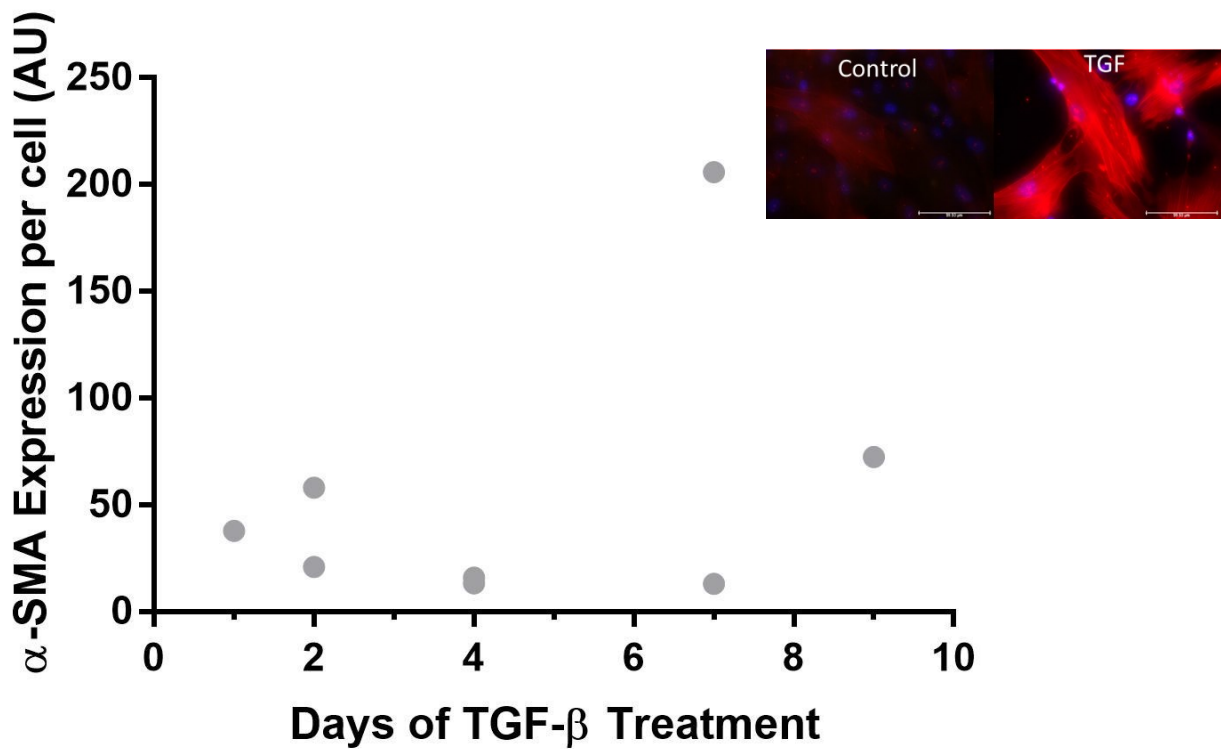


Figure 4.20 - α -SMA expression by pericytes slightly increased with time following TGF- β treatment. Immunostaining performed on pericytes grown in pericyte medium and treated with 10 ng/ml of TGF- β for 24, 48, 96, 168 or 216 hours. Cells were supplemented with TGF- β every 2 days to maintain the treatment. Cells were stained with an anti- α -SMA antibody and intensity of α -SMA stain at 400x magnification was calculated with ImageJ. Intensity of stain per field of view was divided by the number of cells in order to determine α -SMA expression per cell. $n=1-2$, all results are not significant. Inset includes representative staining images. Scale bars = 100 μ m.

The expression of α -SMA was also explored following the same treatment course previously described (Figure 4.17, 4.18, 4.19). TGF- β treatment over 9 days did not cause a significant difference in α -SMA expression, however, in general, treatment for 7 and 9 days caused a slightly higher expression of α -SMA in pericytes. There was a high variation in expression causing a high standard deviation showing that this should be repeated to increase n numbers and reduce the spread of the data.

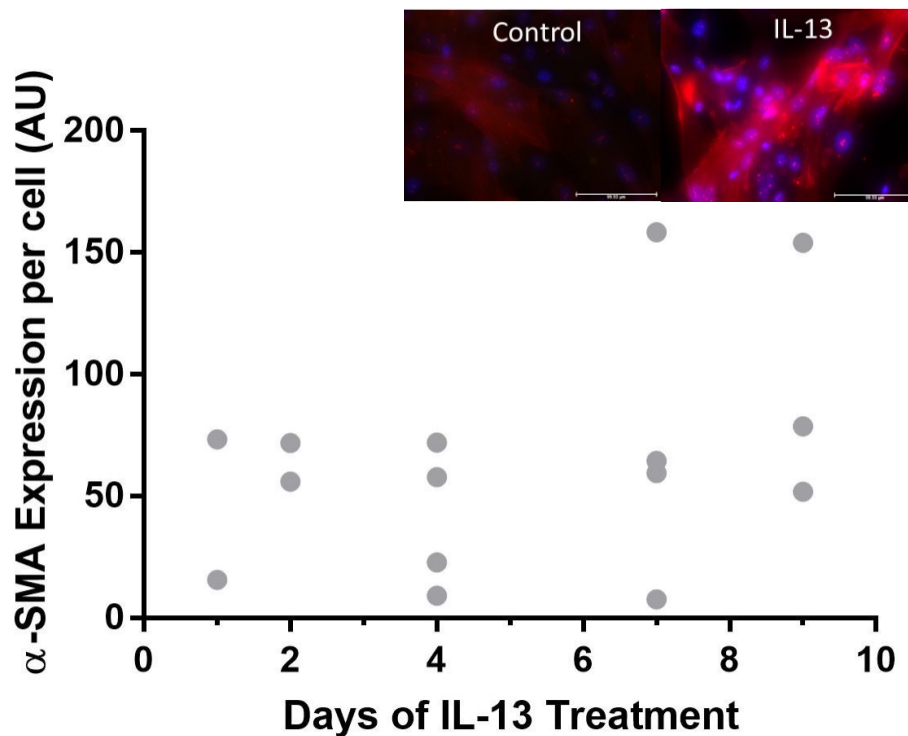


Figure 4.21 - α -SMA expression by pericytes remained relatively constant throughout the 9 days of IL-13 treatment. Immunostaining performed on pericytes grown in pericyte medium and treated with 100 ng/ml of IL-13 for 24, 48, 96, 168 or 216 hours. Cells were supplemented with IL-13 every 2 days to maintain the treatment. Cells were stained with an anti- α -SMA antibody and intensity of α -SMA stain at 400x magnification was calculated with ImageJ. Intensity of stain per field of view was divided by the number of cells in order to determine α -SMA expression per cell. $n=2-4$, all results are not significant. Inset includes representative staining images. Scale bars = 100 μ m.

Again, statistically there was no difference between each treatment group, although there is a slight trend, with increasing the duration of the IL-13 treatment increases the expression of α -SMA by pericytes. There is also a large spread of data within the treatment groups which would be aided by repeating the experiment again. It would also be interesting to extend this experiment beyond 9 days to see if this trend continues or whether it would decrease.

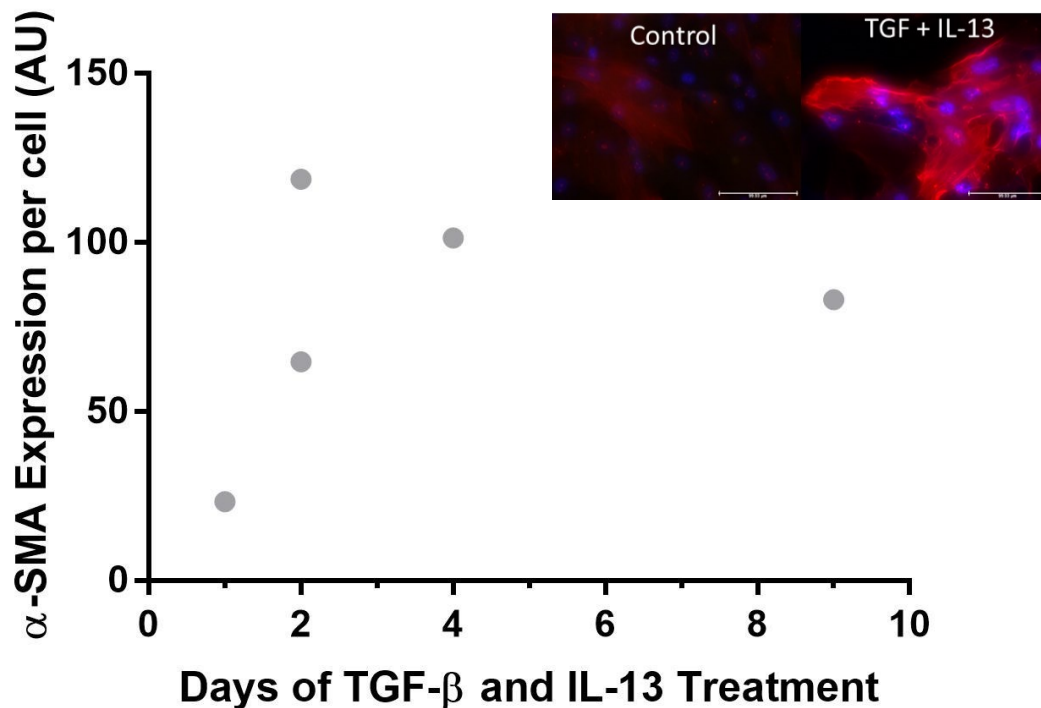


Figure 4.22 - α -SMA expression by pericytes increased with time following a combined TGF- β and IL-13 treatment. Immunostaining performed on pericytes grown in pericyte medium and treated with 10 ng/ml of TGF- β and 100 ng/ml IL-13 for 24, 48, 96, 168 or 216 hours. Cells were supplemented with TGF- β and IL-13 every 2 days to maintain the treatment. Cells were stained with an anti- α -SMA antibody and intensity of α -SMA stain at 400x magnification was calculated with ImageJ. Intensity of stain per field of view was divided by the number of cells in order to determine α -SMA expression per cell. n=1-2, all results are not significant. Inset include representative staining images. Scale bars = 100 μ m.

As with Figure 4.20 and 4.21, a co-treatment with both TGF- β and IL-13 was explored in relation to α -SMA expression in pericytes. Again, these results are not significant although it is suggested that treatment for 2 days and longer increases α -SMA expression. The fact that there is a slight trend, even with an n of 1, suggests that it would be fruitful to repeat this co-treatment and extend the treatment course so fully explore the interplay of these treatments.

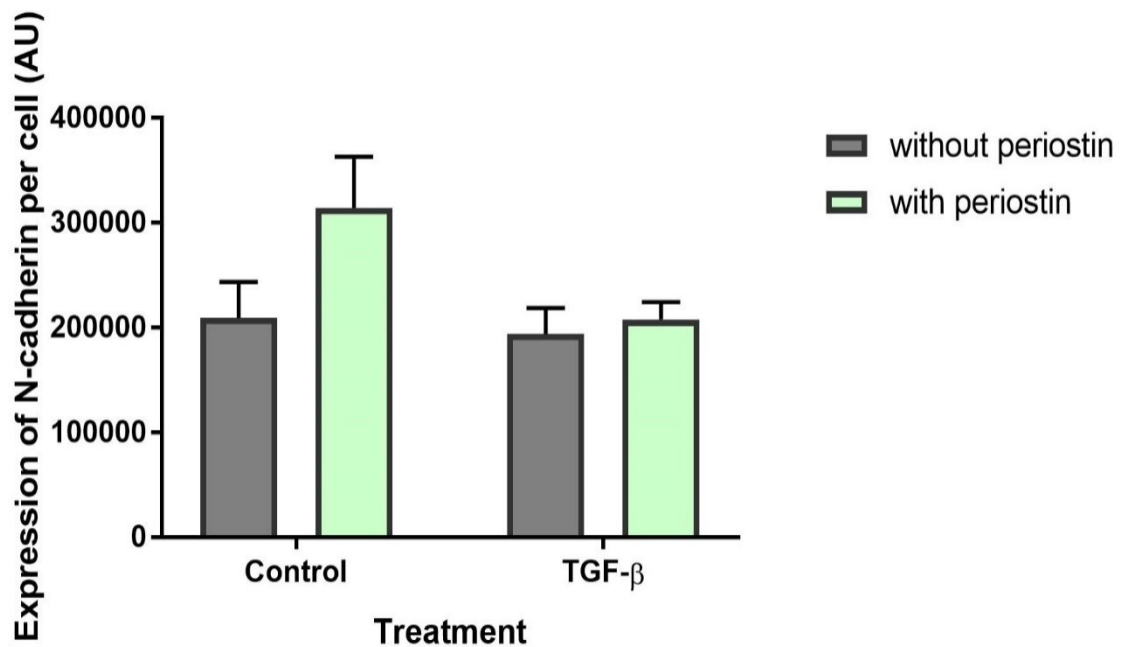


Figure 4.23 – There was no significant difference in the expression of N-cadherin by pericytes following TGF- β and/or periostin treatment. Immunostaining performed on pericytes grown in pericyte medium and treated with 10 ng/ml of TGF- β both with and without 100ng/ml periostin in addition for 5 days. Cells were stained with an anti-N-cadherin antibody and intensity of N-cadherin stain at 400x magnification was calculated with ImageJ. Intensity of stain per field of view was divided by the number of cells in order to determine N-cadherin expression per cell. n=4-6, all results are not significant by two-way ANOVA with Šídák's multiple comparisons test.

This experiment was performed on cultured pericytes and stained for N-cadherin to assess the myofibroblast characteristics and cell-cell interactions following growth factor and periostin treatment. With untreated pericytes, the addition of periostin slightly increased the expression of N-cadherin. However, in pericytes treated with TGF- β , the addition of periostin had no effect at all. In addition, the treatment with TGF- β did not yield a different result than untreated cells. Statistically, there was no difference between the N-cadherin expression following any of these treatments, however you can see a slight change. With a relatively high n number, more repeats may not reveal a more robust trend and other explanations into this similarity can be explored.

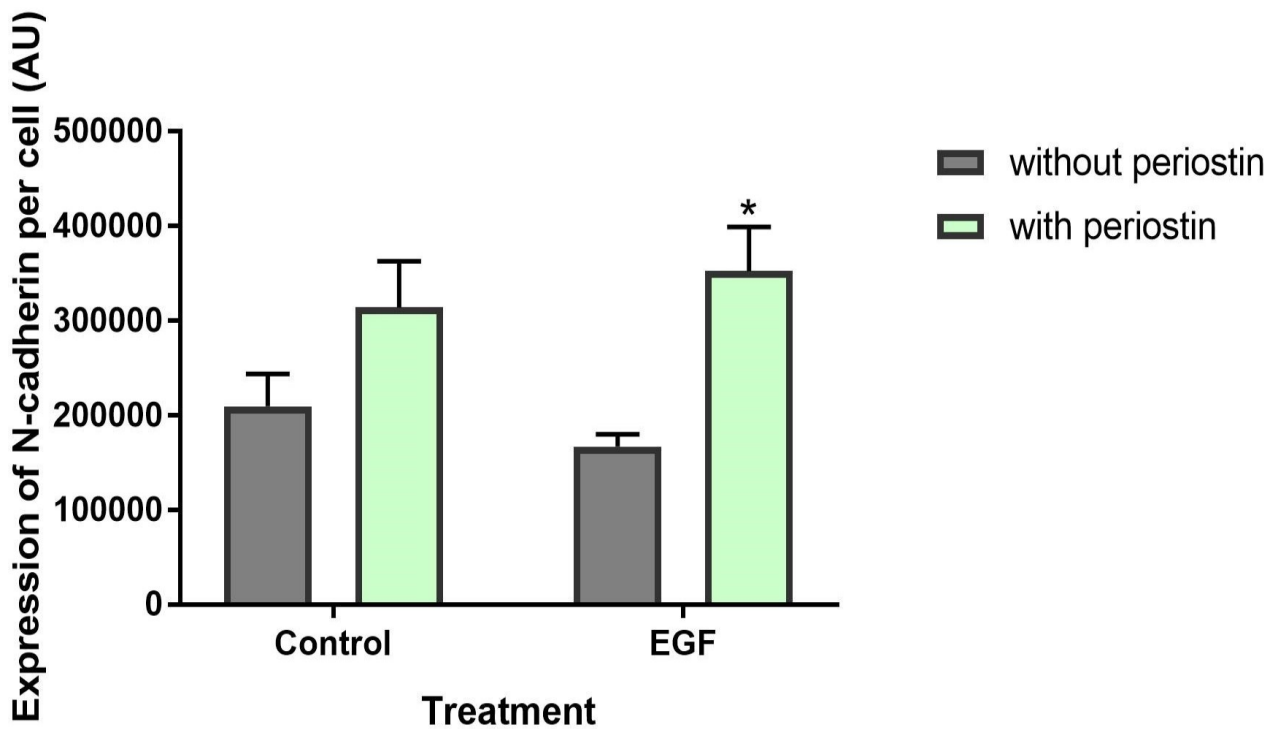


Figure 4.24 – Treatment with EGF and periostin increased the expression of N-cadherin by pericytes. Immunostaining performed on pericytes grown in pericyte medium and treated with 10 ng/ml of EGF both with and without 100ng/ml periostin in addition for 5 days. Cells were stained with an anti-N-cadherin antibody and intensity of N-cadherin stain at 400x magnification was calculated with ImageJ. Intensity of stain per field of view was divided by the number of cells in order to determine N-cadherin expression per cell. n=4-6, “*” = p<0.05 compared to EGF treatment without periostin by two-way ANOVA with Šidák's multiple comparisons test.

In Figure 4.24, control data from Figure 4.23 was included for comparison. Without the addition of periostin, treatment with EGF had a similar yet slightly lower effect on N-cadherin expression than the untreated cells. Yet with the addition of periostin alongside the EGF treatment, N-cadherin expression increased significantly (p=0.0167). Despite this, there was no significant difference between the control and the addition of EGF suggesting that this effect is observed due to the addition of periostin and not because of the presence of EGF.

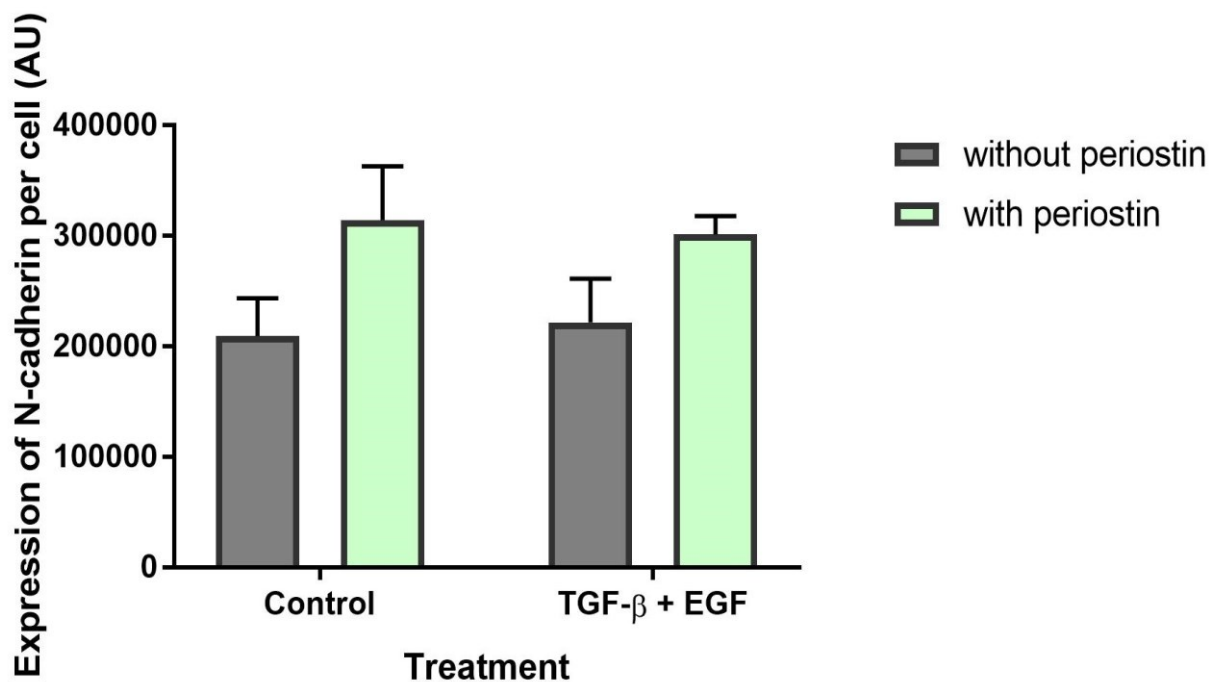


Figure 4.25 - There was no significant difference in the expression of N-cadherin by pericytes following TGF- β , EGF and/or periostin treatment. Immunostaining performed on pericytes grown in pericyte medium and treated with 10 ng/ml of EGF and TGF- β both with and without 100ng/ml periostin in addition for 5 days. Cells were stained with an anti-N-cadherin antibody and intensity of N-cadherin stain at 400x magnification was calculated with ImageJ. Intensity of stain per field of view was divided by the number of cells in order to determine N-cadherin expression per cell. n=4-6, all results are not significant by two-way ANOVA with Šídák's multiple comparisons test.

As with Figure 4.24, control data from Figure 4.23 was included for comparison. The trend observed following treatment with both TGF- β and EGF is very similar to that seen in untreated pericytes as such that the addition of periostin slightly yet insignificantly increases the expression of N-cadherin. The difference between the expression of N-cadherin following EGF and periostin treatment and EGF, TGF and periostin treatment suggests some form of regulation or inhibition by TGF- β which would be interesting to explore further.

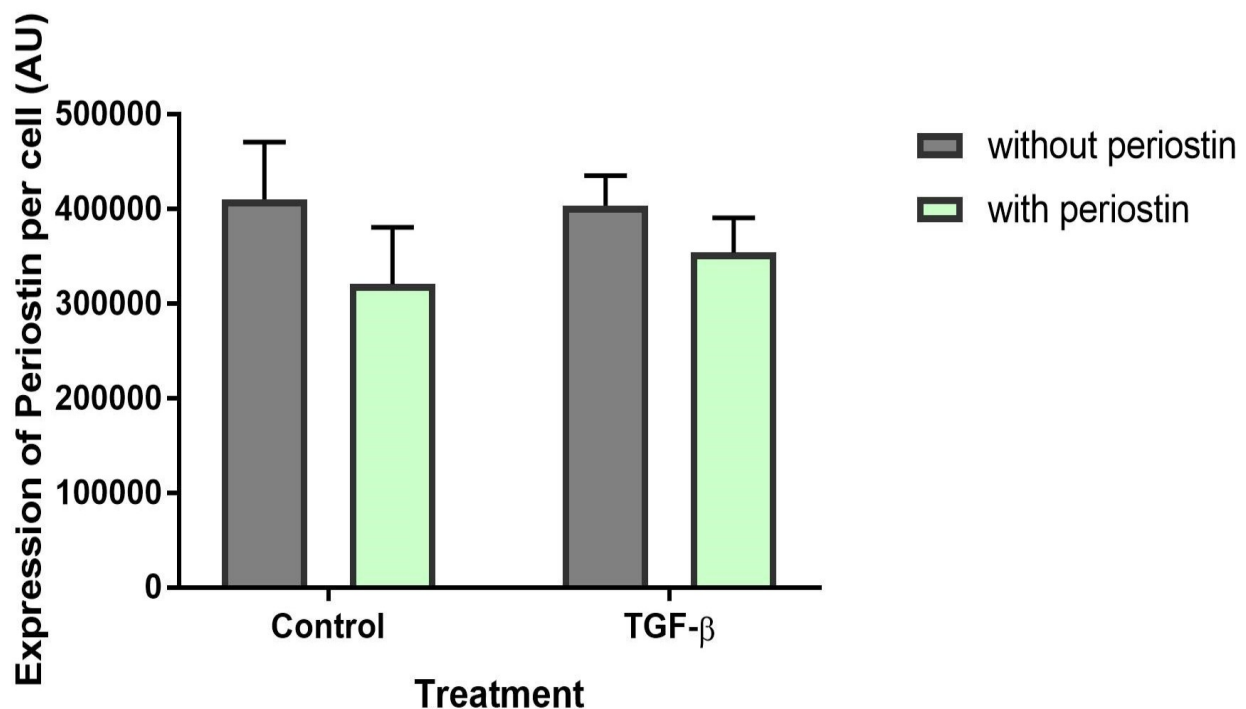


Figure 4.26 - There was no significant difference in the expression of periostin by pericytes following TGF- β and/or periostin treatment. Immunostaining performed on pericytes grown in pericyte medium and treated with 10 ng/ml of TGF- β both with and without 100ng/ml periostin in addition for 5 days. Cells were stained with an anti-periostin antibody and intensity of periostin stain at 400x magnification was calculated with ImageJ. Intensity of stain per field of view was divided by the number of cells in order to determine periostin expression per cell. n=4-6, all results are not significant by two-way ANOVA with Šidák's multiple comparisons test.

Alongside staining for N-cadherin, periostin was also stained for. Following treatment of untreated cells with periostin, the expression of periostin by the pericytes slightly, though insignificantly, decreased. This trend was also observed in pericytes that were treated with TGF- β , with cells treated with TGF- β only having a higher expression of periostin than those treated with both TGF- β and periostin. However, as this trend is also observed within the control condition, it is likely that the addition of TGF- β had no effect on the expression of periostin in this experiment. There was also no significant difference between any of these treatments suggesting that TGF- β treatment does not significantly increase the intracellular production of periostin.

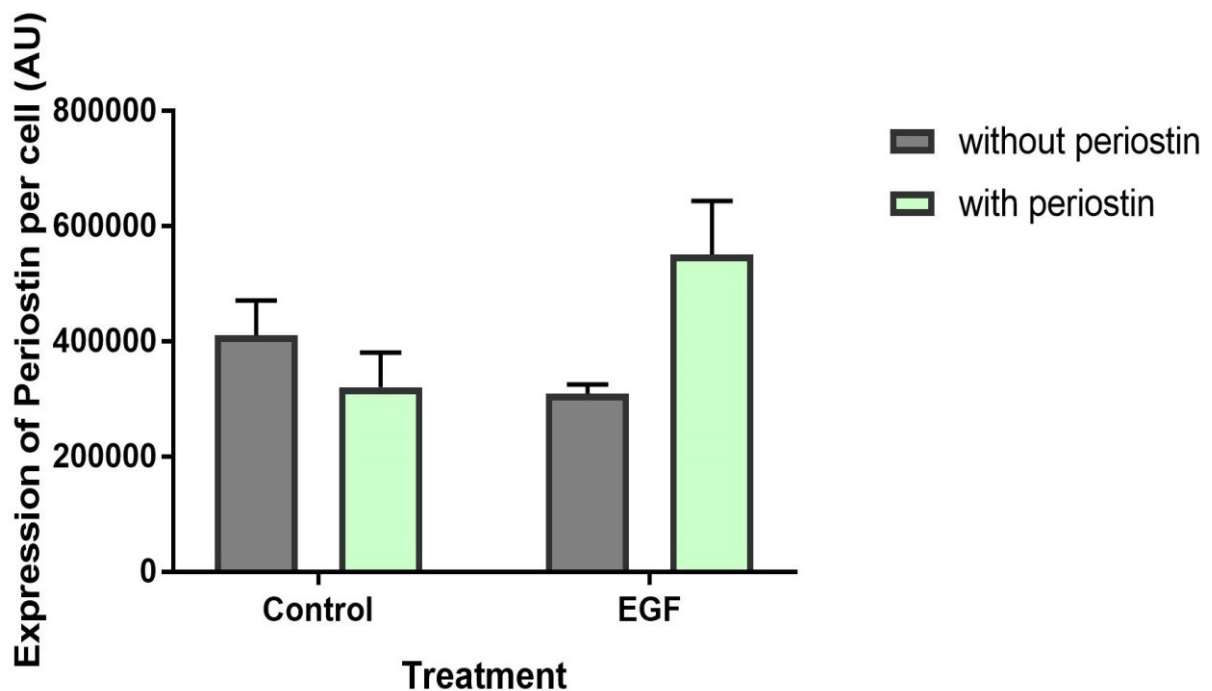


Figure 4.27 - There was no significant difference in the expression of periostin by pericytes following EGF and/or periostin treatment. Immunostaining performed on pericytes grown in pericyte medium and treated with 10 ng/ml of EGF both with and without 100ng/ml periostin in addition for 5 days. Cells were stained with an anti-periostin antibody and intensity of periostin stain at 400x magnification was calculated with ImageJ. Intensity of stain per field of view was divided by the number of cells in order to determine periostin expression per cell. n=4-6, all results are not significant by two-way ANOVA with Šídák's multiple comparisons test t.

Control data from Figure 4.26 was included in Figure 4.27 for comparison. Treatment with EGF only resulted in a slightly lower expression of periostin than the untreated control cells. However, adding periostin to cells treated with EGF increased the expression of periostin, almost significantly ($p < 0.07$). This was similar to the effect on N-cadherin observed in Figure 4.25.

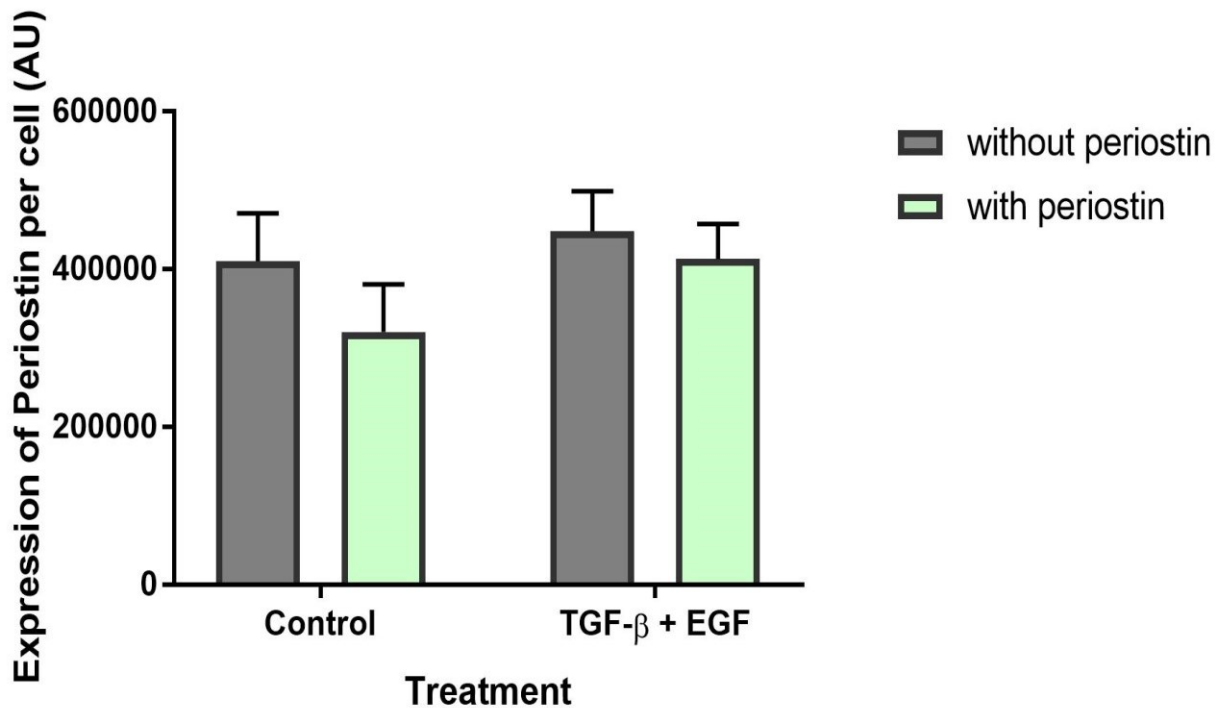


Figure 4.28 - There was no significant difference in the expression of periostin by pericytes following TGF- β , EGF and/or periostin treatment. Immunostaining performed on pericytes grown in pericyte medium and treated with 10 ng/ml of EGF and TGF- β both with and without 100ng/ml periostin in addition for 5 days. Cells were stained with an anti-periostin antibody and intensity of periostin stain at 400x magnification was calculated with ImageJ. Intensity of stain per field of view was divided by the number of cells in order to determine periostin expression per cell. n=4-6, all results are not significant by two-way ANOVA with Šídák's multiple comparisons test.

Again, control data from Figure 4.26 was included in Figure 4.28 for reference. Treatment with TGF- β and EGF both with and without periostin very slightly increased the expression of periostin compared to the untreated cells and untreated cells with periostin added. In addition, periostin with TGF- β and EGF treatment caused a slightly lower expression of periostin than the TGF- β and EGF treatment alone.

Having seen the effect of periostin on pericytes and its co-localisation and increased expression and secretion in diseased tissue, the focus was then moved into the inhibition of periostin in order to

abrogate these effects. As it had been suggested that IL-13 has a strong correlation with the secretion of periostin, cinnamaldehyde, an IL-13 inhibitor, was explored subsequently.

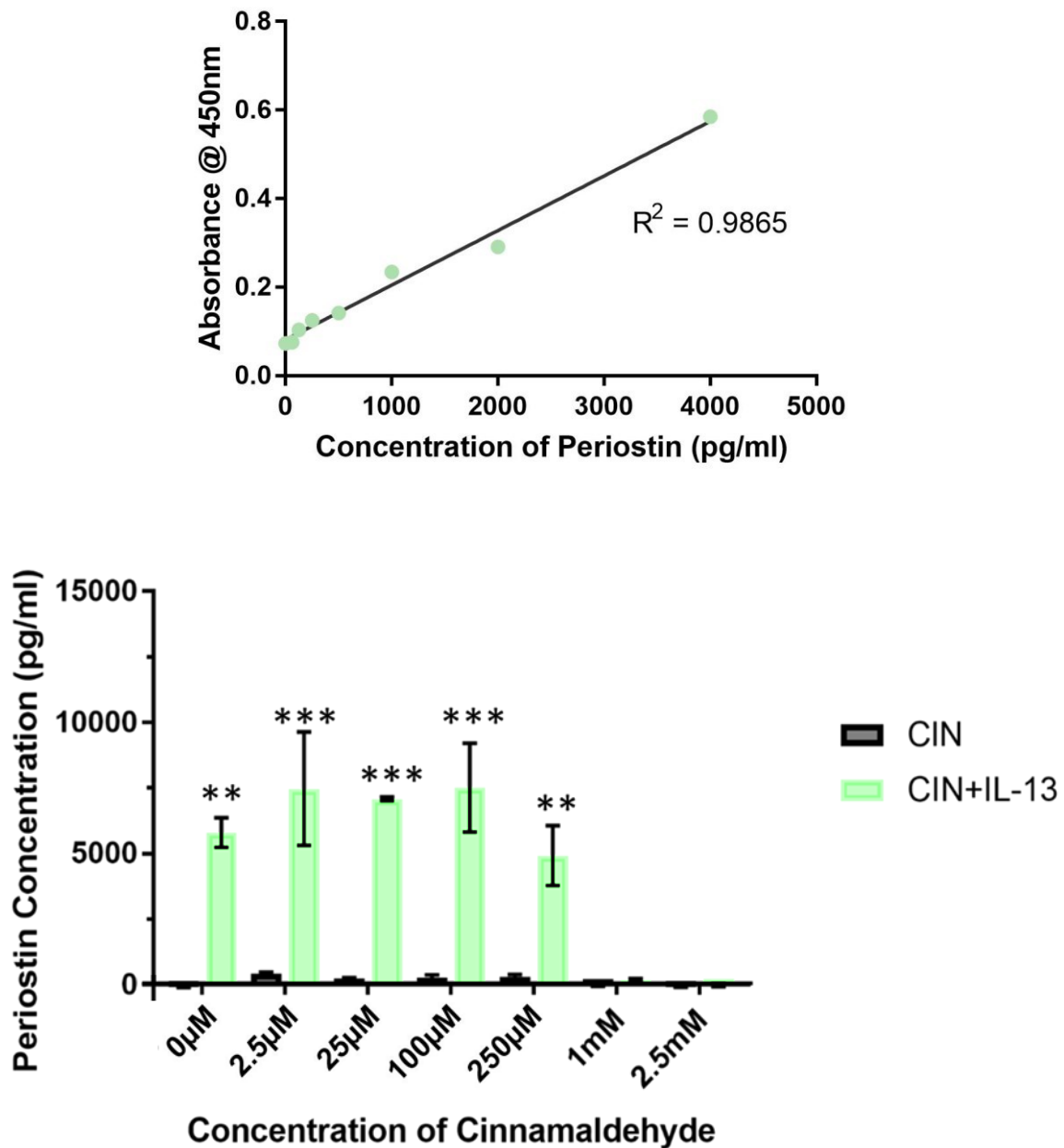


Figure 4.29 – Cinnamaldehyde treatment successfully inhibited IL-13-mediated periostin secretion by pericytes at concentrations higher than 1mM. Cultured pericytes were treated with 100ng/ml IL-13 in pericyte media for 7 days with the addition of cinnamaldehyde for the last 3 days at the concentration stated in A or only cinnamaldehyde at the stated concentration for 3 days. The supernatants were harvested and the periostin content was assessed using an anti-periostin ELISA kit. “**” = $p < 0.01$, “***” = $p < 0.001$ compared to the same concentration without IL-13, $n=2$ by two-way ANOVA with Šidák’s multiple comparisons test.

Cinnamaldehyde, an IL-13 inhibitor, was explored as a way to reduce the production of periostin by pericytes (Mitamura et al., 2018). Periostin was added in the last 3 days of incubation to allow the

effects of IL-13 to establish before attempting to reverse or reduce them. Pericytes treated with only cinnamaldehyde at any concentration did not produce periostin at a detectable concentration. However, when initially treated with IL-13 to increase periostin production and then treated with cinnamaldehyde, a detectable level of periostin was produced. As expected, lower levels of cinnamaldehyde resulted in a higher level of periostin production, but at concentrations of 1mM or higher, periostin production significantly decreases to levels similar to that of pericytes without IL-13 treatment.

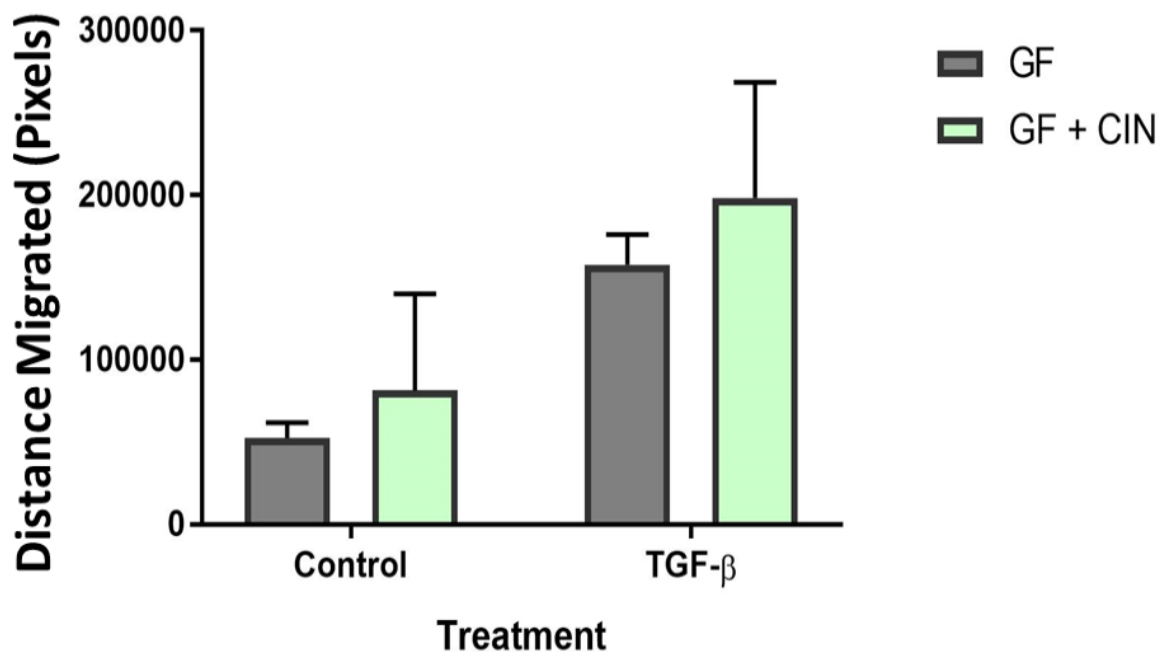


Figure 4.30 – Treatment with cinnamaldehyde did not affect the migration of TGF-β-treated pericytes. with scratch assay performed on pericytes that were grown in pericyte medium and treated with 10 ng/ml of TGF-β for 7 days with 1mM cinnamaldehyde added for the last 3 days. Cells were transferred into media lacking serum and a scratch was made in each monolayer using a p200 pipette tip. Images were taken at 100x magnification immediately after scratching at 24 hours later. The size of the scratches were determined using ImageJ and average difference in sizes were calculated. “GF” = growth factor, n=3, all results were not significant by two-way ANOVA with Šídák's multiple comparisons test.

A scratch assay was used to explore the effect of inhibiting IL-13 on pericyte migration. There was no difference in migration of pericytes that were untreated or treated with only cinnamaldehyde. Treatment increased slightly following treatment with TGF-β although this was not significant. Unusually, adding cinnamaldehyde to TGF-β treated cells also slightly increased pericyte migration

although, again, this was not significant. This may be due to the spread of data; therefore more experiments should be completed to confirm this effect.

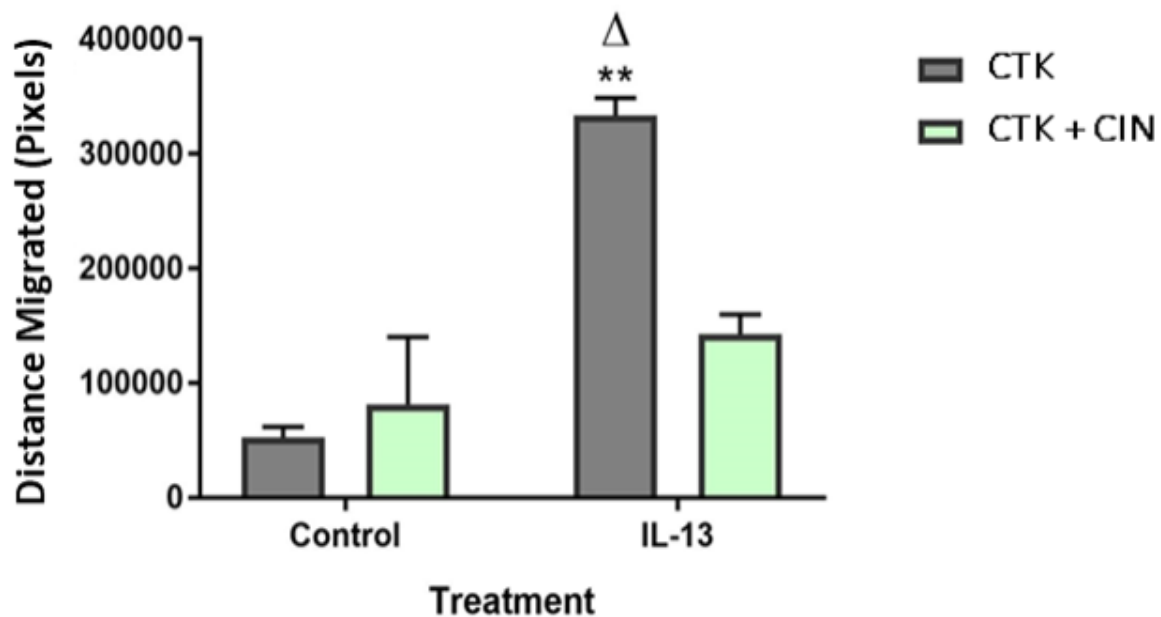


Figure 4.31 – Treatment with cinnamaldehyde reduced the effect of IL-13 treatment on the migration of pericytes. Scratch assay performed on pericytes that were grown in pericyte medium and treated with 100 ng/ml of IL-13 for 7 days with 1mM cinnamaldehyde added for the last 3 days. Cells were transferred into media lacking serum and a scratch was made in each monolayer using a p200 pipette tip. Images were taken at 100x magnification immediately after scratching at 24 hours later. The size of the scratches were determined using ImageJ and average difference in sizes were calculated. “CTK” = cytokine, n=3, “Δ” = $p < 0.05$ to the same growth factor treatment without cinnamaldehyde, “**” = $p < 0.01$ to the control treatment without cinnamaldehyde by two-way ANOVA with Šidák’s multiple comparisons test.

Control data from Figure 4.30 was included for reference. Treatment with IL-13 significantly increased the migration of pericytes compared to untreated pericytes ($p=0.0011$). The addition of cinnamaldehyde to the pericytes treated with IL-13 prevented this increase and instead migration was not significantly different to control untreated cells. This means that cinnamaldehyde treatment significantly reduced pericyte migration following IL-13 treatment ($p=0.0123$).

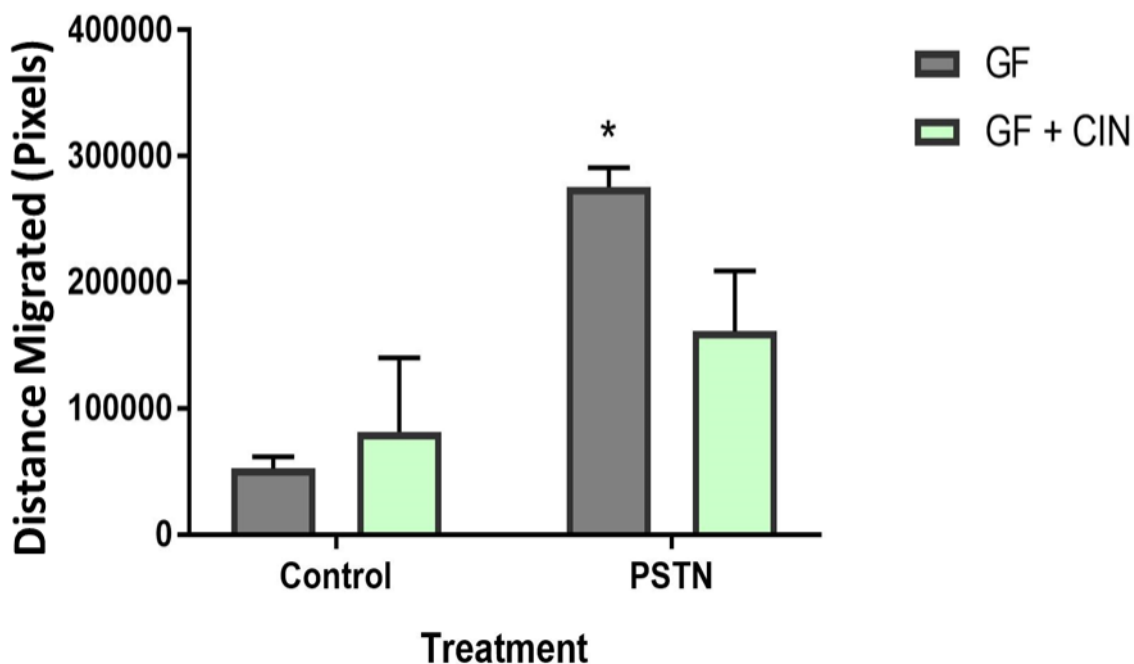


Figure 4.32 – Treatment with cinnamaldehyde reduced the effect of periostin treatment on the migration of pericytes. Scratch assay performed on pericytes that were grown in pericyte medium and treated with 100 ng/ml of periostin for 7 days with 1mM cinnamaldehyde added for the last 3 days. Cells were transferred into media lacking serum and a scratch was made in each monolayer using a p200 pipette tip. Images were taken at 100x magnification immediately after scratching at 24 hours later. The size of the scratches were determined using ImageJ and average difference in sizes were calculated. “GF” = growth factor, n=3, “*” = p<0.05 to the control treatment without cinnamaldehyde by two-way ANOVA with Šídák’s multiple comparisons test.

Again, control data from Figure 4.30 was included for reference. The trend observed in Figure 4.32 is much the same as that seen in Figure 4.31. Treatment with periostin significantly increased the migration of pericytes compared to control cells (p=0.0158). Then, adding cinnamaldehyde to pericytes treated with periostin migration was not significantly different to the control cells and therefore pericyte migration was reduced.

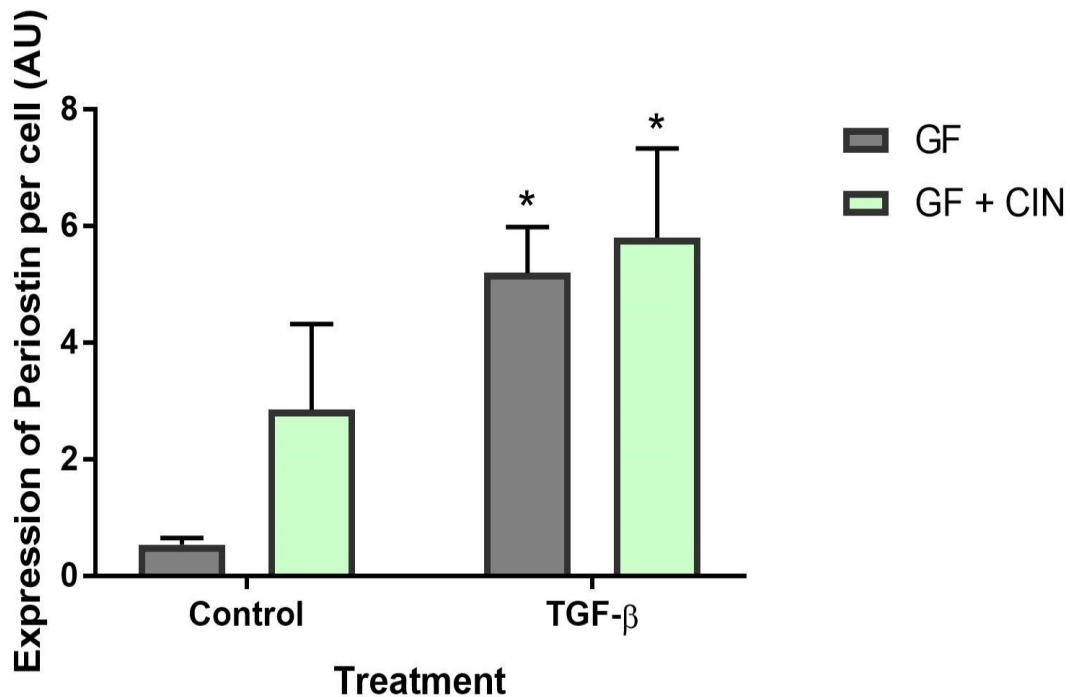


Figure 4.33 – Treatment with cinnamaldehyde did not affect the expression of periostin by TGF-β treated pericytes. Immunostaining performed on pericytes that were grown in pericyte medium and treated with 10 ng/ml of TGF-β for 7 days with 1mM cinnamaldehyde added for the last 3 days. Cells were stained with an anti-periostin antibody and intensity of periostin stain at 400x magnification was calculated with ImageJ. Intensity of stain per field of view was divided by the number of cells in order to determine periostin expression per cell. n=6, “*” = p<0.05 by two-way ANOVA with Šidák’s multiple comparisons test

The addition of cinnamaldehyde alongside growth factors was also explored in relation to the expression of periostin, measured via immunostaining of cultured pericytes. Unusually, though not significantly, the addition of cinnamaldehyde to untreated control pericytes slightly increased the expression of periostin. Outlier calculations were performed in order to ensure this effect was not caused by aberrant results. Treatment of pericytes with TGF-β alone significantly increased the expression of periostin (p=0.05) However the addition of cinnamaldehyde did not reduce this effect as there was no significant difference between treatments with TGF-β and TGF-β with cinnamaldehyde.

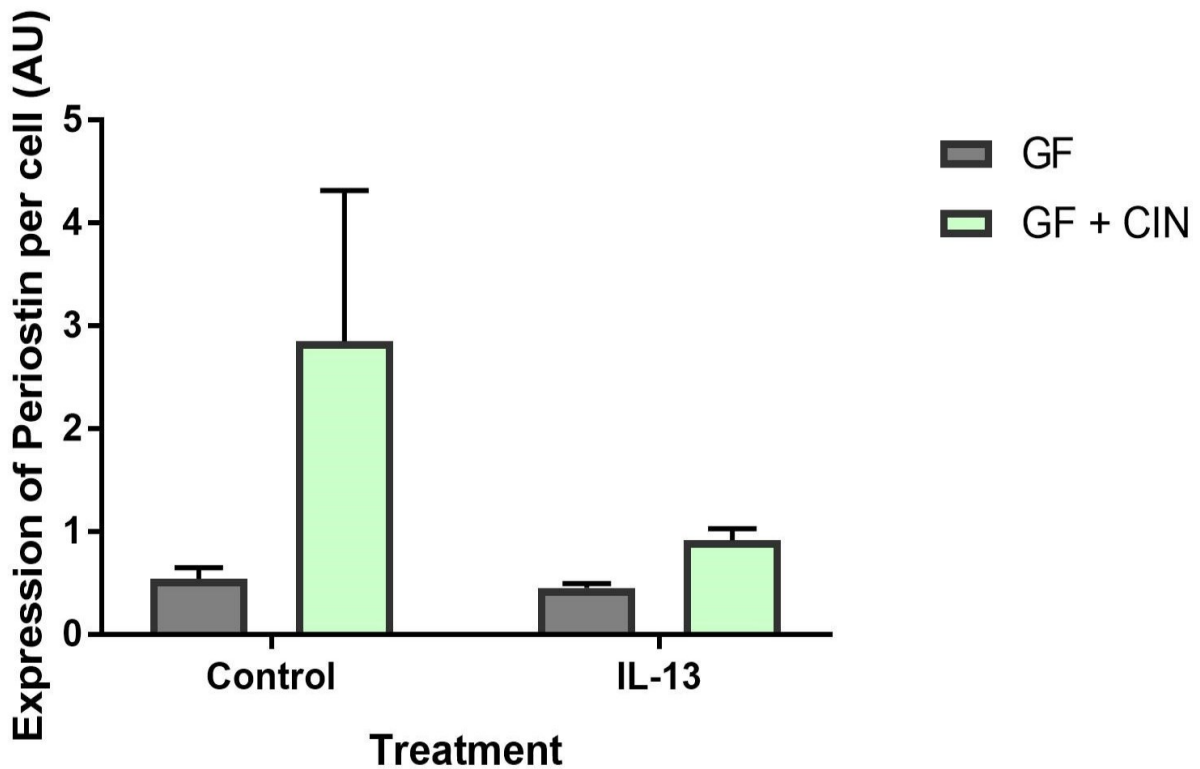


Figure 4.34 - Treatment with cinnamaldehyde did not affect the expression of periostin by IL-13 treated pericytes. Immunostaining performed on pericytes that were grown in pericyte medium and treated with 100 ng/ml of IL-13 for 7 days with 1mM cinnamaldehyde added for the last 3 days. Cells were stained with an anti-periostin antibody and intensity of periostin stain at 400x magnification was calculated with ImageJ. Intensity of stain per field of view was divided by the number of cells in order to determine periostin expression per cell. n=6 by two-way ANOVA with Šidák's multiple comparisons test

Control data from Figure 4.33 was included for reference. Unusually, treatment with IL-13 had no effect on the expression of periostin by pericytes as there was no significant difference between pericytes treated with only IL-13 and those that were untreated. Following the addition of cinnamaldehyde, pericytes treated with IL-13 had a slightly reduced expression of periostin than pericytes that had not received treatment with growth factors. There was also no significant difference between the periostin expressed by the pericytes treated with IL-13 and cinnamaldehyde and those treated with IL-13 only.

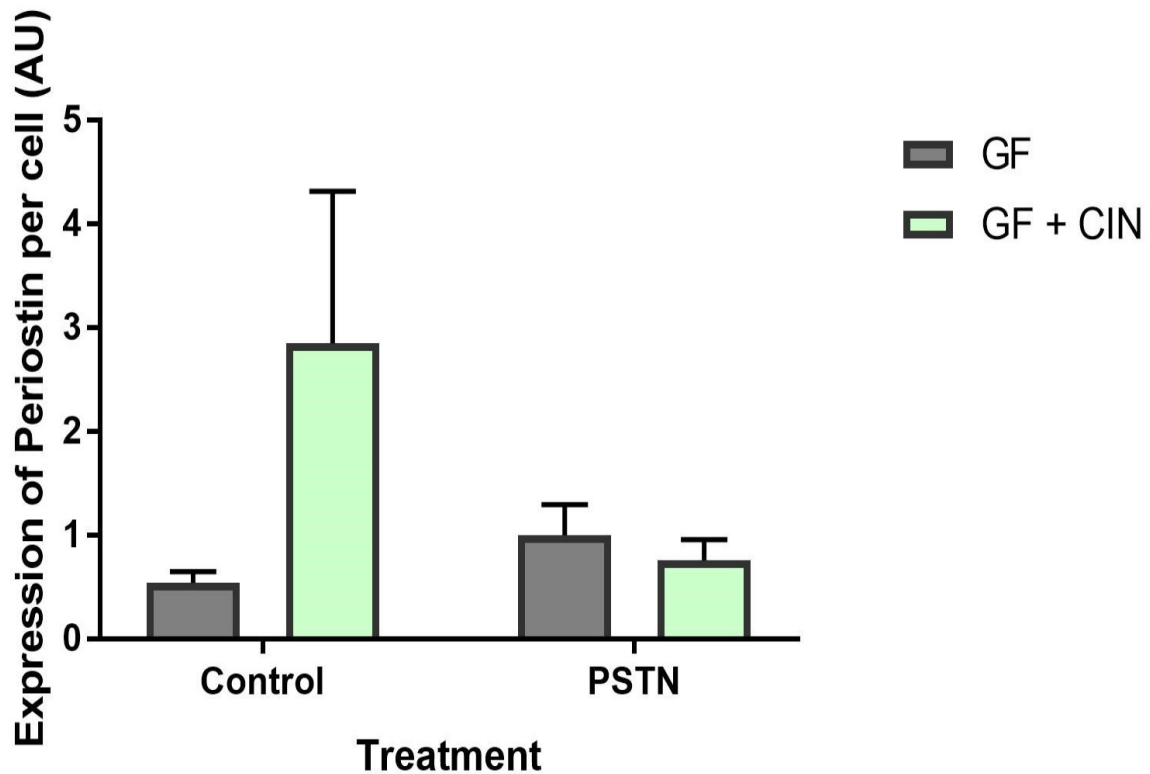


Figure 4.35 - Treatment with cinnamaldehyde did not affect the expression of periostin by periostin treated pericytes. Immunostaining performed on pericytes that were grown in pericyte medium and treated with 100 ng/ml of periostin for 7 days with 1mM cinnamaldehyde added for the last 3 days. Cells were stained with an anti-periostin antibody and intensity of periostin stain at 400x magnification was calculated with ImageJ. Intensity of stain per field of view was divided by the number of cells in order to determine periostin expression per cell. n=5-6 by two-way ANOVA with Šidák's multiple comparisons test

Again, control data from Figure 4.33 was included for comparison. Similar to the trend observed following IL-13 treatment in Figure 4.34, pericyte treatment with periostin resulted in a very similar expression of periostin to untreated cells. Treatment with periostin alongside cinnamaldehyde had a slightly lower, though not significant, expression than untreated cells exposed to cinnamaldehyde. Similar to the treatment with IL-13, with and without cinnamaldehyde, there was no significant difference between periostin expression following treatment with periostin or periostin with cinnamaldehyde.

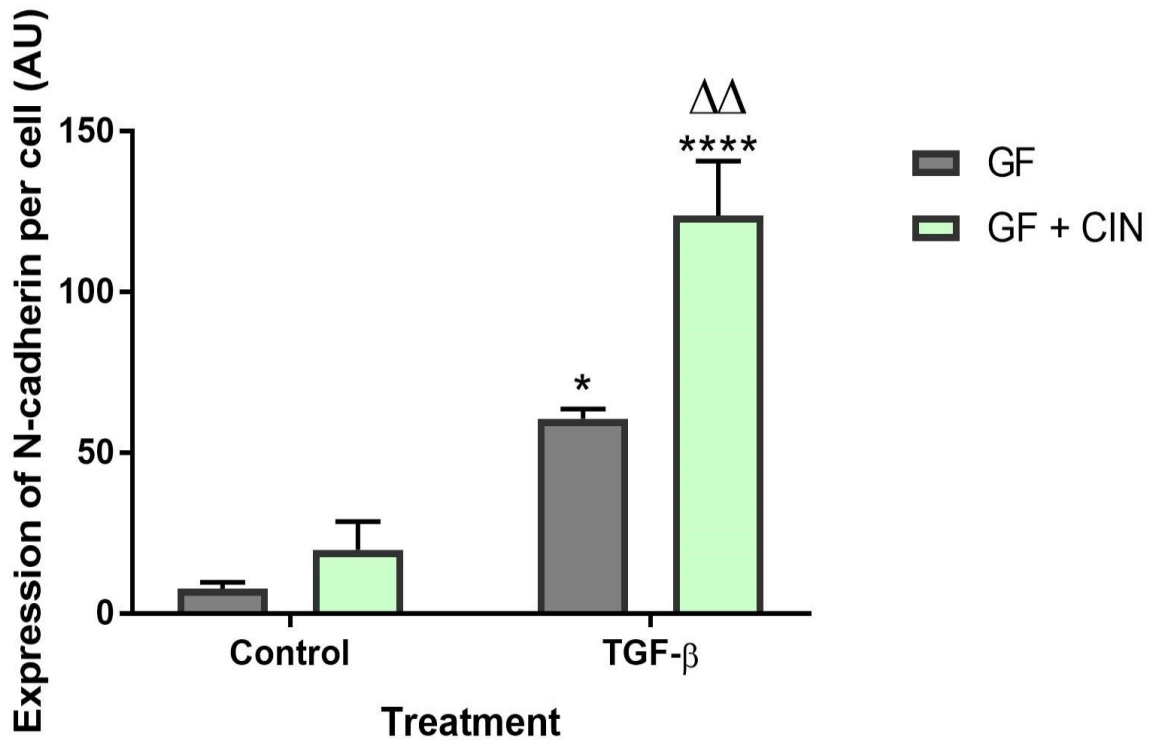


Figure 4.36 – Treatment with cinnamaldehyde significantly increased the expression of N-cadherin in pericytes treated with TGF- β . Immunostaining performed on pericytes that were grown in pericyte medium and treated with 10 ng/ml of TGF- β for 7 days with 1mM cinnamaldehyde added for the last 3 days. Cells were stained with an anti-N-cadherin antibody and intensity of N-cadherin stain at 400x magnification was calculated with ImageJ. Intensity of stain per field of view was divided by the number of cells in order to determine N-cadherin expression per cell. n=5-6, “*” = $p < 0.05$, “****” = $p < 0.0001$ with respect to untreated cells, “ $\Delta\Delta$ ” = $p < 0.01$ with respect to TGF- β treatment by two-way ANOVA with Šidák’s multiple comparisons test .

Untreated control pericytes displayed low levels of N-cadherin expression. The addition of cinnamaldehyde to these untreated pericytes slightly increased expression of N-cadherin, although this difference was not significant. Pericytes treated with TGF- β had significantly increased expression of N-cadherin compared to control cells ($p=0.0112$). Unusually, this expression was also significantly increased further following the addition of cinnamaldehyde ($p < 0.0001$ compared to untreated cells and $p=0.0023$ compared to TGF- β treated cells without cinnamaldehyde).

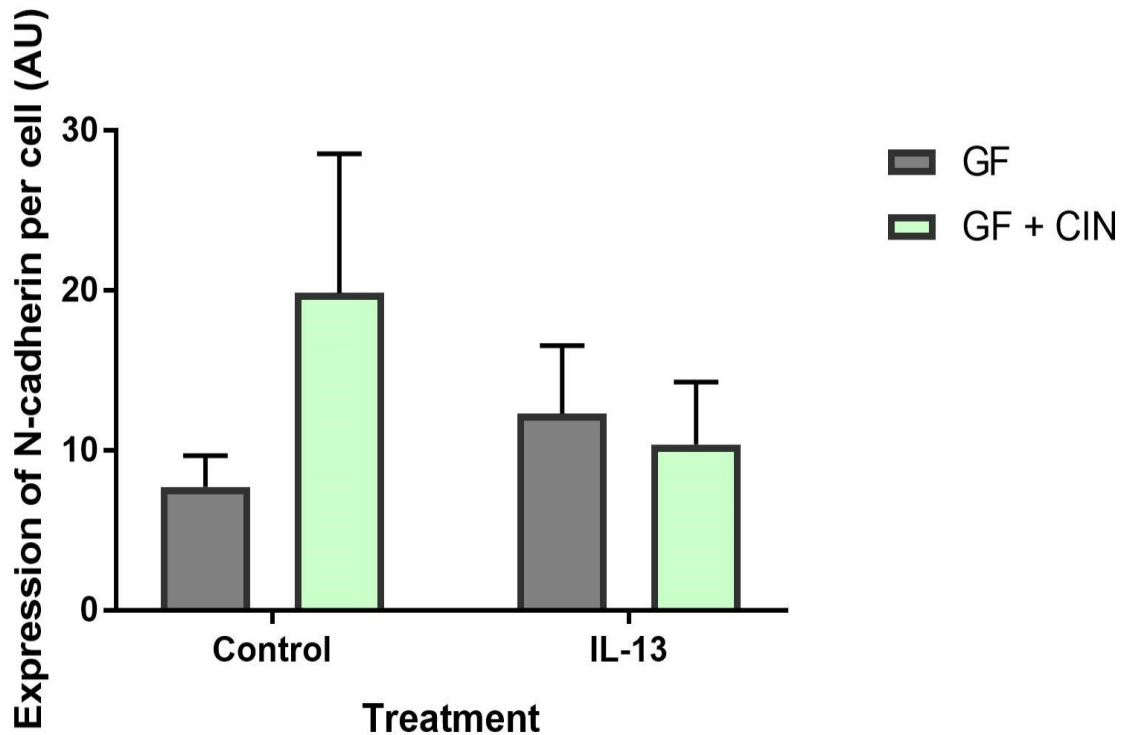


Figure 4.37 - Treatment with cinnamaldehyde did not affect the expression of N-cadherin by IL-13 treated pericytes. Immunostaining performed on pericytes that were grown in pericyte medium and treated with 100 ng/ml of IL-13 for 7 days with 1mM cinnamaldehyde added for the last 3 days. Cells were stained with an anti-N-cadherin antibody and intensity of N-cadherin stain at 400x magnification was calculated with ImageJ. Intensity of stain per field of view was divided by the number of cells in order to determine N-cadherin expression per cell. n=6 by two-way ANOVA with Šídák's multiple comparisons test.

Control data from Figure 4.36 was included for reference. Treating pericytes with IL-13 did not increase the expression of N-cadherin as there was no significant difference in N-cadherin expression between IL-13 treated pericytes and untreated pericytes. There was no significant difference in N-cadherin expression following the addition of cinnamaldehyde to IL-13 treated pericytes, although the expression following both IL-13 and cinnamaldehyde treatment was slightly lower than pericytes treated with solely cinnamaldehyde.

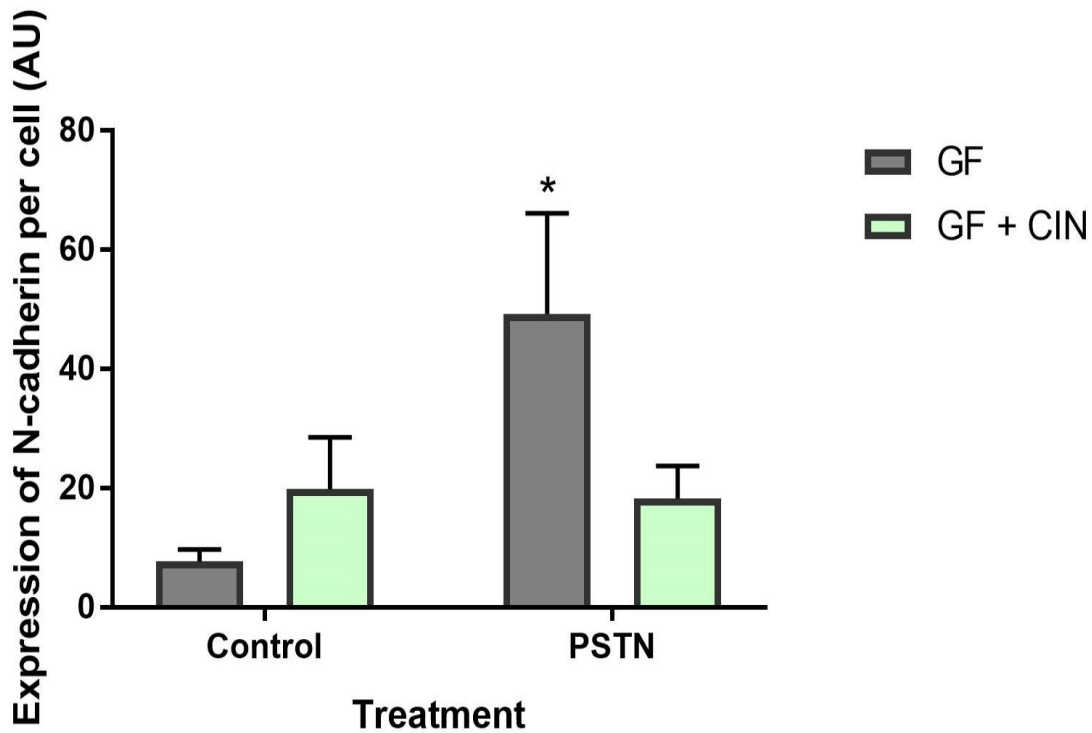


Figure 4.38 - Treatment with cinnamaldehyde decreased the expression of N-cadherin in pericytes treated with periostin. Immunostaining performed on pericytes that were grown in pericyte medium and treated with 100 ng/ml of periostin for 7 days with 1mM cinnamaldehyde added for the last 3 days. Cells were stained with an anti-N-cadherin antibody and intensity of N-cadherin stain at 400x magnification was calculated with ImageJ. Intensity of stain per field of view was divided by the number of cells in order to determine N-cadherin expression per cell. "*" = $p < 0.05$ compared to untreated control. $n = 5-6$ by two-way ANOVA with Šidák's multiple comparisons test.

For reference, control data from Figure 4.36 was included in Figure 4.38. Treatment of pericytes with periostin caused a significant increase in N-cadherin expression ($p = 0.0457$). With the addition of cinnamaldehyde to pericytes treated with periostin slightly reduced the expression of N-cadherin to a level very similar to the pericytes treated with only cinnamaldehyde. However, this is not significant due to the relatively low n number.

4.3 Discussion

Various aspects of periostin have been explored in this chapter, from its production to its effect on physiological effects such as cell migration and the expression of cell adhesion molecules. Periostin is an incredibly important yet often overlooked component of the ECM and therefore aspect of fibrosis and asthma as a whole. The importance of periostin has been determined as, as previously mentioned, it is a biomarker for the severity of asthma (Takahashi et al., 2019). The expression of the gene for periostin (POSTN) has also been shown to be upregulated in several diseases such as asthma and idiopathic pulmonary fibrosis (Figure 4.1, 4.3). This suggests that the inflammation and fibrosis occurring in these lung diseases may cause an increase in expression of periostin at an RNA level. Further bioinformatics analysis also elucidated an expected stimulus or periostin production, as Figure 4.2 highlights that in IL-13 knockout mice, the level of periostin produced was a lot lower than wild type mice. This highlighted IL-13 as an important target in the study of periostin and attempts to reduce its effect ([Gene Expression Omnibus GSE1301](#)). The effect of IL-13 on periostin production is explored experimentally throughout this chapter. There was also an attempt to elucidate the location of this increase in periostin during lung diseases through the use of online databases. Data from Habermann et al. accessed in the IPF Cell Atlas (shown in Figure 4.4, Habermann et al., 2020) suggested that periostin expression localised in endothelial cells and myofibroblasts were greatly increased in interstitial lung disease compared to healthy lungs. Pericytes are tightly associated with endothelial cells in healthy tissue as they reside next to each other in the basement membrane, allowing this increased levels of periostin to affect pericytes and perhaps induce the effects seen in fibrosis. In chronic inflammation, pericytes are also known to differentiate into myofibroblasts and contribute to ECM deposition and fibrosis (Johnson et al., 2011), and therefore may be the ones exhibiting the high levels of periostin following this differentiation. Pericytes also migrate towards the smooth muscle layer during fibrosis and therefore would reside near other myofibroblasts and thus are exposed to increased levels of periostin (Johnson et al., 2015). The inclusion of data from ILD hints to the widespread importance of periostin within several different types of fibrotic lung disease and highlights the importance of any findings regarding the mechanism or inhibition of periostin in fibrosis. The Wellcome Sanger Cell Atlas (data shown in Figure 4.5 (Regev et al., 2017)) also highlights an increase of periostin in asthmatic lungs, specifically in fibroblasts, the smooth muscle layer and the endothelium. However, pericytes share many markers with these three cell types such as PDGFR- α , PDGFR- β , Col1 and vimentin (Hellstrom et al., 1999, Chen et al., 2012, McKleroy, Lee & Atabai, 2013, Rock et al., 2011, Barron, Gharib & Duffield, 2016) and may therefore be mischaracterised in some studies; instead, it may be pericytes that undergo this increased expression of periostin. Periostin has also previously been linked to TGF-

β (Ashley et al., 2017) and so the IntAct protein database was used to explore the interactions between periostin and TGF- β (Orchard et al., 2013). The data in Figure 4.6 clearly shows a strong association between periostin and TGF- β through both physical association and co-localisation and therefore highlights the possibility of important regulation or interactions between these proteins during fibrosis (Ashley et al., 2017)

The migration of pericytes following treatment with either periostin, IL-13 (to induce periostin production) and TGF- β (to compare it to periostin treatment) was investigated using Transwell assays and scratch assays (Figures 4.7, 4.8, 4.9). IL-13 has currently mostly been linked to the induction of EMT and the subsequent increase in motility whereas TGF- β has been known to contribute to pericyte migration both through mesenchymal transition and recruitment during angiogenesis (Wu et al., 2014, Nadal et al., 2002, Wirsik et al., 2020). The Transwell assay in Figure 4.9 was previously discussed in the previous chapter where the lack of change in results following growth factor treatment was attributed to cell clumping and the inability to distinguish between individual cells during processing. This was one of the reasons the experiment was repeated instead using a scratch assay (Figure 4.7, 4.8). With this other method, the treatment of pericytes with TGF- β or periostin causes a significant increase in the migration of these pericytes. This suggests that periostin may contribute towards the migration of pericytes observed during asthma. However, the treatment with IL-13 did not induce a significant increase in migration although there was a slight increase. This warrants further investigation with a properly powered study and a more detailed time course analysis might shed further light on the effect of IL-13 on pericyte migration. In the future, biochemical analysis should be performed to elucidate the mechanism of inducing periostin production by IL-13.

The production of periostin by pericytes was explored through immunostaining for intercellular periostin. Figure 4.10 shows that untreated cultured pericytes are able to spontaneously produce low levels of periostin. This could be slightly increased through the treatment with TGF- β or significantly increased following periostin treatment. This ability of pericytes to produce periostin highlights the possibility that pericytes may both produce and respond to periostin causing a positive feedback loop and a greatly exacerbated fibrotic environment (as hypothesised in Figure 4.39).

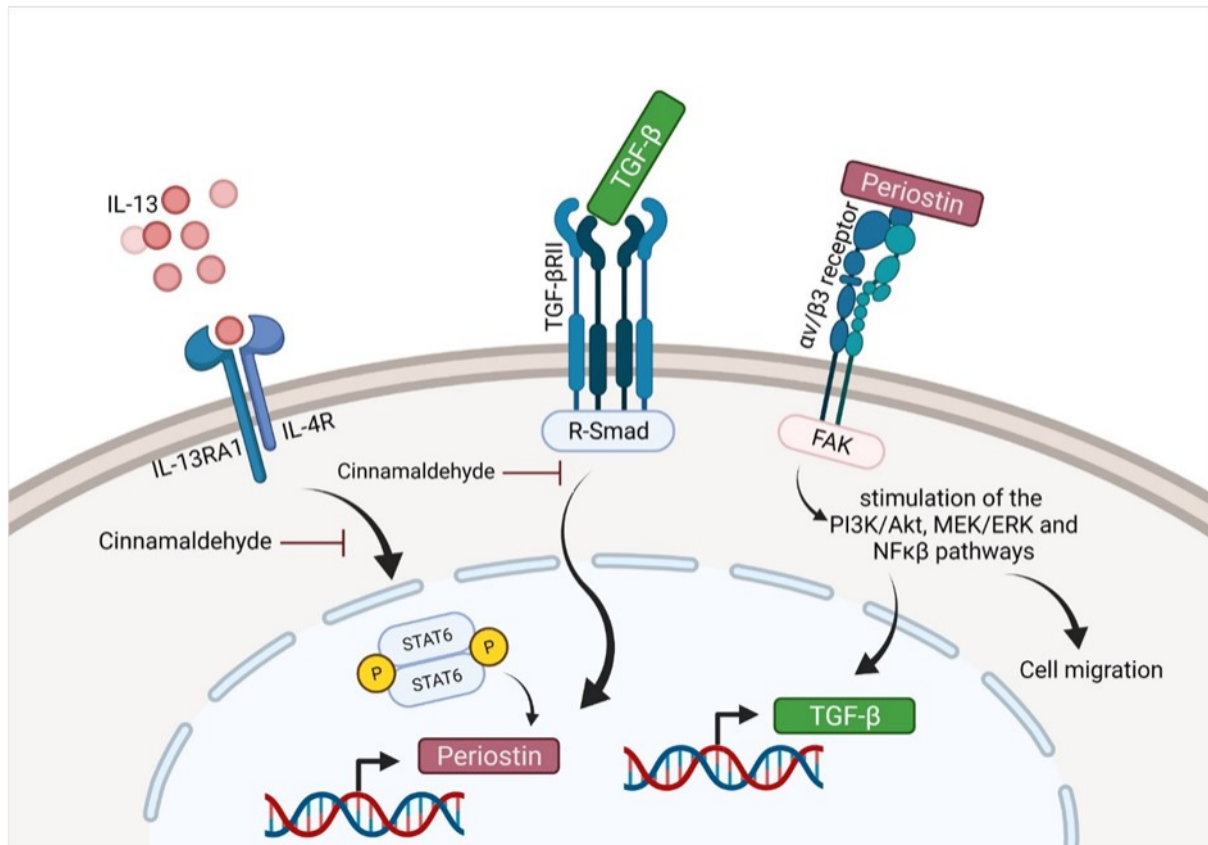


Figure 4.39 - Hypothesised mechanism of periostin and how it contributes to migration and is inhibited by cinnamaldehyde via the activation of Nrf2 thus reducing cell migration and IL-13 and TGF- β induced periostin production (Mitamura et al., 2018). Diagram constructed on BioRender. Originally published in Bignold & Johnson, 2021a.

However, it is difficult to distinguish between periostin produced by the pericytes and residual periostin from the treatments. This may be due to the long half-life of periostin reported by other studies (Michaylira et al., 2010). Therefore, optimisation of staining methods should occur such as the addition of wash steps several hours prior to staining to remove any periostin that was remaining from the treatment. Further exploration was performed into the effect of co-treatment with TGF- β , EGF and periostin (Figures 4.26, 4.27, 4.28). With TGF- β treatment with and without periostin, the expression of periostin was no different to that of the control group. The difference between the results in Figure 4.26 and Figure 4.10 may be due to the difference in treatment times as cells in Figure 4.10 were treated for 2 days and the cells in Figure 4.26 were treated for 5 days. This may indicate that at 2 days treatment more periostin is kept within the cell and therefore would be visible on immunostained images whilst after 5 days the periostin is secreted from the cells into the microenvironment and therefore is washed away during the staining process. It is also possible that periostin exists in a precursor form and may require post-translational processing within the Golgi apparatus before it can be secreted via the conventional protein secretion pathway (Rabouille, 2017). Many ECM proteins exist as pro-proteins including TGF- β , collagen and EGF (Kubiczkova et al., 2012, Canty-Laird, Lu & Kadler, 2012, Le Gall et al., 2003). In Figure 4.28, the expression of periostin following treatment of pericytes with EGF with periostin was slightly higher than with the treatment

of EGF only. This may suggest that EGF may encourage periostin to remain within the cell for longer or produce a greater amount of periostin. However, shown in Figure 4.18, the co-treatment with TGF- β and EGF both with and without periostin reduced this effect to a similar level to the control cells. This may suggest a regulatory pathway between these 3 mediators (Ashley et al. 2017, Michaylira et al., 2010). The interaction between TGF- β , EGF and periostin should be explored and modelled in order to fully explore the regulatory relationship between these proteins. These same conditions were also explored in respect to N-cadherin expression in Figures 4.23, 4.24 and 4.25. A very similar trend was observed in these experiments, with TGF- β treatment with and without periostin and the combined treatment with and without periostin having statistically similar levels of N-cadherin expression to the control cells. Again, the addition of periostin to pericytes treated with EGF caused a significant increase in N-cadherin expression compared to the control cells again highlighting an important interaction between EGF and periostin which should be explored further. N-cadherin was chosen as a second marker for these experiments as it is thought to be elevated during pericyte differentiation to myofibroblasts (Shenoy et al., 2016). N-cadherin mediates cell-cell connections and mediates cell migration via several pathways including the activation of MMPs by activating FGF receptors and regulating RhoA GTPase (Shih & Yamada, 2012).

Figures 4.17 – 4.22 explore the effects of IL-13 and TGF- β treatment over various time points, from 24 hours to 9 days. TGF- β treatment caused a peak of periostin expression between 2 and 4 days, after which the expression reduced slightly. This corroborates the previous results suggesting that intercellular periostin levels are high after 2 days of treatment and drop at 5 days treatment (Hamilton, 2008). IL-13 treatment caused the highest spike in periostin expression following only 1 day of treatment, however, and the combined treatment of both IL-13 and TGF- β caused periostin expression to peak at 9 days. The expression of α -SMA was also explored with the same treatments and time points as α -SMA is increased as pericytes acquire myofibroblast characteristics during differentiation in fibrosis (Hughes & Chan-Ling, 2004, Shinde, Humeres & Frangogiannis, 2017). With all of these treatments, the longer the treatment the higher the expression of α -SMA. This is likely due to the increased differentiation of pericytes into myofibroblasts induced by TGF- β and IL-13. Studies have shown that these cytokines encourage the differentiation of pericytes into myofibroblasts (Zhao et al., 2022, Michalik et al., 2018, Johnson et. al., 2015). The results from all of these experiments may not be accurate however as the n numbers for each condition were very low as these were pilot experiments to identify optimal doses and timings of treatment. This was due to a large amount of cells that had become unadhered throughout the 9 days of these experiments although this was not measured. This longitudinal study should be repeated again in order to collect more repeats or using a long-term imaging system and live stains in order to observe the change

over time with each treatment rather than using different wells for each condition. The apparent non-adherence of the cells should also be monitored in case the prolonged treatment induced cell death. This could be via MTT at the timepoints used in the experiment or by flow cytometry with viability stains such as propidium iodide and Annexin V at the end of the experiment (Rieger, et al., 2011). In addition, further study on the changes to gene expression following prolonged treatment could be investigated but was not looked into in this case due to lack of resources.

As immunostaining was used to determine the levels of intercellular periostin, extracellular periostin produced was measured via ELISA (Kono et al., 2019). A variety of growth factor treatments were explored via ELISA in order to elucidate the factor which initiates the increase of periostin production by pericytes (Figure 4.16). Interestingly, treating pericytes with TGF- β , EGF, VEGF or periostin only caused the same amount of periostin to be produced as the untreated cells. However, treating pericytes with IL-13 caused a 9-fold increase in periostin production. This clearly suggests that IL-13 robustly induces the production of periostin by pericytes. This is corroborated by other studies (Ito et al., 2018, Maeda et al., 2019, Makita et al., 2018).

As periostin is known to be elevated in asthma (Burgess et al., 2021), the house dust mite model was used to simulate asthma in mice. This involved exposing mice to a house dust mite allergen intranasally for 5 weeks in order for inflammation to establish and remodelling to start (Johnson et al., 2004). A schematic diagram of the model is included in Chapter 6 (Figure 6.1). Figure 4.15 depicts the periostin concentration in bronchoalveolar lavage fluid in control mice and mice exposed to house dust mite. This Figure shows that periostin levels were slightly, yet not significantly higher, following house dust mite exposure. This hints to a trend which is well accepted as serum periostin is used as a biomarker for asthma and therefore should be elevated in lavage fluid (Takahashi et al., 2019). The lack of significance is likely impacted by the singular low value in an HDM treated mouse. This mouse did respond to HDM treatment as it experienced symptoms of respiratory distress in line with others within this condition and yet displayed low levels of periostin within its BAL (bronchoalveolar lavage) fluid. It is possible that this mouse had developed a more Th17 skewed asthma than the traditional Th2 as periostin is a known Th2 cytokine and has been shown to be suppressed by IL-17 (Rahmawati et al., 2021, Choy et al., 2015). It has been shown, albeit with a different administration method, that HDM can induce a Th17 asthmatic response in C57/Bl6 mice (Yang et al., 2018). This experiment should be repeated again to increase the number of samples and possibly gain significance. Periostin in vitro was further explored through immunostaining lung section such as in Figures 4.12, 4.13 and 4.14. Figure 4.14 shows that there was a significantly higher expression of periostin in asthmatic lungs which suggests that periostin contributes to the pathology of asthma in some way. The images in Figures 4.12 and 4.13 are able to show the localisation of

periostin within the asthmatic lungs. They show a layer of cells robustly expressing periostin around the airway in asthmatic lung tissue which is not present in the untreated PBS lungs. These lungs from HDM-treated mice also displayed other aspects of remodelling (which can most clearly be seen in Figure 4.12) such as a thickened smooth muscle layer and dysregulated epithelial cells. These cells seem to reside in the subepithelium surrounding the airways and therefore may be pericytes as this is where they migrate to during airway remodelling. A co-stain with a pericyte marker such as PDGFR β or CD146 was also included to characterise the periostin-positive cells. Shown in both 4.12 and 4.13, the highlighted cells within the basement membrane are positive for both periostin and two types of pericyte marker, hence strengthening the hypothesis that these cells are pericytes. Figures 4.12 and 4.13 also suggests that there is a large amount of periostin residing in the epithelium which has been suggested by other studies and also highlights the importance of epithelial cells when discussing periostin within the airway (Burgess et al., 2021).

In an effort to pharmacologically modulate periostin production by pericytes, an upstream initiator of periostin production was targeted. Cinnamaldehyde is an aldehyde previously suggested to be a potent IL-13 inhibitor via the activation of Nrf2 (Mitamura et al., 2018, Huang & Wang, 2017). This was explored as a treatment in order to reduce the concentration of periostin induced by IL-13. Various concentrations of cinnamaldehyde were explored in order to find the optimum concentration to use in future experiments. The ELISA results shown in Figure 4.29 shows that concentrations of cinnamaldehyde lower than 1mM had little effect on the production of periostin by pericytes as levels of periostin following treatment with IL-13 were still high. However, at 1mM and higher, cinnamaldehyde prevented the production of periostin, suggesting that at 1mM cinnamaldehyde successfully inhibits IL-13 and therefore that concentration was selected for future experiments. This agrees with previous studies demonstrating the efficacy of cinnamaldehyde in suppressing IL-13 signalling (Mitamura et al., 2018). However, as cinnamaldehyde was only added in the last 3 days of treatment to allow IL-13 to establish an effect, the complete reduction of periostin secretion suggests that periostin may not be very stable, despite previously being described as having a long half-life (Michaylira et al., 2010). The specificity of cinnamaldehyde at 1mM also comes into question as typical doses have been reported to be between 2.3 μ M-75 μ M (Mei et al., 2020, Roth-Walter et al., 2014). Therefore, further investigations into optimum dosing should be completed. Figures 4.30, 4.31 and 4.32 show the results from a scratch assay performed with TGF- β , IL-13 and periostin treated pericytes alongside cinnamaldehyde. Despite not being a direct inhibitor of TGF- β , cinnamaldehyde was still tested against TGF- β treated pericytes as the crosstalk between TGF- β and periostin is not yet fully understood and therefore may be affected by the activation of Nrf2 as Nrf2 has seen to inhibit certain TGF- β mediated pathways (Ryoo, Ha & Kwak, 2014). These

Figures highlighted that treatment with IL-13 and periostin both significantly increase the migration of pericytes. Interestingly, after treating with cinnamaldehyde alongside these growth factors the migration was reduced until it was not significantly different from the control, untreated pericytes. This suggests that cinnamaldehyde strongly inhibited IL-13 which resulted in the reduction of periostin and therefore the reduction of migration (Bignold & Johnson, 2021a). I hypothesise that the IL-13-mediated periostin production which influences pericyte migration is inhibited via the presence of cinnamaldehyde and the subsequent inhibition of IL-13. Studies have previously shown that IL-13 induces periostin production and that periostin contributes to the migration of certain cell types (Ito et al., 2018, Wu et al., 2017). The fact that cinnamaldehyde treatment was able to abrogate aspects of tissue fibrosis such as pericyte migration in vitro, gives hope to the use cinnamaldehyde as a therapeutic to reduce remodelling in asthma. Figures 4.34, 4.35 and 4.36 show the results of immunostaining targeting the intracellular periostin. Surprisingly treatment with periostin or IL-13 did not cause a significant increase in the expression of periostin by pericytes and yet treatment with TGF- β did. Also, the addition of cinnamaldehyde did not yield significantly different results in any treatment group. This is interesting as it is the opposite of the results seen in the previous migration assay. There are several possible reasons for this. TGF- β treatment may cause more periostin to be accumulated intracellularly and therefore would be more visible in immunostained images and less available for signalling during scratch assays. Conversely, IL-13 and periostin treatment may cause periostin to be secreted a higher rate, allowing it to initiate signalling pathways for migration and be able to be detected in the supernatants used in ELISA assays. Periostin likely needs to be incorporated into the ECM in order to engage with cell surface integrins such as $\alpha_v\beta_3$ or directly with ECM proteins such as fibronectin and subsequently initiate migration pathways (Gonzalez-Gonzalez & Alonso 2018, Hoersch & Andrade-Navarro, 2010, Kii et al., 2010). This would also result in a lower signal observed during immunostaining as incorporation into the ECM may hide the epitope that the primary antibody binds to. Again, alongside periostin staining, N-cadherin was also assessed in order to look for pericyte differentiation into myofibroblasts. As expected, only TGF- β treatment yielded a significant increase in N-cadherin expression, supporting the notion that TGF- β promotes myofibroblast differentiation (Willis & Borok, 2007). However, much is still unknown regarding the importance of N-cadherin in pericyte differentiation and may instead be more indicative of the migratory capacity of the pericytes. The reduction of N-cadherin expression following the addition of cinnamaldehyde to periostin-treated pericytes is surprising, and may hint at crosstalk between pathways responsible for periostin inhibition and differentiation. However, this disagrees with current literature as the activation of Nrf2 by cinnamaldehyde is thought to activate the RhoA-ROCK cascade which is involved in periostin-induced differentiation to

myofibroblasts (Ko et al., 2021, Li et al., 2016, Nikoloudaki et al., 2020). As these cascades are complex, more investigation into their interplay should occur. More studies should also be performed to interrogate the signalling pathways involved in the function of N-cadherin in pericytes before major conclusions can be drawn (Ferrell, et al., 2022). Surprisingly, the addition of cinnamaldehyde increased this even further, which may indicate a relationship between cinnamaldehyde and pericyte differentiation which would not be beneficial if cinnamaldehyde was used for the treatment of asthma as the differentiation of pericytes to myofibroblasts should be discouraged lest they exacerbate the fibrosis. The exact mechanism behind the possible additive effect of TGF- β and cinnamaldehyde is yet unknown but may be, at least in part, due to the complex crosstalk between periostin and TGF- β (Nanri et al., 2019). There is also a concern that cinnamaldehyde may have other adverse effects on lung tissue as in vitro studies have been carried out on cinnamaldehyde-containing vape juices which resulted in impaired glycolytic capacity in human bronchial epithelial cells and reduced cilia movement at concentrations higher than 0.5mM of cinnamaldehyde (Clapp et al., 2019). This suggests that the wider effects of cinnamaldehyde should be explored before pursuing cinnamaldehyde as a possible therapeutic to reduce periostin levels in asthma and thereby mitigate airway wall remodelling.

Taken together, the studies performed in this chapter demonstrate that periostin, a key component of the remodelled airway in allergic airway disease, can be produced and secreted by pericytes in response to mediators known to be highly expressed in chronic allergic inflammation. It was further demonstrated that periostin production by pericytes can be pharmacologically targeted which opens up further avenues to interrogate the mechanisms by which pericytes contribute to tissue fibrosis.

Chapter 5 – A New Dimension: Spheroids Containing a Co-Culture of Endothelial Cells and Pericytes Can Be Constructed Via Magnetic Levitation

5.1 Introduction

In vitro cell culture techniques are the backbone of most biomedical research. The optimisation and innovation of cell culturing techniques have been consistently developed since its development by Ross Granville Harrison in 1907 to study nerve fibres from amphibians (Harrison, 1907). The development of immortalised cell lines, the first of which were derived from the cervical tumour of Henrietta Lacks and dubbed HeLa cells, allowed the continuous study of cells, without the need to generate primary cells (Gey, Coffman & Kubicek, 1952, Masters, 2002). HeLa cells went on to contribute to the understanding of many important scientific topics such as the polio vaccine, HIV (human immunodeficiency virus) infection and cellular ageing (Scherer, Syverton & Gey, 1953, Maddon et al., 1988, Greider & Blackburn, 1985). With advances in media, laboratory plastics, and robust, immortalised cell lines, future innovations have been geared towards the transition from 2D cultures to 3D cultures. There are various different types of 3D cultures which are designed to aid a variety of different tasks and research questions. One of the most prominent of these is bioprinting, and the goal to create personalised organs from patients' cells (Noor et al., 2019). This is done using current 3D printing technology combined with the creation of "Bioink" from pluripotent stem cells. However, this research is still in its early stages and relies on artificial scaffolding and hydrogels which is also a different sector of 3D cell culture research. The exploration of possible cellular scaffolds includes polymer based scaffolds as well as ECM-derived scaffolds around porous electrospun polycaprolactone or silicone bases (Zhu et al., 2019, Jordahl et al., 2019). This would allow the patients' cells to differentiate and associate with each other to form tissue, either for research purposes or, in the future, transplantation. Smaller 3D cultures have also been explored, which involve various different cell types and are often scaffold-free. These are referred to as spheroids or organoids depending on complexity and structure with spheroids being simple cell clusters and organoids being complex with a varied structure, often deriving from stem cells (Gunti et al., 2021).

Several groups have begun to explore the use of these 3D cultures to mimic airways in order to model diseases without the use of animals. Some have used patient derived tissue to isolate cells such as those found in the airway epithelium allowing the formation of airway epithelial spheroids

(Sachs et al., 2019, Boecking et al., 2022). Some have also been able to construct complex 3D cultures consisting of airway epithelial and airway endothelial cell lines alongside patient-derived fibroblasts. These spheroids were able to self-assemble and form lung-like structures which highlights the possibility that these types of cultures would be useful in early-stage disease modelling (Tan et al., 2017).

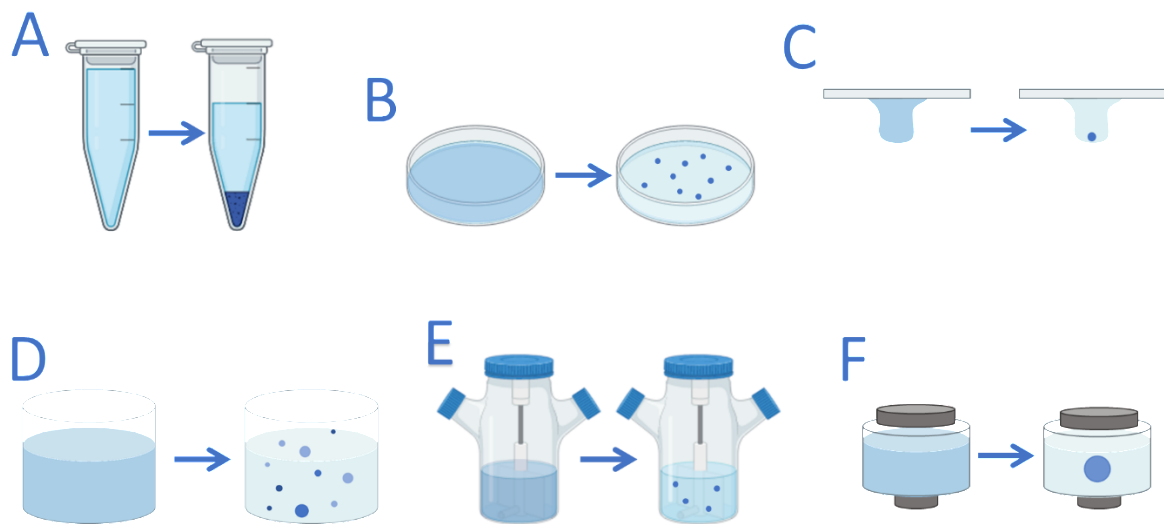


Figure 5.1 - Graphical diagram depicting several methods for spheroid and organoid formation. Methods shown are as follows: A – Centrifugation, B – Liquid Overlay, C – Hanging Drop, D – Hydrogel, E – Spinner Culture, F – Magnetic Levitation. Based on information from (Ryu, Lee & Park, 2019)

There are various methods for creating organoids and spheroids, which rely on a range of different resources as outlines visually in Figure 5.1. One of the simplest methods involves pelleting the cells using centrifugation. This method is mainly used to induce and observe differentiation of mesenchymal stem cells in 3D. This method is simple and, as conditions are similar to normal cell culture, a wide range of analytical techniques can be used on the pellets including immunohistochemical analysis and PCR (polymerase chain reaction)(Bosnakovski et al., 2004). However, the pellets must be imaged in sections due to their large size, and therefore some global information may be missed, such as size difference or 3D organisation. It is also possible that the high density environment formed in the pellet may not be suitable for all cell types and may be restricted in size by gravity and the density which may cause hypoxic conditions in the centre of the mass (Zhang et al., 2010).

Another very simple method is liquid overlay. This utilises non-adherent tissue culture plastic with the addition of a layer of agar or agarose to further prevent adhesion to the plates. Unable to stick to the plate, adherent cells would instead attach to each other, forming spheroid clusters. Much like the pellet method, this method is useful as minimal extra equipment is needed and extra reagents

are commonly used in laboratory environments anyway. However, as this technique results in spontaneously formed spheroids, the lack of control may be a downside as the number and size of the spheroids cannot be predicted and is likely to be variable. Although, studies have shown that using 96-well plates to culture spheroids reliably causes one spheroid per well to form and have even created spheroids of co-cultured cells using this method (Metzger et al., 2011). This highlights the potential of this technique as a basis for creating complex co-culture spheroids.

Much like Metzger et al. saw with their liquid overlay technique, the hanging drop technique allows one spheroid per culture area to form, the size of which can generally be controlled by the number of cells seeded. As the name suggests, the hanging drop method involves suspending cells upside down in drops of cell medium. The drop remains on the upside down plate and spheroids form due to surface tension and the lack of a surface to adhere to (Metzger et al., 2011, Foty 2011, Timmins & Nielsen, 2007). This method removes the effect of the surface of the culture flask, the material and stiffness of which may affect differentiation and proliferation of mesenchymal stem cells (Kozaniti et al., 2022). Again, this technique can be completed using common cell culture materials and requires no specific additional equipment. There are several disadvantages to this method, once cells have been suspended, they are unable to be treated and therefore all treatments must be completed before the suspension. This reduces the flexibility of treatment available using this method as spheroids take several days to establish. It is also not suitable for every cell type, with around half the cancer cell lines explored by Carlsson et al. unable to form spheroids (Carlsson et al., 1983, Costa et al., 2018). This method is an interesting and effective method for spheroid formation, but may not be suitable for all experiment setups.

The incorporation of hydrogels into existing cell culture techniques allows the spontaneous formation of spheroids within a semi solid medium. The gels provide a 3D space whilst still maintaining access to medium and treatments as in normal, 2D cell culture. In addition, the viscosity and composition (such as fibrin, collagen and hyaluronic acid) can be altered to suit the specific cells and experiments desired (Ryu, Lee & Park, 2019). A downside to this technique, however, is the inability to control the exact size or number of spheroids formed, although this can be influenced through different seeding densities. One of the methods which requires slightly more advanced equipment is the spinner culture technique. This technique relies on culturing cells in a bioreactor which prevents cells adhering to the sides of the vessel and so, again, they adhere to each other. This is good for high throughput spheroid formation as bioreactors can be used for large cell numbers (Sutherland et al., 1970, Han et al., 2006). However, the optimisation of the stirring speed is required as too fast and the spheroids would either not form or break apart and too slow and the cells will sink to the bottom and aggregate there.

Another method with specialised equipment, and the one which will be used in this chapter, is the magnetic levitation technique. This involves a magnetic array which encases a culture plate containing cells. Iron nanoparticles are inserted into the cells via centrifugation and the opposing magnetic fields result in the suspension of the cells within the wells. As the cells are suspended, the cell culture plastic has no effect on the cells. In addition, the conditions the spheroids are grown in can be easily manipulated, with different medium or treatments possible at any point in the experiment. It also allows for greater control of the number of spheroids than some methods, as one spheroid will form on each magnetic node (Lewis et al., 2017). However, there have also been downsides to the incorporation of iron nanoparticles and the use of almost weightlessness. These conditions could affect the metabolism or growth of certain cell structures. The use of magnetic levitation to grow spheroids will be explored in this chapter using a co-culture of HPLPCs and HUVECs. Co-cultures were established at a ratio of 1:5 pericytes to endothelial cells as literature estimates that in “normal” tissue, pericyte coverage is between 1:1 and 1:10, with the lung likely having a higher ratio than muscle tissue but less coverage than the blood brain barrier (Armulik et al., 2011, Rowley & Johnson, 2014).

5.2 Results

In order to evaluate the method, spheroids containing both pericytes and endothelial cells were constructed using the method from the Manufacturers website (see Methods section). VEGF and H₂O₂ treatments were undertaken as it was hypothesised that VEGF treatment would encourage pericyte-endothelial connections due to its role in angiogenesis whilst oxidative stress conditions would lead to cell damage and therefore dissociation. DAPI stain was used in isolation in the following images as it allows the overall shape and physiological characteristics of the spheroids to be observed clearly.

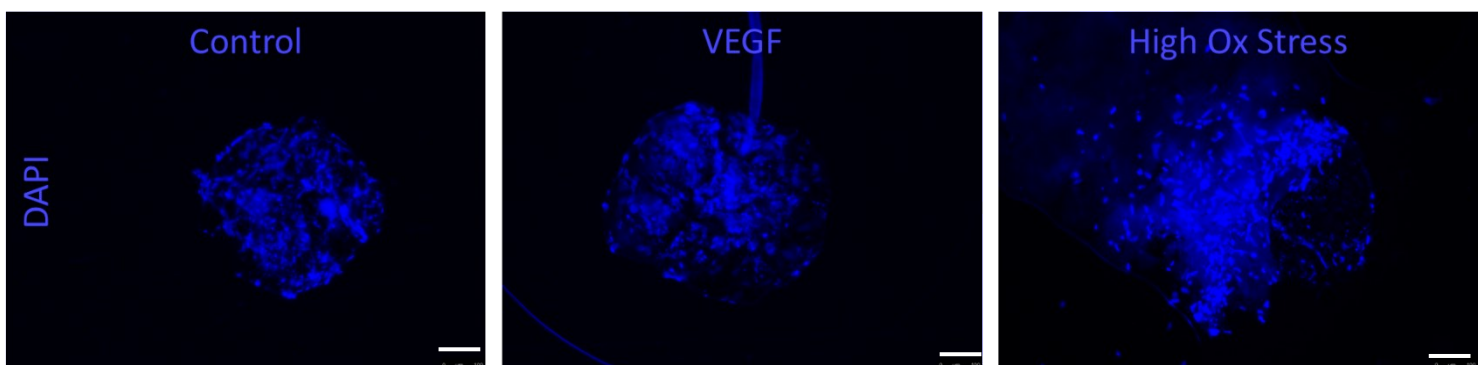


Figure 5.2 – Various characteristics of spheroids can be observed using DAPI staining. Representative images depicting 3D spheroids of HPLPCs and HUVECs. Spheroids were grown for 7 days and treated with 10ng/ml VEGF or 50 µg/ml of H₂O₂ for a further 5 days in order to simulate high oxidative stress conditions. Spheroids were stained with DAPI to visualise nuclei and imaged at x400 using a Leica Widefield microscope. Scale bars = 250µm.

Images shown in Figure 5.2 are representative of all images from these conditions. They depict the nuclei within the 3D structures, although some are not in the plane of focus and so the actual number of nuclei and therefore cells within the spheroid cannot be determined. The images show variable roundness between the conditions, having areas where the cell density decreases (often near the edges) and increases (often near the core). The circumferences of the spheroids are also not smooth or uniform, indicating an issue in the formation of these spheroids. However, this also may be due to the different treatments explored.

Several measurements of the spheroids were taken to explore the variability within the treatment conditions in order to evaluate the effectiveness of this method.

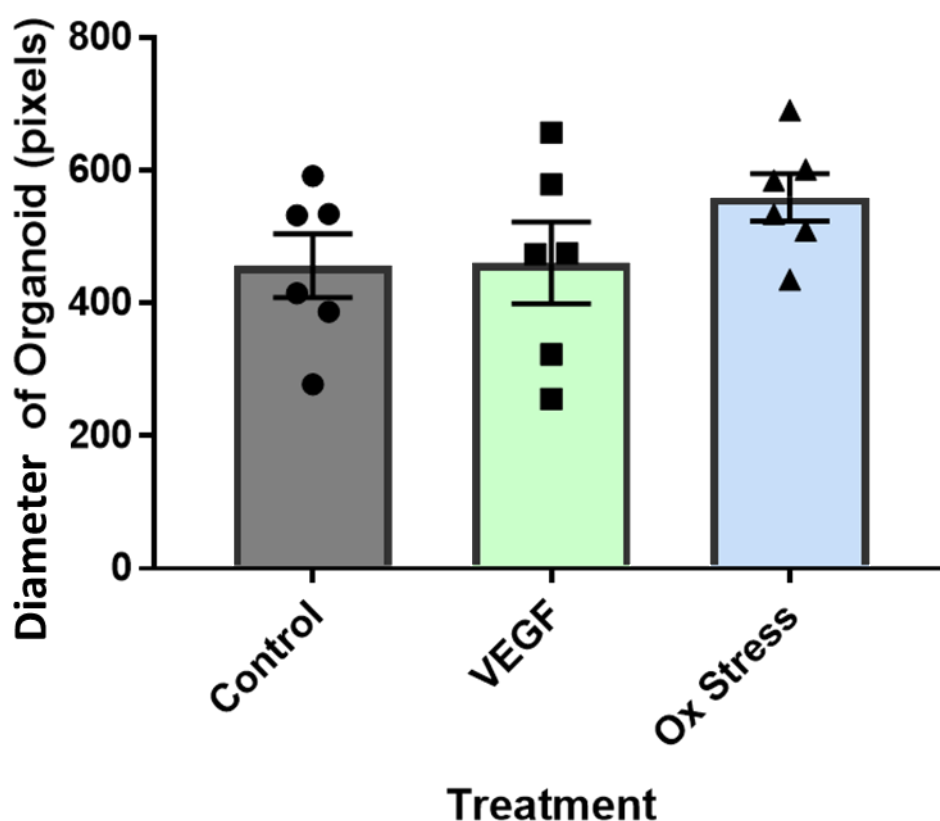


Figure 5.3 – There was no difference in the diameter of the spheroids following VEGF or H₂O₂ treatment. 3D spheroids of HPLPCs and HUVECs were constructed. Spheroids were grown for 7 days and treated with 10ng/ml VEGF or 50 µg/ml of H₂O₂ for a further in order to simulate high oxidative stress conditions. Spheroids were stained with DAPI to visualise nuclei and imaged at x400 using a Leica Widefield microscope. Analysis was performed on these images using ImageJ to measure the diameter of the spheroids at the widest point. Results were not significant to $p < 0.05$, $n = 6$ from 1 independent experiment by one-way analysis of variance (ANOVA) for multiple groups with the Tukey post hoc test.

As each data point is represented on the graph in Figure 5.3 the spread of data within the condition can be examined. This can be seen by examining the CV (coefficient of variance) of the data which is calculated with the formula standard deviation/mean. The CV of both Control and VEGF conditions is 26% and 33%, respectively which is thought to be moderate, indicated a relatively large spread of data. This may suggest that the method is less reliable in creating consistently sized spheroids. There is also no significant difference in the diameter of the spheroids between the treatments observed in this experiment, although it seemed that spheroids treated with H₂O₂ had a slightly greater diameter than those without treatment of those treated with VEGF which had a very similar average diameter.

Another metric of size was also explored through the measurement of the overall area of the spheroids.

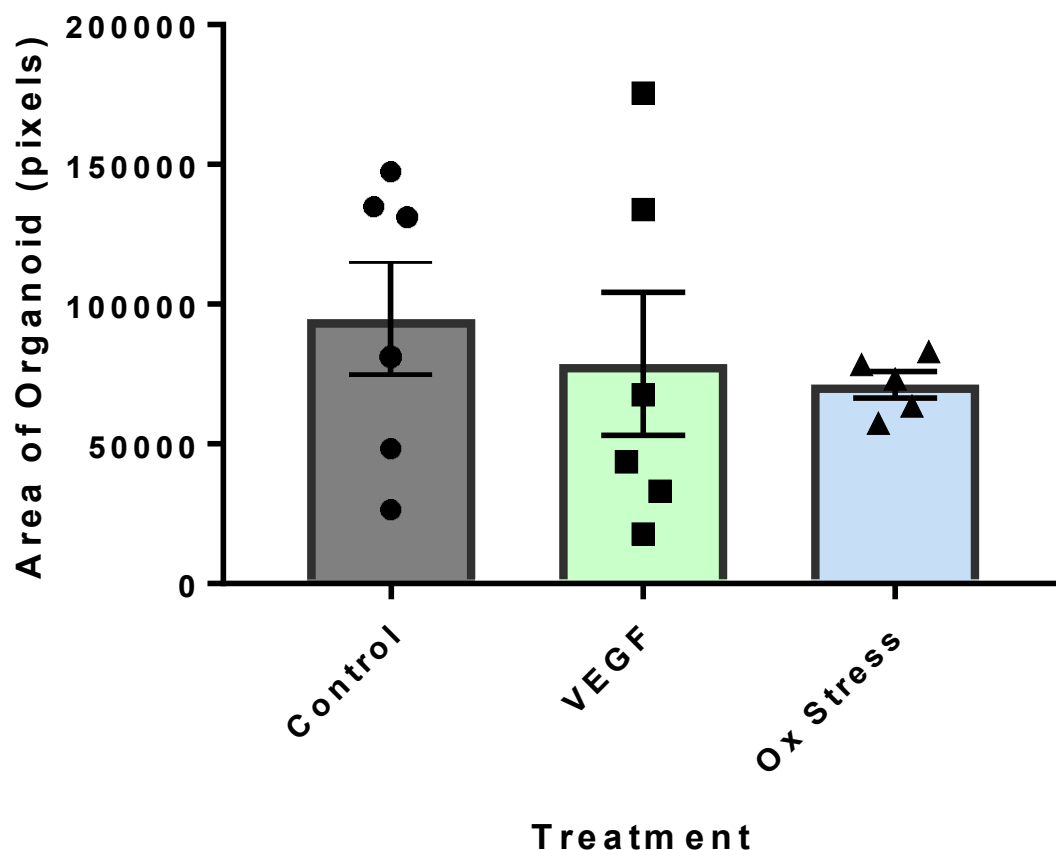


Figure 5.4 – Spheroids treated with H₂O₂ had a more consistent area than VEGF or untreated spheroids. 3D spheroids of HPLPCs and HUVECs were constructed. Spheroids were grown for 7 days and treated with 10ng/ml VEGF or 50 µg/ml of H₂O₂ for a further 5 days in order to simulate high oxidative stress conditions. Spheroids were stained with DAPI to visualise nuclei and imaged at x400 using a Leica Widefield microscope. Analysis was performed on these images using ImageJ to measure the area of the spheroids using “Region of Interest” measurements. Results were not significant to p<0.05, n=5/6 from 1 independent experiment with 1 outlier being removed prior to analysis by one-way analysis of variance (ANOVA) for multiple groups with the Tukey post hoc test.

Similar to in Figure 5.3, the spread of data is clear to see. The CV of the untreated spheroid was 53% and the VEGF-treated spheroid was 80% which was even higher than those seen in Figure 5.4. Therefore the overall size of the spheroids in these conditions may not be very consistent. Again, there was no significant difference of the size of the spheroids between the three treatment groups. However, there is a slight decrease in spheroid size following treatment with either VEGF or H₂O₂.

One aspect of spheroid formation which is slightly more difficult to examine is that of the density. However, this aspect is important as the structure of the spheroid should be consistent to facilitate pericyte-endothelial cell interactions and to properly mimic blood vessel structure.

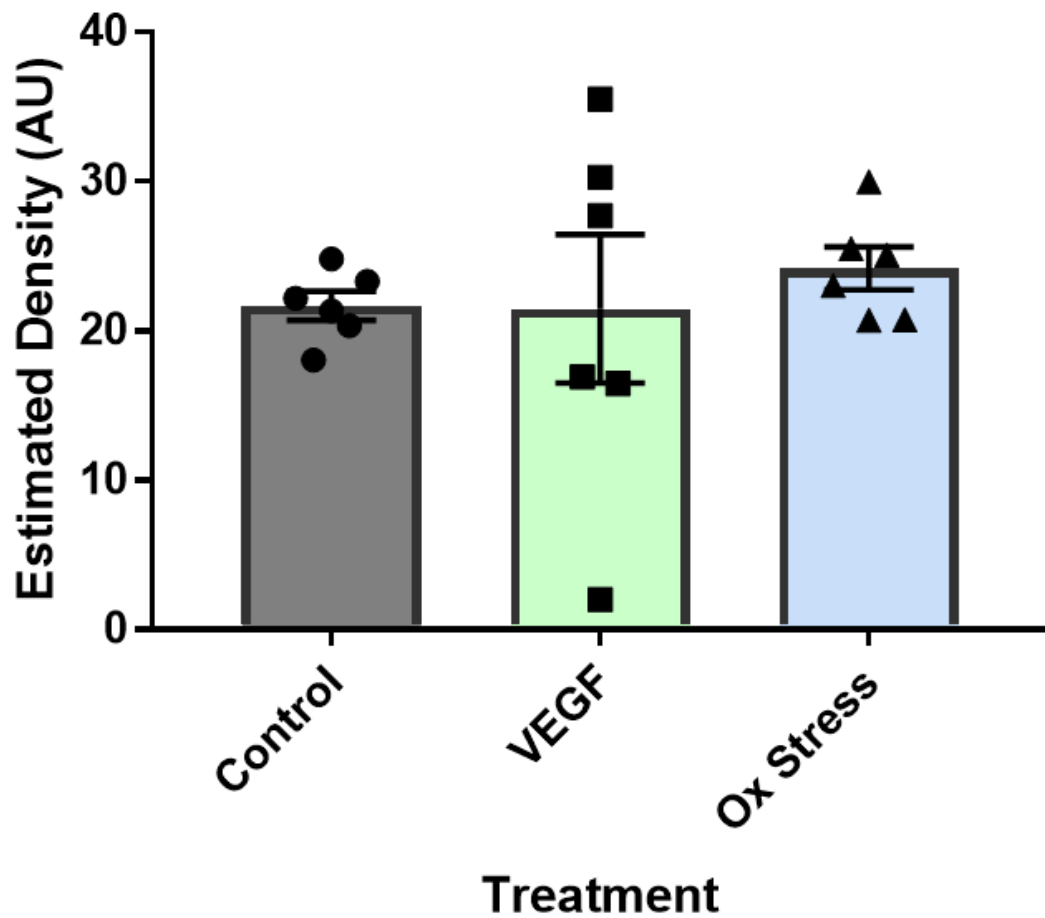


Figure 5.5 – The density of VEGF treated spheroids had a more variable density than the other treatments. 3D spheroids of HPLPCs and HUVECs were constructed. Spheroids were grown for 7 days and treated with 10ng/ml VEGF or 50 µg/ml of H₂O₂ for a further 5 days in order to simulate high oxidative stress conditions. Spheroids were stained with DAPI to visualise nuclei and imaged at x400 using a Leica Widefield microscope. Analysis was performed on these images using ImageJ to estimate the density of the spheroids using the integrated density of DAPI/area. Results were not significant to $p < 0.05$, $n = 6$ from 1 independent experiment by one-way analysis of variance (ANOVA) for multiple groups with the Tukey post hoc test.

Estimated density was calculated by measuring the integrated density of the DAPI stain measure via

ImageJ, per the area, depicted by drawing a region of interest around the circumference of the spheroid. This should measure the amount of DAPI without being influenced by the changes in the area of the spheroids. There was no significant difference in density between these treatments much like the area and length shown in Figures 5.3 and 5.4. Again, we can also look at CV to see the consistency of data within the treatment groups. It is apparent that there was a relatively large spread of data within the VEGF treatment group with a CV of 57% which may indicate high variability of density.

A further batch of spheroids were created using the same method outlined previously. They were additionally stained with fluorescent differential markers to observe the different cell types and attachments.

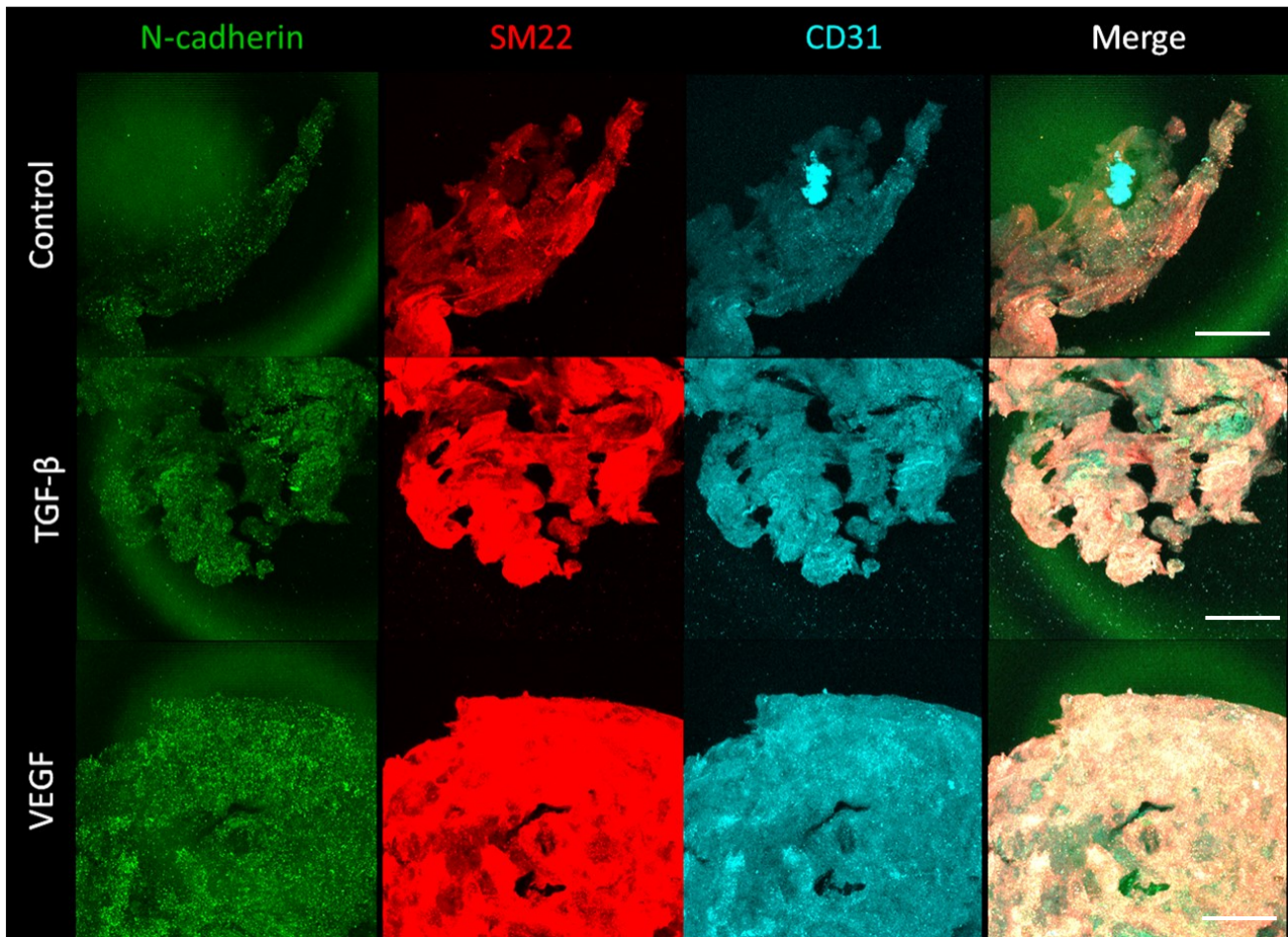


Figure 5.6 – Spheroids can have varying levels of structural integrity and may break apart even in the absence of treatment. Representative images depicting 3D spheroids of HPLPCs and HUVECs. Spheroids were grown for 7 days and treated with 10ng/ml VEGF or 10ng/ml TGF- β for a further 5 days. The magnetic levitation array was only kept on for 24 hours and pericytes and endothelial cells were used at 1:1 as deviations from the method outlined in “Materials and Methods”. Spheroids were stained with SM22 in red to stain pericytes, CD31 in cyan to stain endothelial cells and N-cadherin in green. They were imaged at x630 using a Leica Confocal microscope. Scale bars = 200 μ m.

Spheroid formation in the experiment (Figure 5.6) was not as uniform as shown in Figure 5.2. The images of the untreated cells show an almost crescent structure, indicating some circularity was achieved but may have broken away upon staining. Similarly, the images from spheroids treated with TGF- β showed great irregularity around the edges of the cell mass highlighting the likelihood of structural damage. There also seems to be a high co-localisation of the SM22 (pericyte specific stain) and CD31 (endothelial specific stain) signals, suggesting that endothelial cells and pericytes are orientated similarly within the spheroid.

The expression of these markers were then quantified using ImageJ to assess the effects of the treatments and the structure of the spheroids.

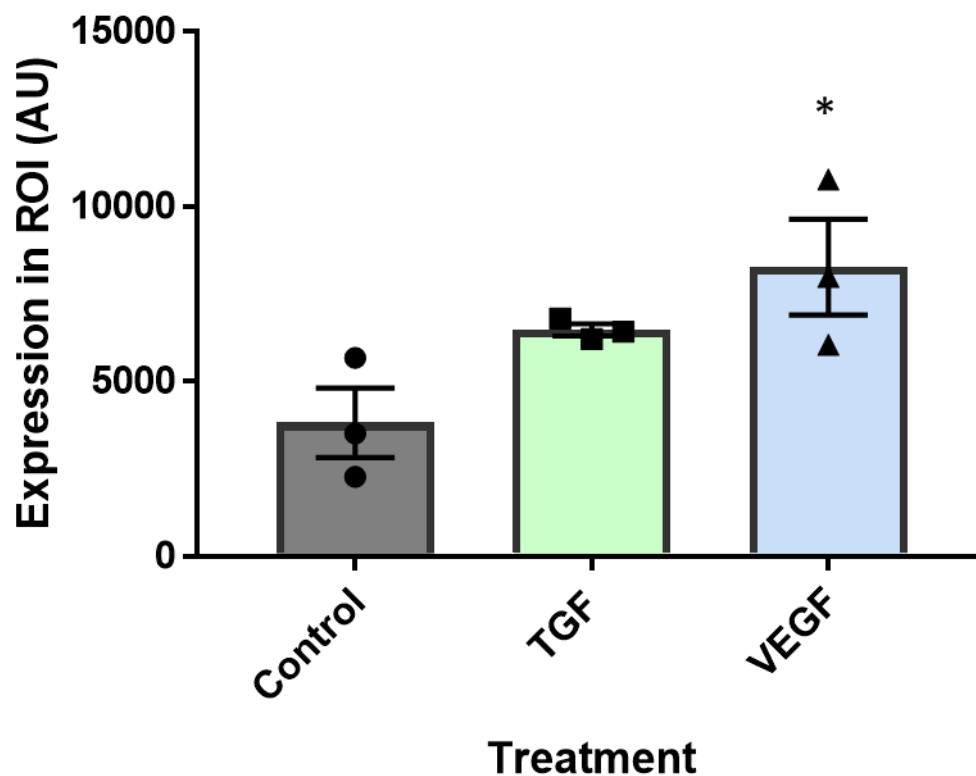


Figure 5.7 – VEGF treated spheroids showed a greater expression of N-cadherin. 3D spheroids of HPLPCs and HUVECs were constructed. Spheroids were grown for 7 days and treated with 10ng/ml VEGF or 10 ng/ml of TGF- β for a further 5 days. Spheroids were stained with N-cadherin, SM22 and CD31, and imaged at x630 using a Leica Confocal microscope. Analysis of the integrated density of the N-cadherin stain in the ROI was performed on these images using ImageJ. “*” = $p < 0.05$, $n = 3$ from 1 independent experiment by one-way analysis of variance (ANOVA) for multiple groups with the Tukey post hoc test..

The expression of N-cadherin was measured in 2D images taken of spheroids. There is a significant increase in the expression of N-cadherin following the treatment of the spheroids with VEGF ($p=0.0423$). However, treatment with TGF- β did not lead to significant changes in N-cadherin expression compared to the untreated spheroids. This may have been due to the structure of the spheroids as, as shown in Figure 5.6, VEGF treated spheroids looked more structurally robust. The number for this calculation is also relatively low and some data is relatively variable, especially the data from the VEGF treated spheroids.

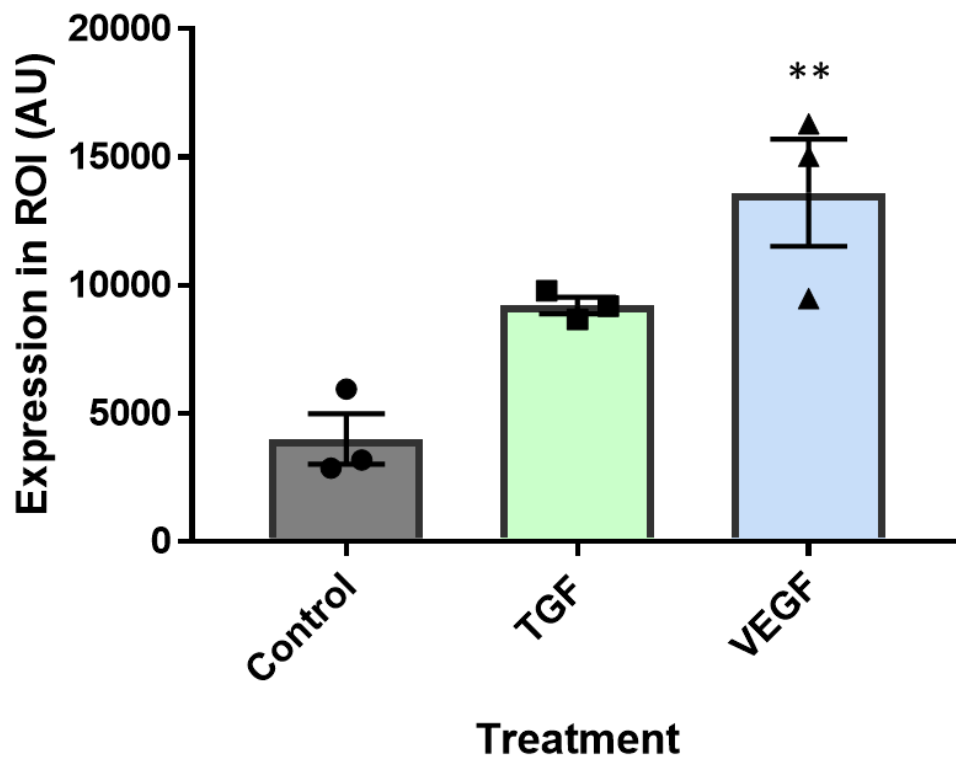


Figure 5.8 - VEGF treated spheroids showed a greater expression of SM22. 3D spheroids of HPLPCs and HUVECs were constructed. Spheroids were grown for 7 days and treated with 10ng/ml VEGF or 10 ng/ml of TGF- β for a further 5 days. Spheroids were stained with N-cadherin, SM22 and CD31, and imaged at x630 using a Leica Confocal microscope. Analysis of the integrated density of the SM22 stain in the ROI was performed on these images using ImageJ. “***” = $p < 0.01$, $n = 3$ from 1 independent experiment by one-way analysis of variance (ANOVA) for multiple groups with the Tukey post hoc test.

Similar to the results seen in Figure 5.7, treating spheroids with VEGF caused a significant increase in expression, this time of SM22 ($p = 0.0057$). There was also, again, a relatively large spread of data observed in the VEGF-treated condition compared to the other conditions which possibly suggests variation in the structure of the spheroids. Treatment with TGF- β caused a slight yet non-significant increase in SM22 expression compared to untreated spheroids. This may be due to an increase in the expression of SM22 by the cells or an increase in the number of cells expressing SM22. This remains unclear due to technical limitations at the time of this study as a higher powered microscope would be required to distinguish between individual cells.

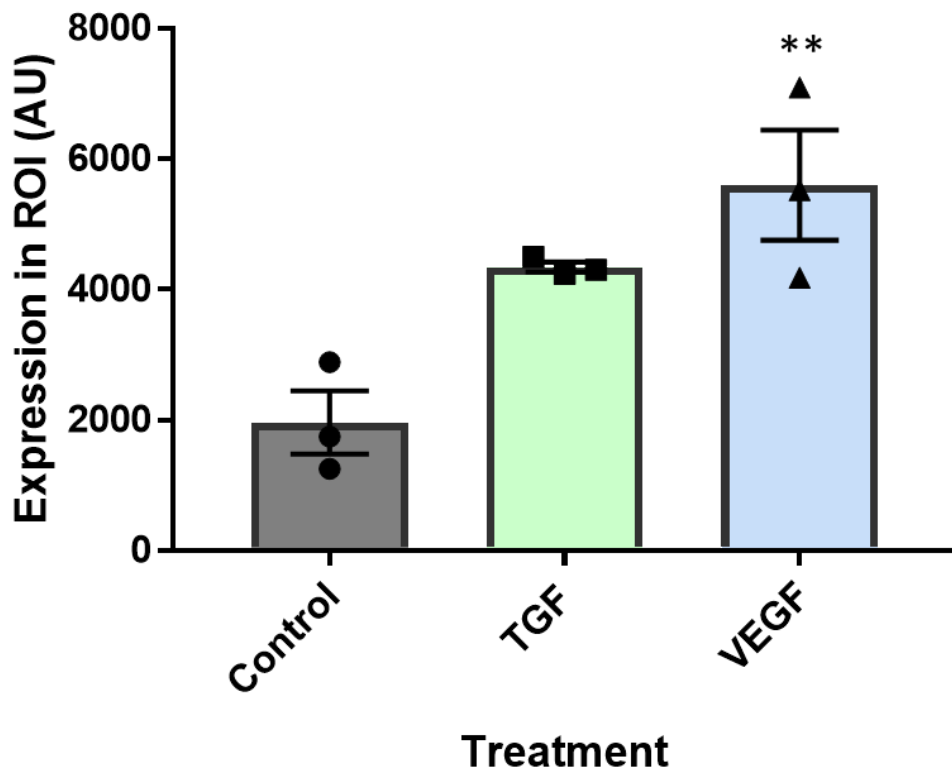


Figure 5.9 - VEGF treated spheroids showed a greater expression of CD31. 3D spheroids of HPLPCs and HUVECs were constructed. Spheroids were grown for 7 days and treated with 10ng/ml VEGF or 10 ng/ml of TGF- β for a further 5 days. Spheroids were stained with N-cadherin, SM22 and CD31, and imaged at $\times 630$ using a Leica Confocal microscope. Analysis of the integrated density of the CD31 stain in the ROI was performed on these images using ImageJ. “**” = $p < 0.01$, $n = 3$ from 1 independent experiment by one-way analysis of variance (ANOVA) for multiple groups with the Tukey post hoc test.

Again, VEGF-treatment of spheroids caused an increase in the expression of CD31. The data in the VEGF-treated condition is once again spread and the low n-number means the data may not be wholly accurate. The TGF- β treated spheroids also showed a slight increase in the expression of CD31 although this was not quite significant. More repeats from more than one independent experiment may lead to this result becoming significant.

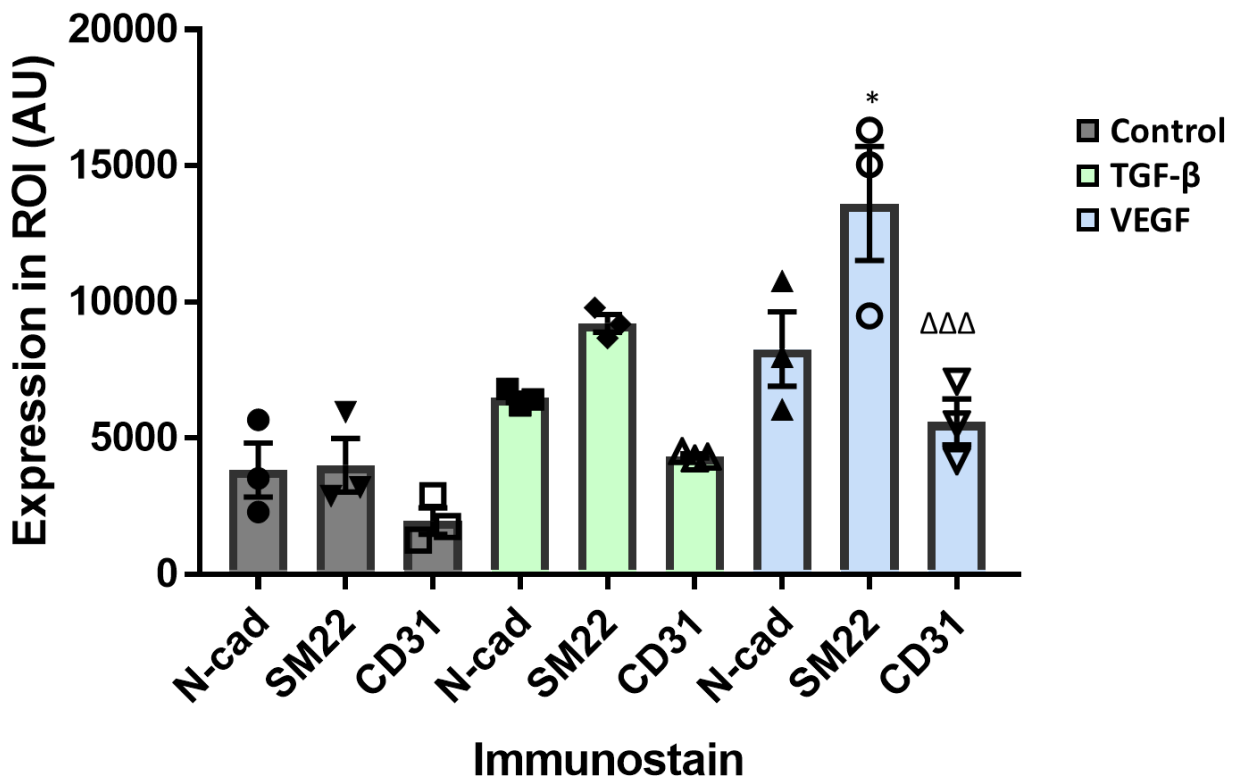


Figure 5.10 – Following all treatments SM22 was the stain with the highest expression, with VEGF treatment resulting in the highest expression overall. 3D spheroids of HPLPCs and HUVECs were constructed. Spheroids were grown for 7 days and treated with 10ng/ml VEGF or 10 ng/ml of TGF- β for a further 5 days. Spheroids were stained with N-cadherin, SM22 and CD31, and imaged at x630 using a Leica Confocal microscope. Analysis of the integrated density of the N-cadherin, SM22 and CD31 stains in the ROI was performed on these images using ImageJ. “*” = $p < 0.05$ compared to VEGF N-cad, “ $\Delta\Delta\Delta$ ” = $p < 0.001$ compared to VEGF SM22, $n=3$ from 1 independent experiment by one-way analysis of variance (ANOVA) for multiple groups with the Tukey post hoc test.

Data in Figure 5.10 is the same data from Figure 5.7, 5.8 and 5.9 but collated to allow the comparison of stains within each treatment group. In each treatment group, the CD31 stain had the lowest expression. In both the groups treated with either TGF- β or VEGF, SM22 was the most highly expressed stain, with the expression of SM22 in VEGF-treated spheroids being significantly higher than the expression of N-cadherin in VEGF-treated spheroids ($p=0.0331$). The expression of SM22 in VEGF-treated spheroids was also significantly higher than the CD31 expression in VEGF-spheroids ($p=0.0007$). However, in the untreated spheroids, the expression of N-cadherin and SM22 was very similar.

Based on the unsatisfactory CD31 staining in figure 5.6, we elected to investigate the use of isolectin staining to identify endothelial cells.

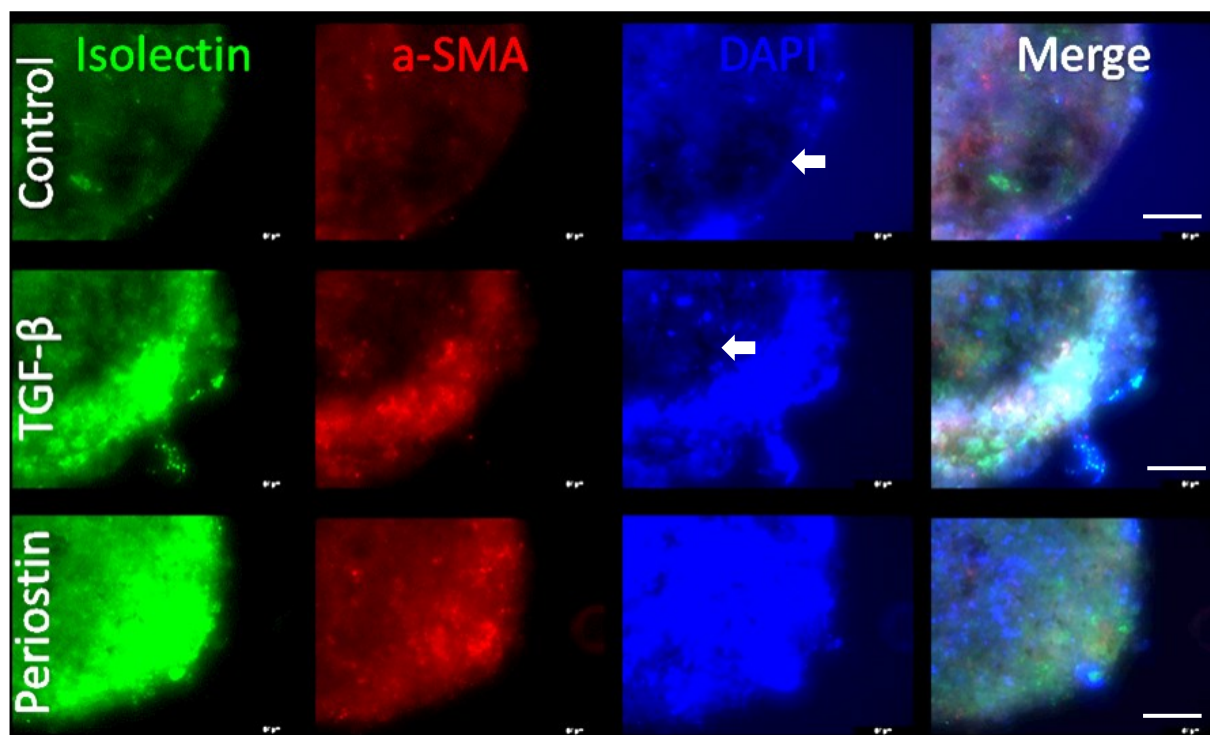
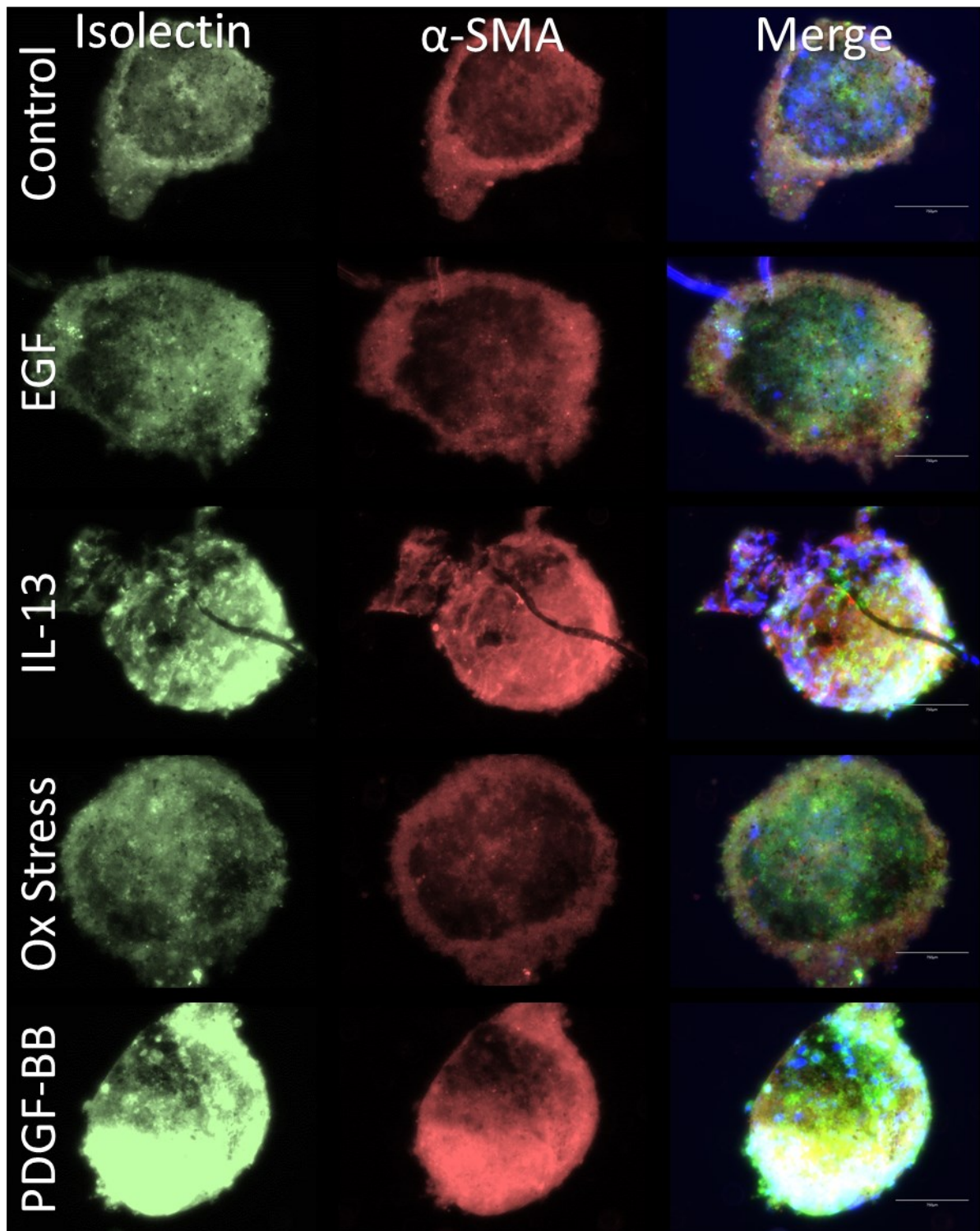


Figure 5.11 – Untreated and TGF- β treated spheroids contained areas with reduced cell densities. Representative images depicting 3D spheroids of HPLPCs and HUVECs. Spheroids were grown for 7 days and treated with 10ng/ml TGF- β or 100ng/ml periostin for a further 5 days. Spheroids were stained with isolectin in green to stain endothelial cells, α -SMA in red to stain pericytes and DAPI in order to visualise cell nuclei. They were imaged at x400 using an EVOS M5000 microscope. White arrow indicates an area with reduced cell mass. Scale bars = 200 μ m.

The Isolectin GS-IB4 from *Griffonia simplicifolia* conjugated to AlexaFluor™ 488 stain was used to mark endothelial cells. These representative images suggest that the untreated spheroids have a lower expression of isolectin and therefore contain fewer endothelial cells. Similarly, pericytes, labelled by the α -SMA stain, increased with treatment from the control baseline. The reduction of both cell types indicated that there may have been less cell mass in the untreated spheroids or an issue with the penetration of the antibodies to the centre of the spheroid. The latter is corroborated by the hole indicated by the white arrow in the DAPI image. The images from the TGF- β -treated spheroids also show an increased expression and cell mass around the edge of the spheroid and reduced cells in the centre (indicated by the white arrow). The periostin-treated spheroid had a more uniform cell layer seen in the DAPI images yet it seemed to still have increased isolectin and α -SMA in cells around the edge of the spheroid.

Expression of these markers were not calculated as many of the spheroids contained auto-fluorescent artefacts which would prevent accurate analysis. These were likely to be dust or hairs introduced when moving the spheroids for mounting. A further round of spheroids was therefore constructed and additional treatments were tested.



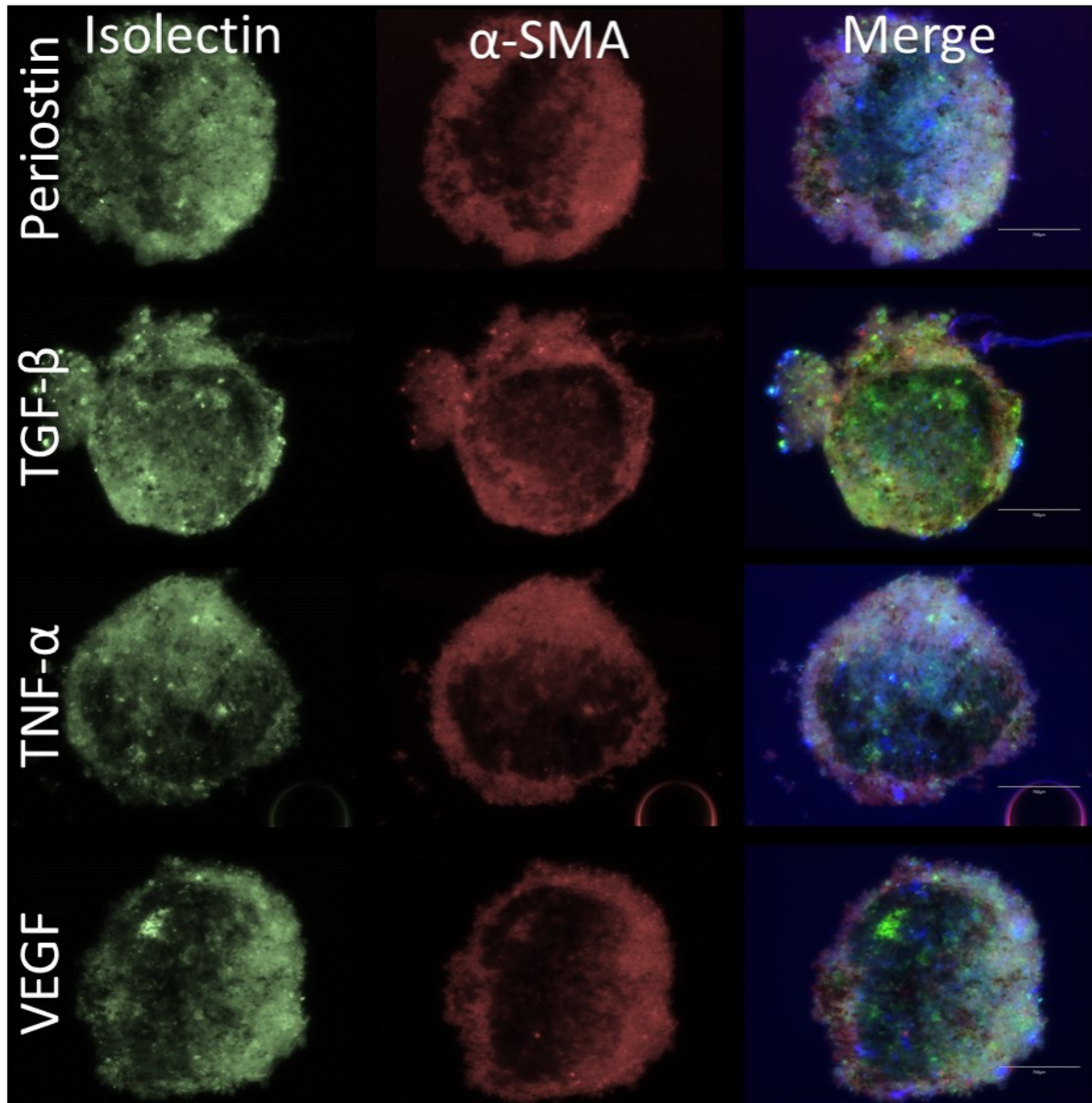


Figure 5.12 – Many treatments resulted in a reduced cell mass in the core of the spheroids as well as irregularities around the outside of the spheroids. Representative images depicting 3D spheroids of HPLPCs and HUVECs. Spheroids were grown for 7 days and treated with 10ng/ml EGF, 100ng/ml IL-13, 50 μ g/ml H₂O₂, 300 μ g/ml PDGF-BB, 100ng/ml periostin, 10ng/ml TGF- β , 10ng/ml TNF- α or 10ng/ml VEGF for a further 5 days. Spheroids were stained with isolectin in green to stain endothelial cells, α -SMA in red to stain pericytes and DAPI in order to visualise cell nuclei. They were imaged at x200 using an EVOS M5000 microscope. Isolectin and α -SMA images were produced as greyscale and colourized using Microsoft Powerpoint for visual purposes. Merged images are raw images, isolectin and α -SMA images are black and white with colour correction performed in Microsoft PowerPoint. Scale bars are 750 μ m.

Treatments were chosen as they had either been previously explored as a stimulant for migration or have been linked to inflammation. Overall, images shown in Figure 5.12 had an overall circular shape showing that this method formed spheroids effectively. Some conditions, such as the TGF- β -treated spheroids and the IL-13 treated spheroids displayed a fragmented edge of the spheroids that was

not observed during culturing, indicating structural damage had occurred during staining. Many of the spheroids, seen most obviously in the α -SMA images, had a decreased cell mass in the centre of the spheroid, suggesting the spheroids forming were hollow, some cell death occurred at the centre of the sphere or antibody was unable to fully perfuse into the centre of the spheroid. This was also highlighted in the previous Figure 5.11, so this phenomenon is replicable. This may be due to the natural organisation of pericytes and endothelial cells when co-cultured and therefore may be an early sign of “blood-vessel” formation. In general, α -SMA-positive pericytes orientate themselves around the edges of the spheroid with the isolectin-positive endothelial cells being more present towards the centre of the sphere. This is most apparent in the control, EGF-treated and H_2O_2 -treated spheroid merged images. In order to further identify the location of the isolectin stain, on either pericytes, endothelial cells or both, more high resolution images need to be taken.

Some variation in the intensity of the stain within treatment groups was observed and so a further comparison was made.

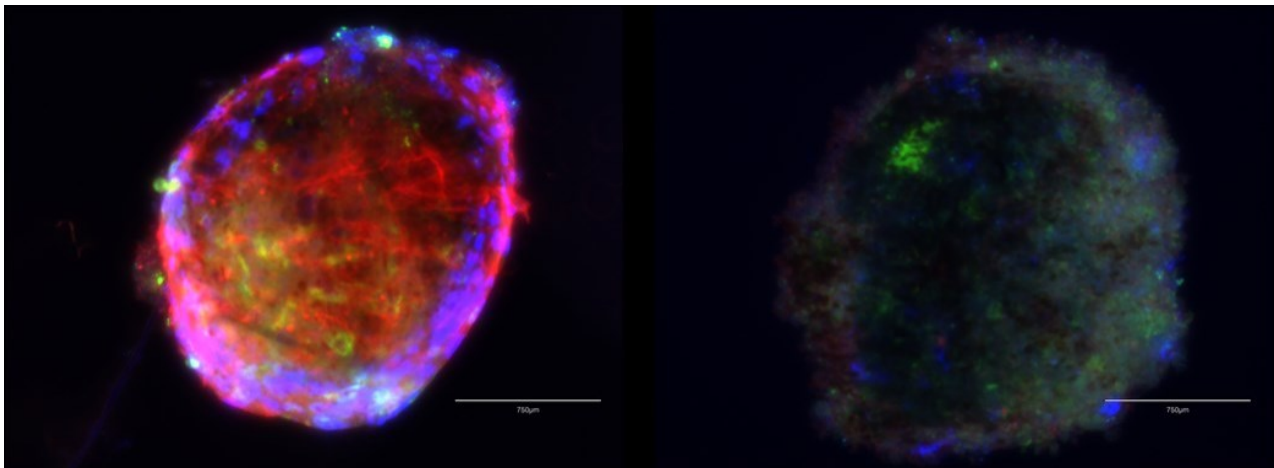


Figure 5.13 – There is great variation in staining intensities within treatment groups. Representative images depicting 3D spheroids of HPLPCs and HUVECs. Spheroids were grown for 7 days and treated with 10ng/ml VEGF for a further 5 days. Spheroids were stained with isolectin in green to stain endothelial cells, α -SMA in red to stain pericytes and DAPI in order to visualise cell nuclei. They were imaged at x200 using an EVOS M5000 microscope. These images are a merge of all 3 stains. Scale bars = 750 μ m.

Both images shown in Figure 5.13 are of VEGF-treated spheroids from the same experiment and were imaged at the same time under the same conditions. This Figure was included to highlight the occasional disparity of this staining and imaging technique and highlighting challenges when analysing the expression of certain markers in order to come to a conclusion about the effect of the treatment. Variants like these were present in several different experiments when imaged on the

EVOS M5000 microscope and may highlight the importance of using a more high powered and sophisticated imaging system.

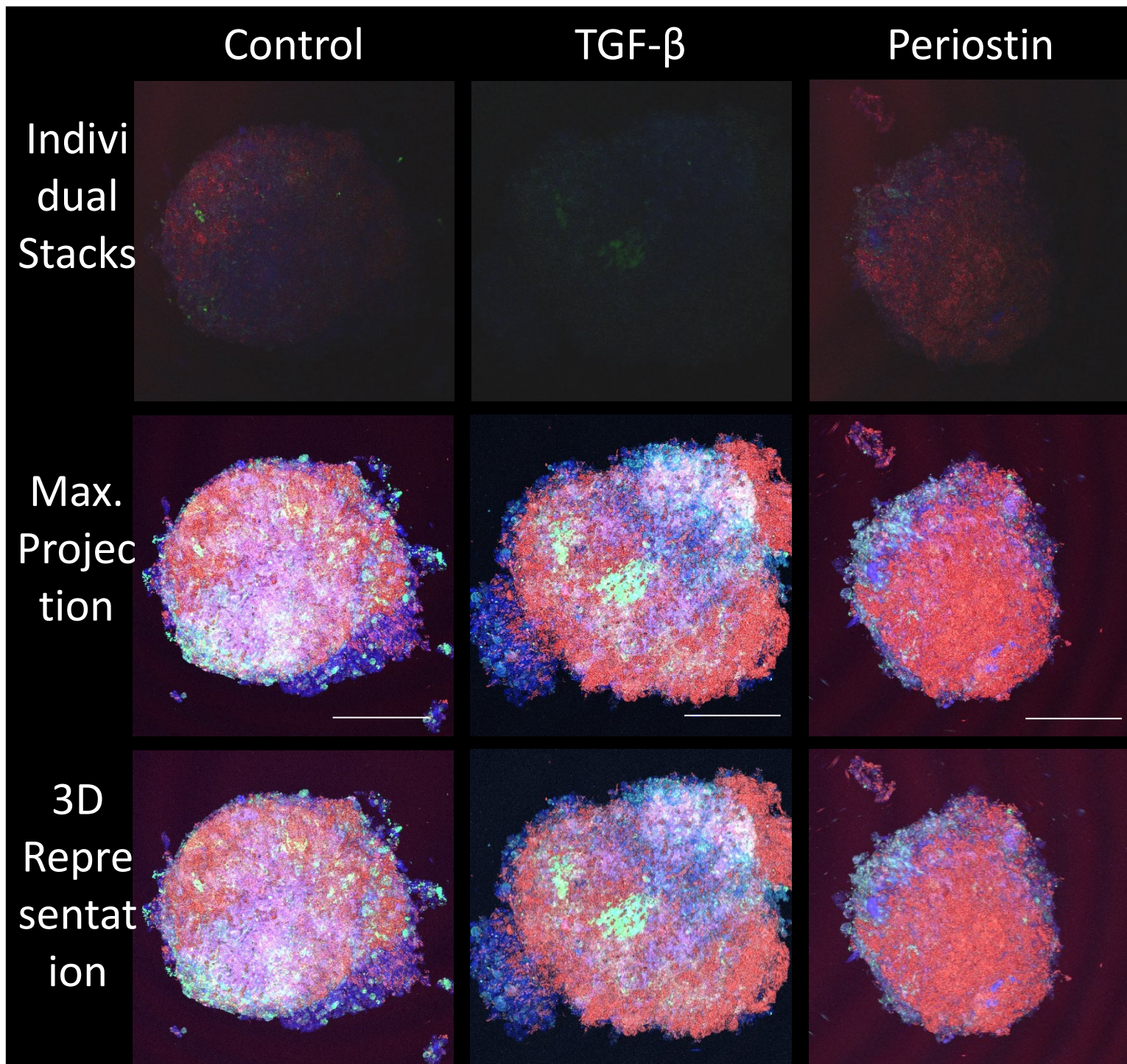


Figure 5.14 – 3D spheroids can be represented in various ways such as maximum projections, 3D representation videos or as a GIF scanning through individual images in the Z-stack. Representative images depicting 3D spheroids of HPLPCs and HUVECs. Spheroids were grown for 7 days and treated with 10ng/ml TGF- β or 100ng/ml periostin for a further 5 days. Spheroids were stained with isolectin in green to stain endothelial cells, α -SMA in red to stain pericytes and DAPI in order to visualise cell nuclei. They were imaged at x200 every 10 μ m using the Z-stack tool on a Leica SP8 confocal microscope and were formatted in ImageJ. The first row links to videos of each image in the stacks. The middle images are maximum projections of the whole spheroid. The lower images link to GIFs of 3D models of the spheroids to visualise their 3D shape. Scale bars = 750 μ m.

Figure 5.14 is designed to demonstrate the many ways of viewing 3D spheroids in order to demonstrate different things. The first and last rows have been hyperlinked to the files on Box so the animations can be viewed. There are also QR codes in the Supplementary Information if needed. The

videos of the individual stacks show each layer throughout the spheroid allowing the observation of structures within the centre of the spheroid. It can also clearly show trends of the staining for example if one marker is only found on the surface of the spheroid rather than at the centre. Maximum projection images are a good way to quickly see all of the staining in the spheroid. As every layer of the stack is viewed at once it would be possible to highlight areas of interest and see the global structure. These images are also used for image analysis as it accurately portrays the staining throughout the whole spheroid. Finally the 3D representation GIFs show the overall 3D shape of the spheroids. As is apparent from the data used in Figure 5.14, when mounted on coverslips the spheroids are very flat and are only a few microns thick when originally they were formed as spheres. This may suggest the need for refining imaging methods.

Another indication that imaging methods needs refinement is what is observed whilst mounting. Images were taken through the eyepiece of a basic light microscope showing spheroids within the growth plate prior and post transferring to the coverslip in order to highlight potentially important material which was often left within the wells.

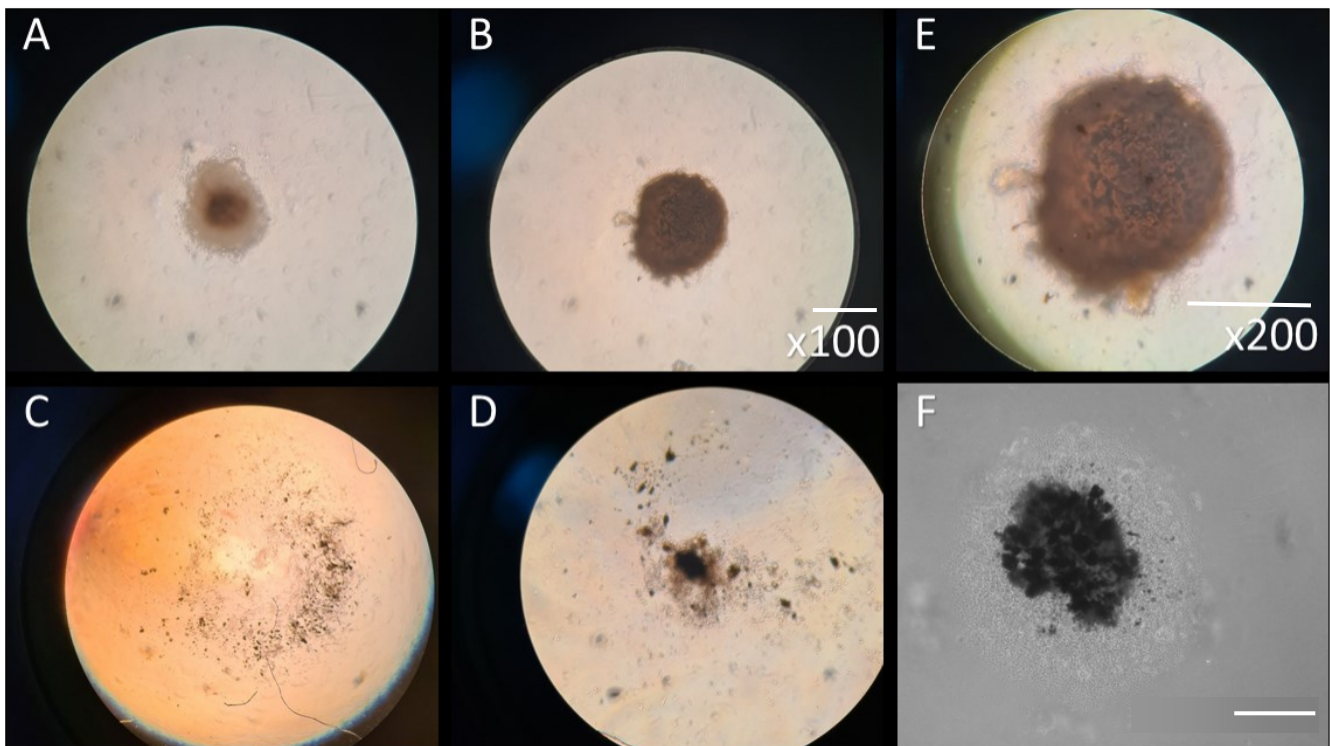


Figure 5.15 – Images of spheroids and growth plates before and after mounting showing rings of cells that are left in the wells after spheroid removal. A,B – Images of spheroids following 7 days of growth and 5 days of cytokine treatment. C,D – Images of the growth plate after spheroid was removed with magnetic pen in order to be mounted. Images A-D were taken through the eyepiece of a standard light microscope at 100x magnification. E – An enlargement of B taken at 200x magnification to show the complexity of the spheroid structure. F – An image of an spheroid in the growth plate taken on a EVOS XL Core brightfield microscope at x100 magnification. Scale bars = 750 μ m.

Image A in Figure 5.15 depicts a standard spheroid in a non-adherent 96-well plate after the magnetic array had been removed. The darker core of cells can be observed as well as the slightly lighter halo of less dense cells around the outside. This juxtaposes image B in which the spheroid is large and opaque throughout. This is seen further in image E where the image is enlarged and the depth and complexity of the spheroid is visible. This contrasts the thin depth of the spheroids seen in Figure 5.14 and suggests the mounting of the spheroids reduces this. Images C and D show the aftermath of removing the spheroid from the plate in order for it to be mounted. The images show a ring of material in the centre of the wells as well as debris, likely introduced during the removal of the spheroid. Image F is a brightfield image taken using an EVOS microscope highlighting the core cell bundle and the ring of less dense material around the outside of the spheroid.

5.3 Discussion

The aim of the work in this chapter is to explore the use of organoids or spheroids constructed *in vivo* in order to simulate disease. This work follows the 3Rs, a principle championed by NC3Rs, with the 3 “R”s being replacement, reduction and refinement (Hubrecht & Carter, 2019). These principles are designed to streamline the use of animal experiments and ensure that animals are being used ethically within research. The work within this chapter is directly relating to the “replacement” keystone which states that *in vitro* models should be developed as a replacement for *in vivo* models to ensure animals are only used when necessary. There is currently large knowledge gap regarding methods of constructing microvascular organoids to perform relevant *in vitro* studies. Through the experiments explored in this chapter, the optimisation of the magnetic levitation technique was undergone to construct spheroids of endothelial cells and pericytes in order to simulate the interactions between these cells in 3D space. As this is a relatively new technique, first developed by Souza et al. in 2010, it is still in the early stages of refinement and therefore requires in depth testing to ensure results are accurate and replicable (Souza et al., 2010). Several groups have attempted to form 3D co-cultures consisting of pericytes and endothelial cells although many of these rely on methods involving semi-solid media such as collagen gel and medium combined with methylcellulose in order to increase its viscosity (Sugihara et al., 2020, Chang et al., 2013). Therefore, this study endeavoured to test this combination of cells using an alternate method to test if it was a viable option to obtain consistent, well-formed spheroids containing both endothelial cells and pericytes.

The overall structure of the spheroids was first assessed in Figures 5.2-5.5. By limiting the number of stains used to just DAPI as a nuclear stain, the complexity of the technique was reduced, and more care could be taken on the formation and mounting of the spheroids. The images in Figure 5.2 highlight the variability observed in the constructed spheroids, with the control image showing a more circular and denser spheroid than the spheroid treated with H₂O₂. This may have been due to the treatments given, as high levels of oxidative stress is thought to contribute to endothelial damage and apoptosis (Hayden et al., 2010). However, as there is a large amount of variation within the treatment groups, which can be seen in the numerical analysis in Figures 5.3-5.5, this is less likely to be the case. Reference has been made to the lack of uniformity to the spheroids formed, especially within Figure 5.2. A hypothesis was made that this lack of uniformity may indicate a less robust interaction between the pericytes and endothelial cells and therefore highlight a limitation with either the culture or the method of spheroid formation. The spread of data can be estimated using the coefficient of variation (CV) of data and is calculated by dividing the sample's standard deviation by its mean and multiplying by 100. For example, the CV of the data from VEGF treated spheroids in Figure 5.4 was 80% which would be relatively large as it meant that the standard deviation was 4/5th the size of the mean. In Figures 5.3-5.5, various measurements of size and shape were taken such as length, area, and estimated density. These were measured to try and represent the overall shape and physical characteristics of the spheroids numerically to allow comparison between treatments and assess the replicability of the formation of the spheroids. An additional measure of roundness could have also been used which follows the formula $\text{perimeter}^2/4\pi\text{area}$ which measures how far the shape deviates from a perfect circle (Bottema, 2000). This was not used in this case as it was a preliminary study and so only several factors were looked at. In future experiments it would be useful to include the measure of circularity to the analysis performed.

Further spheroids were then constructed and stained with immunofluorescent markers in order to visualise the pericytes and endothelial cells. CD31 was used as an endothelial marker and SM22 was used as a pericyte marker. As SM22 is also known to be expressed on smooth muscle cells, it is not a good stain for distinguishing between pericytes and smooth muscle cells (Zhang et al., 2020). However, as only pericytes and endothelial cells from cell lines were used in these experiments, pericytes did not need to be distinguished from smooth muscle cells. N-cadherin was also included to explore the cell-cell interactions between pericytes and endothelial cells. The images shown in Figure 5.6 highlight the varying shape observed in some of the treatment conditions. The TGF- β -treated spheroids seem to show the breakdown of the edges of the spheroid and a fracturing of the overall spheroid shape. Similarly, the untreated spheroid also appeared to have fractured although it had maintained the curvature of the edge of the spheroid and so instead has fractured in the centre

of the spheroid. This is likely to have happened during the mounting process as no damage was observed during the growing or treating phases. However, less damage was observed in the VEGF-treated spheroids which may indicate stronger cell-cell interactions. This may be likely as VEGF is a cytokine involved in angiogenesis which involves forming interactions and associations between pericytes and endothelial cells in order to encourage new vessel growth (Hagedorn et al., 2004). The some of the images in this Figure also contained waves of background interference in the 488 channel which may indicate non-specific binding or errors in the imaging. This also may have been due to the natural autofluorescence of biological tissues which often occurs in the green channel. However, negative controls are always performed in order to help to reduce background stain to the point where only “true signal” remains. The stains from these spheroids were quantified in Figures 5.7-5.10. All three stains had a significantly higher expression in VEGF-treated spheroids. This may be due to the more robust construction of the spheroids observed in this condition as more cells present would lead to more expression. This could be explored further by counting the cell nuclei stained in DAPI and calculating expression per cell. This was not possible in this experiment as the laser responsible for the wavelength that excites DAPI is a high-energy multiphoton laser that has been observed to burn material due to the inclusion of the iron nanoparticles within the cells. Therefore the DAPI stain has not been included in this experiment. The graph in Figure 5.10 was included to compare between the stains in each condition although it is the same data shown in Figures 5.7-5.9. Following the construction of these spheroids I instead decided to seed the endothelial cells and pericytes at a ratio of 5:1 in order to better represent the physiological ranges which is thought to be between 10:1 to 1:1 (Armulik et al., 2011). This would allow us to possibly more accurately observe the organisation and interaction observed in the average blood vessel.

New spheroids were constructed, and images are shown in Figure 5.11. These images highlight the improvement in the shape of the spheroids formed as all images show a mostly intact edge around the outside of the spheroids with only a slight amount of damage to the exterior of the spheroid. This suggests that these spheroids were formed more successfully than previous experiments which is likely due to keeping the magnetic array around the plate for the full growth and treatment period rather than for only 24 hours as was done when constructing spheroids in Figure 5.6. The images in Figure 5.11 seem to show that the centres of the spheroids are less dense than around the edge (as shown by the white arrows). This suggests that there may have been some cell death in the middle of the spheroids and therefore some loss of density due to the reduction of oxygen and required nutrients within the middle of the cell mass. This should be investigated further by including a live/dead stain, for example Zombie Aqua (Nuccitelli et al., 2017) or a stain targeting a measure of metabolic stress such as AMPK (AMP-activated protein kinase) (Tang et al., 2021). This dark area

within the centre of the spheroid, where cells are seemingly not positive for any stain used, could additionally be a problem with antibody penetration. As this is seen relatively consistently throughout treatment groups and with DAPI stain, further optimisation of the staining protocol should occur including the addition of clearing steps such as a “passive clearing technique” developed by Cora et. al to improve organoid imaging (Cora et al., 2019). Additionally, it seems that the green stain is brighter in the centre than the red stain which is more situated around the edge. This may highlight that the core of the spheroid is more likely to contain endothelial cells whilst the pericytes reside around the outside. However, this is difficult to see from the images in 5.11 as they were taken on an EVOS M5000 fluorescent microscope so the plane of focus is not exact and exact location of the stains cannot be accurately determined. To rectify this, images should be taken at higher magnification on a high-resolution microscope as this would result in better resolution images and z-stacks to properly investigate the stains in 3D space. This was not technically feasible on the hardware available.

The method used to create the images in Figure 5.11 was then repeated to investigate a wider range of treatments. A range of treatments were tested in this pilot study in order to see if any of them caused a significant difference in the structure of the spheroid. Representative images of these spheroids are presented in Figure 5.12, although the intensity of the stains were not calculated. This is due to the variability of the intensity of the stains, highlighted in Figure 5.14. These two images are technical replicates and therefore should have relatively similar expression and yet clearly one is much brighter than the other. This may be due to an error in the staining method as this was seen in several different treatment groups as well. It also may be due to the microscope settings or variations when imaging. Therefore it would not yield valid results to quantify the expression of these spheroids. However, structure and shape can still be observed in general to inform on whether the method was successful. The difference in location of the stains is more apparent in the images in Figure 5.12 than in the previous Figure. In particular, the spheroids that were treated with H₂O₂, TNF- α , periostin or TGF- β had stronger isolectin expression in the core and stronger α -SMA expression around the outside. This could be quantified by looking at the expression of each stain in a circle around the centre point and in a ring either side of the outside section of the spheroid. This staining pattern is likely due to issue with either permeabilization of the spheroid or penetration of the reagent. Currently, methods used in this study relied on 0.3% Triton-X in PBS throughout the staining protocol. This concentration is relatively low and so could be optimised at a higher concentration, however this could lead to toxicity due to disruption of the cellular membranes (Fra-Bido et al., 2021, Koley & Bard, 2010). It is also possible to use Tween 20 instead of Triton-X which has an additional advantage of excess protein removal and may aid in background signal removal

(Hoffman & Jump, 1986) as well as being a gentler disinfectant and much harder to depolarise membranes with (Amidzadeh et al., 2014). It is also possible to use methanol as a permeabilization agent as well as a fixative as it dissolves lipids in the membranes although this is a very harsh solvent and can cause deformation of the cell structures (Jamur & Oliver, 2009, Yuan et al., 2017).

In addition to these images shown in Figure 5.12 and 5.13, confocal images were taken of these spheroids and are shown in Figure 5.14. These images do not fully represent each treatment and are mainly included as an example of the uses of confocal imaging when working with 3D spheroids. Max projection images depict each stack taken superimposed on each other in order to observe the expression of markers throughout the spheroid as a whole. These images are useful to see the general trend and can be used to quantify expression as each section is in focus and therefore the location of the stains is more accurate (Jabeen et al., 2019). It is a good way of making a 2D images which contains all the characteristics of a 3D structure (Cromey & Jansma, 2018). The videos constructed scrolling through each stack gives more information on where expression and structures occur along the z-axis. It is useful to see the distribution of the stain, for example if more stain occurred on the top of the spheroid than the bottom. However, it is difficult to quantify this as it is a video and may be made up of a large number of images which can be difficult to analyse. The final images are 3D representations of the z-stack. These are constructed through ImageJ and show the 3D structure of the spheroids. It is very clear that the spheroids have lost their 3D shape upon mounting and so we have lost the information on 3D structure. This highlights the need for in situ mounting as it is likely that squeezing the spheroid between a coverslip and the slide would have caused this shape change. Instead, the spheroids could have been mounted in a semi solid gelatin-based fluid gel and imaged in speciality glass bottomed culture plate which allows for optical length to be similar to that of coverslips (Moxon & Smith, 2016, Felip-Leon et al., 2017) Technological limitations prevented this from being explored as there was not access to an upright confocal microscope at the time of these experiments and therefore the existing mounting method had to be relied on.

This mounting method also raised an issue when moving the spheroids from the plate to the slide. A magnetic pen which was designed to be used alongside the magnetic array was used to pick up the spheroid. However, this was not always successful and could have led to some damage to the spheroids or loss of material. It also became apparent, as evidenced in Figure 5.15, that removing the spheroid from the plate left a residual ring of cells and debris (Figure 5.15.C/D). The debris was likely introduced during this moving stem as it wasn't visible during the growth. The cells that were left behind had likely either not incorporated the iron nanoparticles and therefore were not magnetic (although these were likely to be removed during medium changes) or they had migrated

away from the main cell mass. Therefore, as we are aiming to observe and characterise migrating cells, these cells are very important. If the spheroids were imaged in situ (as shown in Figure 5.15.F) these cells would still be visible and therefore would be able to be included in subsequent analysis.

To conclude, it was possible to construct 3D spheroids of endothelial cells and pericytes using the magnetic levitation method. However, this technique requires more refinement, especially related to the selection of cell-specific markers, mounting and imaging. More exploration into in-situ imaging should be performed making use of an inverted confocal microscope to image z-stacks of the full spheroid and construct 3D models which can further be analysed.

Chapter 6 – CXCL12 Drives Pericyte Accumulation and Airway Remodelling in Allergic Airway Disease

6.1 Introduction

The role of pericytes in allergic asthma is linked to their contributions to airway remodelling, in particular myofibroblast differentiation and airway smooth muscle thickening (Feng, Mantesso & Sharpe, 2010). A key factor in this process is the uncoupling of pericytes from their resident blood vessels and migration towards the inflamed airway, driven by impaired PDGFR β signalling in pericytes in response to chronic allergic inflammation (Feng, Mantesso & Sharpe, 2010). However, little is currently known of the migratory capacity of pericytes. This work aims to fill the important gap in determining the chemotactic stimulus that regulates pericyte migration into areas of inflammation in the search for druggable targets. Bone marrow mesenchymal stem cells (MSC), which have many characteristics in common with tissue pericytes, have been shown to express the receptor CXCR4, and the CXCR4/CXCL12 axis is thought to be the means by which MSCs are retained within the bone marrow (Rankin, 2012). CXCL12 has also been shown to be upregulated during tissue injury, and while the dynamics of this upregulation are disputed, research has shown that the blockade of CXCR4 results in reduced MSC recruitment following burn injury (Diaz-Flores, et al., 2009, Hu et al., 2013) However, other data suggest that binding of the CXCR4 antagonist AMD3100 serves to increase the mobility of MSCs and enhance their recruitment to bone fractures in mice (Kumar & Ponnazhagan, 2012). The relevance of the CXCR4/CXCL12 axis in pericyte recruitment and migration during tissue injury/inflammation is yet to be determined. I aimed to demonstrate in vivo the means by which pericytes migrate to sites of inflammation and fibrosis in the lung. Under fibrotic conditions, characterized by high levels of CXCL12 expression in the airways, pericytes were observed to uncouple from the airway microvasculature and demonstrated enhanced migration toward chemotactic stimuli. Finally, using a novel neutraligand to suppress CXCL12 activity (LIT-927), I was able to mitigate pericyte uncoupling from the airway microvasculature, resulting in decreased airway smooth muscle accumulation and improved symptom scores.

Animal models are an incredibly useful tool in disease research and drug development. They allow the testing of novel drugs and treatment in complex systems, allowing us to predict any aberrant consequences or off-target effects before it can affect humans. There are two main animal models used for simulating asthma in mice: the ovalbumin model and the house dust mite model. The ovalbumin model was first developed in the early 1990s and focuses on the use of the protein ovalbumin, found in eggs, to induce an allergic reaction (Tarayre et al., 1991). It involves the

injection of ovalbumin along with an adjuvant into the perineum to sensitise the mice, followed by several challenges with the allergen most often through aerosolization (Kim, Song & Lee, 2019). Studies have shown that this administration of albumin results in the development of the hallmarks of asthma, including airway, inflammation, increase of IgE, mucus production and influx of eosinophils (Daubeuf & Frossard, 2014, Kim, Song & Lee, 2019). However, the way this inflammation is induced is very artificial and does not translate to the way the human condition is developed and therefore this model is not considered the gold standard in preclinical asthma research. The house dust mite (HDM) model, developed by Johnson et al. in 2004, aims to address this by using a common existing allergen to induce inflammation without the use of an artificial adjuvant to drive the immune response (Johnson et al., 2004). As this method relies on the inhalation of a common aeroallergen in a way similar to how the human disease develops, this model is more comparable to the human disease and therefore the effects of drugs on fibrosis caused by this model are more likely to also be seen in humans. Due to these advantages, the HDM model has now been adopted as the gold standard in preclinical asthma research.

By harnessing the HDM model in order to simulate allergic asthma, the effect of the novel neutraligand LIT-927 was assessed. LIT-927 has previously been used by groups in the context of pulmonary hypertension and allergic airway hypereosinophilia (Bordenave et al., 2019, Regenass et al., 2018). Regenass et al. established a working dose of 300nmol/kg and therefore this was the dose used in the subsequent studies described here (Regenass et al., 2018). Through the use of bronchoalveolar lavage, immunofluorescent staining of both lung sections and tracheal whole mounts as well as the monitoring of respiratory symptoms, the inhibitory effect of LIT-927 was observed, highlighting its potential as a therapeutic in the near future.

6.2 Results

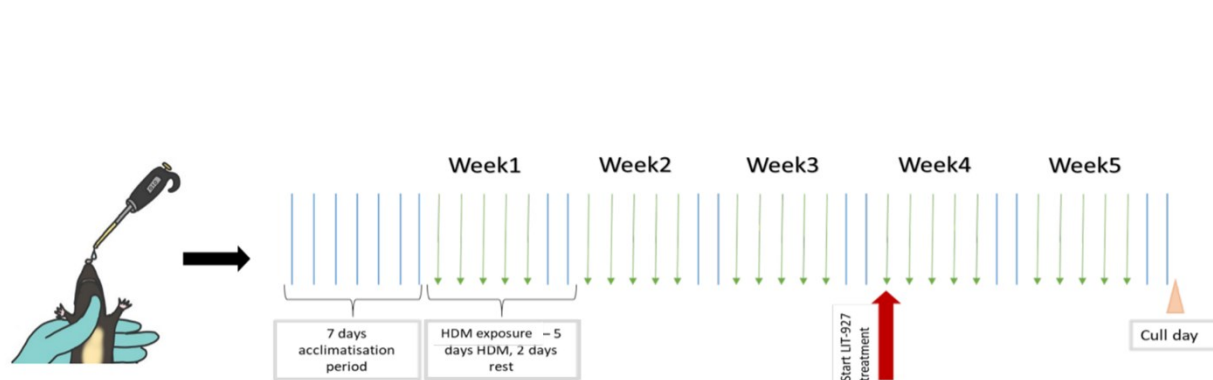


Figure 6.1 -The dosing schedule used in the HDM model. Female C57/B16 mice (6-8 weeks old) were subjected to either sterile PBS (10 μ L) or house dust mite extract (HDM; 25 μ g in 10 μ L) five days a week for 5 consecutive weeks. 10 μ L LIT-927 was given intranasally at a concentration of 197ng/ml in methyl- β -cyclodextrin 10% w/v. for the final 3 weeks. Schematic diagram of the schedule of allergen and drug delivery.

Figure 6.1 depicts the dosing strategy used in the studies performed in this chapter. It involved dosing C57/B16 mice intranasally with 10 μ L of PBS containing 25 μ g of HDM for 5 days followed by 2 days of rest without dosing. This was repeated for 5 weeks to allow fibrosis to develop. After the initial 3 weeks of dosing, a group of mice was treated with 197ng/ml of the LIT-927 drug intranasally in 10 μ L of methyl- β -cyclodextrin 10% w/v in the same dosing pattern as HDM. This group also continued to receive HDM dosing alongside LIT-927 treatment. Several control groups were also included; one which received sterile PBS instead of HDM and only methyl- β -cyclodextrin instead of LIT-927, one receiving HDM and methyl- β -dextrin, and one receiving PBS and LIT-927. Upon completion of the five-week experiment, mice were culled using an intraperitoneal injection of pentobarbital, and various tissues and cells were harvested in accordance with Home Office regulations.

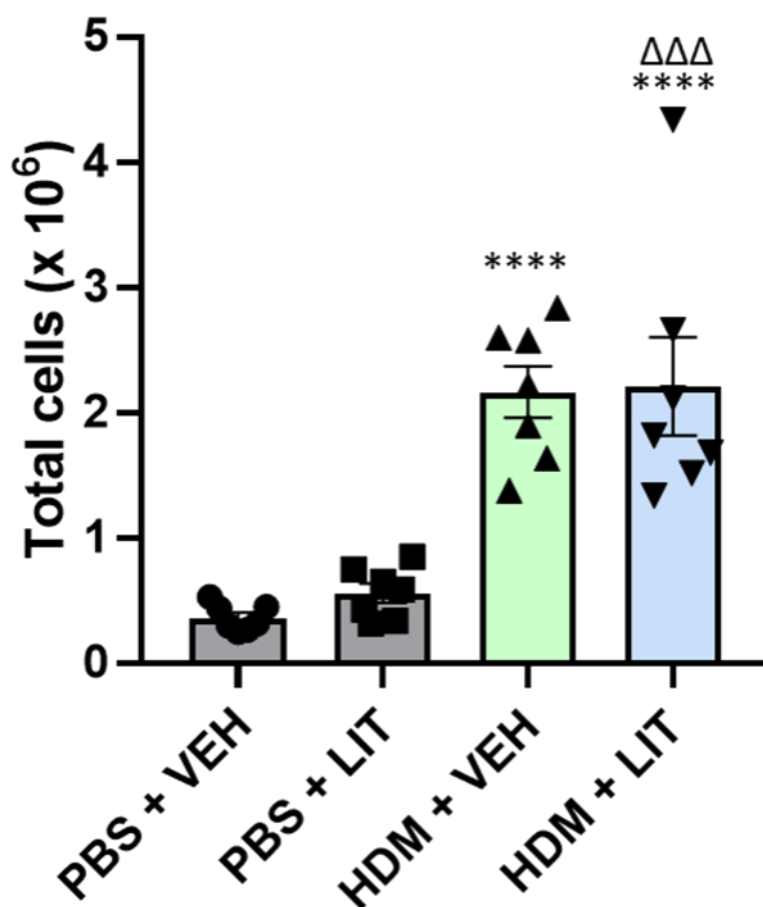


Figure 6.2 – HDM treated mice had more immune cells present in their bronchoalveolar lavage fluid than PBS treated mice. Female C57/BL6 mice (6-8 weeks old) were subjected to either sterile PBS (10 μ L) or house dust mite extract (HDM; 25 μ g in 10 μ L) five days a week for 5 consecutive weeks. 10 μ L LIT-927 was given intranasally at a concentration of 197ng/ml in methyl- β -cyclodextrin 10% w/v. for the final 3 weeks. At the end of the protocol, the lungs were removed and bronchoalveolar lavage (BAL) fluid was collected. Total inflammatory cell infiltrates were enumerated using hematoxylin and eosin stained cytopsin preparations of BAL fluid. n=7, “****” = p<0.0001 with respect to PBS+VEH, “ $\Delta\Delta\Delta$ ” = p<0.001 with respect to PBS+LIT by one-way analysis of variance (ANOVA) for multiple groups with the Tukey post hoc test..

Bronchoalveolar lavage (BAL) involves performing a PBS wash of the lungs post-mortem in order to collect immune cells and soluble mediators present in the airway lumen. The cellular component of the BAL was stained using H&E to visualise the cells and a cell count and differential was performed using a simple brightfield microscope. Both groups of mice given PBS for the 5 weeks had low levels of immune cells present in the bronchoalveolar lavage fluid and the end of the treatment period. Conversely, both groups given HDM for 5 weeks had significantly elevated levels of immune cells in the lavage fluid (p<0.0001). Both of these groups were significantly different to groups given both LIT-927 or just the vehicle (p=0.0002) after receiving PBS although there was no difference in the total cell number present in those given LIT-927 or the vehicle after HDM.

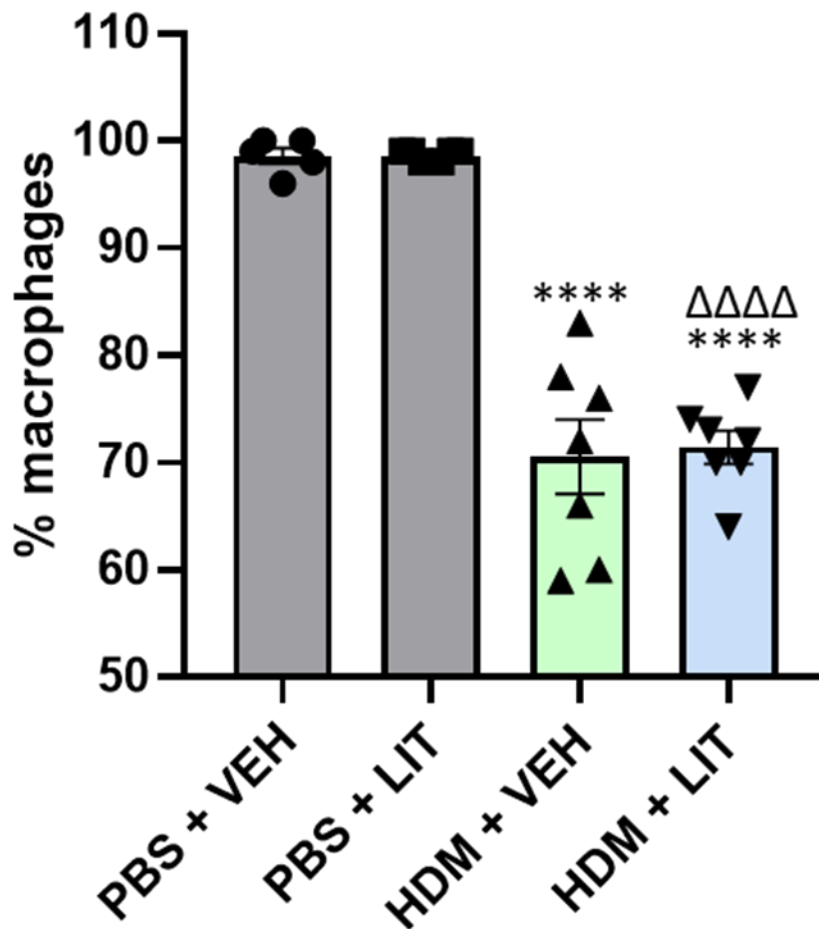


Figure 6.3 – HDM treated mice had a lower percentage of macrophages present in their bronchoalveolar lavage fluid than PBS treated mice. Female C57/Bl6 mice (6-8 weeks old) were subjected to either sterile PBS (10 μ L) or house dust mite extract (HDM; 25 μ g in 10 μ L) five days a week for five consecutive weeks. 10 μ L LIT-927 was given intranasally at a concentration of 197ng/ml in methyl- β -cyclodextrin 10% w/v. for the final 3 weeks. At the end of the protocol, the lungs were removed and bronchoalveolar lavage (BAL) fluid was collected. Macrophage infiltrates were enumerated using hematoxylin and eosin stained cytopsin preparations of BAL fluid. n=7, “****” = $p < 0.0001$ with respect to PBS+VEH, “ΔΔΔΔ” = $p < 0.0001$ with respect to PBS+LIT by one-way analysis of variance (ANOVA) for multiple groups with the Tukey post hoc test.

Figure 6.3 shows that there was a significant decrease in the proportion of macrophages present in both of the groups given HDM compared to those given PBS ($p < 0.0001$). Although the number of cells present in PBS groups was lower (Figure 6.2), a significantly greater percentage of these cells were macrophages ($p < 0.0001$), likely alveolar macrophages that are abundant in the healthy lung. Conversely, the mice given HDM had a higher number of cells but a significantly smaller proportion of them were macrophages. Again, there was no difference following treatment with LIT or vehicle.

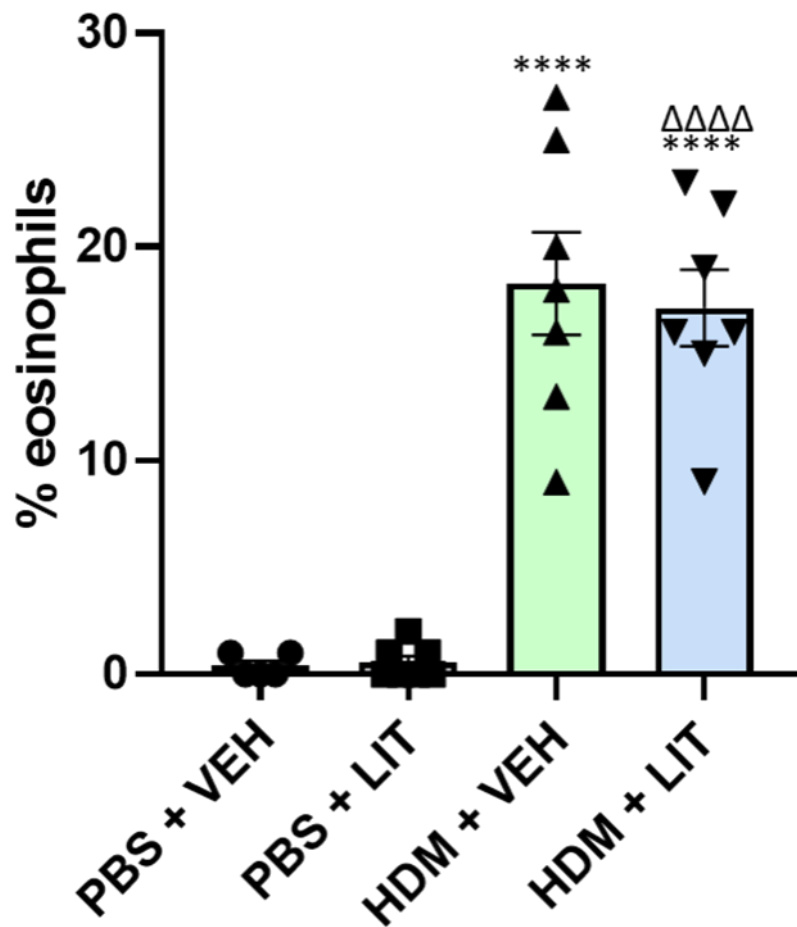


Figure 6.4 - HDM treated mice had a higher percentage of eosinophils present in their bronchoalveolar lavage fluid than PBS treated mice. Female C57/Bl6 mice (6-8 weeks old) were subjected to either sterile PBS (10 μ L) or house dust mite extract (HDM; 25 μ g in 10 μ L) five days a week for five consecutive weeks. 10 μ L LIT-927 was given intranasally at a concentration of 197ng/ml in methyl- β -cyclodextrin 10% w/v. for the final 3 weeks. At the end of the protocol, the lungs were removed and bronchoalveolar lavage (BAL) fluid was collected. Eosinophil infiltrates were enumerated using hematoxylin and eosin stained cytopsin preparations of BAL fluid. n=7, “***” = $p < 0.0001$ with respect to PBS+VEH, “ $\Delta\Delta\Delta\Delta$ ” = $p < 0.0001$ with respect to PBS+LIT by one-way analysis of variance (ANOVA) for multiple groups with the Tukey post hoc test..

In contrast to macrophage levels shown in Figure 6.3, the PBS groups had very few eosinophils present in the BAL fluid. However, mice subjected to allergen challenge with HDM had significantly more eosinophils present than those given PBS. Again, there was no difference in the percentage of eosinophils following treatment with LIT-927 or its vehicle.

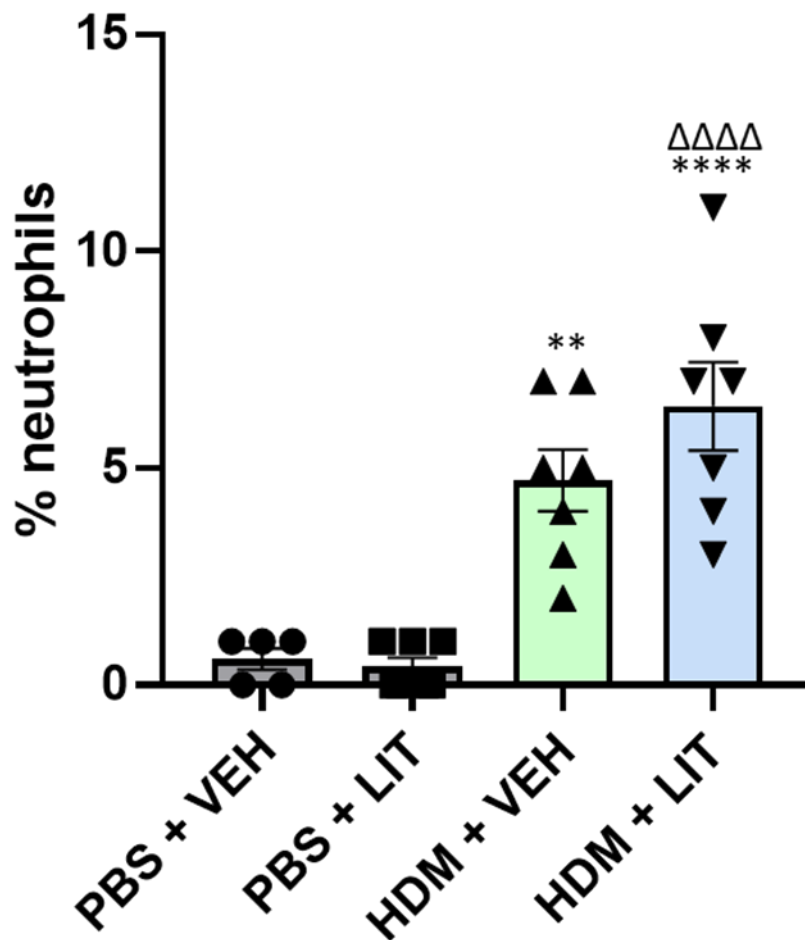


Figure 6.5 - HDM treated mice had a higher percentage of neutrophils present in their bronchoalveolar lavage fluid than PBS treated mice. Female C57/Bl6 mice (6-8 weeks old) were subjected to either sterile PBS (10 μ L) or house dust mite extract (HDM; 25 μ g in 10 μ L) five days a week for five consecutive weeks. 10 μ L LIT-927 was given intranasally at a concentration of 197ng/ml in methyl- β -cyclodextrin 10% w/v. for the final 3 weeks. At the end of the protocol, the lungs were removed and bronchoalveolar lavage (BAL) fluid was collected. Neutrophil infiltrates were enumerated using hematoxylin and eosin stained cytopsin preparations of BAL fluid. n=7, “****” = $p < 0.0001$ and “**” = $p < 0.01$ with respect to PBS+VEH, “ $\Delta\Delta\Delta\Delta$ ” = $p < 0.0001$ and “ $\Delta\Delta\Delta$ ” $p < 0.001$ with respect to PBS+LIT by one-way analysis of variance (ANOVA) for multiple groups with the Tukey post hoc test..

Similar to the results shown in Figure 6.4, the PBS groups had a very low percentage of neutrophils in their BAL fluid. In contrast, mice subjected to allergen challenge with HDM had a significantly higher percentage of neutrophils. Again, there was no significant difference between treatment with LIT-927 and the vehicle, although the group given HDM and LIT-927 had a greater significant difference to both the PBS groups than the group given HDM and vehicle although this was likely due to the one high result in the HDM and LIT-927 group skewing the results.

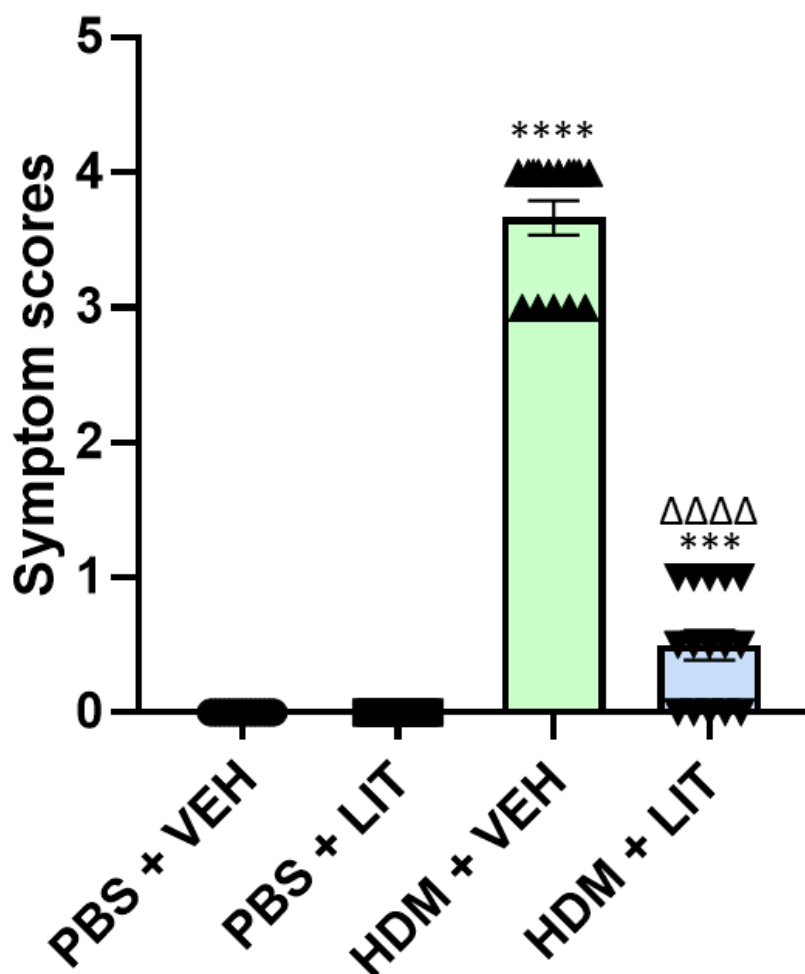


Figure 6.6 – Mice treated with HDM had higher average symptom scores than PBS mice, with those given LIT-927 having significantly lower scores than those given just the vehicle. Female C57/Bl6 mice (6-8 weeks old) were subjected to either sterile PBS (10 μ L) or house dust mite extract (HDM; 25 μ g in 10 μ L) five days a week for five consecutive weeks. 10 μ L LIT-927 was given intranasally at a concentration of 197ng/ml in methyl- β -cyclodextrin 10% w/v. for the final 3 weeks. Symptom scores were monitored throughout the 5-week protocol, with significant differences in symptom score observed between groups at 5 weeks. Graph shows the average symptoms scores during week 5. n=15 per group from two independent experiments. “****” = $p < 0.0001$, “***” = $p < 0.001$ with respect to PBS+VEH, “ $\Delta\Delta\Delta\Delta$ ” = $p < 0.0001$ with respect to HDM+VEH by one-way analysis of variance (ANOVA) for multiple groups with the Tukey post hoc test..

To conform with Home Office regulations, symptom scores were monitored for each mouse upon each interaction throughout the 5 weeks of the study. This was to monitor the wellbeing of the mice to ensure no undue harm was to come of them, as well as to monitor the progression of the allergic asthma by observing the quality of the breathing and the recovery of the animal following anaesthetic. All the mice given PBS had values of 0 as no respiratory distress or behaviour changes were observed throughout the experiment. The mice given HDM and did not get LIT-927 as a treatment had increasing scores as the experiment progressed, averaging around 4.5 as these mice were observed sneezing and wheezing, and took longer to recover from the isoflurane anaesthetic. Mice given HDM and that were treated with LIT-927, however, had statistically decreased averaged

symptom scores. Following treatment with LIT-927, symptom scores drastically reduced compared to the mice given HDM but did not receive treatment. However, at the end of the 5 weeks, the mice given HDM and LIT-927 still had significantly higher average symptom scores than the PBS mice who had not been exposed to HDM.

As these measurements were taken upon every dosing throughout the five-week experiments, they can also be shown according to the week in order to observe the progression of the symptoms.

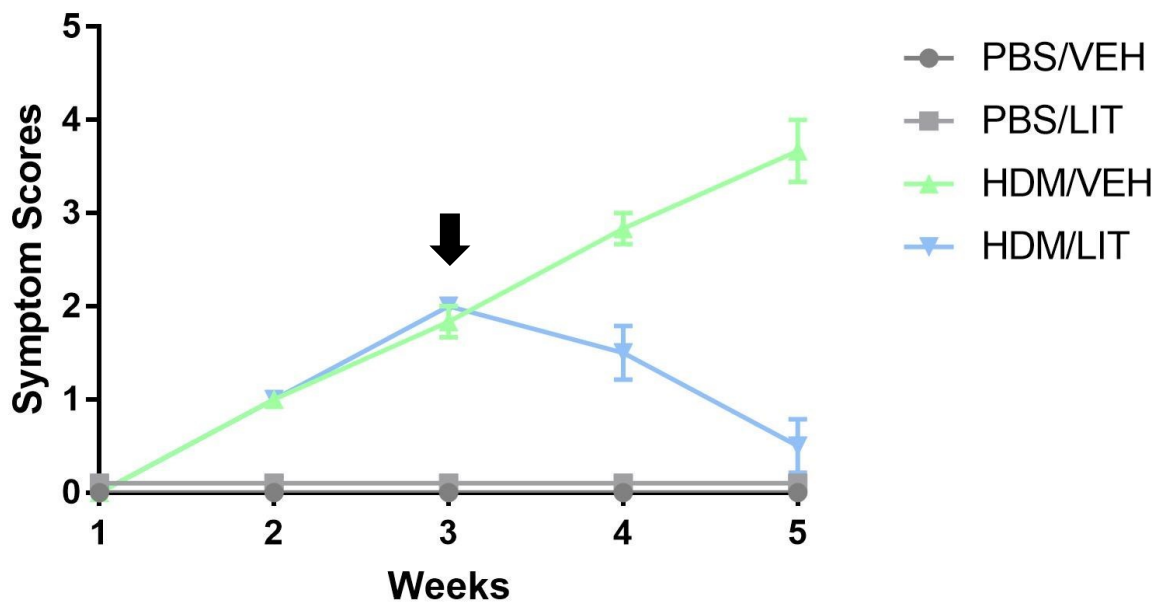


Figure 6.7 - Mice treated with HDM had higher average symptom scores than PBS mice, with those given LIT-927 having significantly lower scores following intervention at week 3. Female C57/Bl6 mice (6-8 weeks old) were subjected to either sterile PBS (10 μ L) or house dust mite extract (HDM; 25 μ g in 10 μ L) five days a week for five consecutive weeks. 10 μ L LIT-927 was given intranasally at a concentration of 197ng/ml in methyl- β -cyclodextrin 10% w/v. for the final 3 weeks. Symptom scores were monitored throughout the 5-week protocol. Plot shows the mean symptoms score each week. n=15 per group from two independent experiments. Black arrow indicated when LIT-927 treatment was initiated.

As expected, mice in both the control conditions, PBS/VEH and PBS/LIT did not exhibit any symptoms of respiratory distress throughout the experiments and their scores remained at baseline. In the first 3 weeks of the experiments, when both the HDM/VEH and HDM/LIT groups were both receiving just HDM, the symptoms scores rose at a similar rate. The group that did not receive the intervention continued to exhibit worsening symptoms until the end of the experiment, yet those that were given LIT-927 alongside HDM began to reduce the severity of their symptoms scores. This indicates that the intervention with LIT-927 reduces signs of respiratory distress soon after treatment. In addition to the BAL fluid, tracheas were harvested and immunostained as described in Chapter 2 – Materials and Methods in order to explore the effect of HDM and LIT-927 treatment on pericytes and to image 3D cell location in situ.

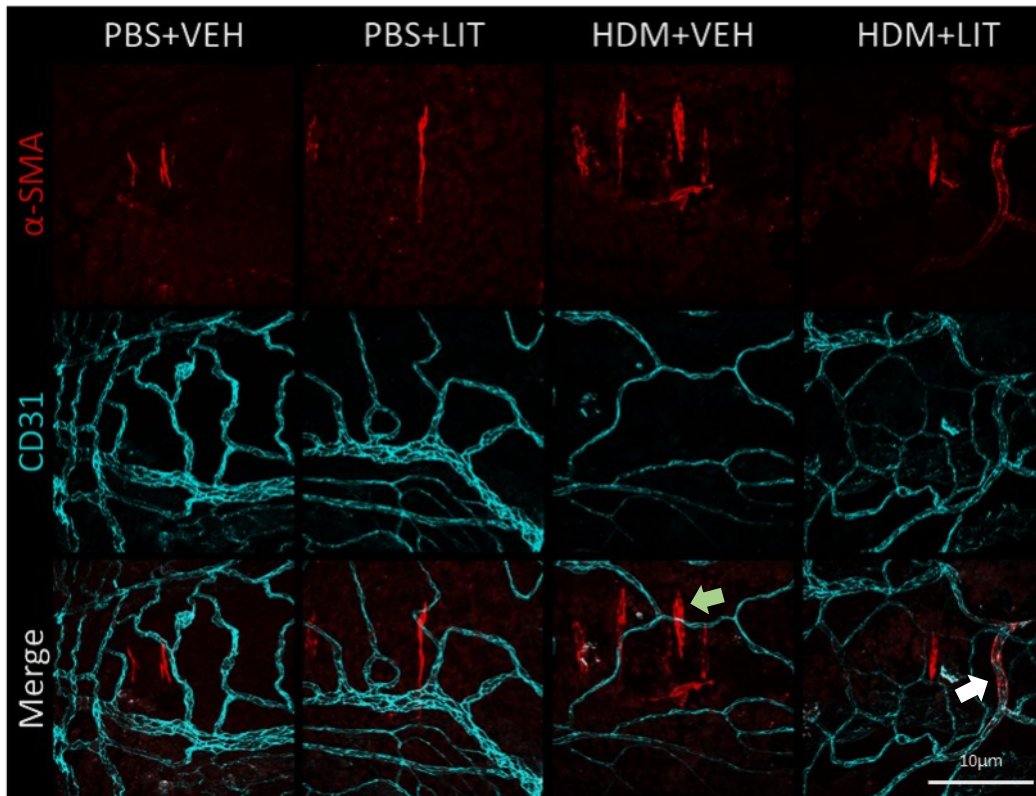


Figure 6.8 – Pericytes were observed uncoupling from the vasculature more in the mice just exposed to HDM than those exposed to HDM and treated with LIT-927. Female C57/Bl6 mice (6-8 weeks old) were subjected to either sterile PBS (10 μ L) or house dust mite extract (HDM; 25 μ g in 10 μ L) five days a week for five consecutive weeks. 10 μ L LIT-927 was given intranasally at a concentration of 197ng/ml in methyl- β -cyclodextrin 10% w/v. for the final 3 weeks. At the end of the protocol, the trachea and bronchi were collected, cleaned, and stained as a whole mount to perform a three-dimensional analysis of uncoupled pericytes. Tracheobronchial whole mounts were stained for the mesenchymal cell marker α -smooth muscle actin (α -SMA; red) and the endothelial cell marker CD31 (cyan) and imaged at x400 magnification using confocal microscopy. Images representative of n=7-8 per group from 2 independent experiments. White arrow indicates coupled pericytes, green arrow indicates uncoupled pericytes.

The images in Figure 6.8 highlight the behaviour of pericytes in fibrotic lung tissue. Pericytes that have decoupled from the vasculature (which is shown in cyan) began to express α -SMA and therefore fluoresce strongly in red. These images are maximum projections taken using z-stacks of the approximately 100 μ m thick trachea harvested from mice given the treatments outlined in Figure 6.1. The images from the mice given PBS showed fewer pericytes present away from the vasculature than in the treatment with HDM but not LIT-927. Interestingly, the tracheas that were exposed to both HDM and LIT-927 also showed less uncoupled pericytes but also showed some α -SMA pericytes around the vessels (white arrow).

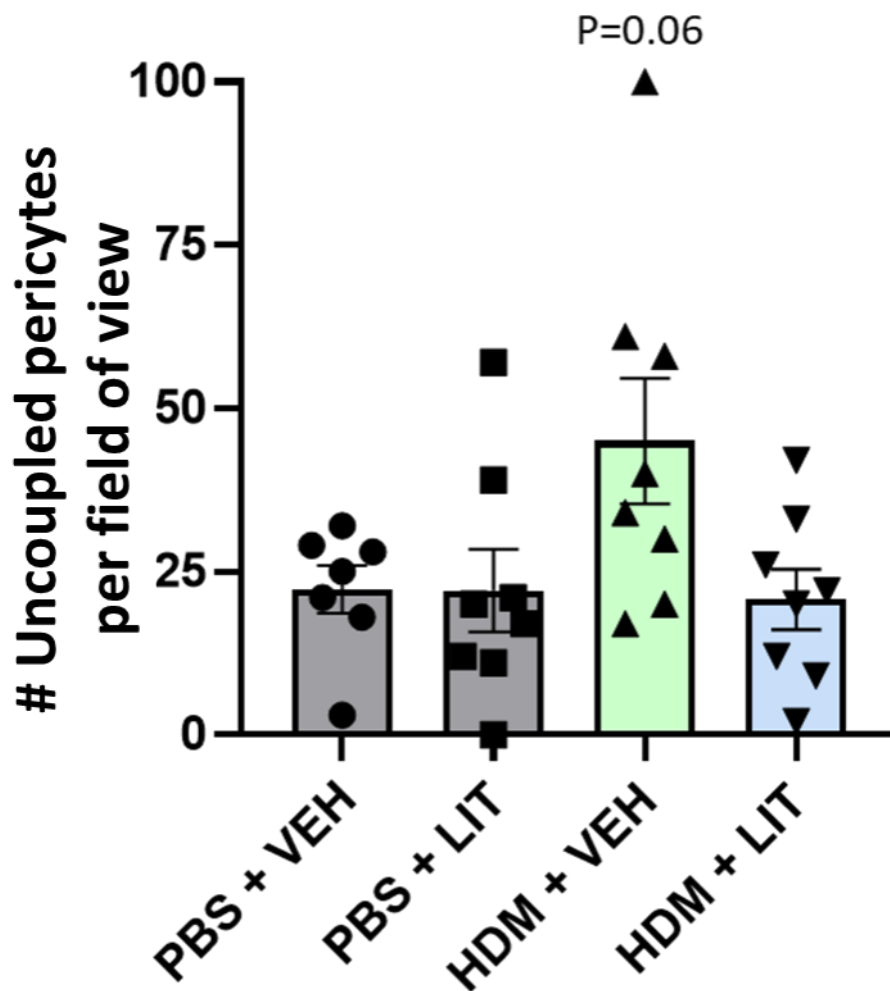


Figure 6.9 – More pericytes had uncoupled in HDM only tracheas than the control tracheas and those given HDM and LIT-927. Female C57/BL6 mice (6-8 weeks old) were subjected to either sterile PBS (10 μ L) or house dust mite extract (HDM; 25 μ g in 10 μ L) five days a week for five consecutive weeks. 10 μ L LIT-927 was given intranasally at a concentration of 197ng/ml in methyl- β -cyclodextrin 10% w/v. for the final 3 weeks. At the end of the protocol, the trachea and bronchi were collected, cleaned, and stained as a whole mount to perform a three-dimensional analysis of uncoupled pericytes. Tracheobronchial whole mounts were stained for the mesenchymal cell marker α -smooth muscle actin and uncoupled α -SMA+ cells were counted. Data presented is the number of uncoupled pericytes per field of view. n=7-8 from 2 independent experiments. P-value is compared to PBS/VEH condition by one-way analysis of variance (ANOVA) for multiple groups with the Tukey post hoc test..

α -SMA positive pericytes were counted along the full length of each trachea and the average was calculated per trachea. The numbers of uncoupled pericytes were very similar in the PBS conditions and the HDM and LIT-927 conditions. However, in the condition that received HDM and vehicle, there was a slight increase in the number of uncoupled pericytes, although this difference was not significant and had a p-value of 0.06. The data in Figure 6.9 had a relatively large spread. This may have been due to natural biological variation or down to imaging issues therefore a counter stain specific to pericytes such as NG2 or vimentin to ensure all α -SMA positive cells counted are pericytes. Tracheas may also not be representative of the pericyte migration occurring within the tissue as much of the migration and therefore remodelling occurs within the bronchi and bronchioles.

As LIT-927 targets the ligand CXCL12, the corresponding receptor, CXCR4 was explored to see if LIT-927 had any effect. This was done through the use of FACS in order to directly calculate the number of pericytes expressing the receptor.

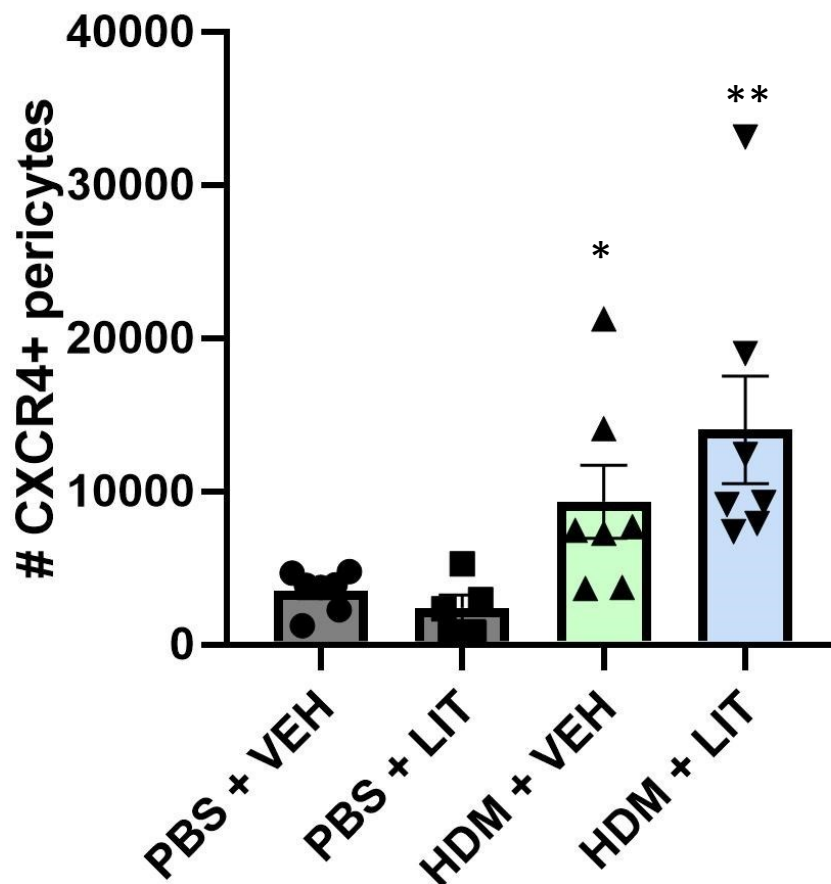


Figure 6.10 – Both conditions exposed to HDM had more CXCR4+ pericytes within their lungs than either control condition. Female C57/Bl6 mice (6-8 weeks old) were subjected to either sterile PBS (10 μ L) or house dust mite extract (HDM; 25 μ g in 10 μ L) five days a week for five consecutive weeks. Lungs were processed into a single cell suspension and submitted to flow cytometric analysis to determine the number of CXCR4+ pericytes. N=7 per group, representative of two independent experiments. "*" = $P < 0.05$, "***" = $p < 0.01$ by one-way analysis of variance (ANOVA) for multiple groups with the Tukey post hoc test.

There is a significant increase in the number of CXCR4+ pericytes following treatment with HDM in both conditions. There was also no difference in the CXCR4+ pericytes between the two control conditions. Interestingly, there was also no significant difference in the number of CXCR4+ pericytes in the mice given HDM, irrespective of if they were also treated with LIT-927 or not. This suggests that treatment with LIT-927 had no effect on the expression of the receptor on pericytes.

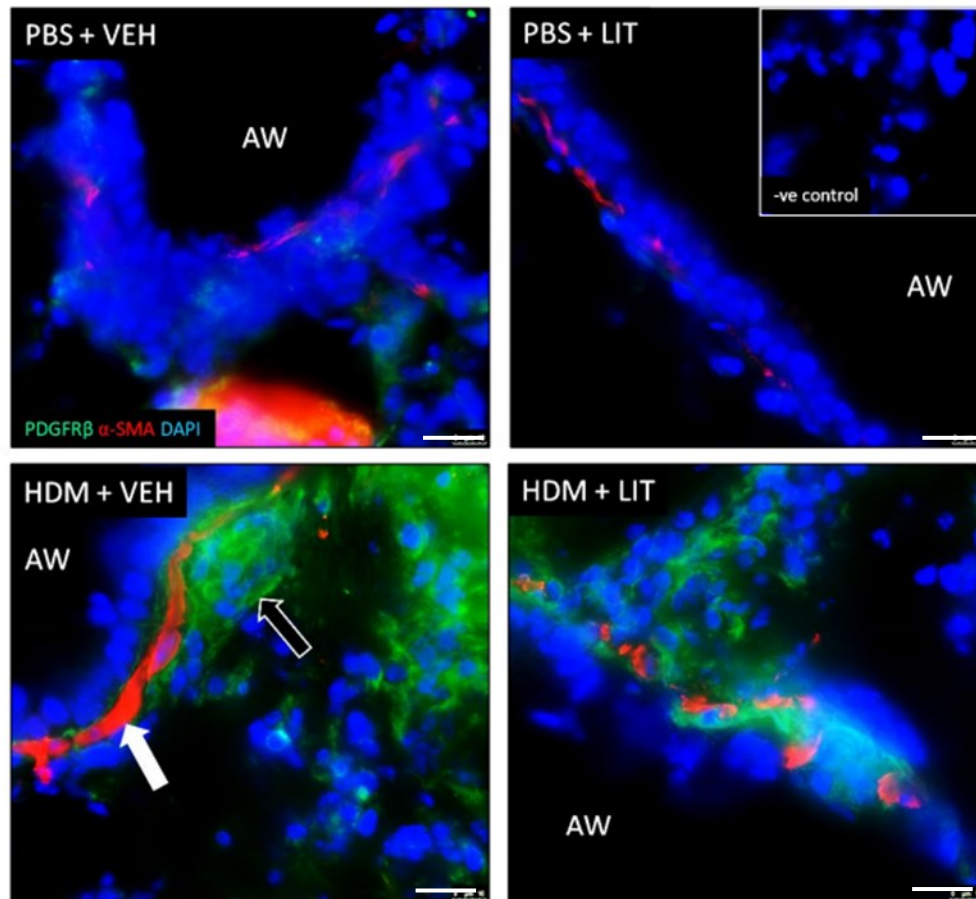


Figure 6.11 – HDM-exposed lungs had a thick and continuous layer of smooth muscle around the airways, which was interrupted following treatment with LIT-927. Female C57/Bl6 mice (6-8 weeks old) were subjected to either sterile PBS (10 μ L) or house dust mite extract (HDM; 25 μ g in 10 μ L) five days a week for five consecutive weeks. 10 μ L LIT-927 was given intranasally at a concentration of 197ng/ml in methyl- β -cyclodextrin 10% w/v. for the final 3 weeks.) At the end of the protocol, lung sections obtained from PBS control and HDM-exposed mice were stained for the pericyte marker PDGFR β (green) and the mesenchymal cell marker α -smooth muscle actin (α -SMA; red) to assess the infiltration of pericytes into airway smooth muscle bundles (white arrow indicates smooth muscle layer and black arrow shows pericytes infiltrating into the smooth muscle layer). Images taken at 400x magnification and are representative of n=8 from 3 independent experiments. Scale bar = 10 μ m.

These images depict cells around the wall of the airway in lung tissue. In the PBS conditions, the red layer of smooth muscle cells is very thin and discontinuous. There is also only a slight presence of PDGFR- β -positive pericytes around these airway walls. In contrast, the image from mice that were given HDM but not LIT-927 had a very thick and continuous band of smooth muscle around the airway wall (shown by the white arrow). There was also a large influx of PDGFR- β -positive pericytes into the subepithelial layer of the airways. However, in the mice given both HDM and LIT-927, the smooth muscle layer still seemed relatively thick but it had become discontinuous. There was also a distinct area of PDGFR- β -positive pericytes although these cells are not as numerous as in the HDM exposed mice given vehicle treatment.

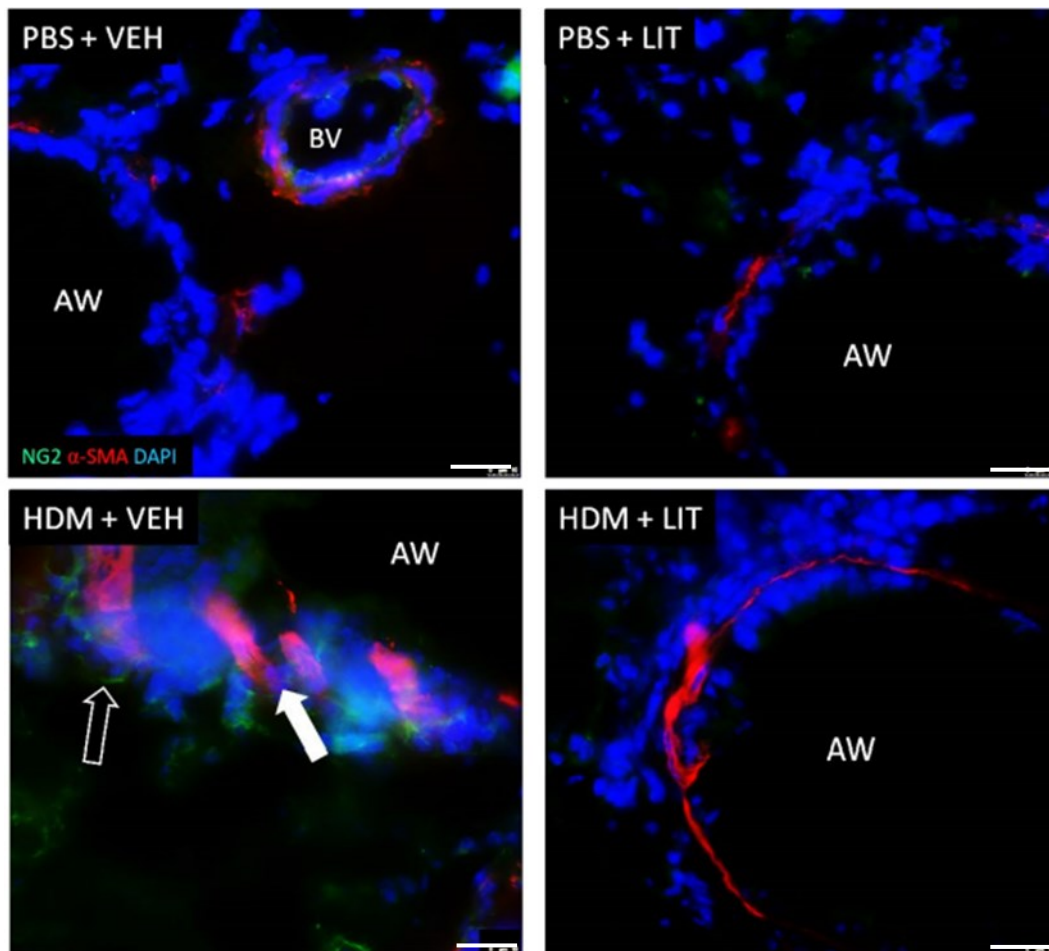


Figure 6.12 - HDM-exposed lungs had a thick and continuous layer of smooth muscle around the airways, which was thinner following treatment with LIT-927. Female C57/Bl6 mice (6-8 weeks old) were subjected to either sterile PBS (10 μ L) or house dust mite extract (HDM; 25 μ g in 10 μ L) five days a week for five consecutive weeks. 10 μ L LIT-927 was given intranasally at a concentration of 197ng/ml in methyl- β -cyclodextrin 10% w/v. for the final 3 weeks.) At the end of the protocol, lung sections obtained from PBS control and HDM-exposed mice were stained for the pericyte marker NG2 (green) and the mesenchymal cell marker α -smooth muscle actin (α -SMA; red) to assess the infiltration of pericytes into airway smooth muscle bundles (white arrow indicates smooth muscle layer and black arrow shows pericytes infiltrating into the smooth muscle layer). Images taken at 400x magnification and are representative of n=8 from 2 independent experiments. Scale bar = 10 μ m.

Again, Figure 6.12 depicts cells within the subepithelial region of the airway wall. Similar to in Figure 6.11, the PBS treated lungs had very thin smooth muscle layers, which are discontinuous throughout the airway wall. There is also a very small amount of NG2-positive pericytes around the airways. These trends are also seen in the lungs given HDM and LIT-927. However, the lungs of the mice given HDM and not LIT-927 contained very thick smooth muscle layers around the airways. There was also an increase of NG2-positive pericytes in the subepithelial layer, which was not present in the other conditions.

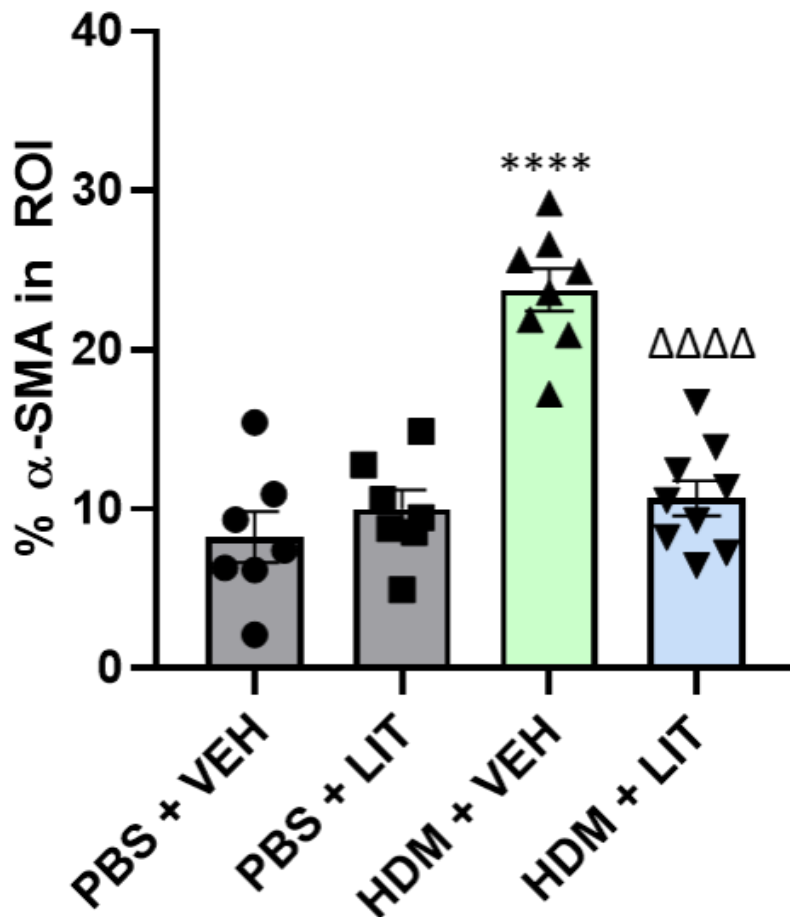


Figure 6.13 – The amount of α -SMA stain was greater in lungs exposed to only HDM compared to controls and the lungs given HDM and LIT-927. Female C57/BL6 mice (6-8 weeks old) were subjected to either sterile PBS (10 μ L) or house dust mite extract (HDM; 25 μ g in 10 μ L) five days a week for five consecutive weeks. 10 μ L LIT-927 was given intranasally at a concentration of 197ng/ml in methyl- β -cyclodextrin 10% w/v. for the final 3 weeks.) At the end of the protocol, lung sections obtained from PBS control and HDM-exposed mice were stained for the pericyte markers NG2 and PDGFR- β (green) and the mesenchymal cell marker α -smooth muscle actin (α -SMA; red) to assess the infiltration of pericytes into airway smooth muscle bundles Airway smooth muscle thickness was quantified morphometrically using ImageJ software. Images taken at 400x magnification and are representative of n=8 from 2 independent experiments. “****” = $p < 0.0001$ with respect to PBS+VEH, “ $\Delta\Delta\Delta\Delta$ ” = $p < 0.0001$ with respect to HDM+VEH by one-way analysis of variance (ANOVA) for multiple groups with the Tukey post hoc test..

The expression of α -SMA from the experiments outlined in Figure 6.9 and Figure 6.10 were calculated within the region of interest around the airway walls. The percentage of α -SMA in the mice given PBS was relatively low, and statistically similar to the levels of α -SMA in the condition with HDM and LIT-927. In contrast, the mice given HDM without the LIT-927 had a percentage of α -SMA that was statistically higher than both the PBS conditions and the HDM + LIT-927 treated lungs.

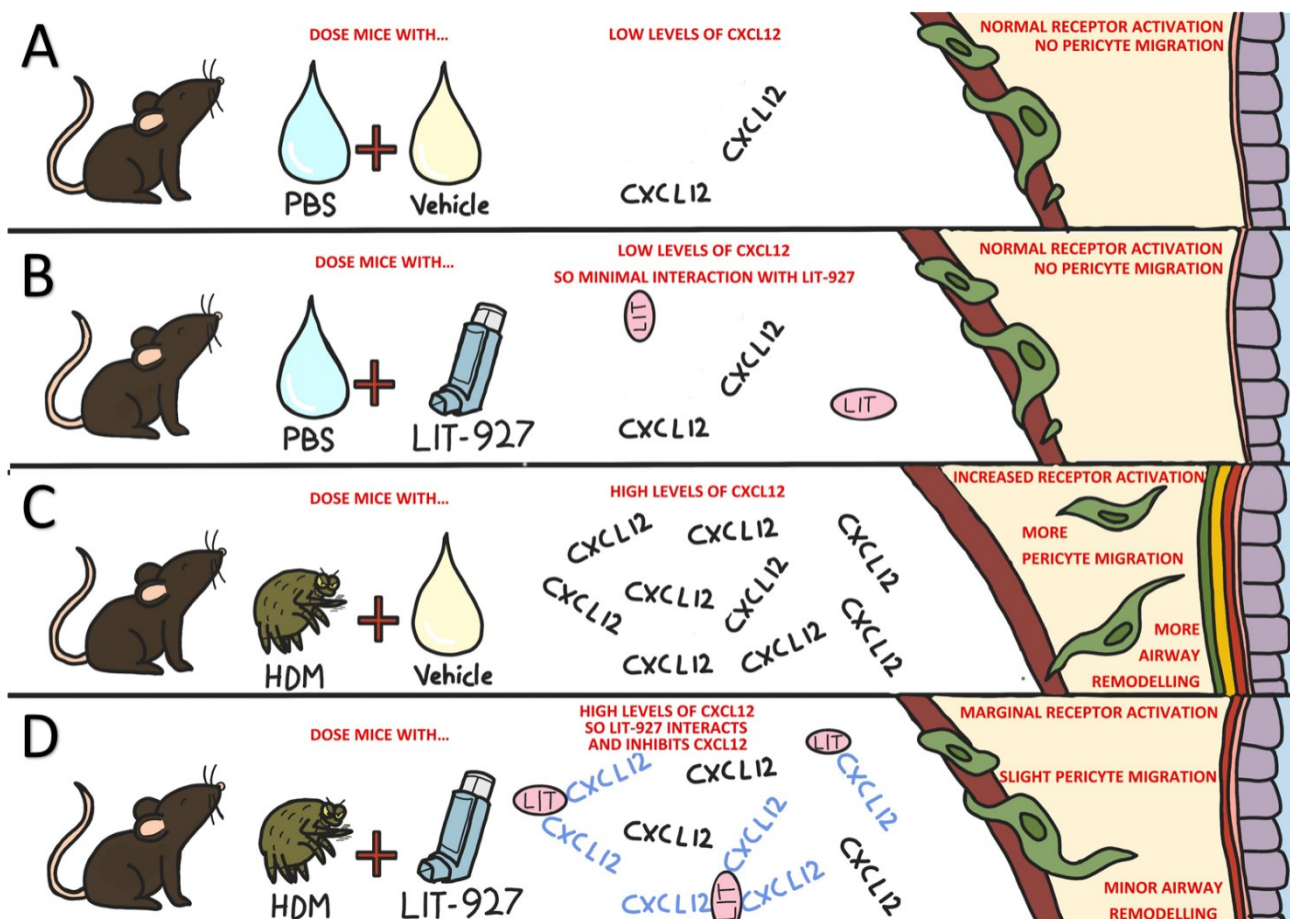


Figure 6.14 – Hypothesis on the effect of HDM and LIT-927 treatment in the different conditions tested. (A) In healthy control mice, lung levels of CXCL12 are low and pericytes stably surround the pulmonary vasculature. (B) A similar situation is observed in PBS control mice given LIT-927. (C) Mice exposed to HDM for 5 weeks demonstrate considerable structural changes in the large airway, including pericyte uncoupling from the supporting vasculature and migration into airway smooth muscle bundles, where they contribute to airway smooth muscle thickening and lung dysfunction. These structural changes are accompanied by Th2-polarized airway inflammation and high levels of CXCL12 expression. (D) Topical (i.n.) administration of LIT-927 to HDM-exposed mice breaks the CXCL12 chemokine gradient at the site of inflammation and prevents pericyte uncoupling and migration, thereby mitigating smooth muscle thickening and improving symptom scores.

Figure 6.14 is a graphical depiction of the conditions explored in this chapter. Part A shows one of the negative control conditions where the mice were given PBS and the vehicle. Under these normal conditions, in the absence of inflammation, low levels of CXCL12 and no LIT-927 are present. CXCR4 is not activated and pericytes do not receive a signal to uncouple from the vasculature, resulting in no airway remodelling. Part B indicates that when LIT-927 is administered, the low concentration of CXCL12 under non-inflamed conditions means that there would be few interactions with LIT-927, resulting in no change to the normal function and location of pericytes. The mice shown in part C were exposed to the allergen HDM and treated with the drug vehicle. HDM exposure induces robust Th2 inflammation and elevated expression of CXCL12, which subsequently activates CXCR4, resulting in pericyte migration from the vasculature and into the subepithelial region of the airway wall,

where these cells contribute to airway remodelling and lung dysfunction. Finally, in panel D, in mice exposed to HDM and treated with LIT-927, CXCL12 interact with the neutraligand LIT-927 is prevented from activating CXCR4 receptors. This results in a reduction in pericyte migration and airway remodelling compared to the scenario depicted in part C.

6.3 Discussion

The results shown in this chapter highlight a promising area of study and showcase a possible new drug to treat the airway remodelling observed in allergic asthma. The basis of this study is the importance of the CXCL12/CXCR4 pathway in allergic asthma. The experimental design, outlined in Figure 6.1 is based on the house dust mite model and is representative of the disease progression in human allergic asthma. House dust mite is an incredibly common allergen and can be found throughout the world with around 1 in 5 adults being sensitised to HDM, making it a useful standard allergen to use in the study of allergic asthma (Calderon et al., 2014, North West Paediatric Allergy Network, 2021). The method of administration of the allergen is also relevant to the human disease, with intranasal administration ensuring the allergen is delivered locally to the lungs which can be seen as equivalent to the inhalation of allergen in the human disease. It is also a less invasive method of administration, compared to intraperitoneal or intravenous injection, leading to less stress for the animal and reducing the effect that increased cortisol levels may have on the response to the allergen (Meijer et al., 2006). In addition, as it is a relatively simple procedure, user error is also reduced. The house dust mite extract was obtained from Citeq Biologics and contained extracts from *Dermatophagoides pteronyssinus*, the most common species of house dust mite (Doras et al., 2018). *D. pteronyssinus* has been shown to contain the allergens Der p 1, Der p 3 and Der p 9, which may be responsible for initiating the immune response to this allergen. Der p 1 has been shown to have proteolytic activity and can increase the permeability of the epithelium via the disruption of tight junctions through the cleavage of occludin, allowing the influx of pro-inflammatory cytokines produced by Th2 cells and macrophages into the surrounding area and the allergen to travel further into the submucosal areas (Wan et al., 1999). It is also thought that Der p 1 induces cytokine release through the activation of PAR-1 receptors, which causes an increase in IL-6 and IL-8, thus contributing to the inflammation (Asokanathan et. al, 2002a, Asokanathan et al., 2002b). Moreover, Der p 3 is thought to activate PAR-4 receptors and is responsible for modulating the opening of calcium ion channels (Lin et al., 2018). This combined approach is likely what leads to the physiological response to house dust mite exposure both in mice and in humans. HDM treatment has also been shown to elicit a strong danger signal as it induces the production of IL-33, an important regulator of the Th2 immune response in allergic inflammation (Dai et al., 2020, Chan et al., 2019).

The other most common method for inducing allergic asthma in mice is referred to as the ovalbumin model. This involves sensitising the mice to ovalbumin via an intraperitoneal injection of ovalbumin, sometimes combined with adjuvants such as aluminium hydroxide, on days 0, 7 and 14 of the experiments. Following this, the immune response must also be challenged through a further injection of ovalbumin at days 26, 27 and 28 before analysis and harvesting could occur on day 30 (Conrad et al., 2009). This method is not very physiologically relevant as it drastically differs from the induction of the disease in humans. Although these challenges with ovalbumin appear to elicit a strong Th2 response characterised by increased eosinophils, IgE and IL-4 (Ban et al., 2013), it has been shown that this is not prolonged and any immune response initiated by ovalbumin administration returns to a baseline eventually. This is known as inhalation tolerance and poses issues in using this model for longitudinal studies, highlighting another deviation from the human disease (Alvarez et al., 2006).

The importance of the CXCL12/CXCR4 gradient in allergic asthma has been discussed as CXCL12 is often elevated in bronchoalveolar lavage fluid of asthmatic patients and inhibition of CXCR4 have been shown to attenuate some symptoms of asthma (Negrete-Garcia et al., 2009, Chen et al., 2015a). It has also been shown that the CXCL12/CXCR4 gradient can contribute to the migration of mesenchymal stem cells and may therefore contribute to pericyte migration in asthma (Chapter 3) (Hu et al., 2013). Studies have also shown that pericytes interacting with CXCL12 via their receptor CXCR4 can encourage pericyte differentiation which may result in increased differentiation into myofibroblasts and therefore more contribution to airway remodelling via ECM deposition and smooth muscle cell hyperplasia (Hamdan, Zhou & Kleinerman, 2014). Previous groups have utilised the small molecule inhibitor AMD3100 in order to block the activity of CXCR4 and disrupt the gradient (Hamdan, Zhou & Kleinerman, 2014, Chen et al., 2015a, Lukacs et al., 2002). However, other studies have suggested that, *in vivo*, AMD3100 may encourage the production and migration of bone marrow mesenchymal stem cells, which also highly express CXCR4, into the periphery and thus result in an exacerbation in allergic airway disease (Kumar & Ponnazhagan, 2012). Therefore, instead of targeting CXCR4 for inhibition, CXCL12 neutralization was the approach chosen here. LIT-927 is a compound that was derived from the small molecule chalcone 4 (Regenass et al., 2018). It interacts directly with CXCL12 and prevents it from binding to CXCR4, thus disrupting the chemokine gradient. As LIT-927 was administered intranasally, this allowed it to exert its action directly at the site of inflammation, *i.e.* the airway wall. Moreover, respiratory delivery of LIT-927 could be a promising addition to current corticosteroid or combination corticosteroid/ β 2-agonist inhalers that are currently available for the treatment of allergic asthma. LIT-927 was administered only after 3 weeks of HDM treatment as studies have shown that remodelling is incipient following 3 weeks of

exposure to HDM (Johnson et al., 2004). This timepoint was targeted in an effort to suppress pericyte migration before it is fully established. The potential reversibility of the remodelling observed in this model has not yet been explored and will require extensive investigation, and is therefore beyond the scope of this thesis.

As shown in Figure 6.2-6.5, following exposure to HDM, immune cell numbers were increased in the bronchoalveolar lavage fluid regardless of whether LIT-927 treatment was provided or not. This suggests that LIT-927 does not interfere with the immune response in allergic asthma and that eosinophils, neutrophils and monocyte-derived macrophages were able to infiltrate the airway wall unimpeded. Despite this, in Figures 6.6 and 6.7 it can be seen that symptom scores were markedly reduced following treatment with LIT-927 compared to those of the mice exposed to house dust mite and treated with vehicle. The reduction of these scores without apparent interference with the immune system highlights the importance of the CXCL12/CXCR4 gradient and the contribution of CXCR4+ mesenchymal cells to airway remodelling, as previous studies have shown that both inflammation and airway remodelling are determinants of increased airway resistance in HDM-exposed mice (Johnson et al., 2008).

This hypothesis, i.e. that pericytes directly contribute to airway smooth muscle thickening and symptom scores, was supported by observing the location of pericytes in the trachea via immunofluorescence (Figures 6.8, 6.9). The cells in these images that were positive for α -SMA were determined to be pericytes that are uncoupling from the capillaries based on their vessel orientation and morphology. The coupled/uncoupled status of pericytes was determined by observing the wholemounts in three dimensions on a widefield microscope and enumerated by blinded, trained personnel. It was seen that slightly more pericytes had uncoupled from the vasculature in the group given house dust mite without LIT-927 than those given house dust mite and LIT-927, and that treatment with LIT-927 reduced pericyte uncoupling, likely by reducing the chemotactic signal for pericytes to migrate rather than by affecting the interaction between pericytes and endothelial cells of the blood vessels, although this should be further investigated by assessing PDGFR β and N-cadherin expression on pericytes under these conditions. This hypothesis was corroborated in Figures 6.10 and 6.11, as these images clearly show a thick band of α -SMA positive cells around the airway wall in the group only given house dust mite which was not present in the group given both house dust mite and LIT-927. This suggests that treatment with LIT-927 prevents the migration of pericytes towards the airway wall which is a characteristic cardinal feature in the airway remodelling observed in allergic asthma (Johnson et al., 2015). The absence of this constrictive barrier of smooth muscle-like cells would contribute to the easing of such symptoms such as airway constriction and therefore impacting the reduction of symptom scores observed in Figures 6.6 and 6.7. The

expression of α -SMA was calculated as a way to quantify the size of these smooth muscle bands, in Figures 6.11 and 6.12. Pericytes and smooth muscle cells represent a continuum of cells, not binary entities and therefore they both stain positive for α -SMA. This is why a secondary pericyte stain, PDGFR β or NG2 was included, to indicate co-localisation. As CXCL12 acts as a chemoattractant in vitro and is upregulated within the HDM model, it is likely to be produced by cells residing around the airways as this was the direction pericytes were migrating. This is corroborated by studies stating that endothelial cells only produce low levels of CXCL12 compared to other cell types, although which is the dominant cell type is in contest, with various cell types being suggested such as fibroblasts, stromal cells and myeloid cells (Greenbaum et al., 2013, Li et al., 2020, Borge et al., 2013). In addition to this, CXCL12 must be secreted around the airway as high concentrations of CXCL12 are observed within the BAL fluid of asthmatics (Negrete-Garcia et al., 2009). Carrying out immunostaining on lung sections for CXCL12 may help to further elucidate the location of CXCL12 within the airway.

Although this “neutraligand” is very recently developed, it has already shown its utility and potential as a therapeutic in several scenarios. Regenss et al have shown that LIT-927 was successful in reducing eosinophil recruitment using the ovalbumin model of eosinophilic asthma (Regenss et al., 2018). Another group have also shown its potential as a treatment for pulmonary arterial hypertension. They showed that it prevented pericyte migration in vitro as well as partially reversing vascular remodelling when administered intraperitoneally (Bordenave et al., 2020). These promising findings corroborate findings outlined within this chapter and hints to future therapeutic used of LIT-927.

In summary, this chapter has outlined evidence demonstrating the mechanism by which lung pericytes migrate to the airway wall in vivo, and contribute to the airway remodelling seen in the lungs of asthmatic patients. Further studies should continue to explore the effects of LIT-927 treatment on the lungs in vivo, for example using precision cut lung slices in order to measure airway hyperresponsiveness following methacholine challenges (Liu et al., 2019a) or using invasive methods such as the Flexivent (McGovern et al., 2013), although these experiments are complicated in the UK as Home Office regulations forbid the use of a paralytic agent in mice undergoing lung function measurements (Home Office, 1986). Further pharmacological assessments should be performed investigating a range of durations and doses of LIT-927 treatment. Clinical studies should also be eventually performed involving LIT-927 to determine the impact of long-term treatment, including the possibility of side effects, and to explore the possibility of a treatment in tandem with existing asthma treatments, such as corticosteroids.

Chapter 7 – General Discussion

The scope of this thesis is the modulation of selected growth factors, the effect of these interventions on tissue-resident mesenchymal stem cells, i.e. pericytes, and how modulating pericyte biology can have an effect on airway remodelling in allergic asthma. This was achieved by harnessing a variety of techniques, from classic techniques such as immunostaining and ELISA, to more complex procedures such as magnetic levitation to form spheroids, and animal experiments. These techniques were utilised as described in four distinct data chapters in this thesis: The Migration of Pericytes In Vitro Can Be Modulated By Growth Factors, Cytokine and Matrikines in the Microenvironment Including TGF- β , VEGF and Periostin, Matricellular Protein Periostin Promotes Pericyte Migration in Fibrotic Airways and Can Be Abrogated By Cinnamaldehyde, A New Dimension: Spheroids Containing a Co-Culture of Endothelial Cells and Pericytes Can Be Constructed Via Magnetic Levitation, and CXCL12 Drives Pericyte Accumulation and Airway Remodelling in Allergic Airway Disease.

7.1 Chapter 3 - The Migration of Pericytes In Vitro Can Be Modulated By Growth Factors, Cytokine & Matrikines in the Microenvironment Including TGF- β , VEGF & Periostin

The migration of pericytes was initially highlighted as a key event within the airway remodelling in allergic asthma (Johnson et al., 2015), and so it was decided to explore the factors effecting the migration of pericytes in order to reduce or reverse this change and therefore reduce the effect of pericytes on airway remodelling in allergic asthma.

Various growth factors were selected to be explored within this set of experiments. Preliminary experiments to narrow down possible cytokines and determine effective doses were previously performed by other lab members and were therefore not included in this thesis. TGF- β was selected as it is widely associated with tissue fibrosis in many conditions, including chronic kidney disease, liver fibrosis, spinal cord injury, asthma and even neurological conditions such as amyotrophic lateral sclerosis (Meng, Nikolic-Paterson & Lan, 2016, Xu et al., 2016, Wang et al., 2018, Doeing & Solway, 2013, Peters et al., 2017). It has been shown that increased TGF- β leads to cell proliferation, migration, and differentiation of mesenchymal stem cells, all of which can exacerbate remodelling due to the differentiation of myofibroblasts and increased contractile cell mass around the airway walls (Xu et al., 2018, Dubon et al., 2018, Willis & Borok, 2009, Johnson et al., 2011). These diverse effects are likely due to the complex canonical and non-canonical signalling pathways by which TGF- β can influence many different pathways. Proliferation of mesenchymal stem cells is thought to be mediated by Wnt signalling induced by Smad (Small mothers against decapentaplegic) 3, whilst the

non-canonical pathway induces many pathways such as Akt (protein kinase B), ERK (extracellular signal-regulated kinase) and p38 and encourages migration of mesenchymal stem cells (Xu et al., 2018, Dubon et al., 2018). Differentiation of mesenchymal stem cells into myofibroblasts and epithelial cells to mesenchymal cells are key sources of myofibroblasts within fibrotic tissue and is greatly influenced by the activation of ILK (integrin-linked kinase) via Smad3 (Willis & Borok, 2009). For these reasons, it was concluded that the impact of TGF- β on pericyte migratory capacity would be a fruitful avenue of exploration. EGF is also known to robustly contribute to increased proliferation of many different cell types, as well as the activation of PLC γ (phospholipase C gamma) through its interaction with its receptor EGFR thusly encouraging migration through the Pyk2/paxillin pathway (Jorissen et al., 2003, Polk, 1998, Choi et al., 2007). VEGF was also included in this investigation, as is traditionally linked to angiogenesis and therefore is also involved in the recruitment and migration of endothelial cells (Wang et al., 2011, Shibuya, 2013). VEGF was therefore tested to see if it could modulate the migration of pericytes as well, as pericytes play an important role in the structural stability of blood vessels (Yamagishi et al., 1999). Periostin was also selected as a matrikine to explore as it has strong links to asthma and TGF- β and so was included to see if it modulates migration of pericytes (Nanri et al., 2020, Izuhara, Ohta & Ono, 2016). Further information on the study of periostin as well as the inclusion of CXCL12 in this study will be explored in subsequent sections in this chapter. In addition to the identification of inflammatory mediators that would be useful to study within the scope of this thesis, a review article was also published describing a number of cytokines that contribute to inflammation and tissue fibrosis (Bignold & Johnson, 2021b).

Two different types of migration assays were used within this chapter to assess the migratory capacity of pericytes. Most of the work was undertaken using Transwell or Boyden chamber assays. Developed in 1962 by Stephen Boyden, the principle of the assay is that cells must actively migrate through a membrane containing pores that are only just big enough for the cell to fit through and often also include a chemoattractant in order to encourage this migration (Boyden, 1962). Transwell assays are thought to be reliable and replicable as they use standard kit and manufactured membranes which would be consistent. They are also able to easily be modified into invasion assays by adding an additional barrier along the membrane such as basement membrane or extracellular matrix (Guy et al., 2017). The addition of a chemoattractant to the bottom well also allows the attraction of various cytokines to be assessed at the same time as cytokine treatment allowing multidimensional analysis (Zhang et al., 2016). However, there are several disadvantages to this method. Firstly, it involves the use of specialised cell culture inserts and so requires additional resources. In addition, depending on the cell visualisation method used, the enumeration of cells

could be very challenging. If using a standard crystal violet stain to colour cell nuclei, the dye also gets stuck within the pores of the membrane and can be falsely included in the cell count. In addition, if staining with DAPI and using ImageJ to automatically count the cells, this is not always accurate as ImageJ is sometimes unable to distinguish between individual nuclei if the cells are in close proximity to each other (as in Figure 3.15). Therefore, it may be advantageous, although time consuming, to count cells by hand.

Scratch assays were also utilised in this chapter and offer a very simple and yet useful method to measure cell migration. Scratch assays may also be referred to as wound healing assays, although that is a gross simplification as wound healing is a much more complex and controlled event including multiple different cell types and signalling pathways. Unlike the previously described Transwell assays, scratch assays need no special equipment as the scratch can simply be made with a pipette tip, although automatic scratch makers are available in order to standardise the size of the scratches (Lee, Kim & Park, 2020). There are several disadvantages to this method, however, with the main issue observed in pericytes being delamination of cells. This occurred frequently when the cell monolayer became too confluent during the treatment period and therefore pulled away from the well bottom when scratched. This was difficult to manage as, in order for the assay to work effectively, cells should be ~80% confluent at the time of the scratch and, as some treatments encourage cell proliferation while other suppress it, getting each treatment group to that confluency at the same time was challenging. However, for all data included, cells were between around 75-90% confluent. In addition, imaging the same section of the scratch before and after incubation was also difficult. Certain identifying topological features were attempted to be matched to ensure it was the same area, although this is relatively unreliable as topography would change when cells migrate. To combat this, live cell imaging could be used to observe cell migration for the whole incubation period and the overall dynamics of the migration could be observed and analysed. This, however, requires expensive long-term cell imaging systems with an incubated stage to provide the necessary conditions for the assay.

The overall findings in this chapter are that treating pericytes with TGF- β , EGF or VEGF significantly increases their migratory capacity, but only when measured via the scratch assay. In Transwell assays, treatment led to decreased migration, although this was likely to be due to increased cell-cell interactions and cell clumping causing multiple cells to be counted as one. This may also link to increased N-cadherin expression observed in several other experiments as N-cadherin mediated cell-cell interactions. The investigation involving pericyte migration also yielded interesting results, with pericytes treated with TGF- β or VEGF migrating towards living macrophages more than untreated pericytes as well as dead macrophages. This has informed several additional projects that have since

started in our lab to further investigate the contribution of macrophage-derived extracellular vesicles to pericyte migration and inflammation as a whole. It was also shown that pericytes migrate towards CXCL12 regardless under all experimental conditions. This led to the investigation and targeting of the CXCL12/CXCR4 gradient, which will be explained in a later section. As well as TGF- β treatment, periostin treatment also increased the migration of pericytes in scratch assays and also induced similar clumping to the TGF- β treated cells. Therefore, periostin was highlighted as a target for further investigation, which will be outlined in the next section.

There are several avenues that could be explored in this research area. One key aspect is the optimisation of the migration assays used. Cell counting on the Transwell membranes could be optimised to allow automatic counting by incorporating machine learning algorithms in order to analyse large data sets quickly and accurately (Moen et al., 2020). Alternatively, the optimum seeding density of pericytes could be explored in order to minimise clumps, but that may be restrictive as pericytes require intercellular connections to thrive. To optimise scratch assays, certain products could be used in order to standardise the size of the scratch such as inserts which create a cell-free space, or automated scratchers (Huang et al., 2019, Yigitbilek et al., 2021). In addition, the use of a live cell imaging system such as the Incucyte SX1 would allow the observation of migration for a continuous 24 hours (Cho et al., 2022).

As one of the most novel and promising cytokines explored in the first chapter, periostin, was selected for more thorough investigation as outlined in the next section.

7.2 Chapter 4 - Matricellular Protein Periostin Promotes Pericyte Migration in Fibrotic Airways and Can Be Abrogated By Cinnamaldehyde

The main scope of this chapter was to explore the relationship between pericytes and the protein periostin and examine its link to allergic asthma. The link to between periostin and allergic asthma is long established, as the serum periostin concentration can be used as a biomarker to indicate severe or late-onset asthma (Matsusaka et al., 2015). It has also been shown to indicate the increased involvement of type 2 immunity and therefore can highlight patients as “Th2-high”. This can inform the likely efficacy of treatments based on targeting IgE or IL-13, such as QGE031, omalizumab or lebrikizumab, as those deemed as “Th2-low” may not respond effectively to those treatments (Izuhara, Ohta & Ono, 2016, Pelaia et al., 2018) There has also been suggestions that periostin is also elevated in other inflammatory lung conditions, such as idiopathic pulmonary fibrosis and interstitial lung disease. In order to explore this avenue, online databases were utilised whilst research laboratories were unavailable due to the COVID-19 pandemic. By using online databases and publicly available data it raises the scope of the research by allowing access to samples and data that would

normally not be available, particularly to small, underfunded labs. The Gene Expression Omnibus by NCBI gives access to microarray data from thousands of samples and by using the search terms POSTN (the gene for periostin) and asthma, 49 experiments with a total of 1,300 samples (Edgar, Domrachev & Lash, 2002). This was then narrowed down to look specifically at allergic asthma, and two data sets were selected as they both involved primary lung tissue. Another database that was used was the “IPF Cell Atlas”, which is a tool that allows researchers to visualise data from six different data sets, all relating to either idiopathic pulmonary fibrosis or interstitial lung disease (Neumark et al., 2020). These data sets were useful, as many were categorised by cell type, thus allowing the expression of periostin to be pinpointed to particular cells or areas. The two data sets from this database highlighted the increase in POSTN expression in endothelial cells, fibroblasts and myofibroblasts. Although none of these are technically pericytes, all may actually point towards pericytes as a source of periostin due to their colocalization and frequent interactions. Fibroblasts and pericytes have very similar surface protein expression and are often mistaken for each other. Similarly, it has been suggested that many myofibroblasts are derived from pericytes and therefore may have a similar expression profile (Humphreys et al., 2010). Another cell atlas was used, i.e. the Wellcome/Sanger Cell Atlas, showing the location and upregulation of POSTN in asthmatic airways (Regev, et al., 2017). The co-localisation of the POSTN gene was also explored using the EMBL-EBI IntAct database, with POSTN having many physical associations with TGFB1, a gene encoding TGF- β 1 (Orchard et al., 2013, <https://www.genecards.org/cgi-bin/carddisp.pl?gene=TGFB1>).

However, there are disadvantages to using databases. Data from several data sets should not be pooled, even if samples seem to be the same, as experimental conditions may differ. If specific to a cell type, cell types may be incorrectly characterised, as previously mentioned with fibroblasts. This could lead to relationships being assumed where none actually occur. In addition, inferring a relationship between two genes from colocalization databases may be dangerous as colocalization does not expressly lead to interactions (Uygun et al., 2016).

This chapter contains some migration data, much like the previous chapter. As first suggested in the previous chapter, data from both Transwells and scratch assays as discussed in this chapter show that pericytes migrate more readily when treated with periostin as well as TGF- β and IL-13. IL-13 was thus included in the treatment panel as it has been shown to encourage the production of periostin (Ito et al., 2018). The fact that periostin elicits a similar effect on migration as TGF- β suggests that further analysis of periostin/TGF- β crosstalk could be important.

Immunostaining was also a technique which was used several times within this chapter, both on cultured cells and lung slices from HDM treated lungs. Initially, cultured pericytes were stained with

an anti-periostin antibody in order to see if periostin was present within pericytes and if cytokine treatments could induce a production of periostin. This hypothesis was supported in Figures 4.10 and 4.11, as unstimulated pericytes had a weak periostin signal that was increased following treatment with TGF- β or recombinant periostin. Several other research groups have also suggested that pericytes may produce periostin under certain conditions, such as within gliomas and following spinal cord injury, but it has yet to be linked to pulmonary pericytes in asthma (Huizer et al., 2020, Yokota et al., 2017). Immunostaining is a good technique to visualise the location of certain proteins and see if they occur in the cytoplasm, along the cell membrane or within the nucleus. It is also useful to identify cells of interest within whole tissue slices. In this chapter, immunostained images were also used to identify a ring of strongly periostin-positive cells around an asthmatic airway wall (Figures 4.12 and 4.13). This narrowed down the type of cells which are likely to interact with periostin as they should be found around the airway walls, thus solidifying our hypothesis that pulmonary pericytes produce and interact with periostin in allergic asthma. In addition, there was also a robust periostin signal within the epithelium which corroborates with studies showing that epithelial cells produce periostin (Burgess et al., 2021). However, as this thesis focuses on the contribution of pericytes, this was not explored further.

The advantages of using immunostaining as a method to identify expression of proteins are numerous. Firstly, it is a very flexible method and can be modified to investigate a wide range of proteins, from cell-surface markers to intracellular proteins and many different target antibodies are commercially available. It is also a relatively easy and forgiving method to complete, with timings and concentrations that can be adjusted to fit experimental or logistical needs. Immunostained images can also provide results very quickly and easily and may not require further numerical analysis if they are merely used as preliminary data. The removal of the need for data analysis is incredibly useful when a quick check is needed to simply see if the protein of interest is present in a cell or environment.

However, immunostaining can also come with disadvantages. Reagents, although widely available, can be expensive, especially if multiple different antibodies are required for each experiment. The quality of antibodies available also varies, with some versions being less effective for certain tissue and so some optimization is required by titrating the antibodies to the optimal working concentration. Due to the limited resources and microscopes available to me at Aston University, only two markers could be tested on a single sample (three stains were possible in one instance although the microscope capable of far red microscopy was only functional and available to me for a very small fraction of time). Identifying a protein of interest within a singular cell type in a complex tissue sample is often not possible with only 2 antibodies that were available to me, especially with

pericytes which often require several markers for identification as their surface proteins are very similar to their surrounding cells such as smooth muscle cells or fibroblasts (Bergers & Song, 2005, Alex et al., 2022) Low quality images may also lead to inaccurate data analysis and therefore a high-quality microscope is required. To overcome some of these disadvantages, a secondary method could be used to analyse the expression of proteins, such as western blot.

ELISA was also used in this chapter to investigate the presence of the protein periostin, although this time in supernatants from cultured pericytes and bronchoalveolar lavage fluid from mice with allergic airway disease. Much like immunostaining, ELISA tests for specific proteins using antibodies although instead of creating an image, a colorimetric reaction occurs in proportion to the amount of protein present. This allows accurate estimation of the concentration of protein in a sample via the use of a standard curve. The difference between ELISA and immunostaining, in the forms used in these experiments, is an important distinction as the latter measures intracellular proteins whilst the former focuses on secreted protein within the microenvironment. However, it is possible to use ELISA to measure intracellular proteins by methods such as Cell-ELISAs or icELISAs although these were not explored within this thesis (Molnar, 2019, Scholer et al., 2020). The ELISA performed in this chapter demonstrated that periostin concentration was slightly elevated in bronchoalveolar lavage fluid from mice exposed to HDM when compared to control saline mice. This is consistent with patient serum, as the periostin concentration is increased in asthmatic patient sera, as previously mentioned (Izuhara et al., 2016).

Several mediators were used to treat cultured pericytes in order to explore what would cause pericytes to produce periostin. The only cytokine to induce a release of periostin from pericytes was IL-13 (Figure 4.16). It is important to compare this to the results of TGF- β and periostin treatment results shown in the immunostaining (Figure 4.10), in which treatment increased intracellular periostin expression. The distinction between what these two methods demonstrate is important here, as immunostaining detects periostin inside the cell, whilst ELISA measures extracellular periostin. These results therefore suggest that treatment of pericytes with TGF- β or periostin causes periostin to be retained within the cell membrane whilst IL-13 treatment causes pericytes to expel periostin into the surrounding medium. The mechanisms between these two very different reactions needs to be elucidated to fully understand the impact of targeting different parts of this reaction cascade. In addition, the importance of the form of periostin, being either the soluble form or ECM-bound form, is vital to furthering knowledge of this interesting matrikine. This requires extensive additional experiments but would be an important and interesting avenue to pursue. In this chapter, ELISAs which did not yield accurate results were also included to demonstrate a disadvantage of the ELISA method. User error can have a significant effect on the quality of data obtained, as an

inaccurate standard curve will always lead to erroneous data since the formula of the curve is used to estimate the concentration and may highlight imprecise pipetting. The quality of the blocking step is also incredibly important and requires high quality BSA, an error that was made in several of these ELISAs, thus preventing specific binding of the periostin or non-specific binding due to incomplete blocking, leading to nonsensical data. There are several alternative methods that could be used instead of ELISA including mass spectrometry or western blots.

A main concept that was explored in this chapter is the inhibition of periostin by targeting the initiator of periostin production, IL-13. This was achieved by using the naturally occurring compound cinnamaldehyde. There has been an increase in naturally derived medicine in recent years, with a review on using natural products as drugs being published in *Nature* as recently as 2021 (Atasnasov et al., 2021). These sources have been explored in relation to cancer therapy and, more relevantly, anti-fibrosis and anti-inflammatory medication (Chen et. al, 2018a, Huang et al., 2021, Andrade et al., 2018). Natural products can be a good inspiration and starting point for developing effective synthetic compounds, suggesting that it may be more time efficient in research as fewer compounds need to be tested in order to find one which proves effective as a treatment (Wright, 2019, Granchi, 2022). Novel chemical structures found in nature also provide an interesting starting point to further optimize and improve the therapeutic nature of these compounds (Dehelean et al., 2021). A recent, large review spanning just over 38 years explored the use of natural compounds in medicine and concluded that 1881 drugs containing natural products had been tested, most of which were anti-cancer drugs or anti-microbial drugs (e.g. anti-bacterial or anti-fungal) (Newman & Cragg, 2020). This shows that naturally-derived medication is still a fruitful avenue to pursue.

Cinnamaldehyde is a phenylpropanoid extracted from cinnamon bark (most often *Cinnamomum verum*, but can be from other members of the *Cinnamomum* family) and often used as a flavouring additive or essential oil (Hastings et al., 2016, Kim et al., 2021). The FDA (Food and Drug Administration) has currently only approved one medical product containing cinnamaldehyde; the T.R.U.E. Test Thin-Layer Rapid Use Patch Test for allergen sensitisation (Wishart et al., 2006, Fischer & Maibach, 1985). Cinnamon-based supplements are also widespread and are thought to possess antimicrobial, antiviral, antioxidant and anti-inflammatory properties (Nabavi et al., 2015, Premanathan et al., 2000, Murcia et al., 2004, Kim et al., 2007, Gruenwald, Freder & Armbruster, 2010). The anti-inflammatory effect of cinnamaldehyde was further explored within this chapter as several studies have suggested an inhibitory effect it has on IL-13, often via the modulation of Nrf2 or NF- κ B (Mitamura et al., 2018, Rangasamy et al., 2005, Kim et al., 2007). The mechanism by which cinnamaldehyde inhibits IL-13 is not fully understood, although several studies have demonstrated that treatment with cinnamaldehyde reduces the effects of IL-13 (Huang & Wang, 2017) with one

study by Mitamura et al. also linking it to the reduction of periostin in fibroblasts via the activation of Nrf2 (Mitamura et al., 2018). The aim of this section was to perform initial experiments to explore the effect of cinnamaldehyde treatment on IL-13 and see if that mitigated the effects of periostin on pericytes observed earlier on in the chapter. Figures 4.29-4.33 demonstrate that treatment with cinnamaldehyde following growth factor dosing with either IL-13 or recombinant periostin reduces the migration of treated pericytes. This effect, however, was not observed following treatment with TGF- β , as there was no difference with or without cinnamaldehyde treatment. This suggests that TGF- β treatment and IL-13 treatment may induce periostin production and secretion via different pathways. This difference may also lead to the difference in location of the periostin following those two treatments, as previously suggested. Cinnamaldehyde treatment was also explored via immunostaining, although there was little effect on the expression of intracellular periostin. This may suggest that cinnamaldehyde may only target the extracellular periostin secreted by pericytes or has little effect within the cell itself.

Further study should also be completed into the toxicity of cinnamaldehyde. This could be done through MTT assays or live/dead staining. This is due to several studies which have highlighted possible damage to cilia within the airways following exposure to cinnamaldehyde (Clapp et al., 2019). However, this is often explored in relation to cinnamon-flavour vape fluid and less on the intranasal administration of cinnamaldehyde. Despite this, prior to in vivo testing, further exploration into the effect of cinnamaldehyde on ciliated columnar epithelial cells should be completed. If the toxicity of cinnamaldehyde is deemed too high and cannot be reduced through the use of analogues, an alternative IL-13 inhibitor can be explored, such as lebrikizumab (Scheerens et al., 2012).

Data from this chapter has been published in *Frontiers in Allergy* and has been presented at the Mercia Stem Cell Alliance Conference in 2019 and at the American Thoracic Society Conference in 2021 and 2022 (Bignold & Johnson, 2021a, Johnson & Bignold, 2021, Johnson & Bignold, 2022).

7.3 Chapter 5 – A New Dimension: Spheroids Containing a Co-Culture of Endothelial Cells and Pericytes Can Be Constructed Via Magnetic Levitation

This chapter focuses on exploring the construction of spheroids containing endothelial cells and pericytes, and hypothesising on their uses in the in vivo modelling of asthma in order to reduce the use of animals in the development of therapeutic interventions. As highlighted within the chapter, many different methods of forming spheroids are available and all have different advantages and disadvantages. The magnetic levitation method was selected for use within this study as it resulted in a consistently sized singular spheroid per well, allowing different treatments to be effectively

compared. However, this method resulted in several experimental disadvantages, such as mounting and imaging as well as the structural integrity of larger spheroids. Many of the experiments included within this chapter involved trying to reduce these factors and optimise the method of forming co-cultured spheroids.

Images in Figures 5.2 and 5.6 clearly show the structural instability of the spheroids formed as each images show either spheroids that have completely fragmented or have areas of considerable cell loss around the edges of the spheroids. It is unclear if this structural damage occurred during growth or treatment of the spheroids or during the mounting step where the cell masses were transferred to a mounting slide using a magnetic pen. This method was incredibly troublesome due to the small size of the spheroids and the weakness of the magnet pen. This often resulted in mechanical damage to the spheroid and therefore prevented any affects caused by the treatments from being observed. As this was mainly due to human error, as practice improved this movement as shown in the images in Figures 5.11, 5.12 and 5.14, where the spheroids had a more consistent and spherical shape. This may pose an issue when using this method with inexperienced lab members, as this technique requires significant practice. Therefore it would be beneficial to further optimise the mounting section of this technique in order to increase reproducibility. This may be done by imaging in situ within the plate rather than transferring onto a glass slide. However, the hardware available at the time of these experiments were not suitable for this, as one confocal microscope was in the upright configuration and therefore could not image plates and another confocal microscope was unable to image through cell culture plastic due to unfavourable optical properties of the plastic compared to glass slides (Thorn, 2016). There are also several additional issues with transferring spheroids from the culture plate to a different coverslip in that some important material may also be lost. In Figure 5.15, images indicate there may have been cell mass left behind in the culture plate when spheroids were removed. As the overall aim of this method was to observe pericyte coverage and even possibly migrating pericytes, the cells that left the spheroids may be very important. However, as these images were brightfield and not stained with something like DAPI, it cannot be confirmed that these are cells and not just cellular debris. Another issue with mounting on glass slides is the use of coverslips when imaging in 3D. Understandably, when building 3D cultures, the aim is to produce a 3D image in order to observe the cell connections completely. However, by using coverslips to mount spheroids, this 3D aspect is greatly reduced. As can be seen in the 3D representations of the spheroids in Figure 5.14, the spheroids have been flattened compared to their spherical form during growth.

Therefore, it may be profitable to explore the use of 96-well plates that are especially designed for imaging with a coverslip base (Xie et al., 2020). By using imaging plates, such as Xie et al. has done,

the compressing effect of the coverslip is negated, yet the issue of successfully moving the spheroid still remains. It would therefore be useful to combine one of these plates with the magnet array and fully culture the spheroids within the imaging plate. However, the problem with this method is that the magnet array is designed to fit normal 96 well plates and may not sit correctly within well plates of a different shape. Also, many of the current imaging plates available are tissue culture coated rather than low attachment, which may affect the formation of the spheroids due to possible attachment to the bottom of the wells. Yet, it is possible to make plates low attachment including using an agar-based solution in the bottom of the wells as well as the use of polyHEMA, a non-adherent polymer (Gao et al., 2018, Chen et al., 2015b). Therefore, this aspect of spheroid use needs to be further optimised in order for this to be a viable method for disease modelling.

Alongside the concerns with mounting, the staining protocol may also need to be optimised further. The images in Figures 5.11 and 5.12 show a decrease in staining, including DAPI within the core of the spheroids. This could be due to several factors. Firstly, the centre of the spheroid could have a reduced density of cells due to increased apoptosis caused by a lack of oxygen diffusing into the cell mass. However, it is commonly reported that oxygen can diffuse between 100-200 μ m, and the spheroids have an average diameter of around 150 μ m and therefore they should be fully oxygenated (Grimes et al., 2016). To test this, EF5 or HIF-1 α , markers for hypoxia, could be included in a staining panel alongside p53 or caspase-3 antibodies to test for apoptosis in order to assess the health of the cells in the core of the spheroids (Grimes et al., 2016, Ward et al., 2008).

To conclude, this chapter outlined a possible method for constructing spheroids containing endothelial cells and pericytes. Aspects of this method should be further optimised, as the mounting and imaging of the spheroids are not yet ideal. This method may be used in the future to observe the interactions between endothelial cells and pericytes following various treatments to replicate an inflammatory and/or fibrotic environment.

7.4 Chapter 6 – CXCL12 Drives Pericyte Accumulation and Airway Remodelling in Allergic Airway Disease

This chapter explores the use of an in vivo model of allergic asthma to investigate the effectiveness of a potential drug targeting CXCL12.

As outlined in this chapter, animal models are an incredibly vital tool in drug development. They allow the detection of off-target effects that can only be observed in an organism. In vivo studies are also an essential step when developing a drug for clinical trials and all data from animal studies must be recorded according to ARRIVE (Animal Research: Reporting of In Vivo Experiments) guidelines (du

Sert et al., 2020). The first consideration when planning an in vivo study is the animal in which the drug will be tested. Many animals have previously been used as models, including drosophila, zebrafish and primates (Hickman et al., 2016). Often, the selection depends on resources available to house and study the particular animals although each animal is useful for studying different aspects of disease. By far the most common animals used for disease modelling, and the one used in this study, is the mouse. It is estimated that 95% of animal experiments take place in mice (Vandamme, 2014). The ability to create transgenic mice to model certain diseases, such as cancer in the 1980s, encouraged researchers to develop these animals for in vivo work (Hanahan, Wagner & Palmiter, 2007). There are many transgenic strains of mice which are kept by various private companies, with the International Mouse Phenotyping Consortium archiving over 6000 strains of transgenic mice with the C57BL/6 background only, showing the scope of biomedical research in mice (Cacheiro et al., 2019). As well as C57BL/6 mice, there are several different mouse strains which are commonly used such as Balb/C, CBA, 129SvEv and CD1 (Sultana, Ogundele & Lee, 2019). Each of these strains have slightly different characteristics and thus must be considered carefully before a suitable strain is selected. This study used C57BL/6 mice rather than Balb/C mice. Balb/C mice are more Th2 skewed than C57BL/6 mice as the former produce more IL-4 whilst the latter produce more IL-12 (Trunova et al., 2011). This suggests that Balb/C mice would be more susceptible to allergens and to presenting an Th2-induced allergic response. Therefore, by using C57BL/6 mice, a more robust immune response must be triggered in order for the Th2 cascade to be initiated.

Mouse models of asthma have been used since 1994, when the first model of asthma was developed using an antigen from a water-borne parasite (*Schistosoma mansoni*). This model resulted in an influx of eosinophils, neutrophils, monocytes and leukocytes as well as an increase in IL-4 in the bronchoalveolar lavage fluid. However, this inflammation resolved after 3-4 days and thus started the years of development to optimise a mouse model of asthma (Lukacs et al., 1994). There are two main allergens used to stimulate an asthmatic response: ovalbumin and house dust mite. Both of these allergens can be administered acutely and chronically in order to model different types of asthma (Nials & Uddin, 2008).

The CXCR4/CXCL12 gradient has long been linked to allergic asthma as well as various other forms of tissue injury (Chen et al., 2015a, Wong et al., 2015) Although the link to pericytes and their migration during allergic asthma and in inflammation is yet to be established, the migration of bone marrow stem cells within injury has been attributed to the CXCR4/CXCL12 gradient (Rankin, 2012, Hu et al., 2013). Many attempts have been made to disrupt this gradient by using inhibitors of CXCR4 with molecules such as AMD3100 and BPRCX807 (Chen et al., 2016, Song et al., 2010, Song et al., 2021). However, as CXCL12 has been seen to be significantly increased in the bronchoalveolar lavage fluid

of asthmatic patients, instead an inhibitor of CXCL12 was selected for this study (Negrete-Garcia et al., 2009, Regenass et al., 2018). LIT-927 is a small molecule derived from chalcone-4, which binds to CXCL12 and prevents it from interacting with CXCR4 through the induction of a conformational change at the site where CXCL12 interacts with CXCR4 (Bignold et al., 2022). In addition to the receptor CXCR4 being expressed on pericytes, some infiltrating macrophages also express CXCR4. This has been assessed by us in the paper Bignold et. al., 2022, and has been suggested that CXCR4+ macrophages still extravasated into the lung but there was slightly less accumulation of these cells in the airways of HDM/LIT mice (Bignold et al., 2022). However, cell number in these experiments were fairly low and it remains unclear as to the contribution of CXCR4+ macrophages on remodelling in allergic airway disease.

To ensure any physiological effects caused by LIT-927 was not due to immune system modulation, immune cells were enumerated and differentiated in the bronchoalveolar lavage (BAL). BAL is a well-established technique which allows the quantification and phenotypic analysis of resident lung inflammatory cells as well as infiltrating inflammatory cells (Van Hoecke et al., 2017). The numbers of immune cells, such as macrophages, eosinophils and neutrophils, remained the same whether mice were treated with LIT-927 or the vehicle, indicating that LIT-927 does not have an anti-inflammatory effect. This is particularly important, as a subset of tissue-infiltrating monocyte-derived macrophages expresses CXCR4; the impact of LIT-927 treatment on macrophage activity in the airways should be more thoroughly examined. These results demonstrate that the observed impact of LIT-927 in improving respiratory symptoms was not due to the inhibition of immune cell infiltration into the airway wall, but rather a non-immune, structural cell type, such as pericytes.

The symptom scores observed throughout the 5 weeks of study highlighted that the treatment with LIT-927 following exposure to HDM reduced the symptoms of respiratory distress brought on by HDM exposure. Mice that were exposed to HDM but were not given LIT-927 began to show symptoms of mild respiratory distress such as sneezing and wheezing (Burkholder et al., 2012). These symptoms were reduced in HDM-exposed mice following treatment with LIT-927. The reduction of symptoms indicated an intervention in the pathology of asthma and highlighted LIT-927 as a potential drug that can be added to the treatment strategy for allergic asthma, with the advantage that this compound targets disease pathways not impacted by currently available treatments.

Various immunostained images were included highlighting pericytes within the trachea and lung sections. The tracheal images show more pericytes uncoupling from the vasculature and migrating in the HDM condition than the negative controls. This was reduced slightly when treated with LIT-927.

This reduction of migration may have aided in preventing the accumulation and subsequent differentiation of pericytes around the airways, which contributes to airway remodelling in allergic asthma (Johnson et al., 2015). This migration of pericytes was also observed in Chapter 3 and Chapter 4 and therefore seems to be a key event in fibrosis. The other images show robust thickening of the airway wall following HDM exposure combined with increased numbers of pericytes residing around the airway wall, indicated by the pericyte markers NG2 and PDGFR β . As previously discussed in Chapter 3, several pericyte markers should be used to ensure proper characterisation of pericytes. This airway wall thickening has been observed in many asthmatic patients and is a key physiological change observed within asthma which contributes to much of the dyspnoea often seen in patients (Awadh et al., 1998, Doeing and Solway, 2013). The airway wall seemed consistently thinner following treatment with LIT-927 and also exhibited reduced accumulation of pericytes. This shows that fewer pericytes were contributing to airway remodelling, although it is uncertain whether this was simply due to a reduction in the migration of pericytes or the reversal of migration, with pericytes moving back towards the blood vessels. Further experiments should be performed to elucidate the main location of pericytes following LIT-927 treatment within the lung tissue at various stages of disease progression.

In this study, only one concentration and treatment schedule of LIT-927 was tested due to time constraints. Although this concentration was taken from previous studies involving LIT-927, a full dose/time-response experiment should be conducted to ensure the dosage of LIT-927 is optimum for treatment and the minimisation of toxicity. In addition, lung function measurements through the use of precision cut lung slices and invasive methacholine challenge should be performed once facilities render this possible. This was initially planned; however, due to the restriction on international travel during the COVID-19 pandemic, the practical training required to acquire skill in the precision-cut lung slice technique could not be undertaken. Additionally, further investigations into the impact of LIT-927 treatment on CXCR4⁺ macrophages in the lung following allergen exposure should be undertaken. Although it was observed that the number of macrophages in the bronchoalveolar lavage fluid was not affected by LIT-927 treatment, further investigations on tissue macrophages are warranted.

This chapter highlighted a promising new drug and outlined its effect on pericytes in vivo. The drug discovery pipeline in asthma is a long one, often dominated by large pharmaceutical companies such as GlaxoSmithKline and Novartis, with particular emphasis lately on anti-IL-4 or anti-IL-5 therapies (Holmes 2012, Moran & Pavord, 2020). However, I hope that work within this chapter, and my thesis as a whole, may aid in the discovery and development of new therapeutics targeting remodelling. Data from this chapter has been submitted to Respiratory Research and can be accessed as a pre-

print article (Bignold et al., 2022). The data were presented at the American Thoracic Society Conference in 2020 (Johnson & Bignold, 2020).

Overall, the findings of this thesis highlighted several fruitful areas of further study to contribute to the advancement of knowledge in this field. These are outlined in Figure 7.1 as well as the main contributions this thesis has had to the literature.

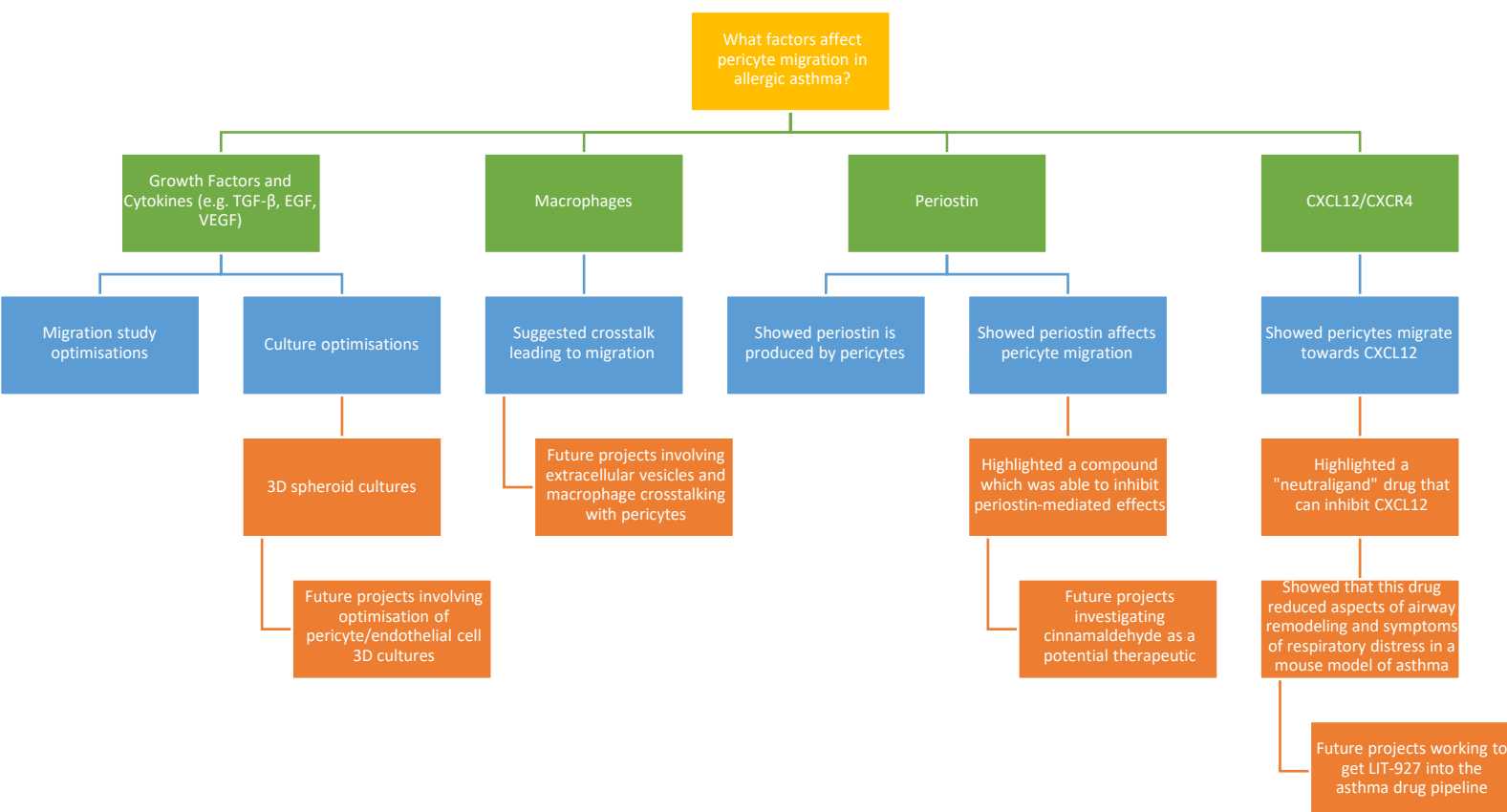


Figure 7.1 – Outcomes of this thesis. A flow chart depicting the main findings and proposed future avenues of study highlighted from findings within this thesis.

7.5 Disruptions

As with many projects that have occurred over the past few years, there have been several disruptions to my study. The majority of these disruptions have been due to the SARS-CoV-2 pandemic and the associated lockdowns and restrictions. Aston University was closed between 23rd March 2020 and 24th June 2020, although due to underlying health conditions which make me more susceptible to the virus, I did not return to the laboratory until 3rd August 2020. During this time, I

was unable to complete any practical work and minimal data analysis due to being unable to access the required software. This greatly impacted me, as many of my experiments relied on cell culture techniques which take several weeks to start up following a closure. Access to facilities and equipment was also reduced for several months due to social distancing and reduced room capacities. This reduced the amount of work and time I was able to spend within the laboratory, further impacting my data collection. As previously mentioned, the restrictions to international travel also prevented me from undertaking training in the preparation of precision cut lung slices, which unfortunately prevented me from including lung function measurements in my final data chapter.

Another large disruption to my studies was caused by the effects of Brexit. This mostly affected the shipping of cells and reagents, which had previously been delivered the day after ordering; after Brexit restrictions came into play, these products could take several weeks to months to arrive. This slowed the rate at which I was able to perform several experiments as well as disruption to cell culture if I was unable to obtain required medium. There were also several issues with receiving shipments of cell lines. The HPLPC cell line used throughout these studies were obtained from Promocell in Germany. They are sent as cryopreserved vials in dry ice which are perfectly viable if shipping is fast, as it had been in previous years. Following Brexit, upon several occasions, these deliveries were held up in customs and the cells thawed, resulting in non-viable material. This caused more delays and disruptions to my cell culture experiments.

There were also many technical limitations that impacted my research. Since November 2021 I was unable to access a new high-resolution confocal microscope due to not being able to access the required training. Prior to this, the confocal microscope that was available to me was only able to produce low-resolution images and was unable to image DAPI due to the laser set-up and the use of a multiphoton laser which damaged my samples. I was also not able to access a live cell imaging system as the one in our facility was out of commission for prolonged periods of time and not replaced until my time in the laboratory was completed. There were also issues with the shared CytoFlex flow cytometer as manufacturing and maintenance issues caused it to be often out of service or inaccurate. This prevented me from undertaking any large-scale FACS experiments.

Chapter 8 - References

ABDELAZIZ, MH., ABDELWAHAB, SF., WAN, J., CAI, W., HUIXUAN, W., JIANJUN, C., KUMAR, KD., VASUDEVAN, A., SADEK, A., SU, Z., WANG, S. & XU, H. 2020. Alternatively activated macrophages; a double-edged sword in allergic asthma. *Journal of Translational Medicine*, 18, 58.

ADAMS, T., SCHUPP, J., POLI, S., AYAUB, E., NEUMARK, N., AHANGARI, F., CHU, S., RABY, B., DETULLIS, G., JANUSZYK, M., DUAN, Q., ARNETT, H., SIDDIQUI, A., WASHKO, G., HOMER, R., YAN, X., ROSAS, I. & KAMINSKI, N. 2020. Single-cell RNA-seq reveals ectopic and aberrant lung-resident cell populations in idiopathic pulmonary fibrosis. *Science Advances*, 6.

AGUILERA, KY. & BREKKEN, RA. 2014. Recruitment and retention: factors that affect pericyte migration. *Cellular and Molecular Life Sciences*, 71(2).

AL-MUHSEN, S., JOHNSON, J. & HAMID, Q. 2011. Remodeling in asthma. *Journal of Allergy and Clinical Immunology*, 128, 451-462.

ALAGAPPAN, V., DE BOER, W., MISRA, V., MOOI, W. & SHARMA, H. 2013. Angiogenesis and Vascular Remodeling in Chronic Airway Diseases. *Cell Biochemistry and Biophysics*, 67, 219-234.

ALEX, L., TULETA, I., HARIKRISHNAN, V. & FRANGOIANNIS, N. 2022. Validation of Specific and Reliable Genetic Tools to Identify, Label, and Target Cardiac Pericytes in Mice. *Journal of the American Heart Association*, 11.

ALVAREZ, D., SWIRSKI, F., YANG, T., FATTOUH, R., CROITORU, K., BRAMSON, J., STAMPFLI, M. & JORDANA, M. 2006. Inhalation tolerance is induced selectively in thoracic lymph nodes but executed pervasively at distant mucosal and nonmucosal tissues. *Journal of Immunology*, 176, 2568-2580.

AMIDZADEH, Z., BEHBAHANI, A., ERFANI, N., SHARIFZADEH, S., RANJBARAN, R., MOEZI, L., ABOUALIZADEH, F., OKHOVAT, M., ALAVI, P. & AZARPIRA, N. 2014. Assessment of different permeabilization methods of minimizing damage to the adherent cells for detection of intracellular RNA by flow cytometry. *Avicenna Journal of Medical Biotechnology*, 6, 38-46

ANDRADE, P. & VALENTAO, P. 2018. Insights into Natural Products in Inflammation. *International Journal of Molecular Sciences*, 19.

ANDRAE, J., GALLINI, R. & BETSHOLTZ, C. 2008. Role of platelet-derived growth factors in physiology and medicine. *Genes & Development*, 22, 1276-1312.

ARMULIK, A., ABRAMSSON, A. & BETSHOLTZ, C. 2005. Endothelial/pericyte interactions. *Circulation Research*, 97, 512-523.

ARMULIK, A., GENOVE, G. & BETSHOLTZ, C. 2011. Pericytes: Developmental, Physiological and Pathological Perspectives, Problems, and Promises. *Developmental Cell*, 21(2), 193-215.

ASHLEY, S., WILKE, C., KIM, K. & MOORE, B. 2017. Periostin regulates fibrocyte function to promote myofibroblast differentiation and lung fibrosis. *Mucosal Immunology*, 10, 341-351.

ASOKANANTHAN, N., GRAHAM, P., BAKKER, A., EIDNE, K., THOMPSON, P. & STEWART, G. 2002a. The house dust mite allergen Der p 1 modulates respiratory epithelial cell function by activation of protease activated receptors (PARs). *Journal of Allergy and Clinical Immunology*, 109, S169-S169.

ASOKANANTHAN, N., GRAHAM, P., FINK, J., KNIGHT, D., BAKKER, A., MCWILLIAM, A., THOMPSON, P. & STEWART, G. 2002b. Activation of protease-activated receptor (PAR)-1, PAR-2, and PAR-4 stimulates IL-6, IL-8, and prostaglandin E-2 release from human respiratory epithelial cells. *Journal of Immunology*, 168, 3577-3585.

ATANASOV, A., ZOTCHEV, S., DIRSCH, V., SUPURAN, C. & TASKFORCE, I. N. P. S. 2021. Natural products in drug discovery: advances and opportunities. *Nature Reviews Drug Discovery*, 20, 200-216.

AUN, M., BONAMICHI-SANTOS, R., ARANTES-COSTA, F., KALIL, J. & GIAVINA-BIANCHI, P. 2017. Animal models of asthma: utility and limitations. *Journal of Asthma and Allergy*, 10, 293-301.

AWADH, N., MULLER, N., PARK, C., ABOUD, R. & FITZGERALD, J. 1998. Airway wall thickness in patients with near fatal asthma and control groups: assessment with high resolution computed tomographic scanning. *Thorax*, 53, 248-253.

BAGLEY, RG., ROULEAU, C., MORGENBESSER, SD., WEBER, W., COOK, BP., SHANKARA, S., MADDEN, SL. & TEICHER, BA. 2006. Pericytes from human non-small cell lung carcinomas: An attractive target for anti-angiogenic therapy. *Microvascular Research*, 71(3), 163-174.

BAGNATO, G. & HARARI, S. 2015. Cellular interactions in the pathogenesis of interstitial lung diseases. *European Respiratory Review*, 24, 102-114.

BAN, M., LANGONNE, I., HUGUET, N., GUICHARD, Y. & GOUTET, M. 2013. Iron oxide particles modulate the ovalbumin-induced Th2 immune response in mice. *Toxicology Letters*, 216, 31-39.

BARNES, P. 2008a. Immunology of asthma and chronic obstructive pulmonary disease. *Nature Reviews Immunology*, 8, 183-192.

BARNES, P. 2008b. The cytokine network in asthma and chronic obstructive pulmonary disease. *Journal of Clinical Investigation*, 118, 3546-3556.

BARRETT, T., WILHITE, SE., LEDOUX, P., EVANGELISTA, C., KIM, IF., TOMASHEVSKY, M., MARSHALL, KA., PHILLIPPY, KH., SHERMAN, PM., HOLKO, M., YEFANOV, A., LEE, H., ZHANG, N., ROBERTSON, CL., SEROVA, N., DAVIS, A. & SOBOLEVA, A. 2013. NCBI GEO: archive for functional genomics data sets – update. *Nucleic Acids Research*, 41(D1), D991-D995.

BARRON, L., GHARIB, S. & DUFFIELD, J. 2016. Lung Pericytes and Resident Fibroblasts Busy Multitaskers. *American Journal of Pathology*, 186, 2519-2531.

BENTLEY, J., CHEN, Q., HONG, J., POPOVA, A., LEI, J., MOORE, B. & HERSHENSON, M. 2014. Periostin is required for maximal airways inflammation and hyperresponsiveness in mice. *Journal of Allergy and Clinical Immunology*, 134, 1433-1442.

BERGERS, G. & SONG, S. 2005. The role of pericytes in blood-vessel formation and maintenance. *Neuro-Oncology*, 7, 452-464.

BIERNACKA, A., DOBACZEWSKI, M. & FRANGOIANNIS, NG. 2011. TGF- β signalling in fibrosis. *Growth Factors*, 29(5), 196-202.

BIGNOLD, R. & JOHNSON, J. 2021a. Matricellular protein periostin promotes pericyte migration in fibrotic airways. *Frontiers in Allergy*, 2, 786034.

BIGNOLD, R. & JOHNSON, J. R. 2021b. Effects of cytokine signaling inhibition on inflammation-driven tissue remodeling. *Current Research in Pharmacology and Drug Discovery*, 2, 100023.

BIGNOLD, R., SHAMMOUT, B., ROWLEY, J., REPICI, M., SIMMS, J. & JOHNSON, J. 2022. CXCL12 drives pericyte accumulation and airway remodeling in allergic airway disease. *Respiratory Research*, 23, 183.

BIRBRAIR, A., ZHANG, T., FILES, D., MANNAVA, S., SMITH, T., WANG, Z., MESSI, M., MINTZ, A. & DELBONO, O. 2014. Type-1 pericytes accumulate after tissue injury and produce collagen in an organ-dependent manner. *Stem Cell Research & Therapy*, 5.

BODNAR, RJ., SATISH, L., YATES, CC. & WELLS, A. 2016. Pericytes: A Newly Recognized Player in Wound Healing. *Wound Repair and Regeneration*, 24(2), 204-214.

BOECKING, CA., WALENTEK, P., ZLOCK, LT., SUN, DL., WOLTERS, PJ., ISHIKAWA, H., JIN, BJ., HAGGIE, PM., MARSHALL, WF., VERKMAN, AS. & FINBEINER, WE. 2022. A simple method to generate human

airway epithelial organoids with externally orientated apical membranes. *American Journal of Physiology Lung Cellular and Molecular Physiology*, 322(3), L420-L437

BONNER, J.C. 2004. Regulation of PDGF and its receptors in fibrotic diseases. *Cytokine & Growth Factor Reviews*, 15(4), 255-273.

BONSER, L. & ERLE, D. 2017. Airway Mucus and Asthma: The Role of MUC5AC and MUC5B. *Journal of Clinical Medicine*, 6.

BOOTH, J., HANNINGTON, G., BAKIR, T., STERN, H., KANGRO, H., GRIFFITHS, P. & HEATH, R. 1982. COMPARISON OF ENZYME-LINKED IMMUNOSORBENT-ASSAY, RADIOIMMUNOASSAY, COMPLEMENT-FIXATION, ANTICOMPLEMENT IMMUNOFLOURESCENCE AND PASSIVE HEMAGGLUTINATION TECHNIQUES FOR DETECTING CYTOMEGALOVIRUS IGG ANTIBODY. *Journal of Clinical Pathology*, 35, 1345-1348.

BORDENAVE, J., THUILLET, R., TU, L., PHAN, C., CUMONT, A., MARSOL, C., HUERTAS, A., SAVALE, L., HIBERT, M., GALZI, J.L., BONNET, D., HUMBERT, M., FROSSARD, N. & GUIGNABERT, C. 2020. Neutralization of CXCL12 attenuates established pulmonary hypertension in rats. *Cardiovascular Research*, 116(3), 686-697.

BORGE, M., NANNINI, P., MORANDE, P., JANCIC, C., BISTMANS, A., BEZARES, R., GIORDANO, M. & GAMBERALE, R. 2013. CXCL12 is a costimulator for CD4(+) T cell activation and proliferation in chronic lymphocytic leukemia patients. *Cancer Immunology Immunotherapy*, 62, 113-124

BOSNAKOVSKI, D., MIZUNO, M., KIM, G., ISHIGURO, T., OKUMURA, M., IWANAGA, T., KADOSAWA, T. & FUJINAGA, T. 2004. Chondrogenic differentiation of bovine bone marrow mesenchymal stem cells in pellet cultural system. *Experimental Hematology*, 32, 502-509.

BOTTEMA, M. & IEEE, S. P. S. 2000. Circularity of objects in images. 2000 IEEE International Conference on Acoustics, Speech, and Signal Processing, Proceedings, Vols I-Vi, 2247-2250.

BOULET, L. 2017. Airway remodeling in asthma: Mechanisms, clinical relevance, treatment, and prevention. *Canadian Journal of Respiratory Critical Care and Sleep Medicine*, 1, 39-42.

BOYDEN, S. 1962. The chemotactic effect of mixtures of antibody and antigen on polymorphonuclear leucocytes. *The Journal of Experimental Medicine*, 115, 453-466.

BURGESS, J., JONKER, M., BERG, M., TEN HACKEN, N., MEYER, K., VAN DEN BERGE, M., NAWIJN, M. & HEIJINK, I. 2021. Periostin: contributor to abnormal airway epithelial function in asthma? *European Respiratory Journal*, 57(2), 2001286.

BURKHOLDER, T., FOLTZ, C., KARLSSON, E., LINTON, C. & SMITH, J. 2012. Health Evaluation of Experimental Laboratory Mice. *Current Protocols in Mouse Biology*, 2, 145-165.

BUTSABONG, T., FELIPPE, A., CAMPAGNOLO, P. & MARINGER, K. 2021. The emerging role of perivascular cells (pericytes) in viral pathogenesis. *Journal of General Virology*, 102(8), 001634.

CACHEIRO, P., HAENDEL, M., SMEDLEY, D., MEEHAN, T., MASON, J., MASHHADI, H., MUNOZ-FUENTES, V., TOCCHINI, G., LLOYD, K., MCKERLIE, C., BOWER, L., CLARY, D., NUTTER, L., FLENNIKEN, A., TEBOUL, L., CODNER, G., WELLS, S., HERAULT, Y., SORG, T., VASSEURM, L., SELLOUM, M., ROUX, M., JACOBS, H., MEZIANE, H., CHAMPY, M., ABOUT, G., MURRAY, S., CHESLER, E., KUMAR, V., WHITE, J., BRAUN, R., BEAUDET, A., DICKINSON, M., HEANEY, J., LORENZO, I., LANZA, D., REYNOLDS, C., WARD, C., SAMACO, R., VEERARAGAVAN, S., HSU, C., CHRISTIANSON, A., GALLEGOS, J., SEAVITT, J., GASPERO, A., GREEN, J., GARZA, GARZA, A., BOHAT, R., SEDLACEK, R., BROWN, S. & M, I. M. P. C. 2019. New models for human disease from the International Mouse Phenotyping Consortium. *Mammalian Genome*, 30, 143-150.

CALDERON, M., LINNEBERG, A., KLEINE-TEBBE, J., BLAY, F., HERNANDEZ FERNANDEZ DE ROJAS, D., VIRCHOW, J. & DEMOLY, P. 2014. Respiratory allergy caused by house dust mites: What do we really know? *Journal of Allergy and Clinical Immunology*, 136.

CAMINATI, M., PHAM, D., BAGNASCO, D. & CANONICA, G. 2018. Type 2 immunity in asthma. *World Allergy Organization Journal*, 11.

CANTY-LAIRD, E., LU, Y. & KADLER, K. 2012. Stepwise proteolytic activation of type I procollagen to collagen within the secretory pathway of tendon fibroblasts in situ. *Biochemical Journal*, 441, 707-717

CARLSSON, J., NILSSON, K., WESTERMARK, B., PONTEN, J., SUNDSTROM, C., LARSSON, E., BERGH, J., PAHLMAN, S., BUSCH, C. & COLLINS, V. 1983. FORMATION AND GROWTH OF MULTICELLULAR SPHEROIDS OF HUMAN-ORIGIN. *International Journal of Cancer*, 31, 523-533.

CARVALHO, C., GASPAR, A., KNIGHT, A. & VICENTE, L. 2019. Ethical and Scientific Pitfalls Concerning Laboratory Research with Non-Human Primates, and Possible Solutions. *Animals*, 9.

CATHERY, W., FAULKNER, A., JOVER, E., RODRIGUEZ-ARABAOLAZA, I., THROMAS, AC., AVOLIO, E., CAPUTO, M. & MADEDDU, P. 2020. Umbilical Cord Pericytes Provide a Viable Alternative to Mesenchymal Stem Cells for Neonatal Vascular Engineering. *Frontier in Cardiovascular Medicine*, 7, 609980.

CHAMBERLAND 2009. A Comparison of Two Sets of Microarray Experiments to Define Allergic Asthma Expression Pattern (vol 35, pg 399, 2009). *Experimental Lung Research*, 35, 539-539.

CHAN, B., LAM, C., TAM, L. & WONG, C. 2019. IL33: Roles in Allergic Inflammation and Therapeutic Perspectives. *Frontiers in Immunology*, 10.

CHANG, FC., CHOU, YH., CHEN, YT. & LIN, SL. 2012. Novel insights into pericyte-myofibroblasts transition and therapeutic targets in renal fibrosis. *Journal of the Formosan Medical Association*, 111(11), 589-598.

CHANG, WG., ANDREJECSK, JW., KLUGER, MS., SALTZMAN, WM. & POBER, JS. 2013. Pericytes modulate endothelial sprouting. *Cardiovascular Research*, 100(3), 492-500.

CHAUDHARY, N., SCHNAPP, A. & PARK, J. 2006. Pharmacologic differentiation of inflammation and fibrosis in the rat bleomycin model. *American Journal of Respiratory and Critical Care Medicine*, 173, 769-776.

CHEN, D., FENG, Y., CAO, G. & ZHAO, Y. 2018a. Natural Products as a Source for Antifibrosis Therapy. *Trends in Pharmacological Sciences*, 39, 937-952.

CHEN, H., XU, X., TENG, J., CHENG, S., BUNJHOO, H., CAO, Y., LIU, J., XIE, J., WANG, C., XU, Y. & XIONG, W. 2015a. CXCR4 inhibitor attenuates allergen-induced lung inflammation by down-regulating MMP-9 and ERK1/2. *International Journal of Clinical and Experimental Pathology*, 8, 6700-6707.

CHEN, H., XU, X., TENG, J., CHENG, S., BUNJHOO, H., CAO, Y., LIU, J., XIE, J., WANG, C., XU, Y. & XIONG, W. 2016. CXCR4 inhibitor attenuates ovalbumin-induced airway inflammation and hyperresponsiveness by inhibiting Th17 and Tc17 cell immune response. *Experimental and Therapeutic Medicine*, 11, 1865-1870.

CHEN, L., ACCIANI, T., LE CRAS, T., LUTZKO, C. & PERL, A. 2012. Dynamic Regulation of Platelet-Derived Growth Factor Receptor alpha Expression in Alveolar Fibroblasts during Realveolarization. *American Journal of Respiratory Cell and Molecular Biology*, 47, 517-527.

CHEN, T., LI, M., FAN, X., CHENG, J. & WANG, L. 2018b. Sodium Tanshinone IIA Sulfonate Prevents Angiotensin II-Induced Differentiation of Human Atrial Fibroblasts into Myofibroblasts. *Oxidative Medicine and Cellular Longevity*, 2018.

CHEN, Y., LOU, X., ZHANG, Z., INGRAM, P. & YOON, E. 2015b. High-Throughput Cancer Cell Sphere Formation for Characterizing the Efficacy of Photo Dynamic Therapy in 3D Cell Cultures. *Scientific Reports*, 5.

CHIARELLI-NETO, O., GARCEZ, ML., PAVANI, C., MARTINS, W., DE ABREU QUINTELA CASTRO, FC., AMBROSIO, RP., MEOTTI, FC. & BAPTISTA, MS. 2023. Inflammatory stimulus worsens the effects of UV-A exposure on J774 cells. *Journal of Photochemistry and Photobiology*. 239, 112647.

CHO, Y., KIM, J., HEO, K., KIM, H., YUN, S., LEE, H., SHIN, H., SHIM, H., YU, H., KIM, Y. & LEE, S. 2022. An internalizing antibody targeting of cell surface GRP94 effectively suppresses tumor angiogenesis of colorectal cancer. *Biomedicine & Pharmacotherapy*, 150.

CHOI, J., YANG, Y., LEE, S., KIM, I., HA, S., KIM, E., BAE, Y., RYU, S. & SUH, P. 2007. Phospholipase C-gamma 1 potentiates integrin-dependent cell spreading and migration through Pyk2/paxillin activation. *Cellular Signalling*, 19, 1784-1796

CHOY, DF., HART, KM., BORTHWICK, LA., SHIKOTRA, A., NAGARKAR, DR., SIDDIQUI, S., JIA, G., OHRI, CM., DORAN, E., VANNELLA, KM., BUTLER, CA., HARGADON, B., SCIURBA, JC., GIESECK, RL., THOMPSON, RW., WHITE, S., ABBAS, AR., JACKMAN, J., WU, LC., EGEN, JG., HEANEY, LG., RAMALINGAM, TR., ARRON, JR., WYNN, TA. & BRADDING, P. 2015. TH2 and TH17 inflammatory pathways are reciprocally regulated in asthma. *Science Translational Medicine*, 7 (301), 301ra129.

CLAPP, P., LAVRICH, K., VAN HEUSDEN, C., LAZAROWSKI, E., CARSON, J. & JASPERS, I. 2019. Cinnamaldehyde in flavored e-cigarette liquids temporarily suppresses bronchial epithelial cell ciliary motility by dysregulation of mitochondrial function. *American Journal of Physiology-Lung Cellular and Molecular Physiology*, 316, L470-L486.

CONRAD, M., YILDIRIM, A., SONAR, S., KILIC, A., SUDOWE, S., LUNOW, M., TEICH, R., RENZ, H. & GARN, H. 2009. Comparison of adjuvant and adjuvant-free murine experimental asthma models. *Clinical and Experimental Allergy*, 39, 1246-1254.

CORA, V., HADERSPECK, J., ANTKOWIAK, L., MATTHEUS, U., NECKEL, PH., MACK, AF., BOLZ, S., UEFFING, M., PASHKOVSKAIA, N., ACHBERGER, K. & LIEBAU, S. 2019. A Cleared View on Retinal Organoids, 8(5), 391.

COSTA, E., DE MELO-DIOGO, D., MOREIRA, A., CARVALHO, M. & CORREIA, I. 2018. Spheroids Formation on Non-Adhesive Surfaces by Liquid Overlay Technique: Considerations and Practical Approaches. *Biotechnology Journal*, 13.

CROMEY, D. & JANSMA, P. 2018. Zeiss ZEN - performing maximum intensity projection of a Z-stack. University of Arizona: UA Microscopy Alliance.

DAI, X., TOHYAMA, M., MURAKAMI, M., SHIRAIISHI, K., LIU, S., MORI, H., UTSUNOMIYA, R., MAEYAMA, K. & SAYAMA, K. 2020. House dust mite allergens induce interleukin 33 (IL-33) synthesis

and release from keratinocytes via ATP-mediated extracellular signaling. *Biochimica Et Biophysica Acta-Molecular Basis of Disease*, 1866.

DAUBEUF, F. & FROSARD, N. 2014. Eosinophils and the ovalbumin mouse model of asthma. *Methods in Molecular Biology*, 1178, 283-293.

DEHELEAN, C., MARCOVICI, I., SOICA, C., MIOC, M., CORICOVAC, D., IURCIUC, S., CRETU, O. & PINZARU, I. 2021. Plant-Derived Anticancer Compounds as New Perspectives in Drug Discovery and Alternative Therapy. *Molecules*, 26.

DEIGELMANN, RF. & EVANS, MC. 2004. Wound healing: an overview of acute, fibrotic and delayed healing. *Frontiers in Bioscience*, 9, 283-9.

DEMOULIN, JB. & MONTANO-ALMENDRAS, CP. 2012. Platelet-derived growth factors and their receptors in normal and malignant hematopoiesis. *American Journal of Blood Research*, 2(1), 44-56.

DIAZ-FLORES, L., GUTIERREZ, R., MADRID, J., VARELA, H., VALLADARES, F., ACOSTA, E. & MARTIN-VASALLO, P. 2009. Pericytes. Morphofunction, interactions and pathology in a quiescent and activated mesenchymal cell niche. *Histology and Histopathology*, 24, 909-969.

DOEING, D. & SOLWAY, J. 2013. Airway smooth muscle in the pathophysiology and treatment of asthma. *Journal of Applied Physiology*, 114, 834-843.

DORAFSHAN, S., RAZMI, M., SAFAEI, S., GENTILIN, E., MADJD, Z. & GHODS, R. 2022. Periostin: biology and function in cancer. *Cancer Cell International*, 22, 315.

DORAS, C., PETAK, F., BAYAT, S., BAUDAT, A., VON GAMIER, C., EIGENMANN, P. & HABRE, W. 2018. Lung responses in murine models of experimental asthma: Value of house dust mite over ovalbumin sensitization. *Respiratory Physiology & Neurobiology*, 247, 43-51.

DORE-DUFFY, P. & ESEN, N. 2018. "The microvascular pericyte: Approaches to isolation, characterization, and cultivation" in *Pericyte biology - novel concepts*. Editor A. Birbrair (Springer International Publishing).

DORE-DUFFY, P., WANG, S., MEHEDI, A., KATYSHEV, V., CLEARY, K., TAPPER, A., REYNOLDS, C., DING, Y., ZHAN, P., RAFOLS, J. & KREIPKE, C. 2011. Pericyte-mediated vasoconstriction underlies TBI-induced hypoperfusion. *Neurological Research*, 33, 176-184.

DRAIJER, C. & PETERS-GOLDEN, M. 2017. Alveolar Macrophages in Allergic Asthma: the Forgotten Cell Awakes. *Current Allergy and Asthma Reports*, 17(2), 12.

DUBON, M., YU, J., CHOI, S. & PARK, K. 2018. Transforming growth factor beta induces bone marrow mesenchymal stem cell migration via noncanonical signals and N-cadherin. *Journal of Cellular Physiology*, 233, 201-213.

DU SERT, N., HURST, V., AHLUWALIA, A., ALAM, S., AVEY, M., BAKER, M., BROWNE, W., CLARK, A., CUTHILL, I., DIRNAGL, U., EMERSON, M., GARNER, P., HOLGATE, S., HOWELLS, D., KARP, N., LAZIC, S., LIDSTER, K., MACCALLUM, C., MACLEOD, M., PEARL, E., PETERSEN, O., RAWLE, F., REYNOLDS, P., ROONEY, K., SENA, E., SILBERBERG, S., STECKLER, T. & WURBEL, H. 2020. The ARRIVE guidelines 2.0: updated guidelines for reporting animal research. *Journal of Physiology-London*, 598, 3793-3801

EDGAR, R., DOMRACHEV, M. & LASH, A. 2002. Gene Expression Omnibus: NCBI gene expression and hybridization array data repository. *Nucleic Acids Research*, 30, 207-210.

EILKEN, HM., DIEGUEZ-HURTADO, R., SCHMIDT, I., NAKAYAMA, M., JEONG, HW., ARF, H., ADAMS, S., FERRARA, N. & ADAMS, RH. 2017. Pericytes regulate VEGF-induced endothelial sprouting through VEGFR1. *Nature Communications*, 8, 1574.

ESERIBESE, M., GOMEZ-CASADO, C., BARBER, D. & DIAZ-PERALES, A. 2015. Immune Polarization in Allergic Patients: Role of the Innate Immune System. *Journal of Investigational Allergology and Clinical Immunology*, 25, 251-258.

FELIP-LEON, C., CEJUDO-MARIN, R., PERIS, M., GALINDO, F. & MIRAVET, J. 2017. Sizing Down a Supramolecular Gel into Micro- and Nanoparticles. *Langmuir*, 33, 10322-10328.

FENG, J., MANTESSO, A. & SHARPE, P. 2010. Perivascular cells as mesenchymal stem cells. *Expert Opinion on Biological Therapy*, 10, 1441-1451.

FERLAND-MCCOLLOUGH, D., SLATER, S., RICHARD, J., RENI, C. & MANGIALARDI, G. 2017. Pericytes, an overlooked player in vascular pathobiology. *Pharmacology & Therapeutics*, 171, 30-42.

FERNANDEZ-MORENO, M., FARR, C., KAGUNI, L. & GARESSE, R. 2007. *Drosophila melanogaster* as a model system to study mitochondrial biology. *Methods in Molecular Biology*, 372, 33-49.

FERRELL, PD., ORISTIAN, KM., COCKRELL, E. & PIZZO, SV. 2022. Pathologic Proteolytic Processing of N-cadherin as a Marker of Human Fibrotic Disease. *Cells*, 11(1), 156.

FISCHER, T. & MAIBACH, H. 1985. THE THIN-LAYER RAPID USE EPICUTANEOUS TEST (TRUE-TEST), A NEW PATCH TEST METHOD WITH HIGH-ACCURACY. *British Journal of Dermatology*, 112, 63-68.

FOTY, R. 2011. A Simple Hanging Drop Cell Culture Protocol for Generation of 3D Spheroids. *Jove-Journal of Visualized Experiments*.

FRA-BIDO, S., WALKER, S., INNOCENTIN, S. & LINTERMAN, M. 2021. Optimized immunofluorescence staining protocol for imaging germinal centres in secondary lymphoid tissues of vaccinated mice. *STAR Protocols*, 2, 100499

GAO, W., WU, D., WANG, Y., WANG, Z., ZOU, C., DAI, Y., NG, C., TEOH, J. & CHAN, F. 2018. Development of a novel and economical agar-based non-adherent three-dimensional culture method for enrichment of cancer stem-like cells. *Stem Cell Research & Therapy*, 9.

GARRISON, AT., BIGNOLD, RE., WU, X. & JOHNSON, JR. 2023. Pericytes: The lung-forgotten cell type. *Frontiers in Physiology*, 14.

GEY, G., COFFMAN, W. & KUBICEK, M. 1952. Tissue culture studies of the proliferative capacity of cervical carcinoma and normal epithelium. *Cancer Research*, 12, 264-265.

GIRODET, PO., NGUYEN, D., MANCINI, JD., HUNDAL, M., ZHOU, X., ISRAEL, E. & CERNADAS. 2016. Alternative Macrophage Activation Is Increased in Asthma. *American Journal of Respiratory Cell and Molecular Biology*, 55(4), 467-475.

GONZALEZ-GONZALEZ, L. & ALONSO, J. 2018. Periostin: A Matricellular Protein with Multiple Functions in Cancer Development and Progression. *Frontiers in Oncology*, 8.

GRANCHI, C. 2022. Biological Activity of Natural and Synthetic Compounds. *Molecules*, 27(12), 3652.

GREENBAUM, A., HSU, Y., DAY, R., SCHUETTELPELZ, L., CHRISTOPHER, M., BORGERDING, J., NAGASAWA, T. & LINK, D. 2013. CXCL12 in early mesenchymal progenitors is required for haematopoietic stem-cell maintenance. *Nature*, 495, 227-230.

GREIDER, C. & BLACKBURN, E. 1985. IDENTIFICATION OF A SPECIFIC TELOMERE TERMINAL TRANSFERASE-ACTIVITY IN TETRAHYMENA EXTRACTS. *Cell*, 43, 405-413.

GRIMES, D., KANNAN, P., WARREN, D., MARKELC, B., BATES, R., MUSCHEL, R. & PARTRIDGE, M. 2016. Estimating oxygen distribution from vasculature in three-dimensional tumour tissue. *Journal of the Royal Society Interface*, 13.

GRUENWALD, J., FREDER, J. & ARMBRUESTER, N. 2010. Cinnamon and Health. *Critical Reviews in Food Science and Nutrition*, 50, 822-834.

GUNTI, S., HOKE, A., VU, K. & LONDON, N. 2021. Organoid and Spheroid Tumor Models: Techniques and Applications. *Cancers*, 13.

GUY, J., ESPENEL, S., VALLARD, A., BATTISTON-MONTAGNE, P., WOZNY, A., ARDAIL, D., ALPHONSE, G., RANCOULE, C., RODRIGUEZ-LAFRASSE, C. & MAGNE, N. 2017. Evaluation of the Cell Invasion and

Migration Process: A Comparison of the Video Microscope-based Scratch Wound Assay and the Boyden Chamber Assay. *Jove-Journal of Visualized Experiments*.

HABERMANN, A., GUTIERREZ, A., BUI, L., YAHN, S., WINTERS, N., CALVI, C., PETER, L., CHUNG, M., TAYLOR, C., JETTER, C., RAJU, L., ROBERSON, J., DING, G., WOOD, L., SUCRE, J., RICHMOND, B., SEREZANI, A., MCDONNELL, W., MALLAL, S., BACCHETTA, M., LOYD, J., SHAVER, C., WARE, L., BREMNER, R., AT WALIA, R., BLACKWELL, T., BANOVIK, N. & KROPSKI, J. 2020. Single-cell RNA sequencing reveals profibrotic roles of distinct epithelial and mesenchymal lineages in pulmonary fibrosis. *Science Advances*, 6.

HAGEDORN, M., BALKE, M., SCHMIDT, A., BLOCH, W., KURZ, H., JAVERZAT, S., ROUSSEAU, B., WILTING, J. & BIKFALVI, A. 2004. VEGF coordinates interaction of pericytes and endothelial cells during vasculogenesis and experimental angiogenesis. *Developmental Dynamics*, 230, 23-33.

HAMDAN, R., ZHOU, Z. & KLEINERMAN, E. 2014. Blocking SDF-1 alpha/CXCR4 Downregulates PDGF-B and Inhibits Bone Marrow-Derived Pericyte Differentiation and Tumor Vascular Expansion in Ewing Tumors. *Molecular Cancer Therapeutics*, 13, 483-491.

HAMILTON, D. 2008. Functional role of periostin in development and wound repair: implications for connective tissue disease. *Journal of Cell Communication and Signaling*, 2, 9-17.

HAN, Y., LIU, X., LIU, H., LI, S., WU, B., YE, L., WANG, Q. & CHEN, Z. 2006. Cultivation of recombinant Chinese hamster ovary cells grown as suspended aggregates in stirred vessels. *Journal of Bioscience and Bioengineering*, 102, 430-435.

HANAHAHAN, D., WAGNER, E. & PALMITER, R. 2007. The origins of oncomice: a history of the first transgenic mice genetically engineered to develop cancer. *Genes & Development*, 21, 2258-2270.

HANNAN, R., MILLER, A., HUNG, R., SANO, C., PEIRCE, S. & BARKER, T. 2020. Extracellular matrix remodeling associated with bleomycin-induced lung injury supports pericyte-to-myofibroblast transition. *Matrix Biology Plus*, 10, 100056.

HARRISON, R. 1907. Observations on the living developing nerve fiber. *The Anatomical Record*, 1, 116-128

HASTINGS, J., OWEN, G., DEKKER, A., ENNIS, M., KALE, N., MUTHUKRISHNAN, V., TURNER, S., SWAINSTON, N., MENDES, P. & STEINBECK, C. 2016. ChEBI in 2016: Improved services and an expanding collection of metabolites. *Nucleic Acids Research*, 44, D1214-D1219.

HAYDEN, M., YANG, Y., HABIBI, J., BAGREE, S. & SOWERS, J. 2010. Pericytopathy Oxidative stress and impaired cellular longevity in the pancreas and skeletal muscle in metabolic syndrome and type 2 diabetes. *Oxidative Medicine and Cellular Longevity*, 3, 290-303.

HELLSTROM, M., KALEN, M., LINDAHL, P., ABRAMSSON, A. & BETSHOLTZ, C. 1999. Role of PDGF-B and PDGFR-beta in recruitment of vascular smooth muscle cells and pericytes during embryonic blood vessel formation in the mouse. *Development*, 126, 3047-3055.

HICKMAN, D., JOHNSON, J., VEMULAPALLI, T., CRISLER, J. & SHEPHERD, R. 2016. Commonly used animal models. *Principles of Animal Research for Graduate and Undergraduate Students*, 117-175.

HINZ, B. 2007. Formation and function of the myofibroblast during tissue repair. *Journal of Investigative Dermatology*, 127, 526-537.

HINZ, B. 2016. The role of myofibroblasts in wound healing. *Current Research in Translational Medicine*, 64, 171-177.

HOERSCH, S. & ANDRADE-NAVARRO, M. 2010. Periostin shows increased evolutionary plasticity in its alternatively spliced region. *Bmc Evolutionary Biology*, 10.

HOFFMAN, W. & JUMP, A. 1986. TWEEN-20 REMOVES ANTIBODIES AND OTHER PROTEINS FROM NITROCELLULOSE. *Journal of Immunological Methods*, 94, 191-196.

HOLMES, D. 2012. Moving from an asthma pipe dram to a pipeline. *Nature Reviews Drug Discovery*, 11, 737-738.

HOME OFFICE. 1986. Guidance on the Operation of the Animals (Scientific Procedures) Act 1986. In: HOME OFFICE (ed.) 5 ed. UK Parliament.

HOWE, K., CLARK, M., TORROJA, C., TORRANCE, J., BERTHELOT, C., MUFFATO, M., COLLINS, J., HUMPHRAY, S., MCLAREN, K., MATTHEWS, L., MCLAREN, S., SEALY, I., CACCAMO, M., CHURCHER, C., SCOTT, C., BARRETT, J., KOCH, R., RAUCH, G., WHITE, S., CHOW, W., KILIAN, B., QUINTAIS, L., GUERRA-ASSUNCAO, J., ZHOU, Y., GU, Y., YEN, J., VOGEL, J., EYRE, T., REDMOND, S., BANERJEE, R., CHI, J., FU, B., LANGLEY, E., MAGUIRE, S., LAIRD, G., LLOYD, D., KENYON, E., DONALDSON, S., SEHRA, H., ALMEIDA-KING, J., LOVELAND, J., TREVANION, S., JONES, M., QUAIL, M., WILLEY, D., HUNT, A., BURTON, J., SIMS, S., MCLAY, K., PLUMB, B., DAVIS, J., CLEE, C., OLIVER, K., CLARK, R., RIDDLE, C., ELIOTT, D., THREADGOLD, G., HARDEN, G., WARE, D., MORTIMER, B., KERRY, G., HEATH, P., PHILLIMORE, B., TRACEY, A., CORBY, N., DUNN, M., JOHNSON, C., WOOD, J., CLARK, S., PELAN, S., GRIFFITHS, G., SMITH, M., GLITHERO, R., HOWDEN, P., BARKER, N., STEVENS, C., HARLEY, J., HOLT, K., PANAGIOTIDIS, G., LOVELL, J., BEASLEY, H., HENDERSON, C., GORDON, D., AUGER, K., WRIGHT, D.,

COLLINS, J., RAISEN, C., DYER, L., LEUNG, K., ROBERTSON, L., AMBRIDGE, K., LEONGAMORNLEERT, D., MCGUIRE, S., GILDERTHORP, R., GRIFFITHS, C., MANTHRAVADI, D., NICHOL, S., BARKER, G., WHITEHEAD, S., KAY, M., et al. 2013. The zebrafish reference genome sequence and its relationship to the human genome. *Nature*, 496, 498-503.

HU, C., YONG, X., LI, C., LU, M., LIU, D., CHEN, L., HU, J., TENG, M., ZHANG, D., FAN, Y. & LIANG, G. 2013. CXCL12/CXCR4 axis promotes mesenchymal stem cell mobilization to burn wounds and contributes to wound repair. *Journal of Surgical Research*, 183, 427-434.

HU, Q., TONG, S., ZHAO, X., DING, W., GOU, Y., XU, K., SUN, C. & XIA, G. 2015. Periostin Mediates TGF-beta-Induced Epithelial Mesenchymal Transition in Prostate Cancer Cells. *Cellular Physiology and Biochemistry*, 36, 799-809.

HUANG, H. & WANG, Y. 2017. The protective effect of cinnamaldehyde on lipopolysaccharide induced acute lung injury in mice. *Cellular and Molecular Biology*, 63, 58-63.

HUANG, M., LU, J. & DING, J. 2021. Natural Products in Cancer Therapy: Past, Present and Future. *Natural Products and Bioprospecting*, 11, 5-13.

HUANG, Y., KUO, H., YANG, Y. & WANG, F. 2019. MicroRNA-29a is a key regulon that regulates BRD4 and mitigates liver fibrosis in mice by inhibiting hepatic stellate cell activation. *International Journal of Medical Sciences*, 16, 212-220.

HUBRECHT, R. & CARTER, E. 2019. The 3Rs and Humane Experimental Technique: Implementing Change. *Animals*, 9.

HUGHES, S. & CHAN-LING, T. 2004. Characterization of smooth muscle cell and pericyte differentiation in the rat retina in vivo. *Investigative Ophthalmology & Visual Science*, 45, 2795-2806.

HUIZER, K., ZHU, C., CHIRIFI, I., KRIST, B., ZORGMAN, D., VAN DER WEIDEN, M., VAN DEN BOSCH, T., DUMAS, J., CHENG, C., KROS, J. & MUSTAFA, D. 2020. Periostin Is Expressed by Pericytes and Is Crucial for Angiogenesis in Glioma. *Journal of Neuropathology and Experimental Neurology*, 79, 863-872.

HUMPHREYS, B., LIN, S., KOBAYASHI, A., HUDSON, T., NOWLIN, B., BONVENTRE, J., VALERIUS, M., MCMAHON, A. & DUFFIELD, J. 2010. Fate Tracing Reveals the Pericyte and Not Epithelial Origin of Myofibroblasts in Kidney Fibrosis. *American Journal of Pathology*, 176, 85-97.

HUNG, C., LINN, G., CHOW, Y., KOBAYASHI, A., MITTELSTEADT, K., ALTEMEIER, W., GHARIB, S., SCHNAPP, L. & DUFFIELD, J. 2013. Role of Lung Pericytes and Resident Fibroblasts in the

Pathogenesis of Pulmonary Fibrosis. *American Journal of Respiratory and Critical Care Medicine*, 188, 820-830.

HUNG, CF., WILSON, CL. & SCHNAPP, LM. 2019. "Pericytes in the lung," in *Pericyte biology in different organs*. Editor A. Birbrair. (Springer International Publishing).

IACOBUCCI, G. 2019. Asthma deaths rise 33% in past decade in England and Wales. *Bmj-British Medical Journal*, 366.

ITO, Y., AL MUBARAK, R., ROBERTS, N., CORRELL, K., JANSSEN, W., FINIGAN, J., MISHRA, R. & CHU, H. 2018. IL-13 induces periostin and eotaxin expression in human primary alveolar epithelial cells: Comparison with paired airway epithelial cells. *Plos One*, 13.

IZADPANA, R., TRYGG, C., PATEL, B., KRIEDT, C., DUFOUR, J., GIMBLE, J. & BUNNELL, B. 2006. Biologic properties of mesenchymal stem cells derived from bone marrow and adipose tissue. *Journal of Cellular Biochemistry*, 99, 1285-1297.

IZUHARA, K., OHTA, L. & ONO, J. 2016. Using Periostin as a Biomarker in the Treatment of Asthma. *Allergy Asthma & Immunology Research*, 8, 491-498.

JABEEN, N., QURESHI, R., SATTAR, A. & BALOCH, M. 2019. Diagnostic Accuracy of Maximum Intensity Projection in Diagnosis of Malignant Pulmonary Nodules. *Cureus*, 11.

JACKSON-BOETERS, L., WEN, W. & HAMILTON, D. 2009. Periostin localizes to cells in normal skin, but is associated with the extracellular matrix during wound repair. *Journal of Cell Communication and Signaling*, 3, 125-133.

JAFFAR, J., GRIFFITHS, K., OVEISSI, S., DUAN, M., FOLEY, M., GLASPOLE, I., SYMONS, K., ORGAN, L. & WESTALL, G. 2020. CXCR4+ cells are increased in lung tissue of patients with idiopathic pulmonary fibrosis. *Respiratory Research*, 21, 221.

JAMES, A. & WENZEL, S. 2007. Clinical relevance of airway remodelling in airway diseases. *European Respiratory Journal*, 30, 134-155.

JAMUR, M. & OLIVER, C. 2009. *Permeabilization of Cell Membranes. Immunocytochemical Methods and Protocols*. Humana Press.

JANSON, S. & BECKER, G. 1998. Reasons for delay in seeking treatment for acute asthma: The patient's perspective. *Journal of Asthma*, 35, 427-435.

JATAKANON, A., UASUF, C., MAZIAK, W., LIM, S., CHUNG, K. & BARNES, P. 1999. Neutrophilic inflammation in severe persistent asthma. *American Journal of Respiratory and Critical Care Medicine*, 160, 1532-1539.

JOHNSON, J. & BIGNOLD, R. 2020. CXCL12 Inhibition Attenuates Pericyte Mobilization and Ameliorates Airway Remodeling in Chronic Allergic Airway Disease. *American Journal of Respiratory and Critical Care Medicine*, 201.

JOHNSON, J. & BIGNOLD, R. 2021. Periostin Expression Is Elevated in HDM-Driven Allergic Airway Disease and Associated with Increased Pericyte Migration. *American Journal of Respiratory and Critical Care Medicine*, 203.

JOHNSON, J. & BIGNOLD, R. 2022. The Matricellular Protein Periostin Is Produced by Pericytes and Contributes to Airway Wall Remodelling in Allergic Airway Disease. *American Journal of Respiratory and Critical Care Medicine*, 205.

JOHNSON, J., FOLESTAD, E., ROWLEY, J., NOLL, E., WALKER, S., LLOYD, C., RANKIN, S., PIETRAS, K., ERIKSSON, U. & FUXE, J. 2015. Pericytes contribute to airway remodeling in a mouse model of chronic allergic asthma. *American Journal of Physiology-Lung Cellular and Molecular Physiology*, 308, L658-L671.

JOHNSON, J., PACITTO, SR., WONG, J., ARCHER, EW., EIREFELT, S., MILLER-LARSSON, A. & JORDANA, M. 2008. Combined budesonide/formoterol therapy in conjunction with allergen avoidance ameliorates house dust mite-induced airway remodeling and dysfunction. *American Journal of Physiology-Lung Cellular and Molecular Physiology*, 295(5), L780-8.

JOHNSON, J., ROOS, A., BERG, T., NORD, M. & FUXE, J. 2011. Chronic Respiratory Aeroallergen Exposure in Mice Induces Epithelial-Mesenchymal Transition in the Large Airways. *Plos One*, 6.

JOHNSON, J., WILEY, R., FATTOUH, R., SWIRSKI, F., GAJEWSKA, B., COYLE, A., GUTIERREZ-RAMOS, J., ELLIS, R., INMAN, M. & JORDANA, M. 2004. Continuous exposure to house dust mite elicits chronic airway inflammation and structural remodeling. *American Journal of Respiratory and Critical Care Medicine*, 169, 378-385.

JONES, R., NOBLE, P., ELLIOT, J., MITCHELL, H., MCFAWN, P., HOGG, J. & JAMES, A. 2016. Airflow obstruction is associated with increased smooth muscle extracellular matrix. *European Respiratory Journal*, 47, 1855-1857.

JORDAHL, S., SOLORIO, L., NEALE, D., MCDERMOTT, S., JORDAHL, J., FOX, A., DUNLAY, C., XIAO, A., BROWN, M., WICHA, M., LUKER, G. & LAHANN, J. 2019. Engineered Fibrillar Fibronectin Networks as Three-Dimensional Tissue Scaffolds. *Advanced Materials*, 31.

JORISSEN, R., WALKER, F., POULIOT, N., GARRETT, T., WARD, C. & BURGESS, A. 2003. Epidermal growth factor receptor: mechanisms of activation and signalling. *Experimental Cell Research*, 284, 31-53.

KALLURI, R. & WEINBERG, RA. 2009. The basics of epithelial-mesenchymal transition. *Journal of Clinical Investigation*, 119(6), 1420-1428.

KANAOKA, M., YAMAGUCHI, Y., KOMITSU, N., FEGHALI-BOSTWICK, C., OGAWA, M., ARIMA, K., LZUHARA, K. & AIHARA, M. 2018. Pro-fibrotic phenotype of human skin fibroblasts induced by periostin via modulating TGF-beta signaling. *Journal of Dermatological Science*, 90, 199-208.

KAPANCI, Y., RIBAUUX, C., CHAPONNIER, C. & GABBIANI, G. 1992. Cytoskeletal features of alveolar myofibroblasts and pericytes in normal human and rat lung. *Journal of Histochemistry & Cytochemistry*, 40, 1955-1963.

KEMP, SS., AGUERA, KN., CHA, B. & DAVIS, GE. 2020. Defining Endothelial Cell-Derived Factors That Promote Pericyte Recruitment and Capillary Network Assembly. *Atherosclerosis, Thrombosis and Vascular Biology*, 40, 2632-2648.

KEMP, SS., LIN, PK., SUN, Z., CASTANO, MA., YRIGOIN, K., PENN, MR. & DAVIS, GE. 2022. Molecular basis for pericyte-induced capillary tube network assembly and maturation. *Frontiers in Cell and Developmental Biology*, 10, 943533.

KII, I., NISHIYAMA, T., LI, M., MATSUMOTO, K., SAITO, M., AMIZUKA, N. & KUDO, A. 2010. Incorporation of Tenascin-C into the Extracellular Matrix by Periostin Underlies an Extracellular Meshwork Architecture. *Journal of Biological Chemistry*, 285, 2028-2039.

KIM, D., KIM, C., KIM, M., KIM, J., JUNG, K., CHUNG, J., AN, W., LEE, J., YU, B. & CHUNG, H. 2007. Suppression of age-related inflammatory NF-kappa B activation by cinnamaldehyde. *Biogerontology*, 8, 545-554.

KIM, D., SONG, M. & LEE, K. 2019. Comparison of asthma phenotypes in OVA-induced mice challenged via inhaled and intranasal routes. *Bmc Pulmonary Medicine*, 19.

KIM, S., CHEN, J., CHENG, T., GINDULYTE, A., HE, J., HE, S., LI, Q., SHOEMAKER, B., THIESSEN, P., YU, B., ZASLAVSKY, L., ZHANG, J. & BOLTON, E. 2021. PubChem in 2021: new data content and improved web interfaces. *Nucleic Acids Research*, 49, D1388-D1395.

KO, E., KIM, D., MIN, DW., KWON, SH. & LEE, JY. 2021. Nrf2 regulates cell motility through RhoA-ROCK1 signalling in non-small-cell lung cancer cells. *Nature Scientific Reports*, 11, 1247.

KOLEY, D. & BARD, A. 2010. Triton X-100 concentration effects on membrane permeability of a single HeLa cell by scanning electrochemical microscopy (SECM). *Proceedings of the National Academy of Sciences of the United States of America*, 107, 16783-16787.

KONO, Y., TO, M., TSUZUKI, R., HARUKI, K. & TO, Y. 2019. Elevated serum periostin level in patients with chronic cough and airway hyperresponsiveness. *Respiratory Investigation*, 57, 122-125.

KOZANITI, F., DELIGIANNI, D., GEORGIU, M. & PORTAN, D. 2022. The Role of Substrate Topography and Stiffness on MSC Cells Functions: Key Material Properties for Biomimetic Bone Tissue Engineering. *Biomimetics*, 7.

KRATZER, A., CHU, H., SALYS, J., MOUMEN, Z., LEBERL, M., BOWLER, R., COOL, C., ZAMORA, M. & TARASEVICIENE-STEWART, L. 2013. Endothelial cell adhesion molecule CD146: implications for its role in the pathogenesis of COPD. *Journal of Pathology*, 230, 388-398.

KUBICZKOVA, L., SEDLARIKOVA, L., HAJEK, R. & SEVCIKOVA, S. 2012. TGF-beta - an excellent servant but a bad master. *Journal of Translational Medicine*, 10.

KUMAR, S. & PONNAZHAGAN, S. 2012. Mobilization of bone marrow mesenchymal stem cells in vivo augments bone healing in a mouse model of segmental bone defect. *Bone*, 50, 1012-1018.

KUPPE, C., IBRAHIM, M., KRANZ, J., ZHANG, X., ZIEGLER, S., PERALES-PATON, J., JANSEN, J., REIMER, K., SMITH, J., DOBIE, R., WILSON-KANAMORI, J., HALDER, M., XU, Y., KABGANI, N., KAESLER, N., KLAUS, M., GERNHOLD, L., PUELLES, V., HUBER, T., BOOR, P., MENZEL, S., HOOGENBOEZEM, R., BINDELS, E., STEFFENS, J., FLOEGE, J., SCHNEIDER, R., SAEZ-RODRIGUEZ, J., HENDERSON, N. & KRAMANN, R. 2021. Decoding myofibroblast origins in human kidney fibrosis. *Nature*, 589, 281-+.

LEE, CG., MAN, B., TAKYAR, S., AHANGARI, F., DELACRUZ, C., HE, CH. & ELIAS, JA. 2011. Studies of Vascular Endothelial Growth Factor in Asthma and Chronic Obstructive Pulmonary Disease. *Proceedings of the American Thoracic Society*, 8(6), 512-515.

LEE, L., KHAKOO, AY. & CHINTALGATTU, V. 2019. Isolation and Purification of Murine Cardiac Pericytes. *Journal of Visualised Experiments*, 16(150).

LEE, T., KIM, H. & PARK, S. 2020. A lab-made wound maker for analysis of cell migration in a 96-well plate. *Korean Journal of Clinical Laboratory Science*, 52, 53-61.

LE GALL, S., AUGER, R., DREUX, C. & MAUDUIT, P. 2003. Regulated cell surface Pro-EGF ectodomain shedding is a zinc metalloprotease-dependent process. *Journal of Biological Chemistry*, 278, 45255-45268.

LEMOS, DR., MARSH, G., HUANG, A., CAMPANHOLLE, G., ABURATANI, T., DANG, L., GOMEZ, I., FISHER, K., LIGRESTI, G., PETI-PETERDI, J. & DUFFIELD, JS. 2016 Maintenance of vascular integrity by pericytes is essential for normal kidney function. *American Journal of Physiology Renal Physiology*, 311(6), F1230-F1242.

LEWIS, N., LEWIS, E., MULLIN, M., WHEADON, H., DALBY, M. & BERRY, C. 2017. Magnetically levitated mesenchymal stem cell spheroids cultured with a collagen gel maintain phenotype and quiescence. *Journal of Tissue Engineering*, 8.

LI, C., ZHEN, G., CHAI, Y., XIE, L., CRANE, JL., FARBER, E., FARBER, CR., LUO, X., GAO, P., CAO, X. WAN, M. 2016. RhoA determines lineage fate of mesenchymal stem cells by modulating CTGF-VEGF complex in extracellular matrix. *Nature Communications*, 7, 11455.

LI, F., XU, X., GENG, J., WAN, X. & DAI, H. 2020. The autocrine CXCR4/CXCL12 axis contributes to lung fibrosis through modulation of lung fibroblast activity. *Experimental and Therapeutic Medicine*, 19, 1844-1854.

LI, W., GAO, P., ZHI, Y., XU, W., WU, Y., YIN, J. & ZHANG, J. 2015. Periostin: its role in asthma and its potential as a diagnostic or therapeutic target. *Respiratory Research*, 16.

LIN, S., KISSELEVA, T., BRENNER, D. & DUFFIELD, J. 2008. Pericytes and Perivascular Fibroblasts Are the Primary Source of Collagen-Producing Cells in Obstructive Fibrosis of the Kidney. *American Journal of Pathology*, 173, 1617-1627.

LIN, Y., NELSON, C., KRAMER, H. & PAREKH, A. 2018. The Allergen Der p3 from House Dust Mite Stimulates Store-Operated Ca²⁺ Channels and Mast Cell Migration through PAR4 Receptors. *Molecular Cell*, 70, 228-+.

LIU, G., BETTS, C., CUNOOSAMY, D., ABERG, P., HORNBERG, J., SIVARS, K. & COHEN, T. 2019a. Use of precision cut lung slices as a translational model for the study of lung biology. *Respiratory Research*, 20.

LIU, G., PHILP, AM., CORTE, T., TRAVIS, MA., SCHILTER, H., HANSBRO, NG., BURNS, CJ., EAPEN, MS., SOHAL, SS., BURGESS, JK. & HANSBRO, PM. 2021. Therapeutic targets in lung tissue remodelling and fibrosis. *Pharmacology & Therapeutics*, 225, 107839.

LIU, Z., YI, L., DU, M., GONG, G. & ZHU, Y. 2019b. Overexpression of TGF-beta enhances the migration and invasive ability of ectopic endometrial cells via ERK/MAPK signaling pathway. *Experimental and Therapeutic Medicine*, 17, 4457-4464.

LOPEZ-GUISA, J., POWERS, C., FILE, D., COCHRANE, E., JIMENEZ, N. & DEBLEY, J. 2012. Airway epithelial cells from asthmatic children differentially express proremodeling factors. *Journal of Allergy and Clinical Immunology*, 129, 990-U496.

LUKACS, N., BERLIN, A., SCHOLS, D., SKERLJ, R. & BRIDGER, G. 2002. AMD3100, a CXCR4 antagonist, attenuates allergic lung inflammation and airway Hyperreactivity. *American Journal of Pathology*, 160, 1353-1360.

LUKACS, N., STRIETER, R., CHENSUE, S. & KUNKEL, S. 1994. INTERLEUKIN-4-DEPENDENT PULMONARY EOSINOPHIL INFILTRATION IN A MURINE MODEL OF ASTHMA. *American Journal of Respiratory Cell and Molecular Biology*, 10, 526-532.

MADDON, P., MCDUGAL, J., CLAPHAM, P., DALGLEISH, A., JAMAL, S., WEISS, R. & AXEL, R. 1988. HIV INFECTION DOES NOT REQUIRE ENDOCYTOSIS OF ITS RECEPTOR, CD4. *Cell*, 54, 865-874.

MAEDA, D., KUBO, T., KIYA, K., KAWAI, K., MATSUZAKI, S., KOBAYASHI, D., FUJIWARA, T., KATAYAMA, T. & HOSOKAWA, K. 2019. Periostin is induced by IL-4/IL-13 in dermal fibroblasts and promotes RhoA/ROCK pathway-mediated TGF-beta 1 secretion in abnormal scar formation. *Journal of Plastic Surgery and Hand Surgery*, 53, 288-294.

MAKITA, K., MIKAMI, Y., MATSUZAKI, H., MIYASHITA, N., TAKESHIMA, H., NOGUCHI, S., HORIE, M., URUSHIYAMA, H., IIKURA, M., HOJO, M., NAGASE, T. & YAMAUCHI, Y. 2018. Mechanism of Periostin Production in Human Bronchial Smooth Muscle Cells. *International Archives of Allergy and Immunology*, 175, 26-35.

MANGIALARDI, G., FERLAND-MCCOLLOUGH, D., MASELLI, D., SANTOPAOLLO, M., CORDARO, A., SPINETTI, G., SAMBATARO, M., SULLIVAN, N., BLOM, A. & MADEDDU, P. 2019. Bone marrow pericyte dysfunction in individuals with type 2 diabetes. *Diabetologia*, 62, 1275-1290.

MARCONI, GD., FONTICOLI, L., RAJAN, TS., PIERDOMENICO, SD., TRUBIANI, O., PIZZICANNELLA, J. & DIOMEDE, F. 2021. Epithelial-Mesenchymal Transition (EMT): The Type-2 EMT in Wound Healing, Tissue Regeneration and Organ Fibrosis. *Cells*, 10(7), 1587.

MASTERS, J. 2002. HeLa cells 50 years on: the good, the bad and the ugly. *Nature Reviews Cancer*, 2, 315-319.

MATSUSAKA, M., KABATA, H., FUKUNAGA, K., SUZUKI, Y., MASAKI, K., MOCHIMARU, T., SAKAMAKI, F., OYAMADA, Y., INOUE, T., OGUMA, T., SAYAMA, K., KOH, H., NAKAMURA, M., UMEDA, A., ONO, J., OHTA, S., IZUHARA, K., ASANO, K. & BETSUYAKU, T. 2015. Phenotype of asthma related with high serum periostin levels. *Allergology International*, 64, 175-180.

MCCURLEY, A., ALIMPERTI, S., CAMPOS-BILDERBACK, SB., SANDOVAL, RM., CALVINA, JE., REYNOLDS, TL., QUIGLEY, C., MUGFORD, JW., POLACHECK, WJ., GOMEZ, IG., DOVEY, J., MARSH, G., HUANG, A., QIAN, F., WEINREB, PH., DOLINSKI, BM., MOORE, S., DUFFIELD, JS., CHEN, CS., MOLITORIS, BA., VIOLETTE, SM. & CRACKOWER, MA. 2017. Inhibition of $\alpha\beta 5$ Integrin Attenuates Vascular Permeability and Protects against Renal Ischemia-Reperfusion Injury. *Journal of the American Society of Nephrology*, 28(6), 1741-1752.

MCGOVERN, T., ROBICHAUD, A., FEREDDOONZAD, L., SCHUESSLER, T. & MARTIN, J. 2013. Evaluation of Respiratory System Mechanics in Mice using the Forced Oscillation Technique. *Jove-Journal of Visualized Experiments*.

MCKLEROY, W., LEE, T. & ATABAI, K. 2013. Always cleave up your mess: targeting collagen degradation to treat tissue fibrosis. *American Journal of Physiology-Lung Cellular and Molecular Physiology*, 304, L709-L721.

MEDERACKE, I., HSU, C., TROEGER, J., HUEBENER, P., MU, X., DAPITO, D., PRADERE, J. & SCHWABE, R. 2013. Fate tracing reveals hepatic stellate cells as dominant contributors to liver fibrosis independent of its aetiology. *Nature Communications*, 4.

MEI, J., MA, J., XU, Y., WANG, Y., HU, M., MA, F., QIN, Z., XUE, R. & TAO, N. 2020. Cinnamaldehyde Treatment of Prostate Cancer-Associated Fibroblasts Prevents Their Inhibitory Effect on T Cells Through Toll-Like Receptor 4. *Drug Design, Development and Therapy*, 14, 3363-3372

MEIJER, M., SPRUIJT, B., VAN ZUTPHEN, L. & BAUMANS, V. 2006. Effect of restraint and injection methods on heart rate and body temperature in mice. *Laboratory Animals*, 40, 382-391.

MELZER, C., VON DER OHE, J., HASS, R. & UNGEFROREN, H. 2017. TGF-beta-Dependent Growth Arrest and Cell Migration in Benign and Malignant Breast Epithelial Cells Are Antagonistically Controlled by Rac1 and Rac1b. *International Journal of Molecular Sciences*, 18.

MENG, X., NIKOLIC-PATERSON, D. & LAN, H. 2016. TGF-beta: the master regulator of fibrosis. *Nature Reviews Nephrology*, 12, 325-338.

MENG, Y.M., JIANG, X., ZHAO, X., MENG, Q., WU, S., CHEN, Y., KONG, X., QIU, X., SU, L., HUANG, C., WANG, M., LIU, C. & WONG, P.P. 2021. Hexokinase 2-driven glycolysis in pericytes activates their contractility leading to tumor blood vessel abnormalities. *Nature Communications*, 12, 6011.

METZGER, W., SOSSONG, D., BACHLE, A., PUTZ, N., WENNEMUTH, G., POHLEMANN, T. & OBERRINGER, M. 2011. The liquid overlay technique is the key to formation of co-culture spheroids consisting of primary osteoblasts, fibroblasts and endothelial cells. *Cytotherapy*, 13, 1000-1012.

MICHALIK, M., WOJCIK-PSZCZOLA, K., PAW, M., WNUK, D., KOCZURKIEWICZ, P., SANAK, M., PEKALA, E. & MADEJA, Z. 2018. Fibroblast-to-myofibroblast transition in bronchial asthma. *Cellular and Molecular Life Sciences*, 75, 3943-3961.

MICHAYLIRA, C., WONG, G., MILLER, C., GUTIERREZ, C., NAKAGAWA, H., HAMMOND, R., KLEIN-SZANTO, A., LEE, J., KIM, S., HERLYN, M., DIEHL, J., GIMOTTY, P. & RUSTGI, A. 2010. Periostin, a Cell Adhesion Molecule, Facilitates Invasion in the Tumor Microenvironment and Annotates a Novel Tumor-Invasive Signature in Esophageal Cancer. *Cancer Research*, 70, 5281-5292.

MIRZOYAN, Z., SOLLAZZO, M., ALLOCCA, M., VALENZA, A., GRIFONI, D. & BELLOSTA, P. 2019. *Drosophila melanogaster*: A Model Organism to Study Cancer. *Frontiers in Genetics*, 10.

MITAMURA, Y., MURAI, M., MITOMA, C. & FURUE, M. 2018. NRF2 Activation Inhibits Both TGF-beta 1-and IL-13-Mediated Periostin Expression in Fibroblasts: Benefit of Cinnamaldehyde for Antifibrotic Treatment. *Oxidative Medicine and Cellular Longevity*, 2018.

MOEN, E., BANNON, D., KUDO, T., GRAF, W., COVERT, M. & VAN VALEN, D. 2019. Deep learning for cellular image analysis. *Nature Methods*, 16, 1233-1246.

MOHLE, R., BAUTZ, F., RAFII, S., MOORE, M., BRUGGER, W. & KANZ, L. 1998. The chemokine receptor CXCR-4 is expressed on CD34(+) hematopoietic progenitors and leukemic cells and mediates transendothelial migration induced by stromal cell-derived factor-1. *Blood*, 91, 4523-4530.

MOLNAR, ELEK. 2019. Cell-Based Enzyme-Linked Immunosorbent Assay (Cell-ELISA) Analysis of Native and Recombinant Glutamate Receptors. *Methods in Molecular Biology*, 1941, 47-54.

MORAN, A. & PAVORD, ID. 2020. Anti-IL-4/IL-13 for the treatment of asthma: the story so far. *Expert Opinion on Biological Therapy*, 20(3), 283-294.

MORELLI, R., CLISSA, L., AMICI, R., CERRI, M., HITREC, T., LUPPI, M., RINALDI, L., SQUARCIO, F. & ZOCCOLI, A. 2021. Automating cell counting in fluorescent microscopy through deep learning with c-ResUnet. *Nature Scientific Reports*, 11, 22920.

MOXON, S. & SMITH, A. 2016. Controlling the rheology of gellan gum hydrogels in cell culture conditions. *International Journal of Biological Macromolecules*, 84, 79-86.

MURAOKA, RS., DUMONT, N., RITTER, CA., DUGGER, TC., BRANTLEY, DM., CHEN, J., EASTERLY, E., ROEBUCK, LR., RYAN, S., GOTWALS, PL., KOTELIANSKY, V. & ARTEAGA, CL. 2002. Blockade of TGF-beta inhibits mammary tumor cell viability, migration, and metastases. *Journal of Clinical Investigation*, 109(12), 1551-9

MURCIA, M., EGEE, I., ROMOJARO, F., PARRAS, P., JIMENEZ, A. & MARTINEZ-TOME, M. 2004. Antioxidant evaluation in dessert spices compared with common food additives. Influence of irradiation procedure. *Journal of Agricultural and Food Chemistry*, 52, 1872-1881.

NABAVI, S., DI LORENZO, A., IZADI, M., SOBARZO-SANCHEZ, E., DAGLIA, M. & NABAVI, S. 2015. Antibacterial Effects of Cinnamon: From Farm to Food, Cosmetic and Pharmaceutical Industries. *Nutrients*, 7, 7729-7748.

NADAL, JA., SCICLI, GM., CARBINI, LA. & SCICLI, AG. 2002. Angiotensin II stimulates migration of retinal microvascular pericytes: involvement of TGF- β and PDGF-BB. *American Journal of Physiology Heart and Circulatory Physiology*, 282(2), H739-H748

NAIK, P., BOZYK, P., BENTLEY, J., POPOVA, A., BIRCH, C., WILKE, C., FRY, C., WHITE, E., SISSON, T., TAYOB, N., CARNEMOLLA, B., ORECCHIA, P., FLAHERTY, K., HERSHENSON, M., MURRAY, S., MARTINEZ, F., MOORE, B. & INVESTIGATORS, C. 2012. Periostin promotes fibrosis and predicts progression in patients with idiopathic pulmonary fibrosis. *American Journal of Physiology-Lung Cellular and Molecular Physiology*, 303, L1046-L1056.

NAKAMA, T., YOSHIDA, S., ISHIKAWA, K., KUBO, Y., KOBAYASHI, Y., ZHOU, Y., NAKAO, S., HISATOMI, T., IKEDA, Y., TAKAO, K., YOSHIKAWA, K., MATSUDA, A., ONO, J., OHTA, S., IZUHARA, K., KUDO, A., SONODA, K. & ISHIBASHI, T. 2017. Therapeutic Effect of Novel Single-Stranded RNAi Agent Targeting Periostin in Eyes with Retinal Neovascularization. *Molecular Therapy-Nucleic Acids*, 6, 279-289.

NANRI, Y., NUNOMURA, S., TERASAKI, Y., YOSHIHARA, T., HIRANO, Y., YOKOSAKI, Y., YAMAGUCHI, Y., FEGHALI-BOSTWICK, C., AJITO, K., MURAKAMI, S., CONWAY, S. & IZUHARA, K. 2020. Cross-Talk between Transforming Growth Factor-beta and Periostin Can Be Targeted for Pulmonary Fibrosis. *American Journal of Respiratory Cell and Molecular Biology*, 62, 204-216.

NASEER, M., ZUBAIR, H., IKRAMULLAH & KLIM, M. 2009. EFFECT OF FETAL CALF SERUM ON CELLULAR PROLIFERATION OF MOUSE Y1 ADRENOCORTICAL CELLS IN VITRO. *Pakistan Journal of Medical Sciences*, 25, 500-504.

NEGRETE-GARCIA, M., POPOCA-COYOTL, A., MONTES-VIZUET, A. & TERAN, L. 2009. CXCL12 is Released in the Bronchoalveolar Lavage of Asthmatic Subjects. *Journal of Allergy and Clinical Immunology*, 123, 731-732.

NEUMARK, N., COSME, C., ROSE, K. & KAMINSKI, N. 2020. The Idiopathic Pulmonary Fibrosis Cell Atlas. *American Journal of Physiology-Lung Cellular and Molecular Physiology*, 319, L887-L892.

NEWMAN, D. & CRAGG, G. 2020. Natural Products as Sources of New Drugs over the Nearly Four Decades from 01/1981 to 09/2019. *Journal of Natural Products*, 83, 770-803.

NIALS, A. & UDDIN, S. 2008. Mouse models of allergic asthma: acute and chronic allergen challenge. *Disease Models & Mechanisms*, 1, 213-220.

NIKOLOUDAKI, G., SNIDER, P., SIMMONS, O., CONWAY, SJ. HAMILTON, DW. 2020. Periostin and matrix stiffness combine to regulate myofibroblast differentiation and fibronectin synthesis during palatal healing. *Matrix Biology*, 94, 31-56.

NOLAN-STEVAUX, O., TRUITT, MC., PHLER, JC., OLSON, P., GUINTO, C., LEE, DC. & HANAHAN, D. 2010. Differential Contribution to Neuroendocrine Tumorigenesis of Parallel Egfr Signalling in Cancer Cells and Pericytes. *Genes & Cancer*, 1(2), 125-141.

NOOR, N., SHAPIRA, A., EDRI, R., GAL, I., WERTHEIM, L. & DVIR, T. 2019. 3D Printing of Personalized Thick and Perfusable Cardiac Patches and Hearts. *Advanced Science*, 6.

NORTH WEST PAEDIATRIC ALLERGY NETWORK. 2021. House Dust Mite Avoidance [Online]. NHS North West Paediatric Allergy Network. Available: <http://www.allergynorthwest.nhs.uk/resources/allergy-leaflets/housedustmiteavoidance/> [Accessed 24 June 2022].

NOVAK, M. 2004. Housing for captive nonhuman primates: the balancing act. In: RESEARCH, N. R. C. I. F. L. A. (ed.) *The Development of Science-based Guidelines for Laboratory Animal Care: Proceedings of the November 2003 International Workshop*. Washington DC: National Academies Press (US).

NUCCITELLI, R., MCDANIEL, A., ANAND, S., CHA, J., MALLON, Z., BERRIDGE, J. & UECKER, D. 2017. Nano-Pulse Stimulation is a physical modality that can trigger immunogenic tumor cell death. *Journal For Immunotherapy of Cancer*, 5.

O'DWYER, D. & MOORE, B. 2017. The role of periostin in lung fibrosis and airway remodeling. *Cellular and Molecular Life Sciences*, 74, 4305-4314.

OKAMOTO, M., HOSHINO, T., KITASATO, Y., SAKAZAKI, Y., KAWAYAMA, T., FUJIMOTO, K., OHSHIMA, K., SHIRAIISHI, H., UCHIDA, M., ONO, J., OHTA, S., KATO, A., IZUHARA, K. & AIZAWA, H. 2011. Periostin, a matrix protein, is a novel biomarker for idiopathic interstitial pneumonias. *European Respiratory Journal*, 37(5), 1119-27.

ORCHARD, S., AMMARI, M., ARANDA, B., BREUZA, L., BRIGANTI, L., BROACKES-CARTER, F., CAMPBELL, N., CHAVALI, G., CHEN, C., DEL-TORO, N., DUESBURY, M., DUMOUSSEAU, M., GALEOTA, E., HINZ, U., IANNUCELLI, M., JAGANNATHAN, S., JIMENEZ, R., KHADAKE, J., LAGREID, A., LICATA, L., LOVERING, R., MELDAL, B., MELIDONI, A., MILAGROS, M., PELUSO, D., PERFETTO, L., PORRAS, P., RAGHUNATH, A., RICARD-BLUM, S., ROECHERT, B., STUTZ, A., TOGNOLLI, M., VAN ROEY, K., CESARENI, G. & HERMJAKOB, H. 2013. The MIntAct project-IntAct as a common curation platform for 11 molecular interaction databases. *Nucleic Acids Research*, 42, D358-D363.

OUANOUI, A., LAMY, S. & ANNABI, B. 2018. Periostin, a signal transduction intermediate in TGF- β -induced EMT in U-87MG human glioblastoma cells, and its inhibition by anthocyanidins. *Oncotarget*, 9(31), 22023-22037.

PANDEY, U. & NICHOLS, C. 2011. Human Disease Models in *Drosophila melanogaster* and the Role of the Fly in Therapeutic Drug Discovery. *Pharmacological Reviews*, 63, 411-436.

PELAIA, C., CALABRESE, C., TERRACCIANO, R., DE BLASIO, F., VATRELLA, A. & PELAI, G. 2018. Omalizumab, the first available antibody for biological treatment of severe asthma: more than a decade of real-life effectiveness. *Therapeutic Advances in Respiratory Disease*, 12.

PETERS, S., ZITZELSPERGER, E., KUESPERT, S., IBERL, S., HEYDN, R., JOHANNESSEN, S., PETRI, S., AIGNER, L., THAL, D., HERMANN, A., WEISHAUPT, J., BRUUN, T. & BOGDAHN, U. 2017. The Tgf-beta system as a Potential Pathogenic Player in Disease Modulation of amyotrophic lateral sclerosis. *Frontiers in Neurology*, 8.

PHILLIPS, K., BALES, K., CAPITANIO, J., CONLEY, A., CZOTY, P., 'T HART, B., HOPKINS, W., HU, S., MILLER, L., NADER, M., NATHANIELSZ, P., ROGERS, J., SHIVELY, C. & VOYTKO, M. 2014. Why Primate Models Matter. *American Journal of Primatology*, 76, 801-827.

PICOLI, C., COIMBRA-CAMPOS, L., GUERRA, D., SILVA, W., PRAZERES, P., COSTA, A., MAGNO, L., ROMANO-SILVA, M., MINTZ, A. & BIRBRAIR, A. 2019. Pericytes Act as Key Players in Spinal Cord Injury. *American Journal of Pathology*, 189, 1327-1337.

PIJUAN, J., BARCELO, C., MORENO, DF., MAIQUES, O., SISO, P., MARTI, RM., MACIA, A. & PANOSA, A. 2019. In vitro Cell Migration, Invasion, and Adhesion Assays: From Cell Imaging to Data Analysis. *Frontiers in Cell and Developmental Biology*, 7, 107.

POLK, D. 1998. Epidermal growth factor receptor-stimulated intestinal epithelial cell migration requires phospholipase C activity. *Gastroenterology*, 114, 493-502.

PRAZERES, PHDM., SENA, IFG., BORGES, IDT., DE AZEVEDO, PO., ANDREOTTI, JP., DE PAIVA, AE., DE ALMEIDA, VM., GUERRA, DADP., SANTOS, GSPD., MINTZ, A., DELBONO, O. & BIRBRAIR, A. 2017. Pericytes are heterogeneous in their origin within the same tissue. *Developmental Biology*, 427(1), 6-11.

PREMANATHAN, M., RAJENDRAN, S., RAMANATHAN, T., KATHIRESAN, K., NAKASHIMA, H. & YAMAMOTO, N. 2000. A survey of some Indian medicinal plants for anti-human immunodeficiency virus (HIV) activity. *Indian Journal of Medical Research*, 112, 73-77.

PROEBSTL, D., VOISIN, M., WOODFIN, A., WHITEFORD, J., D'ACQUISTO, F., JONES, G., ROWE, D. & NOURSHARGH, S. 2012. Pericytes support neutrophil subendothelial cell crawling and breaching of venular walls in vivo. *Journal of Experimental Medicine*, 209, 1219-1234.

RABOUILLE, C. 2017. Pathways of Unconventional Protein Secretion. *Trends in Cell Biology*, 27, 230-240.

RAHMAWATI, SF., TE VELDE, M., KERSTJENS, HAM., DOMLING, ASS., GROVES, MR. & GOSENS, R. 2021. Pharmacological Rationale for Targeting IL-17 in Asthma. *Frontiers in Allergy*, 2.

RANGASAMY, T., GUO, J., MITZNER, W., ROMAN, J., SINGH, A., FRYER, A., YAMAMOTO, M., KENSLER, T., TUDER, R., GEORAS, S. & BISWAL, S. 2005. Disruption of Nrf2 enhances susceptibility to severe airway inflammation and asthma in mice. *Journal of Experimental Medicine*, 202, 47-59.

RANKIN, S. 2012. Chemokines and adult bone marrow stem cells. *Immunology Letters*, 145, 47-54.

REGENASS, P., ABBOUD, D., DAUBEUF, F., LEHALLE, C., GIZZI, P., RICHE, S., HACHET-HAAS, M., ROHMER, F., GASPARIK, V., BOEGLIN, D., HAIECH, J., KNEHANS, T., ROGNAN, D., HEISSLER, D., MARSOL, C., VILLA, P., GALZI, J., HIBERT, M., FROSSARD, N. & BONNET, D. 2018. Discovery of a Locally and Orally Active CXCL12 Neutraligand (LIT-927) with Anti-inflammatory Effect in a Murine Model of Allergic Airway Hypereosinophilia. *Journal of Medicinal Chemistry*, 61, 7671-7686.

REGEV, A., TEICHMANN, S., LANDER, E., AMT, I., BENOIST, C., BIRNEY, E., BODENMILLER, B., CAMPBELL, P., CARNINCI, P., CLATWORTHY, M., CLEVERS, H., DEPLANCKE, B., DUNHAM, I., EBERWINE, J., ELIS, R., ENARD, W., FARMER, A., FUGGER, L., GOTTGENS, B., HACHOHEN, N., HANIFFA,

M., HEMBERG, M., KIM, S., KLENERMAN, P., KRIEGSTEIN, A., LEIN, E., LINNARSSON, S., LUNDBERG, E., LUNDEBERG, J., MAJUMDER, P., MARIONI, J., MERAD, M., MHLANGA, M., NAWIJIN, M., NETEA, M., NOLAN, G., PE'ER, D., PHILLIPAKIS, A., PONTING, C., QUAKE, S., REIK, W., ROZENBLATT-ROSEN, O., SANES, J., SATIJA, R., SCHUMACHER, T., SHALEK, A., SHAPIRO, E., SHARMA, P., SHIN, J., STEGLE, O., STRATTON, M., STUBBINGTON, M., THEIS, F., UHLEN, M., VAN OUDENAARDEN, A., WAGNER, A., WATT, F., WEISSMAN, J., WOLD, B., XAVIER, R., YOSEF, N. & MEETING, H. C. A. 2017. The Human Cell Atlas. *Elife*, 6.

RIBATTI, D., NICO, B. & CRIVELLATO, E. 2011. The role of pericytes in angiogenesis. *International Journal of Developmental Biology*, 55, 261-268.

RIEGER, AM., NELSON, KL., KONOWALCHUK, JD. & BARREDA, DR. 2011. Modified Annexin V/Promidium Iodide Apoptosis Assay For Accurate Assessment of Cell Death. *Journal of Visualized Experiments*, 50, 2597.

ROCK, J., BARKAUSKAS, C., CRONCE, M., XUE, Y., HARRIS, J., LIANG, J., NOBLE, P. & HOGAN, B. 2011. Multiple stromal populations contribute to pulmonary fibrosis without evidence for epithelial to mesenchymal transition. *Proceedings of the National Academy of Sciences of the United States of America*, 108, E1475-E1483.

ROTH-WALTER, F., MOSKOVSKICH, A., GOMEZ-CASADO, C., DIAZ-PERALES, A., OIDA, K., SINGER, J., KINACIYAN, T., FUCHS, HC. & JENSEN-JAROLIM, E. 2014. Immune Suppressive Effect of Cinnamaldehyde Due to Inhibition of Proliferation and Induction of Apoptosis in Immune Cells: Implications in Cancer. *PLoS ONE*, 9(10), e108402.

ROWLEY, J. & JOHNSON, J. 2014. Pericytes in Chronic Lung Disease. *International Archives of Allergy and Immunology*, 164, 178-188.

RYOO, IG., HA, H. & KWAK, MK. 2014. Inhibitory Role of the KEAP1-NRF2 Pathway in TGF β 1-Stimulated Renal Epithelial Transition to Fibroblastic Cells: A Modulatory Effect on SMAD Signaling. *PLoS ONE*, 9(4), e93265.

RYU, N., LEE, S. & PARK, H. 2019. Spheroid Culture System Methods and Applications for Mesenchymal Stem Cells. *Cells*, 8.

SACHS, N., PAPASPYROPOULOS, A., ZOMER-VAN OMMEN, DD., HEO, I., BOTTINGER, L., KLAY, D., WEEBER, F., HUELSZ-PRINCE, G., IAKOBACHVILI, N., AMATNGALIM, GD., DE LIGHT, J., VAN HOECK, A., PROOST, N., VIVEEN, MC., LYUBIMOVA, A., TEEVEN, L., DERAKHSHAN, S., KORVING, J., BEGTHEL, H.,

DEKKERS, JF., KUMAWAT, K., RAMOS, E. & CLEVERS, H. 2019. Long-term expanding human airway organoids for disease modelling. *The EMBO Journal*, 38(4), e100300.

SANCHEZ-MARTIN, A., ESTECHA, A., SAMANIEGO, R., SANCHEZ-RAMON, S., VEGA, MA. & SANCHEZ-MATEOS, P. 2011. The chemokine CXCL12 regulates monocyte-macrophage differentiation and RUNX3 expression. *Blood*, 117(1), 88-97.

SCHEERENS, H., ARRON, J., CHOY, D., MOSESOVA, S., LAL, P. & MATTHEWS, J. 2012. Lebrikizumab reduces serum periostin in asthma patients with elevated baseline periostin. *European Respiratory Journal*, 40.

SCHERER, W., SYVERTON, J. & GEY, G. 1953. Studies on the propagation in vitro of poliomyelitis viruses. IV. Viral multiplication in a stable strain of human malignant epithelial cells (strain HeLa) derived from an epidermoid carcinoma of the cervix. *Journal of Experimental Medicine*, 97, 695-710

SCHNEIDER, CA., RASBAND, WS. & ELICEIRI, KW. 2012. NIH Image to ImageJ: 25 years of image analysis. *Nature Methods*, 9, 671-675.

SCHOLER, L., LE-TRILLING, VTK., EILBRECHT, M., MENNERICH, D., ANASTASIOU, OE., KRAWCZYK, A., HERRMANN, A., DITTMER, U. & TRILLING, M. 2020. A Novel In-Cell ELISA Assay Allows Rapid and Automated Quantification of SARS-CoV-2 to Analyze Neutralizing Antibodies and Antiviral Compounds. *Frontiers in Immunology*, 11.

SHAW, I., RIDER, S., MULLINS, J., HUGHES, J. & PEULT, B. 2018. Pericytes in the renal vasculature: roles in health and disease. *Nature Reviews Nephrology*, 14, 521-534.

SHENOY, A., JIN, Y., LUO, H., TANG, M., PAMPO, C., SHAO, R., SIEMANN, D., WU, L., HELDERMON, C., LAW, B., CHANG, L. & LU, J. 2016. Epithelial-to-mesenchymal transition confers pericyte properties on cancer cells. *Journal of Clinical Investigation*, 126, 4174-4186.

SHIBUYA, M. 2013. Vascular endothelial growth factor and its receptor system: physiological functions in angiogenesis and pathological roles in various diseases. *Journal of Biochemistry*, 153, 13-19.

SHIH, W. & YAMADA, S. 2012. N-cadherin as a key regulator of collective cell migration in a 3D environment. *Cell Adhesion & Migration*, 6, 513-517.

SHINDE, A., HUMERES, C. & FRANGOIANNIS, N. 2017. The role of alpha-smooth muscle actin in fibroblast-mediated matrix contraction and remodeling. *Biochimica Et Biophysica Acta-Molecular Basis of Disease*, 1863, 298-309.

SMITH, BN. & BHOWMICK, NA. 2016. Role of EMT in Metastasis and Therapy Resistance. *Journal of Clinical Medicine*, 5, 17.

SONG, J., CHANG, C., WU, C., DINH, T., JAN, J., HUANG, K., CHOU, M., SHIUE, T., YEH, K., KE, Y., YEH, T., TA, Y., LEE, C., HUANG, J., SUNG, Y., SHIA, K. & CHEN, Y. 2021. A highly selective and potent CXCR4 antagonist for hepatocellular carcinoma treatment. *Proceedings of the National Academy of Sciences of the United States of America*, 118.

SONG, J., KANG, C., KANG, H., YOON, H., KIM, Y., KIM, K., MOON, H. & PARK, S. 2010. Inhibitory effect of CXC chemokine receptor 4 antagonist AMD3100 on bleomycin induced murine pulmonary fibrosis. *Experimental and Molecular Medicine*, 42, 465-476.

SOUZA, G., MOLINA, J., RAPHAEL, R., OZAWA, M., STARK, D., LEVIN, C., BRONK, L., ANANTA, J., MANDELIN, J., GEORGESCU, M., BANKSON, J., GELOVANI, J., KILLIAN, T., ARAP, W. & PASQUALINI, R. 2010. Three-dimensional tissue culture based on magnetic cell levitation. *Nature Nanotechnology*, 5, 291-296.

STEPHENSON, SE., WILSON, CL., BIND, NG., KAUR, A., ALVAREZ, X., MIDKIFF, CC. & SCHNAPP, LM. 2020. Pericytes as novel targets for HIV/SIV infection in the lung. *American Journal of Physiology Lung Cellular and Molecular Physiology*, 319(5), 848-853.

STRATMAN, AN., SCHWINDT, AE., MALOTTE, KM. & DAVIS, GE. 2010. Endothelial-derived PDGF-BB and HB-EGF coordinately regulate pericyte recruitment during vasculogenic tube assembly and stabilisation. *Blood*, 116(22), 4720-4730.

SU, H., CANTRELL, AC., ZENG, H., ZHU, SH. & CHEN, JX. 2021. Emerging Role of Pericytes and Their Secretome in the Heart. *Cells*, 10(3), 548.

SUGIHARA, K., SASAKI, S., UEMUR, A., KIDOAKI, S. & MIURA, T. 2020. Mechanisms of endothelial cell coverage by pericytes: computational modelling of cell wrapping and in vitro experiments. *Journal of The Royal Society Interface*, 17, 20190739.

SULTANA, R., OGUNDELE, O. & LEE, C. 2019. Contrasting characteristic behaviours among common laboratory mouse strains. *Royal Society Open Science*, 6.

SUN, R., KING, X., QIU, X., HUANG, C. & WONG, PP. 2021. The Emerging Roles of Pericytes in Modulating Tumor Microenvironment. *Frontiers in Cell and Developmental Biology*, 9.

SUTHERLAND, R., INCH, W., MCCREDIE, J. & KRUVU, J. 1970. MULTI-COMPONENT RADIATION SURVIVAL CURVE USING AN IN-VITRO TUMOUR MODEL. *International Journal of Radiation Biology and Related Studies in Physics Chemistry and Medicine*, 18, 491-+.

SWEENEY, M. & FOLDES, G. 2018. Takes Two: Endothelial-Perivascular Cell Cross-Talk in Vascular Development and Disease. *Frontiers in Cardiovascular Medicine*, 5.

SWIRSKI, F., GAJEWSKA, B., ROBBINS, C., D'SA, A., JOHNSON, J., POULADI, M., INMAN, M. & STAMPFLI, M. 2004. Concomitant airway expression of granulocytemacrophage colony-stimulating factor and decorin, a natural inhibitor of transforming growth factor-beta, breaks established inhalation tolerance. *European Journal of Immunology*, 34, 2375-2386.

TAKAHASHI, K., MEGURO, K., KAWASHIMA, H., KASHIWAKUMA, D., KAGAMI, S., OHTA, S., ONO, J., IZUHARA, K. & IWAMOTO, I. 2019. Serum periostin levels serve as a biomarker for both eosinophilic airway inflammation and fixed airflow limitation in well-controlled asthmatics. *Journal of Asthma*, 56, 236-243.

TAKAMASU, T., ENOMOTO, Y., ORIHARA, K., MATSUDA, A., GON, Y., SAITO, H., RA, C. & OKAYAMA, Y. 2011. An Acute Asthma Attack Induces Tissue Remodeling By Hypersecretion of Epidermal Growth Factor (EGF) And Amphiregulin (AREG) In The Airway. *Journal of Allergy and Clinical Immunology*, 127(2).

TAKESHITA, S., KIKUNO, R., TEZUKA, K. & AMANN, E. 1993. OSTEObLAST-SPECIFIC FACTOR-II - CLONING OF A PUTATIVE BONE ADHESION PROTEIN WITH HOMOLoGY WITH THE INSECT PROTEIN FASCICLIN-I. *Biochemical Journal*, 294, 271-278.

TAN, Q., CHOI, KM., SICARD, D. & TSCHUMPERLIN, DJ. 2017. Human Airway Organoid Engineering as a Step toward Lung Regeneration and Disease Modeling. *Biomaterials*, 113, 118-132.

TANG, C., XU, J., YE, H. & WANG, X. 2021. Metformin prevents PFKFB3-related aerobic glycolysis from enhancing collagen synthesis in lung fibroblasts by regulating AMPK/mTOR pathway. *Experimental and Therapeutic Medicine*, 21.

TARAYRE, J., ALIAGA, M., BARBARA, M., TISSEYRE, N., VIEU, S. & TISNEVERSAILLES, J. 1991. PHARMACOLOGICAL MODULATION OF A MODEL OF BRONCHIAL INFLAMMATION AFTER AEROSOL-INDUCED ACTIVE ANAPHYLACTIC SHOCK IN CONSCIOUS GUINEA-PIGS. *International Journal of Immunopharmacology*, 13, 349-356.

TATARI, N., MOVASSAGH, H., SHAN, L., KOUSSIH, L. & GOUNNI, A. 2019. Semaphorin 3E Inhibits House Dust Mite-Induced Angiogenesis in a Mouse Model of Allergic Asthma. *American Journal of Pathology*, 189, 762-772.

THANNICKAL, VJ., LEE, DY., WHITE, ES., CUI, Z., LARIOS, JM., CHACON, R., HOROWITZ, JC., DAY, RM. & THOMAS, RE. 2003. Myofibroblast differentiation by transforming growth factor-beta1 is

dependent on cell adhesion and integrin signaling via focal adhesion kinase. *The Journal of Biological Chemistry*, 278, 12384–9

THIERY, JP., ACLOQUE, H., HUANG, RYJ. & NIETO, MA. 2009. Epithelial-mesenchymal transitions in development and disease. *Cell*, 139(5), 871-90.

THORN, K. 2016. A quick guide to light microscopy in cell biology. *Molecular Biology of the Cell*, 27, 219-222.

TIGGES, U., WELSER-ALVES, J., BOROUJERDI, A. & MILNER, R. 2012. A novel and simple method for culturing pericytes from mouse brain. *Microvascular Research*, 84, 74-80.

TIMMINS, N. & NIELSEN, L. 2007. Generation of multicellular tumor spheroids by the hanging-drop method. *Tissue Engineering*. Humana Press.

TOLWINSKI, N. 2017. Introduction: *Drosophila*-A Model System for Developmental Biology. *Journal of Developmental Biology*, 5.

TRUNOVA, G., MAKAROVA, O., DIATROPTOV, M., BOGDANOVA, I., MIKCHAILOVA, L. & ABDULAEVA, S. 2011. Morphofunctional Characteristic of the Immune System in BALB/c and C57Bl/6 Mice. *Bulletin of Experimental Biology and Medicine*, 151, 99-102.

UYGUN, S., PENG, C., LEHTI-SHIU, M., LAST, R. & SHIU, S. 2016. Utility and Limitations of Using Gene Expression Data to Identify Functional Associations. *Plos Computational Biology*, 12.

VAN DIJK, C., NIEUWEBOER, F., PEI, J., XU, Y., BURGISSER, P., VAN MULLIGEN, E., EL AZZOUZI, H., DUNCKER, D., VERHAAR, M. & CHENG, C. 2015. The complex mural cell: Pericyte function in health and disease. *International Journal of Cardiology*, 190, 75-89.

VANDAMME, T. 2014. Use of rodents as models of human diseases. *Journal of Pharmacy & BioAllied Sciences*, 6, 2-9.

VAN HOECKE, L., JOB, ER., SAELENS, X. & ROOSE, K. 2017. Bronchoalveolar Lavage of Murine Lungs to Analyze Inflammatory Cell Infiltration. *Journal of Visualized Experiments*, 123, 55398.

VANLANDEWIJCK, M., HE, L., MAE, MA., ANDRAE, MA., ANDRAE, J., ANDO, K., DEL GAUDIO, F., NAHAR, K., LÉBOUVIER, T., LAVINA, B., GOUVEIA, L., SUN, Y., RASCHPERGER, E., RASANEN, M., ZARB, Y., MOCHIZUKI, N., KELLER, A., LENDAHL, U. & BETSHOLTZ, C. 2018. A molecular atlas of cell types and zonation in the brain vasculature. *Nature*, 554, 475-480.

VASIUKOV, G., NOVITSKAYA, T., ZIJLSTRA, A., OWENS, P., YE, F., ZHAO, Z., MOSES, HL., BLACKWELL, T., FEOKTISTOV, I. & NOVITSKIY, SV. 2020. Myeloid Cell-Derived TGF β Signaling Regulates ECM

Deposition in Mammary Carcinoma via Adenosine-Dependent Mechanisms. *Cancer Research*, 80(12), 2628-2638.

VELDMAN, M. & LIN, S. 2008. Zebrafish as a Developmental Model Organism for Pediatric Research. *Pediatric Research*, 64, 470-476.

VIEIRA BRAGA, FA., KAR, G., BERG, M., CARPAIJ, OA., POLANSKI, K., SIMON, LM., BROUWER, S., GOMES, T., HESSE, L., JIANG, J., FASOULI, ES., EFREMOVA, M., VENTO-TORMO, R., TALAVERA-LOPEZ, C., JONKER, MR., AFFLECK, K., PALIT, S., STRZELECKA, PM., FIRTH, HV., MAHBUBANI, KT., CVEJIC, A., MEYER, KB., SAEB-PARSY, K., LUINGE, M., BRANDSMA, CA., TIMENS, W., ANGELIDIS, I., STRUNZ, M., KOPPELMAN, GH., VAN OOSTERHOUT, AJ., SCHILLER, HB., THEIS, FJ., VAN DEN BERGE, M., MAWIJN, SC. & TEICHMANN, SA. 2019. A cellular census of human lungs identifies novel cell states in health and in asthma. *Nature Medicine*, 25, 1153-1163.

WALTERS, E., SOLTANI, A., REID, D. & WARD, C. 2008. Vascular remodelling in asthma. *Current Opinion in Allergy and Clinical Immunology*, 8, 39-43.

WAN, H., WINTON, H., SOELLER, C., TOVEY, E., GRUENERT, D., THOMPSON, P., STEWART, G., TAYLOR, G., GARROD, D., CANNELL, M. & ROBINSON, C. 1999. Der p 1 facilitates transepithelial allergen delivery by disruption of tight junctions. *Journal of Clinical Investigation*, 104, 123-133.

WANG, W., LIU, R., SU, Y., LI, H., XIE, W. & NING, B. 2018. MicroRNA-21-5p mediates TGF-beta-regulated fibrogenic activation of spinal fibroblasts and the formation of fibrotic scars after spinal cord injury. *International Journal of Biological Sciences*, 14, 178-188.

WANG, Y., ZANG, Q., LIU, Z., WU, Q., MAASS, D., DULAN, G., SHAUL, P., MELITO, L., FRANTZ, D., KILGORE, J., WILLIAMS, N., TERADA, L. & NWARIAKU, F. 2011. Regulation of VEGF-induced endothelial cell migration by mitochondrial reactive oxygen species. *American Journal of Physiology-Cell Physiology*, 301, C695-C704.

WANG, Y., ZHAO, M., LIU, S., GUO, J., LU, Y., CHENG, J. & LIU, J. 2020. Macrophage-derived extracellular vesicles: diverse mediators of pathology and therapeutics in multiple diseases. *Cell Death & Disease*, 11, 924.

WARD, T., CUMMINGS, J., DEAN, E., GREYSTOKE, A., HOU, J., BACKEN, A., RANSON, M. & DIVE, C. 2008. Biomarkers of apoptosis. *British Journal of Cancer*, 99, 841-846.

WEI, W., CHEN, W. & HE, N. 2021. HDAC4 induces the development of asthma by increasing Slug-upregulated CXCL12 expression through KLF5 deacetylation. *Journal of Translational Medicine*, 19, 258.

WILLIS, B. & BOROK, Z. 2007. TGF-beta-induced EMT: mechanisms and implications for fibrotic lung disease. *American Journal of Physiology-Lung Cellular and Molecular Physiology*, 293, L525-L534.

WILSON, CL., STEPHENSON, SE., HIGUERO, JP., FEGHALI-BOSTWICK, C., HUNG, CF. & SCHNAPP, LM. 2018. Characterization of human PDGFR- β -positive pericytes from IPF and non-IPF lungs. *American Journal of Physiology Lung Cell and Molecular Physiology*, 315, 991-1002.

WINKLER, J., ABISOYE-OGUNNIYAN, A., METCALF, KJ. & WERB, Z. 2020. Concepts of extracellular matrix remodelling in tumour progression and metastasis. *Nature Communications*, 11, 5120.

WIRSIK, NM., EHLER, J., MADER, L., ILINA, EI., BLANK, AE., GROTE, A., FEUERHAKE, F., BAUMGARTEN, P., DEVRAJ, K., HARTER, PN., MITTELBRONN, M. & NAUMANN, U. 2020. TGF- β activates pericytes via induction of the epithelial-to-mesenchymal transition protein SLUG in glioblastoma. *Neuropathology and Applied Neurobiology*, 47, 768-780.

WISHART, D., KNOX, C., GUO, A., SHRIVASTAVA, S., HASSANALI, M., STOTHARD, P., CHANG, Z. & WOOLSEY, J. 2006. DrugBank: a comprehensive resource for in silico drug discovery and exploration. *Nucleic Acids Research*, 34, D668-D672.

WONG, S., ROWLEY, J., REDPATH, A., TILMAN, J., FELLOUS, T. & JOHNSON, J. 2015. Pericytes, mesenchymal stem cells and their contributions to tissue repair. *Pharmacology & Therapeutics*, 151, 107-120.

WRIGHT, G. 2019. Unlocking the potential of natural products in drug discovery. *Microbial Biotechnology*, 12, 55-57.

WU, X., WANG, Z., QIAN, M., WANG, L., BAI, C. & WANG, X. 2014. Adrenaline stimulates proliferation and migration of mesenchymal stem cells towards the LPS-induced lung injury. *Journal of Cells and Molecular Medicine*, 18(8), 1612-1622.

WU, Z., DAI, W., WANG, P., ZHANG, X., TANG, Y., LIU, L., WANG, Q., LI, M. & TANG, C. 2018. Periostin promotes migration, proliferation, and differentiation of human periodontal ligament mesenchymal stem cells. *Connective Tissue Research*, 59, 108-119.

XAVIER, S., SAHU, R., LANDES, S., YU, J., TAYLOR, R., AYYADEVARA, S., MEGYESI, J., STALLCUP, W., DUFFIELD, J., REIS, E., LAMBRIS, J. & PORTILLA, D. 2017. Pericytes and immune cells contribute to complement activation in tubulointerstitial fibrosis. *American Journal of Physiology-Renal Physiology*, 312, F516-F532.

XIANG, DN., FENG, YF., WANG, J., ZHANG, X., SHEN, JJ., ZOU, R. & YUAN, YZ. 2019. Platelet-derived growth factor-BB promotes proliferation and migration of retinal microvascular pericytes by up-

regulating the expression of C-X-C chemokine receptor types 4. *Experimental and Therapeutic Medicine*, 10(5), 4022-4030.

XIE, B., HANSEL, J., MUNDORF, V., BETZ, J., REIMCHE, I., ERKAN, M., BUDEYRI, I., GESELL, A., KERR, R., ARIANTARI, N., YU, H., PROKSCH, P., TEUSCH, N. & MRSNY, R. 2020. Pseudopterosin and O-Methyltylophorinidine Suppress Cell Growth in a 3D Spheroid Co-Culture Model of Pancreatic Ductal Adenocarcinoma. *Bioengineering-Basel*, 7.

XU, F., LIU, C., ZHOU, D. & ZHANG, L. 2016. TGF- β /SMAD Pathway and Its Regulation in Hepatic Fibrosis. *Journal of Histochemistry & Cytochemistry*, 64, 157-167.

XU, J., LI, D., HSU, CY., TIAN, Y., ZHANG, L., WANG, Y., TOWER, RJ., CHANG, L., MEYERS, CA., GAO, Y., BRODERICK, K., MORRIS, C., HOOPER, JE., NIMMAGADDA, S., PEULT, B. & JAMES, AW. 2020. Comparison of skeletal and soft tissue pericytes identifies CXCR4⁺ bone forming mural cells in human tissues. *Bone Research*, 8, 22

XU, J., MORA, A., SHIM, H., STECENKO, A., BRIGHAM, KL. & ROJAS, M. 2006. Role of the SDF-1/CXCR4 Axis in the Pathogenesis of Lung Injury and Fibrosis. *American Journal of Respiratory Cell and Molecular Biology*, 37(2).

XU, X., ZHENG, L., YUAN, Q., ZHEN, G., CRANE, J., ZHOU, X. & CAO, X. 2018. Transforming growth factor-beta in stem cells and tissue homeostasis. *Bone Research*, 6.

YAMAGISHI, S., YONEKURA, H., YAMAMOTO, Y., FUJIMORI, H., SAKURAI, S., TANAKA, N. & YAMAMOTO, H. 1999. Vascular endothelial growth factor acts as a pericyte mitogen under hypoxic conditions. *Laboratory Investigation*, 79, 501-509.

YAMAGUCHI, M., HIRAI, S., TANAKA, Y., SUMI, T., TADA, M., TAKAHASHI, H., WATANABE, A. & SAKUMA, Y. 2020. Pericyte-myofibroblast transition in the human lung. *Biochemical and Biophysical Research Communications*, 528, 269-275.

YANG, Y., DONG, P., ZHAO, J., ZHOU, W., ZHOU, Y., XU, Y., MEI, C., GUO, F., ZHENG, Y. & YANG, JQ. 2018. PKC λ /I regulates Th17 differentiation and house dust mite-induced allergic airway inflammation. *Biochimica et Biophysica Acta – Molecular Basis of Disease*, 1864(2), 934-941.

YIGITBILEK, F., CONLEY, S., TANG, H., SAADIQ, I., JORDAN, K., LERMAN, L. & TANER, T. 2021. Comparable in vitro Function of Human Liver-Derived and Adipose Tissue-Derived Mesenchymal Stromal Cells: Implications for Cell-Based Therapy. *Frontiers in Cell and Developmental Biology*, 9.

YOKOTA, K., KOBAYAKAWA, K., SAITO, T., HARA, M., KIJIMA, K., OHKAWA, Y., HARADA, A., OKAZAKI, K., ISHIHARA, K., YOSHIDA, S., KUDO, A., IWAMOTO, Y. & OKADA, S. 2017. Periostin Promotes Scar

Formation through the Interaction between Pericytes and Infiltrating Monocytes/Macrophages after Spinal Cord Injury. *American Journal of Pathology*, 187, 639-653.

YTREHUS, K., HULOT, J., PERRINO, C., SCHIATTARELLA, G. & MADONNA, R. 2018. Perivascular fibrosis and the microvasculature of the heart. Still hidden secrets of pathophysiology? *Vascular Pharmacology*, 107, 78-83.

YUAN, F., XIONG, G., COHEN, N. & COHEN, A. 2017. Optimized Protocol of Methanol Treatment for Immunofluorescent Staining in Fixed Brain Slices. *Applied Immunohistochemistry & Molecular Morphology*, 25, 221-224.

YUAN, K., LIU, Y., ZHANG, Y., NATHAN, A., TIAN, W., YU, J., SWEATT, AJ., SHAMSHOU, EA., CONDON, D., CHAKRABORTY, A., AGARWAL, S., AUER, N., ZHANG, S., WU, JC., ZMANIAN, RT., NICOLLS, MR. & DE JESUS PEREZ, VA. 2020. Mural Cell SDF1 Signalling Is Associated with the Pathogenesis of Pulmonary Arterial Hypertension. *American Journal of Respiratory Cell and Molecular Biology*. 62(6), 747-759.

YUAN, K., ORCHOLSKI, ME., PANARONI, C., SHUFFLE, EM., HUANG, NF., JIANG, X., TIAN, W., VLADAR, EK., WANG, L., NICOLLS, MR., WU, JY. & DE JESUS PEREZ, VA. 2015. Activation of the Wnt/Planar Cell Polarity Pathway Is Required for Pericyte Recruitment during Pulmonary Angiogenesis. *American Journal of Pathology*, 185(1), 69-84.

ZHANG, C., BARRIOS, M., ALANI, R., CABODI, M. & WONG, J. 2016. A microfluidic Transwell to study chemotaxis. *Experimental Cell Research*, 342, 159-165.

ZHANG, L., SU, P., XU, C., YANG, J., YU, W. & HUANG, D. 2010. Chondrogenic differentiation of human mesenchymal stem cells: a comparison between micromass and pellet culture systems. *Biotechnology Letters*, 32, 1339-1346.

ZHANG, X., YAN, X., CAO, J., YANG, Z., CAO, X., ZHANG, Y., LIANG, L., ZHENG, M., LIU, X., ZHANG, J. & HAN, H. 2020. SM22 α vascular mural cells are essential for vessel stability in tumors and undergo phenotype transition regulated by Notch signaling. *Journal of Experimental & Clinical Cancer Research*, 39, 124.

ZHAO, W., WANG, C., LIU, R., WEI, C., DUAN, J., LIU, K., LI, S., ZOU, H., ZHAO, J., WANG, L., QI, Y., LIANG, W., JIANG, J., ZHANG, W., PANG, L. & LI, F. 2016. Effect of TGF-beta 1 on the Migration and Recruitment of Mesenchymal Stem Cells after Vascular Balloon Injury: Involvement of Matrix Metalloproteinase-14. *Scientific Reports*, 6.

ZHAO, Z., ZHANG, Y., ZHANG, C., ZHANG, J., LUO, X., QUI, Q., LUO, D. & ZHANG, J. 2022. TGF- β promotes pericyte-myofibroblast transition in subretinal fibrosis through the Smad2/3 and Akt/mTOR pathways. *Experimental & Molecular Medicine*, 54, 673-684.

ZHOU, W., KE, S., HUANG, Z., FLAVAHAN, W., FANG, X., PAUL, J., WU, L., SLOAN, A., MCLENDON, R., LI, X., RICH, J. & BAO, S. 2015. Periostin secreted by glioblastoma stem cells recruits M2 tumour-associated macrophages and promotes malignant growth. *Nature Cell Biology*, 17, 170-+.

ZHU, L., SU, Q., JIE, X., LIU, A., WANG, H., HE, B. & JIANG, H. 2016. NG2 expression in microglial cells affects the expression of neurotrophic and proinflammatory factors by regulating FAK phosphorylation. *Nature Scientific Reports*, 6, 27983.

ZHU, M., LI, W., DONG, X., YUAN, X., MIDGLEY, A., CHANG, H., WANG, Y., WANG, H., WANG, K., MA, P., WANG, H. & KONG, D. 2019. In vivo engineered extracellular matrix scaffolds with instructive niches for oriented tissue regeneration. *Nature Communications*, 10.

Chapter 9 - Supplementary Information



Supplementary Figure 9.1 – alternative access to multimedia shown in Figure 5.14. QR code linking to 3D representation of untreated spheroid.



Supplementary Figure 9.2 – alternative access to multimedia shown in Figure 5.14. QR code linking to 3D representation of TGF- β treated spheroid.



Supplementary Figure 9.3 – alternative access to multimedia shown in Figure 5.14. QR code linking to 3D representation of periostin treated spheroid.



Supplementary Figure 9.4 – alternative access to multimedia shown in Figure 5.14. QR code linking to video of individual stacks of an untreated spheroid.



Supplementary Figure 9.5 – alternative access to multimedia shown in Figure 5.14. QR code linking to video of individual stacks of a TGF- β treated spheroid.



Supplementary Figure 9.6 – alternative access to multimedia shown in Figure 5.14. QR code linking to video of individual stacks of a periostin treated spheroid.

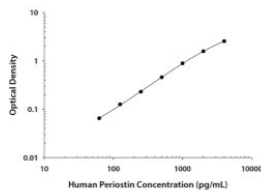
CALCULATION OF RESULTS

Average the duplicate readings for each standard, control, and sample and subtract the average zero standard optical density (O.D.).

Create a standard curve by reducing the data using computer software capable of generating a four parameter logistic (4-PL) curve-fit. As an alternative, construct a standard curve by plotting the mean absorbance for each standard on the y-axis against the concentration on the x-axis and draw a best fit curve through the points on the graph. The data may be linearized by plotting the log of the human Periostin concentrations versus the log of the O.D. and the best fit line can be determined by regression analysis. This procedure will produce an adequate but less precise fit of the data. If samples have been diluted, the concentration read from the standard curve must be multiplied by the dilution factor.

TYPICAL DATA

This standard curve is only for demonstration purposes. A standard curve should be generated for each set of samples assayed.



SPECIFICITY

The following factors prepared at 50 ng/mL were assayed and exhibited no cross-reactivity or interference.

Recombinant human:	Recombinant mouse:
βIG-H3	Periostin
Integrin αVβ3	
Integrin αVβ5	

OTHER MATERIALS & SOLUTIONS REQUIRED

DuoSet® Ancillary Reagent Kit 2 (5 plates): (R&D Systems®, Catalog # DY008) containing 96 well microplates, plate sealers, substrate solution, stop solution, plate coating buffer (PBS), wash buffer, and Reagent Diluent Concentrate 2.

The components listed above may be purchased separately:

96 well microplates: (R&D Systems®, Catalog # DY990).

Plate Sealers: (R&D Systems®, Catalog # DY992).

PBS: 137 mM NaCl, 2.7 mM KCl, 8.1 mM Na₂HPO₄, 1.5 mM KH₂PO₄, pH 7.2-7.4, 0.2 µm filtered (R&D Systems®, Catalog # DY006).

Wash Buffer: 0.05% Tween® 20 in PBS, pH 7.2-7.4 (R&D Systems®, Catalog # WA126).

Reagent Diluent Concentrate 2: 1% BSA in PBS, pH 7.2-7.4, 0.2 µm filtered (R&D Systems®, Catalog # DY995).

Quality of BSA is critical (see Technical Hints).

Substrate Solution: 1:1 mixture of Color Reagent A (H₂O₂) and Color Reagent B (Tetramethylbenzidine) (R&D Systems®, Catalog # DY999).

Stop Solution: 2 N H₂SO₄ (R&D Systems®, Catalog # DY994).

PRECAUTIONS

Some components in this kit contain a preservative which may cause an allergic skin reaction. Avoid breathing mist.

The Stop Solution suggested for use with this kit is an acid solution.

The Color Reagent B suggested for use with this kit may cause skin, eye, and respiratory irritation. Avoid breathing fumes.

Wear protective gloves, clothing, eye, and face protection. Wash hands thoroughly after handling. Refer to the SDS on our website prior to use.

CALIBRATION

This DuoSet® is calibrated against a highly purified NS0-expressed recombinant human Periostin produced at R&D Systems®.

TECHNICAL HINTS & LIMITATIONS

- We recommend the use of R&D Systems™ Reagent Diluent Concentrate 2 (Catalog # DY995) to prepare Reagent Diluent for use in this assay.
- The use of high quality Bovine Serum Albumin (BSA) for the Reagent Diluent is crucial for the optimum performance of the DuoSet® ELISA Development kit. Impurities such as proteases, binding proteins, soluble receptors or other interfering substances can be found to varying degrees in virtually all BSA preparations and can inhibit or interfere with the detection of certain analytes. If the standard curve appears suppressed, consider evaluating a different preparation of BSA.
- It is suggested to start Reagent Diluent optimization for serum and plasma samples by using PBS supplemented with 10-50% animal serum. Do not use buffers with animal serum to reconstitute or dilute the Detection Antibody or Streptavidin-HRP A.
- It is important that the Reagent Diluent selected for reconstitution and dilution of the standard reflects the environment of the samples being measured.
- Avoid microbial contamination of reagents and buffers.
- A thorough and consistent wash technique is essential for proper assay performance. Wash Buffer should be dispensed forcefully and removed completely from the wells by aspiration or decanting. Remove any remaining Wash Buffer by inverting the plate and blotting it against clean paper towels.
- Individual results may vary due to differences in technique, plasticware and water sources.
- It is recommended that all standards and samples be assayed in duplicate.
- The use of PBS from tablets may interfere in this assay.

TROUBLESHOOTING

Note: For more detailed troubleshooting, please visit: www.RnDSystems.com/ELISADevelopment

Poor Standard Curve

- Impure BSA used for Reagent Diluent preparation.
- Improper reconstitution and/or storage of standard.
- Improper dilution of highest standard and standard curve.
- Incomplete washing and/or aspiration of wells.
- Unequal volumes added to wells/pipetting error.
- Incorrect incubation times or temperatures.

Poor Precision

- Unequal volumes added to wells/pipetting error.
- Incomplete washing and/or aspiration of wells.
- Unequal mixing of reagents.

Low or No color Development

- Inadequate volume of substrate added to wells.
- Incorrect incubation times or temperatures.
- Impure BSA used for Reagent Diluent preparation.

7170322

4/18

DuoSet® ELISA
DEVELOPMENT SYSTEM

Human Periostin/OSF-2

Catalog Number: DY3548B (15 plates)

INTENDED USE

For the development of sandwich ELISAs to measure natural and recombinant human Periostin. The Reagent Diluent recommended may be suitable for most cell culture supernate, serum, and plasma samples. The Reagent Diluent selected for use can alter the performance of an immunoassay. Reagent Diluent optimization for samples with complex matrices such as serum and plasma, may improve their performance in this assay.

This kit contains sufficient materials to run ELISAs on at least fifteen 96 well plates, provided the following conditions are met:

- The reagents are prepared as described in this package insert.
- The assay is run as described in the General ELISA Protocol.
- The recommended microplates, buffers, diluents, substrates, and solutions are used.

This package insert must be read in its entirety before using this product. Refer to the Certificate of Analysis for component concentrations as they may vary. For research use only. Not for use in diagnostic procedures.

MANUFACTURED AND DISTRIBUTED BY:

USA & Canada | R&D Systems, Inc.
614 McKinley Place NE, Minneapolis, MN 55413, USA
TEL: (800) 343-7475 (612) 379-2956 FAX: (612) 656-4400
E-MAIL: info@RnDSystems.com

DISTRIBUTED BY:

UK & Europe | R&D Systems Europe, Ltd.
19 Barton Lane, Abingdon Science Park, Abingdon OX14 3NB, UK
TEL: +44 (0)1235 529449 FAX: +44 (0)1235 533420
E-MAIL: info@RnDSystems.co.uk

China | R&D Systems China Co., Ltd.

24A1 Hua Min Empire Plaza, 726 West Yan An Road, Shanghai PRC 200050
TEL: +86 (21) 52380373 FAX: +86 (21) 52371001
E-MAIL: info@RnDSystemsChina.com.cn

R&D SYSTEMS
a biotechnie brand

www.RnDSystems.com

MATERIALS PROVIDED & STORAGE CONDITIONS

Store the unopened kit at 2-8 °C. Do not use past kit expiration date.

DESCRIPTION	PART #	# VIALS	STORAGE OF OPENED/ RECONSTITUTED MATERIAL
Human Periostin Capture Antibody	B4441	1 vial	Refer to the lot-specific Certificate of Analysis (C of A) for storage conditions.
Human Periostin Detection Antibody	B4442	1 vial	
Human Periostin Standard	B4200	3 vials	
Streptavidin-HRP A	B9003	1 vial	

REAGENT PREPARATION

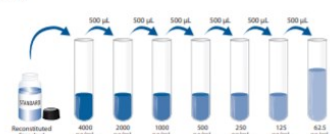
Bring all reagents to room temperature before use. Allow all components to sit for a minimum of 15 minutes with gentle agitation after initial reconstitution. Working dilutions should be prepared and used immediately.

Streptavidin-HRP A: 1.0 mL of streptavidin conjugated to horseradish-peroxidase. Dilute to the working concentration specified on the vial label using Reagent Diluent.

Mouse Anti-Human Periostin Capture Antibody: Refer to the lot-specific C of A for amount supplied. Reconstitute with 1.0 mL of PBS. Dilute in PBS without carrier protein to the working concentration indicated on the C of A.

Biotinylated Mouse Anti-Human Periostin Detection Antibody: Refer to the lot-specific C of A for amount supplied. Reconstitute with 1.0 mL of Reagent Diluent. Dilute in Reagent Diluent to the working concentration indicated on the C of A.

Recombinant Human Periostin Standard: Refer to the lot-specific C of A for amount supplied. Reconstitute each vial with 0.5 mL of Reagent Diluent. A seven point standard curve using 2-fold serial dilutions in Reagent Diluent is recommended. Prepare 1000 µL of high standard per plate assayed at the concentration indicated on the C of A.



Supplementary Figure 9.7 – Manufacturers protocol for the human periostin ELISA DuoSet by R&D Systems. (accessed at https://www.rndsystems.com/products/human-periostin-osf-2-duo-set-elisa_dy3548b#product-datasheets)